DECLINE CURVE ANALYSIS AND ENHANCED SHALE OIL RECOVERY BASED ON EAGLE FORD SHALE DATA

By

Dieudonne K. Delaihdem

RECOMMENDED:

Dr. Mohabbat Ahmadi

Dr. Catherine Hanks

Dr. Abhijit Dandekar

Dr. Abhijit Dandekar
Chair, Department of Petroleum Engineering

APPROVED:

Dr. Doug Goering
Dean, College of Engineering and Mines

Dr. John C. Eichelberger
Dean of the Graduate School

11/28/13

Date

DECLINE CURVE ANALYSIS AND ENHANCED SHALE OIL RECOVERY BASED ON EAGLE FORD SHALE DATA

A

THESIS

Presented to the Faculty

of the University of Alaska Fairbanks

in Partial Fulfillment of the Requirements

for the Degree of

MASTER OF SCIENCE

By

Dieudonne K. Delaihdem, B.S.

Fairbanks, Alaska

December 2013

ABSTRACT

Transient and fracture dominated flow regimes in tight permeability shale reservoirs with hydraulically fractured horizontal wells impose many unconventional challenges. These include execution of appropriate shale decline curve analysis and the optimization of hydrocarbons recovery. Additionally, short production profiles available are inadequate for accurate production decline analysis.

This research assessed the effectiveness of Arps' decline curve analysis and recently established methods--power law exponential analysis, logistic growth analysis, Duong's method and the author's approach--to predict future production of horizontal wells in the Eagle Ford Shale. Simulation models investigated history matching, enhanced shale oil recovery, and drainage area beyond stimulated reservoir volume.

Traditional Arps' hyperbolic method sufficiently analyzed past production rates, but inaccurately forecasted cumulative productions. The recent decline models show slight variations in their past performance evaluations and forecasting future production trends. The technique proposed and used in this work enhanced the successful application of Arps' hyperbolic decline from 32.5% to 80%.

Simulation results indicate 4.0% primary oil recovery factor and 5.8% enhanced shale oil recovery factor using CO_2 miscible injection. Based on pressure observed outside of the stimulated reservoir volume, limited to the range of data used in this study, drainage area outside stimulated reservoir volume is not significant.

DEDICATION

To God is the Glory
Praises to the Lord; His Love Endures Forever

TABLE OF CONTENTS

LIST OF FIGURES

LIST OF TABLES

ACKNOWLEDGEMENT

I would like to thank my advisor Dr. Mohabbat Ahmadi, and other members of my graduate study committee; Dr. Catherine Hanks and Dr. Abhijit Dandekar for all their support and contributions. Without their intellectual advice and feedback during the entire study this work would not have been academically successful. I appreciate their input of talent and time in carefully evaluating every stage of my work.

I would also like to thank Dr. Jim Erdle of CMG for making available their simulation software for me to use even while on vacation in Ghana. I am deeply grateful to CMG support staff for their assistance on numerous occasions.

I extend my thanks also to the staff and students of the Petroleum Engineering department at UAF.

Finally, I express my sincere gratitude to my wife and children, parents and siblings, and my Christian fellowship brothers for believing strongly in me and for their prayerful supports.

Finally, my praise and worship for this accomplishment belong to GOD the Invincible, Author of Life, Alpha and Omega.

Dieudonne K. Delaihdem

Chapter 1 Introduction

1.1 Shale Oil Reservoirs

Hydrocarbon accumulations in petroleum reservoirs around the world migrated from very fine-grained, dark-gray or black organic-rich sedimentary source rocks, referred to as organic-rich shales. For decades, organic-rich shale formations have been regarded as source rocks from which hydrocarbons originated and migrated into sandstone and limestone of various reservoir qualities. Oil- and gas-prone shales form when massive amounts of organic debris deposition occur in swamps, lakes, marine environments, followed by rapid burial without decay (Passey et al., 2010). Subsequently, over geologic time, these organic constituents convert into hydrocarbons under the effect of temperature and pressure changes in the subsurface due to burial. Thus, these organic-rich shales undergo the necessary geologic processes from diagenesis to catagenesis to convert dead organic contents into useful hydrocarbons. The Eagle Ford Shale, located within the Maverick Basin in south Texas, is a perfect example of organic-rich shale, and it is a world-class source rock for a number of conventional petroleum systems such as the Austin Chalk and the East Texas oilfields (Sondhi, 2011). The geochemical evidence of Eagle Ford Shale sourcing the Austin Chalk is the presence of similar kerogen type II found in both reservoirs (Martin et al., 2011). The Eagle Ford Shale oil, however, is generated from kerogen type I, I/II and III, which implies that the overall hydrocarbon composition of the Eagle Ford Shale and Austin Chalk may be significantly different.

The decline in the conventional hydrocarbon reserves, especially in the United States, motivated researchers to explore organic-rich shales as potential hydrocarbon reservoirs. Geoscientists recognized the reservoir potential of the ultra-low permeability organic-rich shale formations saturated with and/or still “cooking” petroleum. Petroleum engineers have undertaken to develop

technologies for economic and commercial development of these resources. Technological innovations over the years, coupled with increasing demands and rising prices of petroleum products, generated considerable interest in developing shale oil and shale gas reservoirs, particularly in the United States and Canada (Mullen, 2010).

Shale oil and conventional oil reservoirs require different development strategies for economic oil recovery. Low permeability shale reservoirs require extensive hydraulic fracture stimulation treatments at the onset of economic oil recovery (Miskimins, 2008). On the other hand, conventional reservoirs have relatively good permeability, and therefore produce at economic rates without hydraulic fractures. Understanding petrophysical and geomechanical properties is essential for optimum stimulation treatment of shale reservoirs.

1.2 Shale Oil- What is it?

Shale oil is crude oil produced from, and still residing in, organic-rich, dark-gray, black shale formations (source rocks) that are in the oil window of thermal maturity (Chaudhary, 2011). Shale reservoir rocks are characterized by nano-Darcy permeability and micro porosity and are classified as ultra-low or tight permeability formations. The nano-Darcy permeability, the non-communicating micro porosity and lack of structural conduits prevented the migration of the hydrocarbons generated in these shales into conventional reservoirs. As a result, economic recovery is particularly challenging without the current innovations in petroleum technology (Medeiros et al., 2008). Shale oil should not be confused with oil shale, organic-rich shale which contains kerogen (solid organic matter) that has not yet reached the thermal maturity for generating any hydrocarbon phases (Chaudhary, 2011). Shale oil is liquid hydrocarbon (crude oil)

trapped in micro porous source rocks due to lack of conventional formation permeability and natural migration pathways; consequently, shale oil requires unconventional recovery processes.

1.3 Shale Play Development

Economic development of a shale oil play depends on the shale's total organic content (TOC), petrophysical characteristics, and reservoir properties (Mullen, 2010). A TOC in excess of 3% is usually a good cut-off-grade (McFarland, 2010). The Eagle Ford TOC is 2.0% to 6.5% (Vassilellis et al., 2010). Rock-Eval pyrolysis, vitrinite reflectance, and burial history of shale deposits are used to evaluate the type of kerogen present and level of thermal maturity in order to determine the petroleum potential of the shale play (McFarland, 2010). Vitrinite reflectance (VF) between 0.6% and greater than 1.35% in an oil-prone shale correlates with a hydrocarbon generation window, which is 60 to 120 degrees Celsius (McFarland, 2010). Another important factor in determining the viable development of shale oil is the areal extent and thickness of the organic-shale deposits (McFarland, 2010).

Successful exploitation of shale oil reservoirs requires sufficient liquid-conductive fractures in the otherwise impervious shale. This enhances fluid flow from the oil-saturated matrix into horizontal wellbores. Thus, shale formations are normally impermeable except for the presence of natural fractures. Natural fractures form as a result of tectonic activities, overburden pressure and/or pressurized liquid expulsion (Berg and Gangi, 1999). Consequently, effective characterization of shale reservoirs requires knowledge of the geology (lithology and mineralogy) of a formation in order to understand and predict the petrophysical parameters such as natural fracture density and distribution, hardness, and brittleness index (Mullen, 2010). Major engineering challenges,

therefore, include adequate reservoir characterization for the appropriate wellbore stimulation design (Vassilellis et al., 2010). The challenges include numerical analysis of natural fracture networks, determination of rock geomechanical properties, and proper selection of hydro-fracturing fluids (Vassilellis et al., 2010).

Shale plays' geomechanical and geochemical attributes vary, and individualized developmental approaches may be required for different shale reservoirs (Rickman, et al., 2008). The Eagle Ford is not only mineralogically unique but also produces three hydrocarbon types, requiring different development strategies within the play (Mullen, 2010).

1.4 Purpose and Scope of Study

Decline curve analysis of past production data is an essential tool petroleum reservoir engineers use to estimate reserves, evaluate well performance, improve well completion effectiveness, and determine reservoir properties. In the first part of this study, the available production decline techniques assessed the past wells' performance, forecasted the future performance rates and estimated reserves for selected wells in the Texas Eagle Ford Shale play. These various techniques include Arp's empirical decline curve analysis (DCA), logistic growth analysis (LGA), power law exponential analysis, and Duong's method. In addition, a new approach, involving the use of logistic growth analysis cumulative production data in Arps' hyperbolic decline model, to eliminate the dominance of decline exponents greater than one was proposed and used. The techniques evaluated production profiles for forty hydraulically fractured horizontal wells in the Eagle Ford for expected ultimate recovery (EUR) and future performance.

In the second part of the study, numerical simulation models (NSM) with realistic researched data: reservoir rocks, fluids, wellbore and hydraulic fracture were used to history match the past

production of two wells in the Eagle Ford Shale play and generate future performance predictions. Furthermore, NSM accomplishes other goals such as:

1. Compares and contrasts the practical effects of miscible gas injectants such as CO_2, CH_4, CO_2-CH_4 1:1 mixture and other combinations of CO_2, CH_4, N_2, C_2H_6, C_3H_8, to enhance shale oil recovery beyond primary depletion,
2. Explores the technical feasibility of enhanced shale oil recovery (ESOR) by miscible gas injection displacement process using different numbers and arrangements of, and
3. Defines the drainage area of several horizontal wells in a reservoir of similar modeling parameters as for ESOR using observation wells outside of the stimulated reservoir volumes (SRV).

Chapter 2 Literature Review

2.0 Introduction

The Eagle Ford Shale play is both gas and liquid hydrocarbon-rich (Stegent et al., 2010 and Vassilellis et al., 2010). The hydrocarbon resources of the Eagle Ford are roughly 3.35 billion barrels of oil and 20.80 trillion standard cubic feet of natural gas (Government-Report, 2011). The Eagle Ford Shale is an unconventional hydrocarbon resource; thus, economic recovery is not possible without the implementation of advanced petroleum recovery technology (Holditch, 2003).

The Eagle Ford Shale is of Upper Cretaceous (Cenomanian-Turonian) age (Tuttle, 2010). It is the source of hydrocarbon accumulations in the overlying Austin Chalk and the massive East Texas Woodbine sands fields (Fan et al., 2011 and Tuttle, 2010). It is currently one of the most attractive source reservoirs in Texas due to its relatively high total organic content (TOC) of 2.0-6.5% (Fertl and Rieke III, 1980; Mullen, 2010; Vassilellis et al., 2010).

Three distinct hydrocarbon phases are produced from the Eagle Ford Shale and, depending upon the development site (county, lease and depth); they include dry gas, gas condensate, and oil (Mullen, 2010). As a result, hydrocarbon production requires reservoir engineering techniques tailored to the phases of hydrocarbon production (Mullen, 2010).

Production rates of the Eagle Ford oil wells decline rapidly after the first two or three months of high liquid withdrawal (TRRC-Website, 2012). About 40% of the Eagle Ford wells' cumulative production could be achieved within five years despite the projected 30-year longevity for most of the wells (Hart, 2011). Thereafter, the wells will experience low recovery of fluids unless there

is additional intervention such as re-fracturing of the formation and/or application of enhanced oil recovery (EOR) techniques (e.g., gas injection) (Hart, 2011).

The oil recovery factor for the Eagle Ford Shale play during primary energy reservoir depletion will be roughly 5%. However, improvement in fracking technology, fracturing of wells multiple times, longer laterals, closely spaced well intervals, and miscible displacement (especially using CO_2 solvents) all can improve shale oil recovery factors (Hart, 2011).

2.1 Geology

The Eagle Ford Shale play, located in the Maverick Basin of southeast Texas, is a SW-NE trending source and reservoir rock. It stretches approximately 400 miles long and 50 miles wide, from the Mexican border in the SW into the NE of Texas (Wang and Liu, 2011 and Vassilellis et al., 2010) (**Figures 2.1 and 2.2)**. The Eagle Ford Shale formed in the Upper Cretaceous (Cenomanian-Turonian) due to major anoxic extinction of microorganisms and rapid sedimentation in restricted marine basins (Tuttle, 2010 and Martin et al., 2011).

The Eagle Ford Shale covers almost 11 million acres. The stratigraphic column in **Figure 2.3** shows the Eagle Ford Shale underlain unconformably by the Buda Limestone and overlain by the Austin Chalk. The gross thickness of the formation ranges from 20 to 500 ft, while the formation top varies between subsea elevations of 2500 ft to 14000 ft (Mullen, 2010; Nwabuoku, 2011 and Wang and Liu, 2011). The rejuvenated mid-Cretaceous Sabine uplift and subsequent erosion of the Eagle Ford Shale after it had been deposited account for the reduction in the thickness of the

formation to about 50 ft in the NE from the average gross thickness of 350 ft in the SW (Martin et al., 2011).

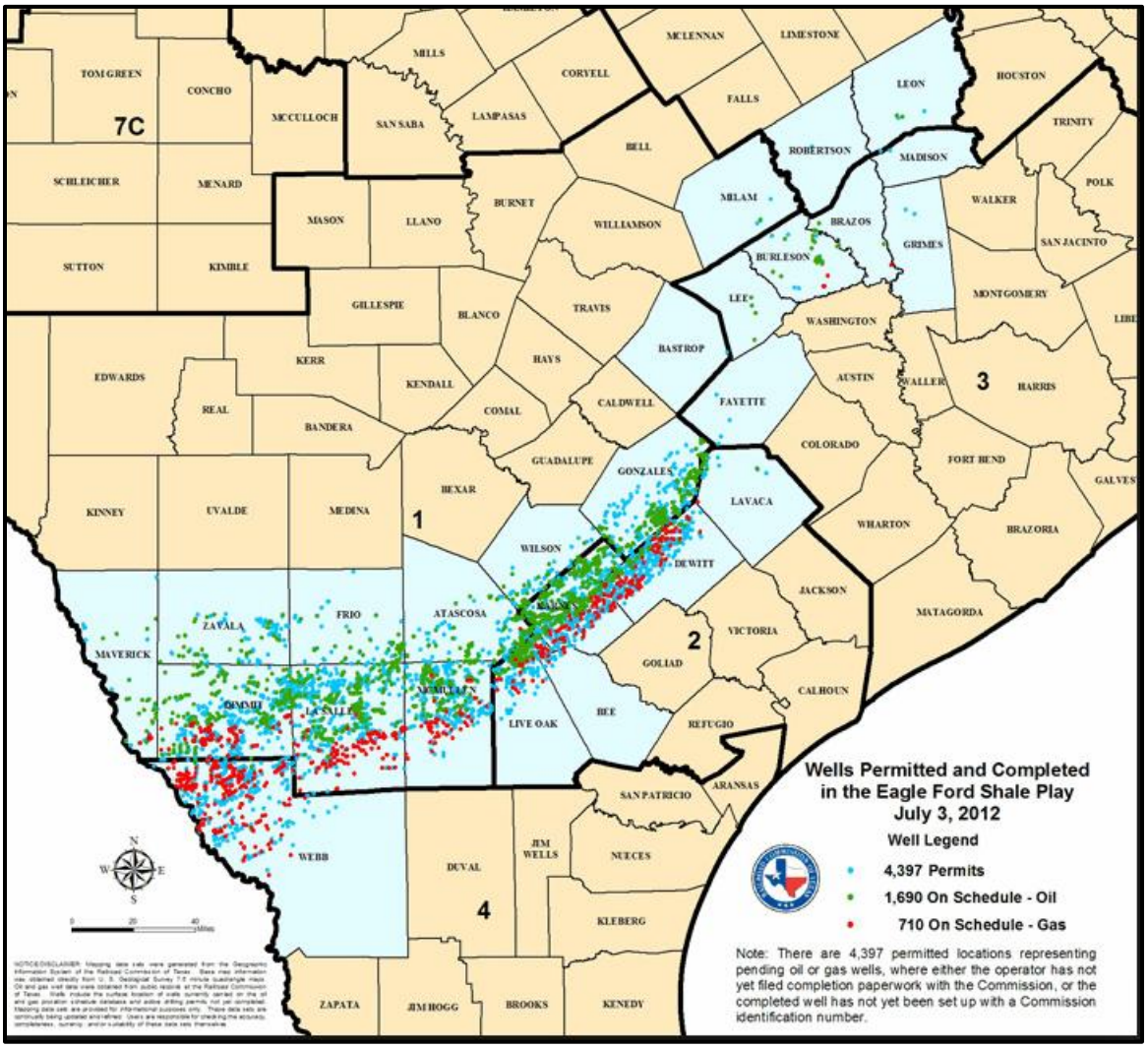

Figure 2.1: Map view of southern Texas showing Eagle Ford Shale resource play, counties, scheduled oil and gas and permitted wells locations (TRRC, 2012).

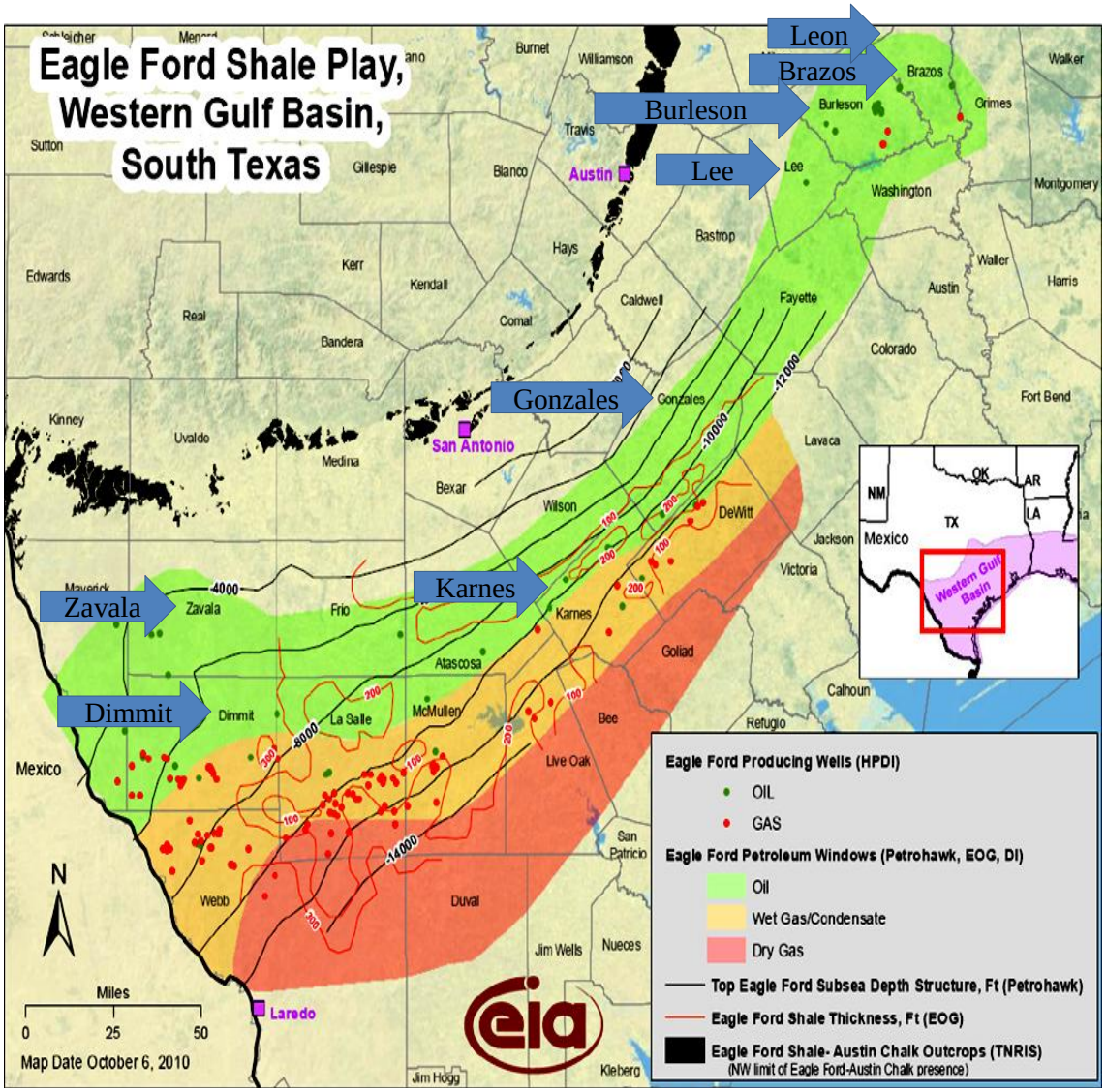

Figure 2.2: Map view of the Eagle Ford Shale hydrocarbon phases and windows of thermal maturity with arrow labels indicating the researched counties' locations (Wang and Liu, 2011).

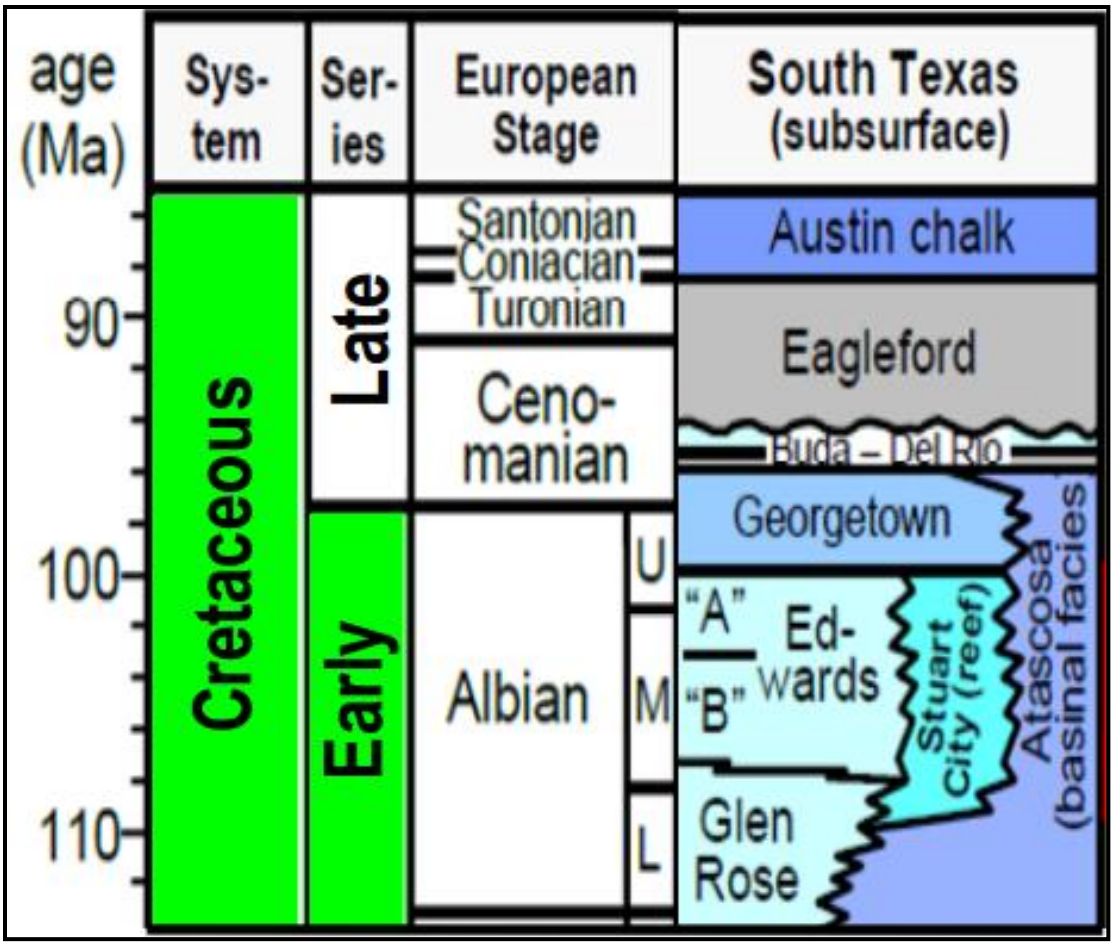

Figure 2.3: Cretaceous stratigraphic column from south Texas showing stratigraphic location of the Eagle Ford shale (Fan et al., 2011).

Hydrocarbon accumulations within the Eagle Ford Shale are closely related to local stratigraphy. The stratigraphic sequence consists of two main clastic depositional environments. These include a lower transgressive sequence of black, organic-rich, laminated shale and an upper regressive sequence of quartz-rich siltstone, bentonites, limestone, and calcareous black shale. Both of these sequences have natural fractures, sealing faults, and variable thicknesses (Martin et al., 2011). The increased permeability associated with natural fractures augments oil and gas storability in localized sweet spots, and sealing faults confine and trap hydrocarbon accumulations in the fractures while also preventing migration out of the source rock (Mullen, 2010 and Martin et al.,

2011). Consequently, the amount of recoverable hydrocarbon varies across the Eagle Ford Shale play due to the sequence stratigraphy, facies changes, and natural fracture distribution.

2.2 Decline Curve Analysis

Analysis of past production decline to predict future production performance is valuable to oil and gas industry operators and financial resource institutions. Arps (1945) developed methods to analyze decline trends in conventional reservoirs with great success. Hydrocarbon recovery from unconventional shale reservoirs is increasingly crucial, especially in the US and Canada; it is crucial to evaluate current production trends, predict future production performance and evaluate the effectiveness of different hydraulic fracture stimulations and completion designs. The traditional Arps decline models have not successfully estimated reserves or future production in tight permeability reservoirs (Duong, 2010). One of the assumptions in Arps' empirical equations is the existence of a boundary-dominated flow regime, which is observed historically for most conventional reservoirs. This assumption does not apply to tight permeability shales, which are dominated by long transient flow regimes. As a result, traditional Arps' decline relations may result in decline exponent (b) greater than one (i.e., $b>1$) for shale reservoirs. The effect of $b>1$ is unrealistic infinite cumulative production forecast with time. Thus, Arp's hyperbolic models tend to overestimate the expected ultimate recovery, despite closely fitting the past production rate profiles.

To ensure accurate prediction mechanisms, researchers have proposed other analytical models to predict future production and estimate reserves for shale reservoirs (Duong, 2010). The recent

decline analysis techniques used to specifically address production forecasting in shale reservoirs include:

1. Power Law Exponential (PLE) Analysis by Ilk et al., 2008,
2. Logistic Growth Analysis (LGA) by Clark, 2011, and
3. Duong method by Duong, 2011.

McNeil et al. (2009) recommended that erratic production profiles be filtered by elimination of data points that deviate from a reasonable decline trend.

2.2.1 Arps Decline Curve Analysis

Arps (1945) developed the mathematical relations for three types of graphical representation of production decline for conventional reservoirs. These empirical equations define the historical exponential, hyperbolic, and harmonic decline types observed for different qualities of traditional reservoirs. The basic concept of decline analysis involves fitting a trendline through a well's historical performance on a semi-log plot and extrapolating that line to estimate future production performance, assuming the past trend will not change under constant operational conditions. Mathematically, it is the concept of loss-ratio (1/D) and the derivative of the loss-ratio (b), where D and b are the decline parameter and decline exponent, respectively, expressed as follows (Arps, 1945):

$$\frac{1}{D} = -q/\left(\frac{dq}{dt}\right) \qquad (2.1)$$

$$\text{and } b = \frac{d}{dt}\left(\frac{1}{D}\right) = -\frac{d}{dt}\left(\frac{q}{dq/dt}\right); \text{ where } 0 \leq b \leq 1 \qquad (2.2)$$

Equation 2.1 translates into three diagnostic equations corresponding to the three decline types (exponential, harmonic and hyperbolic). When b=0, the decline type is exponential or constant

percentage which, graphically, is a straight line fitting historical performance on a semi-log plot of rate versus time or rate versus cumulative production (Arps, 1945). The empirical equations for exponential decline are:

$$q = q_i * e^{-Dt} \qquad (2.3)$$

and

$$N_p = \frac{q_i - q}{D} \qquad (2.4)$$

where

D =Decline constant, 1/day or 1/time

q = Production rate at time t, stb/day or stb/time

q_i = Initial rate, stb/day or stb/time, and

N_p = Cumulative production at time t, STB

When b=1, decline is harmonic and a straight line on the semi-log plot of rate versus cumulative production. The empirical equations for harmonic decline are:

$$q = \frac{q_i}{e^{Np*\frac{Di}{qi}}} = q_i * e^{-\frac{Di}{qi}*Np} \qquad (2.5)$$

and

$$Np = \frac{qi}{Di} \ln \frac{qi}{q} \qquad (2.6)$$

where;

Di =Initial decline constant, 1/day or stb/time

q = Production rate at time t, stb/day or stb/time

q_i = Initial rate, stb/day or stb/time, and

N_p = Cumulative production at time t, STB

Hyperbolic decline is for the limit 0<b<1. The hyperbolic decline plot is a curve (concave upwards) on the semi-log rate-time, since decline exponents change with time, in contrast to the constant percentage decline (Clark, 2011). Low productivity wells exhibit hyperbolic-harmonic decline behavior (Clark, 2011). Arps' hyperbolic modeling equations are as follows:

$$q = qi(1 + bD_i t)^{-\frac{1}{b}} \qquad (2.7)$$

$$N_p = \frac{q_{ib}}{(1-b)D_i}(q_i^{1-b} - q^{1-b}) \qquad (2.8)$$

In case of adequate production data, a horizontal shale well's performance is commonly analyzed using Arps' hyperbolic rate decline (Duong, 2010 and Shelley et al., 2012). As expected in fracture-dominated, extremely tight formations, initial production rates are extremely high, followed by rapid decline ruled by the unusually long transient flow regimes (Medeiros at al., 2008 and Duong, 2010). The benefit of using the hyperbolic model for shales is that a reasonable match is usually obtained for wellbore performances that are characterized by long transient flow regimes (Duong, 2010). The downside is that cumulative production becomes infinite due to matching data with b>1. The transient flow regime behavior portrays an infinite-acting reservoir because the pressure response profile in the reservoir constantly moves outward, apparently never able to reach the finite dimensional boundaries, resulting in an erroneous EUR (Clark, 2011).

2.2.2 Power Law Exponential Analysis

This model, proposed by Ilk et al., 2008, models the loss-ratio and its derivative for production decline by a power law relationship observed in transient linear and bilinear flow regimes. In contrast to Arps' exponential decline model, it represents decay as a power law function instead of a constant decline (Clark, 2011). Ilk et al. (2008) stated that the production profile usually follows exponential rate decline, aside from the early-time rapid decline rate; therefore, PLE analysis can estimate reserves. According to McNeil et al. (2009), the first one or two data points from the production profile may not count towards having a good data production fit.

With the power law exponential loss-ratio method, Ilk et al. (2008) define the decline parameter (D) and production rate (q) respectively as

$$D = D_{\infty} + D_1 * t^{-(1-n)} \qquad (2.9)$$

$$q = \hat{q}_i \, e^{\left(-D_{\infty} * t - \frac{D_1}{n} t^n\right)} \qquad (2.10)$$

With further modification by Ilk et al., (2008), the PLE **Equation 2.10** becomes

$$q = \hat{q}_i \, e^{\left(-D_{\infty} t - \hat{D}_i t^n\right)} \qquad (2.11)$$

where,

D_1 = Decline constant "intercept" at 1 time unit, (t=1,$time^{-1}$)

D_{∞} = Decline constant at "infinite time"($t = \infty, time^{-1}$)

$\hat{D}_i$ = Decline constant ($\hat{D}_i = D_1/n$), $time^{-1}$

n = Time exponent, dimensionless

q = Production rate, stb/d

$\hat{q}_i$ = Rate "intercept", (t=0, stb/d)

t =production time (days)

The model parameters $\hat{q}_i$, D_∞, $\widehat{D}_i$ and n are required to make data adjustments for early-time transient flow and late-time constant decline behavior. Also the t^n term (**Equations 2.10 and 2.11**) matches early-time transient flow regime, while D_∞ models late-time decline behavior (Clark 2011). According to Ilk et al. (2008), **Equation 2.9** approximates the loss-ratio by a decaying power law relation where D_∞ is constant for late-time behaviors.

To estimate the EUR, decline parameters (initial rate (q_i) and decline rate (D)) are determined from the semi-log plot of rate versus time using the PLE-generated profile. This diagnostic plot must linearly fit a trendline of least square regression $R^2 \geq 0.97$ to estimate expected ultimate recovery EUR and generate future production curves.

2.2.3 Logistic Growth Analysis

Logistic growth analysis (LGA) is an empirical mathematical technique used to analyze numerous physical trends such as population (Clark 2011). LGA is able to analyze well production performance and predict future reserves, especially in shale oil reservoirs (Clark, 2011). Clark (2011) clearly explained the use of LGA with original concepts and modifications necessary for its application to tight permeability formations.

The recommended approach starts with the least square regression of cumulative production (Q (t)) versus time (t) by means of the mathematical expression:

$$Q(t) = \frac{Kt^n}{a+t^n} \qquad (2.12)$$

where,

K = Carrying capacity (maximum physically recoverable oil) (stb)

a = Constant of t^n when half the oil has been recovered, (day), and

n= Exponential parameter (hyperbolic exponent) (Clark, 2011).

Subsequently, the corresponding equation for production rate (q) versus time (t) is given as

$$q(t) = n\left(\frac{K}{a}\right)^{\frac{1}{n}} Q^{1-\left(\frac{1}{n}\right)} \left(1 - \frac{Q}{K}\right)^{1+\left(\frac{1}{n}\right)} \qquad (2.13)$$

2.2.4 Duong's Method

Duong's method addresses the fracture-dominated flow in shale reservoirs due to the lack of matrix permeability. Traditional decline curve analysis (DCA) is based on a drainage area with relatively good matrix permeability, which subsequently establishes pseudo-radial and boundary-dominated flows (BDF). However, in a shale reservoir, the drainage zone consists primarily of natural fractures and the stimulated reservoir volume (SRV); thus, it is a fracture-dominated flow reservoir and no BDF is established due to nano-Darcy matrix permeability. Duong (2011) stated that with negligible matrix contribution compared to that of fluid flow in fractures, the determination of EUR based on the traditional concept of drainage area is inaccurate.

Duong (2011) outlines the detailed procedure for evaluating and forecasting cumulative production using his model. It involves two diagnostic plots by means of the empirical equations below (**Equations 2.14 and 2.15)**.

$$\frac{q}{N_p} = at^{-m} \qquad (2.14)$$

where,

a = Intercept constant, day^{-1}

N_p = Cumulative oil production, STB

m = Slope (which must be greater than unity for unconventional tight formations)

q = Oil rate, stb/day

t = Production time, days

A log-log plot of the above relation (q/Np vs. t) gives a straight line with a negative slope, -m, and an intercept, a, which are two of the four unknown parameters in Duong's decline curve analysis method. Note that the slope is negative, but m is always a positive value. The value of m must be greater than one (1) to indicate unconventional tight reservoirs.

Another unknown parameter q_1- oil rate at Day 1- is determined using the relationship (Duong 2011):

$$q = q_1 t(a, m) \qquad (2.15)$$

$$q = q_1 t(a, m) + q_\infty \qquad (2.16)$$

$$\text{Note: } t(a, m) = t^{-m} e^{\left(\frac{a}{1-m}\left(t^{1-m}-1\right)\right)} \qquad (2.17)$$

where,

q_1 = Oil rate at Day 1

q_∞ = Oil rate at infinite time

t = Production time, days

$t_{(a, m)}$ = Time function based on **Equation 2.17**

If the resulting linear plot for any production profile using **Equation 2.15** fails to pass through the origin, Duong (2010) proposed the use of **Equation 2.16**. The modification term q_∞, defined as the production rate at infinite time, is an anomaly related to wellbore operating conditions (Duong 2010). The two diagnostic plots are used to determine variables a (Intercept constant, day^{-1}), m (Slope of q/Np versus t), q_1 (Oil rate at Day 1), and q_∞ (Oil rate at infinite time).

Rate-time and cumulative production-time relationships to estimate forecast at abandonment are given as (Duong 2011):

$$\frac{q}{q_1} = t^{-m} e^{\left(\frac{a}{1-m}\left(t^{1-m}-1\right)\right)} \qquad (2.18)$$

$$N_p = \frac{q_1}{a} e^{\left(\frac{a}{1-m}\left(t^{1-m}-1\right)\right)} \qquad (2.19)$$

2.3 Analyses of the Eagle Ford Shale

2.3.1 Reservoir Fluids

The Eagle Ford Shale reservoir has dry gas, wet gas, and liquid hydrocarbon depending upon the depth and temperature of the reservoir. The maturity windows corresponding to the liquid, wet gas and dry gas zones across the entire formation are shown in colors of green, orange, and red,

respectively, in **Figure 2.2**. The phases' distribution in the Eagle Ford source rock reservoir is not gravity segregated as associated with traditional reservoirs due to the different maturity windows for in-situ, self-sourcing shale reservoir hydrocarbon phases. The oil-rich zone is in shallower depths than the less dense gas strata in the Eagle Ford Shale instead of the conventional gas cap and underlying liquid in multi-phase reservoirs. Thus, in a multi-phase conventional reservoir; gravity controls the segregation of the fluids. On the other hand, tight permeability shale reservoir multi-phases are zoned according to hydrocarbon maturity windows depending on reservoir depth and temperature. The liquid-rich, wet gas, and dry gas regions occur at estimated depths of 8000 ft, 10000 ft, and 14000 ft, respectively (Chaudhary et al., 2011).

2.3.2 Natural Fractures

Cores from the Eagle Ford Shale indicate the presence of mineralized vertical natural fractures (Orangi et al., 2011). Orangi et al. (2011) also confirmed the presence of micro fractures. Micro-fracturing of rock formations occurs naturally by liquid pore pressure (Berg and Gangi, 1999). Also, increasing pore pressure typically associated with the conversion of high density kerogen to light hydrocarbon fluids creates natural fractures in source reservoir rocks (Berg and Gangi, 1999). In this model, natural fractures are due to the differential pore volume resulting from kerogen conversion into crude.

The brittle and calcareous zones of the Eagle Ford Shale are easily fractured and could result in localized sweet spots. These oil-saturated natural fractures extend between 10 ft and 30 ft within brittle, carbonate rich (dolomitic shale) inter-bedded shale layers rich in calcite, chert, and silt (Fertl and Rieke III, 1980). Brittle, naturally fractured zones within the organic-rich source rock

are targets for optimal well placement, hydraulic fracture staging, and completion designs (Fertl and Rieke III, 1980).

According to Stegent et al. (2010), outcrop- scale natural fractures are rare in the calcareous portion of the Eagle Ford Shale. He pointed out evidence of dense micro-fractures, as shown in **Figure 2.4**.

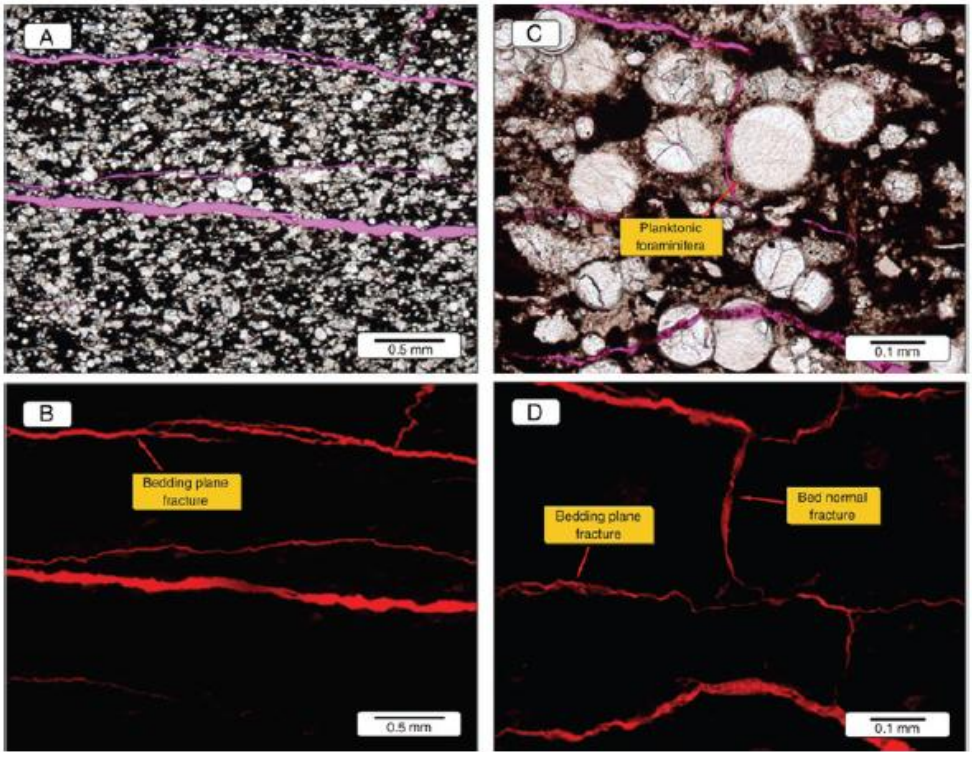

Figure 2.4: Micro-fractures in Eagle Ford Shale cores (Stegent et al., 2010).

2.3.3 Reservoir Stimulation and Wellbore Completions

Shale reservoirs are economically viable as a result of technological advancements in petroleum engineering tools and methodologies. These advanced technologies include horizontal wellbore drilling with multistage and transverse hydraulic fracturing (Wei and Economides, 2005; Mullen, 2010). Drilling horizontal wellbores along the direction of the least principal in-situ stress ensures propagation of transverse fractures (Nwabuoku, 2011).

Hydraulic fracturing increases reservoir contact with the horizontal wellbores, decreases wells' drawdown, and ultimately increases conductivity to wellbores (Medeiros et al., 2008). Near wellbore stimulation by multiple transverse fractures effectively creates reservoir contacts for ultra-low permeability reservoirs with horizontal wellbores (Vincent, 2011). The ultra-low permeability Eagle Ford Shale reservoirs, therefore, require horizontal wellbores stimulated with optimal hydraulic fracturing techniques (Medeiros et al., 2007).

Stegent et al. (2010) concluded that successful hydraulic fracture treatment and strategic wellbore completions of the Eagle Ford Shale reservoir required a thorough understanding of its petrophysical properties. Comprehensive petrophysical analysis and reservoir quality assessment may involve gathering the following information:

1. Geochemical data to assess hydrocarbon maturity and kerogen types
2. Shale or gamma ray logs to calculate TOC, kerogen, free gas volume, formation shaliness and brittleness
3. Electric logs and resistivity logs for fluid saturation determination
4. Sonic logs to assess stress orientations, Poisson's ratio, and Young Modulus, and

5. Borehole images and dipmeter logs to identify structures and sedimentary features and their orientations (Mullen, 2010 and Stegent et al., 2010).

The Eagle Ford Shale consists of 38-88% clay, with ~ 50% of that clay being smectite, a clay mineral susceptible to swelling. As a result, potential clay swelling during development is a considerable challenge (Hsu and Nelson, 2002).

As of late 2008, horizontal wells of the Eagle Ford Shale reservoir typically had 12-20 hydraulic fractures in multiple stages along the lateral leg (Martin et al., 2011). Review of some of the earlier horizontal wells drilled within the Eagle Ford Shale had as many as 4 clusters per 14-16 stages. Hydraulic fracture stages have been spaced at equal intervals of about 250 ft over a lateral length of about 4000 ft (Nwabuoku, 2011).

Optimal placement of hydraulic fractures needs to be based on shale log data which can be used to identify the brittle and TOC rich zones. This may result in uneven hydraulic fracture intervals, contrary to the common approach of equal spacing of hydraulic fracture stages (Mendoza at al., 2011). Evaluation of optimal fracture staging and perforation clusters per stage is essential for effective shale reservoir drainage; too closely spaced fractures can lead to undesired fracture geometry and less productive Stimulated Reservoir Volume (SRV), while largely spaced fracture stages will generate fractures with less reservoir contact (Nwabuoku, 2011). Closely spaced adjacent transverse fractures may create zones of attraction that can cause interference between successive fracture stages through stress shadowing (Roussel et al., 2012). Stress shadowing can result in disruption of transverse fracture patterns, re-stimulation of previously generated transverse fractures, and failure to initiate new fractures (Roussel et al., 2012). Roussel et al.

(2012) observed that fracture spacing greater than 200-300 ft propagates fractures perpendicular to the lateral in brittle zones. Ductile regions along the wells' trajectories, however, can accommodate closely spaced fracture stages with only a small amount of proppant and smaller fracture widths (Roussel et al., 2012).

The effective drainage area in most tight permeability reservoirs is confined, usually to a rectangular region containing systemic complex fractures. This drainage area consists of both natural fractures, if present, and the SRV generated by hydraulic fracturing of the reservoir unit (Medeiros et al., 2008).

Perkins and Kern (1961) observed that competent reservoir rocks with high brittleness (or with low ductile characteristics) respond in elastic fashion to applied pressure. As a result, the dimensions (width and length) of fractures propagated in hydraulic fracture operations depend on the intensity of applied pressure (fracturing fluid injection rate) and the fluid's viscosity.

Hydraulic fractures at depths of producing intervals in the Eagle Ford Shale propagate perpendicularly to minimum horizontal stresses, resulting in mostly vertical fractures (Wei and Economides, 2005). Consequently, horizontal wells' orientations are key considerations for drilling, stimulation, and completion designs, in order to create the most efficient network of transverse fractures (Wei and Economides, 2005).

2.3.4 Simulation

This section reviews the simulation parameters used to characterize reservoir models of the Eagle Ford Shale play. **Table 2.1** shows the different ranges of porosity and absolute permeability values that different authors incorporated in previous reservoir simulations models. The different values correspond to different parts of the Eagle Ford Shale.

Table 2.1: Porosity and permeability values used in Eagle Ford Shale simulation models

Porosity (%)	**Absolute Matrix Permeability (Nano-Darcy)**	**Hydrocarbon zone/Sources referenced**
5.0-14.0	40-1300	Oil/Wang and Liu, 2011
3.0-10.0	3-405	Oil and Gas/Martin et al., 2011
3.4-14.6	10	Gas/Vassilellis, et al., 2010
9.0-12.0	420	Oil and Gas/Mendoza et al., 2011
8.0-18.0	20-1200	Oil and Gas/Stegent and Ingram, 2011 and Mullen, 2010
6.0	100	Oil/Chaudhary et al., 2011
9.0	25-500	Oil/Orangi et al., 2011

Wang and Liu (2011) conducted a sensitivity analysis of the following reservoir and wellbore parameters with respect to the wells' performance: natural fracture permeability, reservoir-pay volume (pay thickness and matrix porosity), natural fracture spacing, stimulated reservoir volume (SRV) half-length, SRV enhanced permeability, and matrix permeability. They concluded that well performance was least sensitive to matrix permeability and most sensitive to natural fracture permeability.

The Eagle Ford Shale also has variable pressure regimes and is over-pressured in some places (Mullen, 2010). **Table 2.2** shows some of the reported pressure gradients from the Eagle Ford Shale.

Table 2.2: Eagle Ford pressure gradients

Pressure gradient (psi/ft)	**Sources referenced**
0.62	Wang and Liu, 2011
0.43-0.65	Vassilellis, et al., 2010
0.55-0.85	Chaudhary et al., 2011

Table 2.3 contains reservoir temperatures, water saturation and rock compressibility parameters found in the literature.

Table 2.3: Eagle Ford Shale parameters previously used in simulation

Temperature (^{o}F)	**Water Saturation (%)**	**Rock compressibility (10^{-6} psi^{-1})**	**Hydrocarbon zone/ Sources referenced**
315			Oil and Gas/ Mendoza et al., 2011
	7-31		Oil and Gas/ Stegent and Ingram, 2011 and Mullen, 2010
150-350	30	5	Oil/Chaudhary et al., 2011
273		20-100	Oil/Orangi et al., 2011

The natural fracture distribution in the Eagle Ford Shale is particularly complex and difficult to represent in simulation grid models (Wang and Liu, 2011). Wang and Liu's (2012) simulation

model used a composite fracture width of 0.001 ft, incorporating natural, re-activated and hydraulic fractures.

Waters et al. (2009) pointed out that the pressure drop within a low permeability shale reservoir is extremely small due to the nano-Darcy scale of the matrix permeability. The greatest decline occurs near wellbores and fracture zones. Depending on fracture density, shale reservoirs may only deplete to about 50% of initial pressure in 60 years, or show minimal pressure depletion in after 10 years of production (Waters et al., 2009).

Hydrocarbon fluid flow in horizontal wellbores in fractured media in ultra-low permeability formations goes through a long transient flow regime (Medeiros et al., 2008). The transient decline may last the entire productive life of the hydraulically fractured horizontal wellbore (Medeiros et al. 2007). Adequate representation of the transient flow regime in simulation models of shale reservoirs requires logarithmic, locally-refined grid sizes. This provision captures the impact of high pressure depletion and saturation changes near the matrix-fracture boundary and the horizontal wellbore fracture interface (Rubin, 2010).

Orangi et al. (2011) provided synthetic Eagle Ford crude oil data generated and recombined from typical stock tank oil and separator compositions. The Eagle Ford Shale synthetic crude's properties and compositions are shown in **Table 2.4** (Orangi et al., 2011). The synthetic crude compositional model was developed based on the Peng-Robinson equation of state (EOS) (Orangi et al. 2011).

Table 2.4: Equation of State parameters and Compositions of a Synthetic Eagle Ford Shale Oil (Orangi et al., 2011)

Fluid	GOR (scf/stb)	API	Gas density (lb/ft^3)	Gas gravity	Initial pressure (psi)	Temperature (^oF)	Saturation pressure (psi)	Boi (RB/STB)	Viscosity (cp)
Oil	500	41	0.06906	0.905	6300	237	2053	1.3534	0.58

Component	Pc (psia)	Tc (^oF)	Acentric Factor	Molecular Weight	Specific Gravity	Composition (mole fraction)
N2	492.3	-232.3	0.04	28.01	0.808	0.00073
CO2	1071.3	88.4	0.225	44.01	0.8159	0.01282
C1	673.1	-116.1	0.013	16.04	0.35	0.31231
C2	708.4	90.6	0.0986	30.07	0.48	0.04314
C3	617.4	206.7	0.1524	44.1	0.5077	0.04148
IC4	529.1	275.5	0.1848	58.12	0.5631	0.0135
NC4	550.7	306.3	0.201	58.12	0.5844	0.03382
IC5	483.5	369.7	0.2223	72.15	0.6248	0.01805
NC5	489.5	386.6	0.2539	72.15	0.6312	0.02141
NC6	439.7	455.3	0.3007	86.18	0.6641	0.04623
C7+	402.8	601.7	0.3739	114.4	0.7563	0.16297
C11+	307.7	764.9	0.526	166.6	0.8135	0.12004
C15+	241.4	909.8	0.6979	230.1	0.8526	0.10044
C20+	151.1	1155.8	1.0456	409.2	0.9022	0.07306

Orangi et al. (2011) again provided a pressure-volume-temperature (PVT) plot for the synthetic crude of the Eagle Ford Shale (EFS) (**Figure 2.5)**. It is not known whether the plot of formation volume factor (FVF) versus pressure was generated by correlation or by simulation.

Pressure (psi)	Oil FVF (rb/stb)
6000	1.3534
3500	1.358
3000	1.365
2500	1.372
2000	1.38
1800	1.355
1600	1.335
1400	1.31
1200	1.29
1000	1.26
750	1.23
500	1.2
250	1.16
14.7	1.05

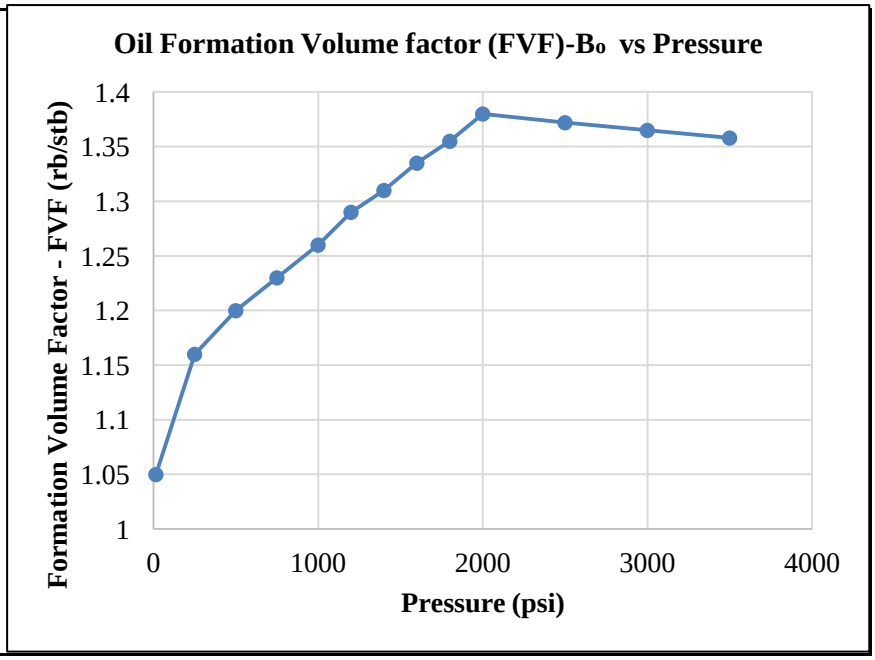

Figure 2.1: Pressure versus FVF at reservoir temperature of EFS. The table and corresponding graph in this figure were approximated from the pressure-FVF curve provided by Orangi et al. (2011).

2.4 Improving Shale Oil Recovery by CO_2 Injection and CO_2 as Frac Fluid

The oil recovery factor for the Eagle Ford Shale play during primary drive reservoir depletion is roughly 5% (Hart, 2011). However, improvements in fracking technology such as repeated fracturing of wells, longer laterals, closely spaced wells, and miscible displacement using CO_2 solvents can lead to enhanced shale oil recovery (Hart, 2011).

Liquid CO_2 has minimal near-wellbore effects. It is non-damaging to fractures, generating clean fractures when used as hydraulic fracturing fluid, either as an additive or a sole proppant-laden frac fluid (Lillies and King, 1982). Sinal and Lancaster (1987) stated that the main purpose of CO_2 in stimulation "frac jobs" is the ability to produce cleaner hydraulic fractures that eliminate

formation damage such as near-wellbore relative permeability reduction, especially in tight and low pressure formations.

Eagle Ford Shale play development can benefit from using liquid CO_2 with proppants in hydraulic fracturing in a number of ways. CO_2 as a hydro-fracturing fluid can reduce or eliminate effects of clay swelling (Gupta and Bobier, 1998; Hsu and Nelson, 2002 and Stegent and Ingram, 2011). Furthermore, CO_2 enhances the sand-propped integrity of fractures and reduces fracture closure caused by reservoir pressure depletion, because CO_2 flow-back to the wellbore is not dependent on reservoir pressure (Lillies and King, 1982). Using CO_2 also eliminates water flow-back, a characteristic of conventional fracturing fluids.

The main drawback in CO_2 hydraulic fracturing is that of its phase behavior-- it must remain a liquid phase to ensure stimulation "fracking" of the formation to the desired fracture geometry. Unlike the conventional high viscosity fracturing fluids, CO_2 lacks the ability to transport proppants well into the fractures before vaporizing (Lillies and King, 1982; Settari et al., 1986 and Sinal and Lancaster, 1987). Unless viscosifying agents are incorporated, 100% liquid CO_2 fracking generates less stimulated volume and low conductivity fractures. Because of this, its usefulness in tight oil reservoirs may be limited (Settari at al., 1986 and Sinal and Lancaster 1987).

However, CO_2 also enhances oil recovery in tight permeability formations because of its high injectivity (Lillies and King, 1982). CO_2 typically attains miscibility at most reservoir pressures and temperatures (Lillies and King, 1982).

Holm, (1986) explained miscibility in reservoirs to mean the formation of a homogeneous, single phase fluid without any interfaces (**Figure 2.6**) when two or more reservoir fluids and injected fluid combine at a certain physical condition. The presence of two or more phases creates separation of the interfaces, resulting in high interfacial tension. Both first-contact and multi-contact miscible displacement eliminate interfacial tension between the oil and the injected fluid, which removes or lowers residual oil saturation (Holm, 1986).

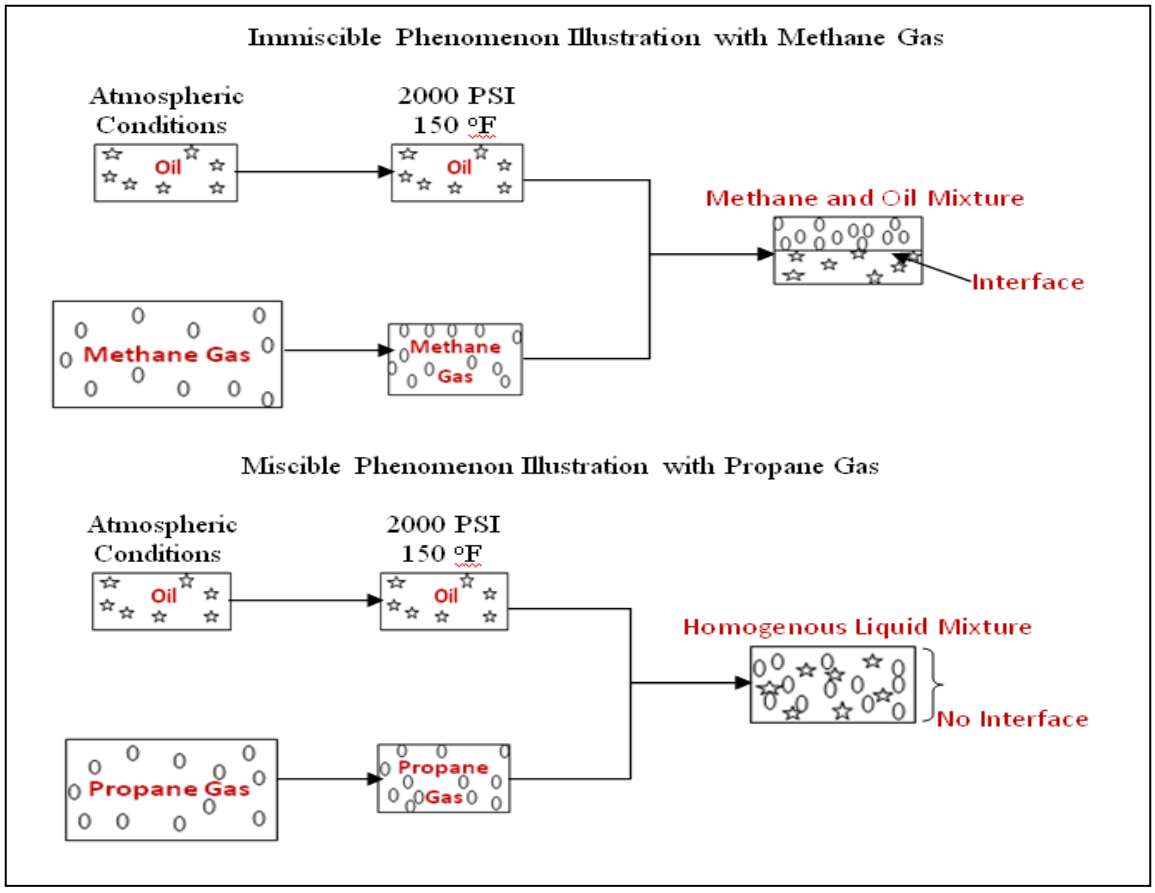

Figure 2.2: Illustration of miscible and immiscible (Holm, 1986).

CO_2 flooding enhances light and medium crude oil recovery from tight reservoir units such as shale plays due to its favorable phase behavior such as CO_2 solubility and development of multi-contact miscibility of CO_2-oil systems depending on reservoir parameters (Gui et al. 2008).

Extraction of intermediate hydrocarbon components by CO_2 initiates miscibility between CO_2 and the in-situ oil; the enriched CO_2 dissolution as more reservoir oil is contacted leads to miscible or near miscible displacement of the crude by the CO_2 (Malik and Islam, 2000).

CO_2 flooding displaces oil from reservoirs by vaporizing and/or condensing gas drive. This phenomenon is multi–contact miscible displacement, where CO_2 eventually becomes miscible with oil in the reservoir after it sufficiently vaporizes intermediate hydrocarbons. Miscibility develops when injected gas and reservoir fluid come into contact above threshold minimum miscibility pressure (MMP) (Holm, 1986 and Rahmatabadi, 2011). MMP is a function of reservoir conditions (i.e. temperature) and injection gas and oil compositions.

CO_2 flooding can be a miscible or near-miscible process (Gui et al., 2008; Bui, 2010 and Rahmatabadi, 2011). If injected gas and reservoir oil mix to produce a single phase fluid in the reservoir, then the gas is said to have a first contact miscible (FCM) displacement of the reservoir oil (Rahmatabadi, 2011). On the other hand, multiple contact miscible (MCM) displacement takes place when miscibility develops through mass transfer of the gas; i.e., CO_2 seeps through the reservoir to contact fresh oil (Rahmatabadi, 2011).

However, MMP is often impractical to reach, since the depth of many hydrocarbon reservoirs may be relatively shallow and characterized by lower pressures relative to the threshold for dynamic mixing of CO_2 and crude oil in the reservoir (Bui, 2010). In these cases, CO_2 causes

viscosity reduction and swelling of the reservoir oil by near-miscible displacement process due to phase behavior changes when CO_2-oil systems form in the reservoir.

Malik and Islam (2000) and Nielson (1989) mentioned that CO_2 and reservoir oil are not first contact miscible; however, the CO_2 creates a miscible front for the vaporized hydrocarbon components. Miscibility occurs dynamically beyond the minimum miscibility pressures between 1500 and 6000 psia (Nielson, 1989). At these pressures, the density of the CO_2 increases sufficiently for solubility with the oil hydrocarbon components (Nielson, 1989). Dynamic miscibility is achievable in crude oil with at least 25^o API gravity (Malik and Islam, 2000 and Nielson, 1989).

Depending on the reservoir oil composition, dissolution of CO_2 in crude oil during miscible displacement can cause problems with asphaltene precipitation in the reservoir (Ghoodjani and Bolouri, 2012 and Nielson, 1989). As a result, plugging and clogging in reservoirs by asphaltene deposition may lead to permeability impairment (Ghoodjani and Bolouri, 2012).

Successful enhanced oil recovery by gas injection partly depends on the reservoir wettability. Organic-rich shales deposited in swamps, lakes, and marine environments are primarily water-wet. When petroleum diagenesis progresses, the wettability converts to strongly oil-wet and weakly water-wet as a result of the mineralogy and organic content (Odusina et al., 2011). This was supported by a Nuclear Magnetic Resonance (NMR) study which found that organic-rich shale formations are mainly oil-wet (Odusina et al., 2011).

CO_2 high injectivity into tight reservoirs makes the choice of CO_2 injection for enhanced oil recovery effective compared to secondary recovery scheme such as water flooding (Holm, 1986). Also, CO_2 injection is preferred to Nitrogen (N_2) and hydrocarbon gas injection because of CO_2's greater relative ability to reduce rock-fluid interfacial tension and oil viscosity (Ghoodjani and Bolouri, 2011; Ghoodjani and Bolouri, 2012).

Pure CO_2, though expensive, has a viscosity and density closer to that of crude oil than natural gas does (Holm, 1986). This is one of CO_2's advantages over methane in gas injection enhanced oil recoveries. Also, CO_2 attains minimum miscibility pressure at lower reservoir pressures and can be used in shallower reservoirs than natural gas can (Holm, 1986).

Another matter to consider is that CO_2 gas viscosity is low compared to oil, which makes CO_2 extremely mobile. Consequently, early breakthrough and bypassing of oil may occur, especially in shale reservoirs with high induced conductivity (Gui et al., 2008).

The optimum CO_2 injection rate depends on the price of oil, original oil in place (OOIP), span of injection (short or long term), oil viscosity, reservoir size, and reservoir heterogeneity (Ghoodjani and Bolouri, 2012). To avoid CO_2 leaking, especially in the case of both EOR and geologic sequestration, injection pressure should not exceed the reservoir fracturing pressure (Ghoodjani and Bolouri, 2012). However, relatively high OOIP, high oil prices, and short term application may require high CO_2 injection rates in order to maximize oil recovery (Ghoodjani and Bolouri, 2012).

Typical successful examples of using CO_2 in tight permeability reservoirs to enhance oil recovery include:

1. The Saskatchewan ultra-low permeability limestone and dolomitic shale member had a predicted 3.64% OOIP recovery factor over 100 years of primary recovery (Wang et al., 2010). However, enhanced oil recovery during CO_2 flooding increased the predicted recovery factor to over 34%; and
2. Oil production from Elm Coulee Field in Montana from the Bakken Formation of the Williston Basin had a 5-10% primary recovery factor. CO_2 flooding increased oil recovery factor for the 8-12 ft thick upper shale and the underlying sandy dolomitic layer by 20% of the OOIP (Shoaib and Hoffman, 2009).

Chapter 3 Eagle Ford Production History Assessment Using Various Decline Curve Analysis Techniques

3.0 Introduction

This chapter discusses the methods and results of different decline curve analysis techniques the author has used to analyze past production profiles of forty horizontal wells in the Eagle Ford. These techniques include Arps' decline analyses relations, power-law exponential (PLE) analysis, logistic growth analysis (LGA), Duong method and, finally, my own proposed method, Logistic Arps' Hyperbolic Approach (LAHA). The analyses cover production profiles of oil-producing horizontal wellbores selected from eight different counties in the Eagle Ford Shale play. The selection of the counties is based on their locations in the oil window of thermal maturity, proximity to one another, extension across most of the oil-prone zones and, finally, publicly available field development and production data from the Texas Rail Road Commission (TRRC) website. Counties include Leon, Brazos, Burleson, Lee, Gonzales, Karnes, Dimmit and Zavala Counties (**Figure 2.2**).

The objectives of my analyses are to assess the ability of the different decline analysis methods to match the wells' past production rates and cumulative production, and generate the future production trends. The minimum abandonment rate used was 2 STB/day, since many of the wells are currently operating close to this rate. Most of these wells have short production histories, which imply decline trends may not have been well established by the wellbores or the reservoirs at the time of the analyses. The production profiles of wells made publicly available by TRRC varied from 9-50 months between 2008 and January 2013. Despite this limitation, the importance of generating early future production forecasts for the shale reservoirs cannot be overemphasized.

The results are categorized into two segments. The general results are observations regarding the respective effectiveness of the different decline curve analysis techniques. The county-well specific results are considered case studies for the individual counties and wells, and are discussed separately in **Chapter 4**. For detailed results, refer to **Appendix 1** and **2.**

3.1 Methods

3.1.1 Data Preparation before the Analysis

At the start of every analysis, I examined the original data set and plotted the production rates against time. This made possible the identification of reasonable decline trends established by the well's performance data. Data points that did not follow a relatively smooth decline trend were eliminated and not incorporated in the analysis. Not all the profiles have observable sections of relatively smooth decline to isolate for the analyses. Consequently, I could not define the decline paths for all of the forty production profiles, especially for cases where the data is extremely erratic.

3.1.2 Arps' Decline Models Applications

I applied the Arps' decline curve relations, namely exponential, harmonic, and hyperbolic, to analyze the forty production profiles of the Eagle Ford Shale.

Arps' exponential or harmonic declines involve using past production data to generate decline diagnostic plots: rate versus time, cumulative production and the semilog rate versus time, or cumulative production with the constraint of least square regression $R^2 \geq 0.95$. I generated similar diagnostic plots for all forty profiles, which I interpreted for either exponential or harmonic

decline. Using the decline parameters obtainable from the equation of the trendline, I proceeded to calculate expected ultimate recovery (EUR) and future production.

The Arps' hyperbolic decline relation applications involved the use of Microsoft Office's Excel multivariable solver tool to determine the decline rate (D_i), initial production rate (q_i) and the decline exponent (b) using model **Equation 2.7**.

$$q = qi(1 + bD_i t)^{-\frac{1}{b}} \qquad (2.7)$$

With these parameters (D_i, q_i, and b) established for the best fits for each of the production declines, I plotted the production rate against time resulting from Arps' hyperbolic model. I also calculated the expected ultimate recoveries, the remaining recoverable reserves, and time to reach abandonment for all the forty oil-producing wellbores using **Equation 2.8**.

$$N_p = \frac{q_i b}{(1-b)D_i}(q_i^{1-b} - q^{1-b}) \qquad (2.8)$$

3.1.3 Power Law Exponential (PLE) Analysis Application

I evaluated the forty production profiles from Eagle Ford Shale oil wells according to the power law exponential decline model. First, I applied **Equation 2.11** using the solver tool in Microsoft Excel to determine values for $\hat{q}_i$ (rate intercept at time t=0, stb/d), D_∞ (decline constant at infinite time($t = \infty, \text{time}^{-1}$)), $\widehat{D}_i$ (decline constant ($\widehat{D}_i = D_1/n$),time^{-1}), and n (time exponent, dimensionless), such that the least square regression is maintained between the real and the PLE generated data.

$$q = \hat{q}_i\, e^{(-D_\infty t - \widehat{D}_i t^n)} \qquad (2.11)$$

Subsequently, diagnostic semi-log rate versus time was plotted to obtain the exponential decline rate ($\widehat{D}_i$) and the initial production rate ($\hat{q}_i$). I calculated the EUR, remaining reserve, and time to reach the abandonment rate of 2 barrels/day using exponential decline relations. This diagnostic plot must linearly fit a trendline of least square regression $R^2 \geq 0.97$ for optimal benefit in estimating expected ultimate recovery EUR and generating future production curves.

Alternatively, EUR at the well's abandonment rate can be evaluated from integral q with respect with time t. Substituting **Equation 2.11** into $\int_0^t q dt$ gives cumulative production (N_p) at abandonment:

$$N_p = \int_0^t \hat{q}_i \, e^{(-D_\infty t - \widehat{D}_i t^n)} \, dt = \hat{q}_i \int_0^t \frac{dt}{e^{(D_\infty t + \widehat{D}_i t^n)}}$$

The solution to the above integral is beyond the scope of this research and has, therefore, not been considered.

3.1.4 Logistic Growth Analysis (LGA) Application

To apply the logistic growth model, I used the least square regression method to determine K (the carrying capacity or maximum physically recoverable barrels of oil), a (the constant of time (t) to the nth (t^n) when half the oil has been recovered), and n (the exponential parameter or hyperbolic exponent equivalent), by means of **Equation 2.12**. I also generated the plots of cumulative production versus time to verify a close match between the actual and the model profiles for the forty production profiles in the Eagle Ford.

$$Q(t) = \frac{Kt^n}{a+t^n} \qquad (2.12)$$

With the values K, n, and a determined above, I calculated the model's production rate decline and generated profiles of rate versus time using **Equation 2.13**.

$$q(t) = n\left(\frac{K}{a}\right)^{\frac{1}{n}} Q^{1-\left(\frac{1}{n}\right)}\left(1-\frac{Q}{K}\right)^{1+\left(\frac{1}{n}\right)} \qquad (2.13)$$

Finally, I calculated the expected ultimate recoveries, the remaining recoverable reserves, and time to reach abandonment for the forty wells.

3.1.5 Duong's Decline Curve Analysis Method

For all the forty production profiles researched in the Eagle Ford, I generated two diagnostic plots to determine the initial variables a, m, q_1 and q_∞**,** where,

a = Intercept constant, day^{-1}

m = Slope (which must be greater than unity for unconventional tight formations)

q_i = Oil rate at Day 1 (stb)

q_∞ = Oil rate at infinite time (stb)

These diagnostic plots were obtained using the relationships expressed in **Equations 2.14, 2.15** and **2.16.** I plotted the ratios of production rate and cumulative production (q/Np) to time (t) to determine the slope (m) and the intercept (a), and also, the production rate against the time function t(a,m), defined by **Equation 2.17**. I model both **Equation 2.15** and **2.16** to investigate the effects of q_∞ (the production at infinite time), which, in practice, no reservoir will attain.

$$\frac{q}{N_p} = at^{-m} \quad (2.14)$$

$$q = q_1 t(a, m) \quad (2.15)$$

$$q = q_1 t(a, m) + q_\infty \quad (2.16)$$

$$t(a, m) = t^{-m} e^{\left(\frac{a}{1-m}\left(t^{1-m}-1\right)\right)} \quad (2.17)$$

where,

a = Intercept constant, day^{-1}

N_p = Cumulative oil production, STB

m = Slope (which must be greater than unity for unconventional tight formations)

q = Oil rate, stb/day

t = Production time, days

q_1 = Oil rate at Day 1

q_∞ = Oil rate at infinite time

$t_{(a, m)}$ = Time function based on **Equation 2.17**

3.1.6 Logistic Arps' Hyperbolic Approach (LAHA)

This section explains my version of the decline curve analysis technique. The motivation to investigate this is as a result of the critical observation that the logistic growth analysis technique has robustly fitted the past cumulative production and the production rates decline trends for all forty wells. The logistic Arps' hyperbolic approach (LAHA) seeks to maintain the benefits of the traditional Arps' hyperbolic relation, which include the good fit to the past production rates. In

addition, LAHA results are expressed in terms of conservative decline curve analysis parameters to which industry analysts and investors are accustomed.

After the analyses of all forty production profiles, I used the smoother reasonable decline trend generated from the logistic growth analysis (LGA) model as input for Arps' hyperbolic decline relation. By the least square regression method, I obtained new sets of traditional decline curve analysis parameters, namely the decline rate (D_i), the initial rate (q_i) and the decline exponent (b) for the new decline profile generated by LGA. Further, I match the resultant curve with the original data output by LGA and Arps' hyperbolic decline models. The expectation of my approach is to normalize the values of decline exponents b>1, which subsequently will leads to generating forecasts of realistic values similar to those of LGA. Therefore, I again calculated the EUR, remaining reserves, and abandonment time resulting from my approach.

3.2 General Results

3.2.1 Data Preparation before the Analysis

Figure 3.1 presents an example of the numerous cases where at least one offset data point was removed from the profile so that a reasonable decline trend could be achieved and analyzed. This profile (**Figure 3.1**) is of the production data of the Simms lease horizontal wellbore, and it shows some offset data at the beginning and towards the end on the rate versus time plot **(Figure 3.1 A)**. The semilog rate versus time plot of the same production profile in **Figure 3.1 B** also supports the need to eliminate the most erratic data points; the equation of the trendline, with the highest degree of least square regression, cannot be validated without reasonably excluding sections of the data.

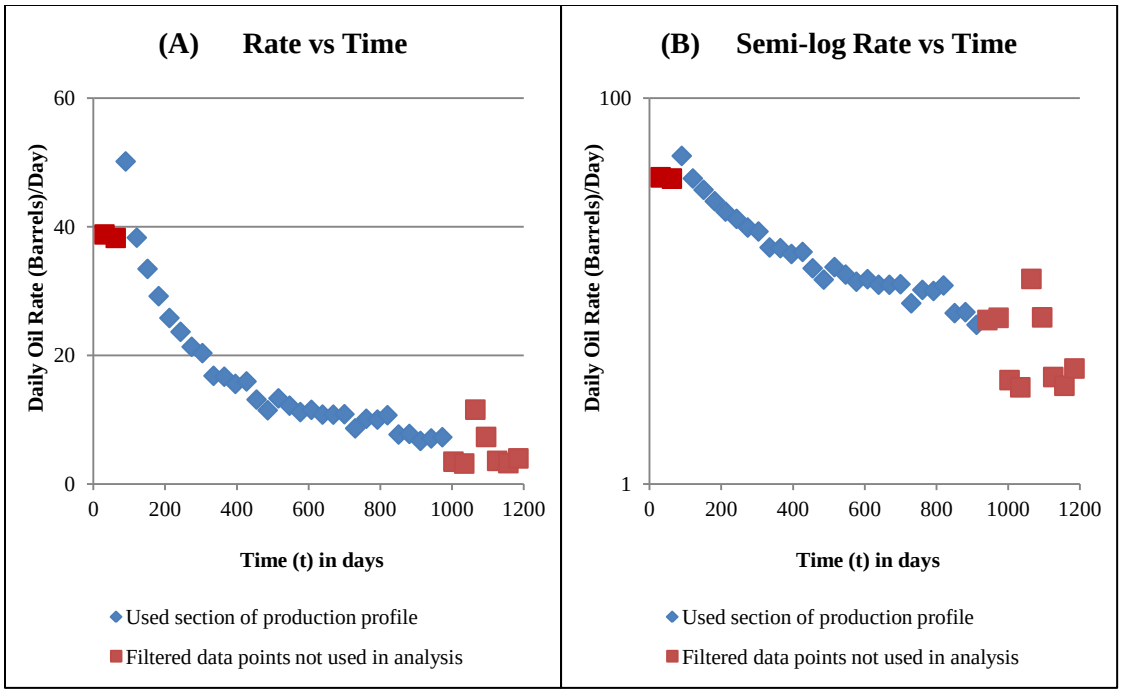

Figure 3.1 (A, B): Rate and semi-log rate versus time of the Simms lease #03914 production profile, in which the use of the blue marked trend is justified compared to the erratic (red marked) sections.

Some of the profiles are extremely erratic, making it difficult to make sense of declining production trends. Examples of these kinds of profiles are presented in **Figure 3.2 (A, B)**. The analyses these production profiles resulted, for example, in unusual parameter values such as the Arps' decline exponent associated with Arps' hyperbolic model **Figure 3.3 (A, B)**. Further examples are reported with respect to the specific techniques later in the text.

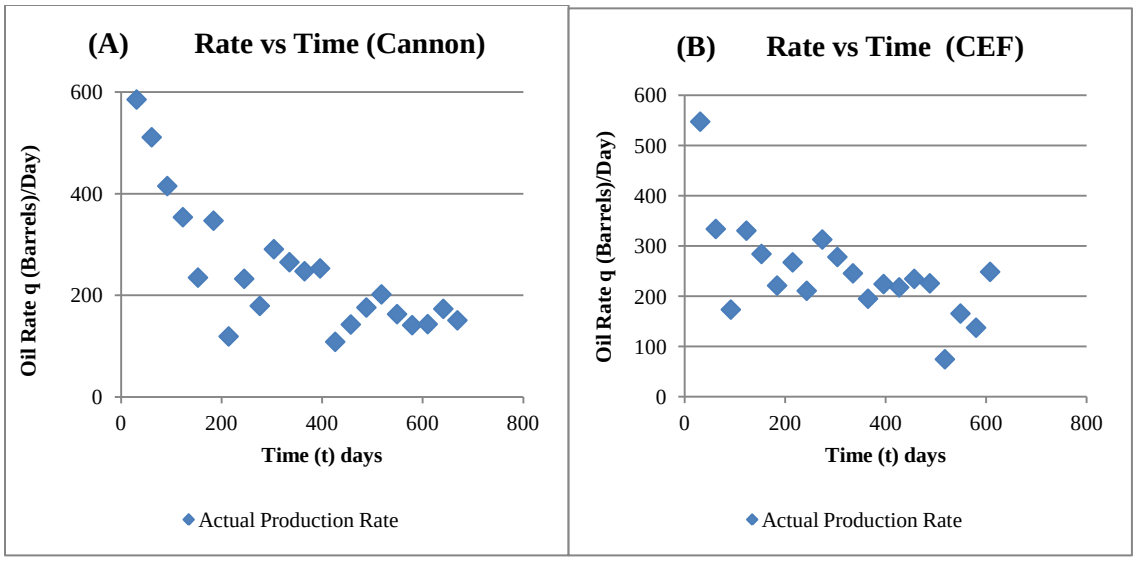

Figure 3.2 (A, B): Rate versus time plots for Cannon #09607 lease and CEF #09608, presented as examples for erratic production profiles.

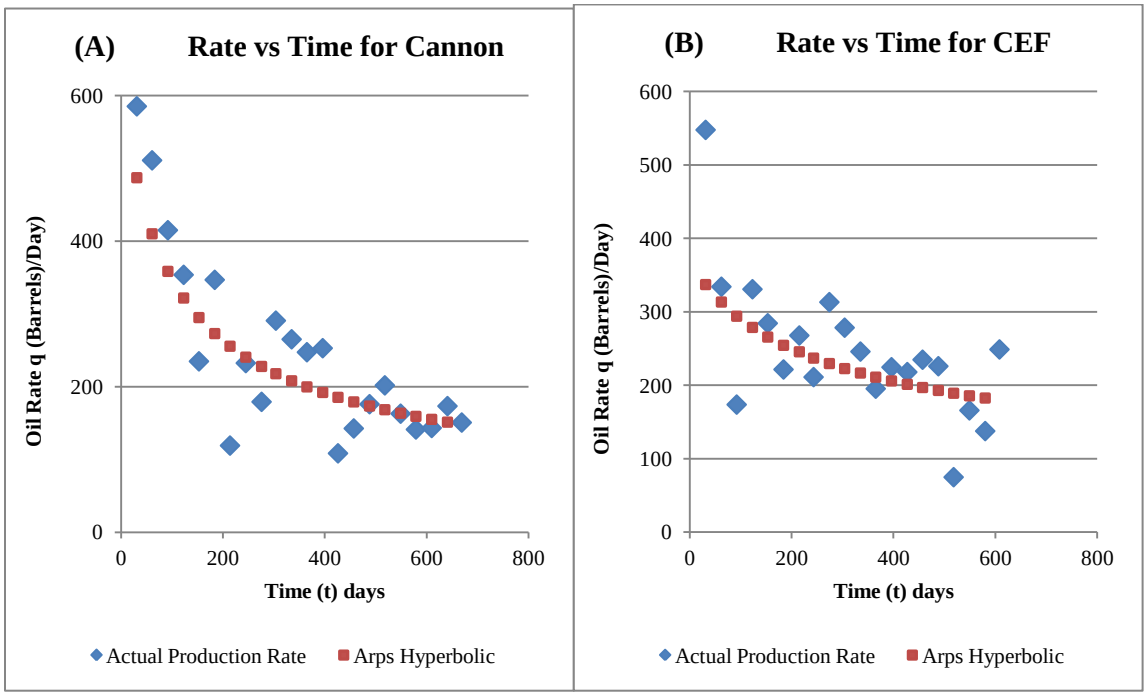

Figure 3.3 (A, B): (A) Arps' hyperbolic decline analysis for the erratic production profiles of the CEF #09608 and Cannon #09607 lease wellbores resulted in abnormally high Arps' decline exponent; i.e., b=3.05 for (A) and b=1.84 (B) respectively.

3.2.2 Arps' Decline Curve Analysis

Figure 3.4 shows four diagnostic plots I generated in order to verify Arps' exponential or harmonic decline for one of the production profiles in Burleson County (Giesenschlag W.H.C Unit). Similar kinds of diagnostic plots were created for each of the forty production profiles. **Figure 3.5** is also one example of the forty results obtained for Arps' decline curve analysis using the hyperbolic relation.

The pie chart (**Figure 3.6**) summarizes the relative extent to which the different types of Arps' decline curve analysis successfully modeled the forty production profiles of the Eagle Ford Shale oil reservoirs. Normalized 6.45% and 29.03% of the production profiles are observed to exhibit exponential and harmonic decline respectively. A higher percentage was observed for Arps' harmonic decline when a least square regression $R^2 \geq 0.85$ was imposed to classify Arps' exponential and harmonic decline. This is consistent with preliminary findings presented in Agboada and Ahmadi (2013). On the other hand, Arps' hyperbolic relation fitted the rate profiles of all forty past production profiles (**Figure 3.7**). Thus, the Arps' hyperbolic model closely fits the production rates well but the corresponding cumulative production is not very close to the actual history cumulative production. Relative to Arps' exponential and harmonic decline models, the Arps' hyperbolic relation had 20.97% normal decline exponents such as $0<b<1$, and 43.55% abnormal decline exponent $b>1$(**Figure 3.6**).

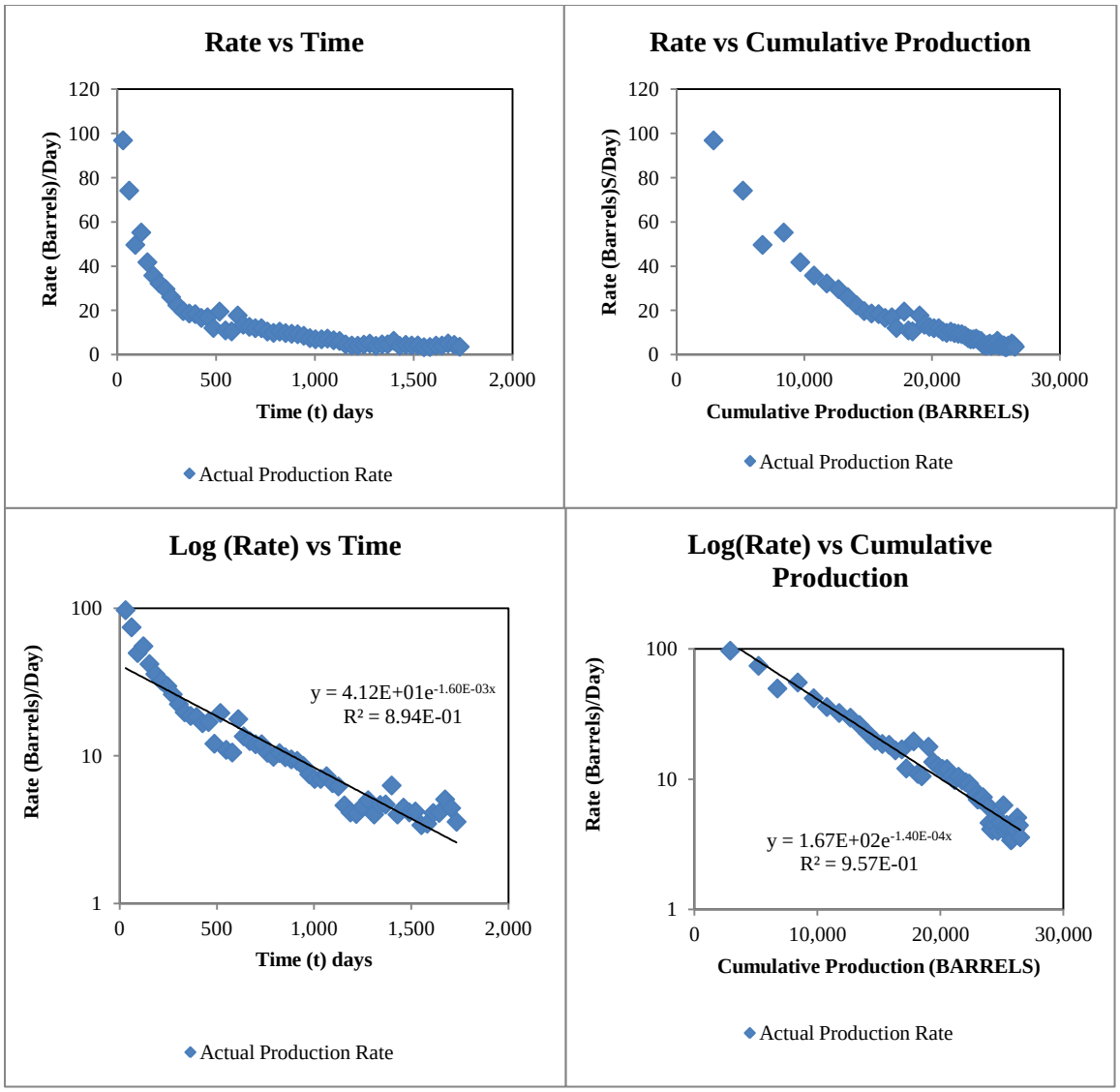

Figure 3.4: Four diagnostic plots used to determine Arps' exponential or harmonic decline.

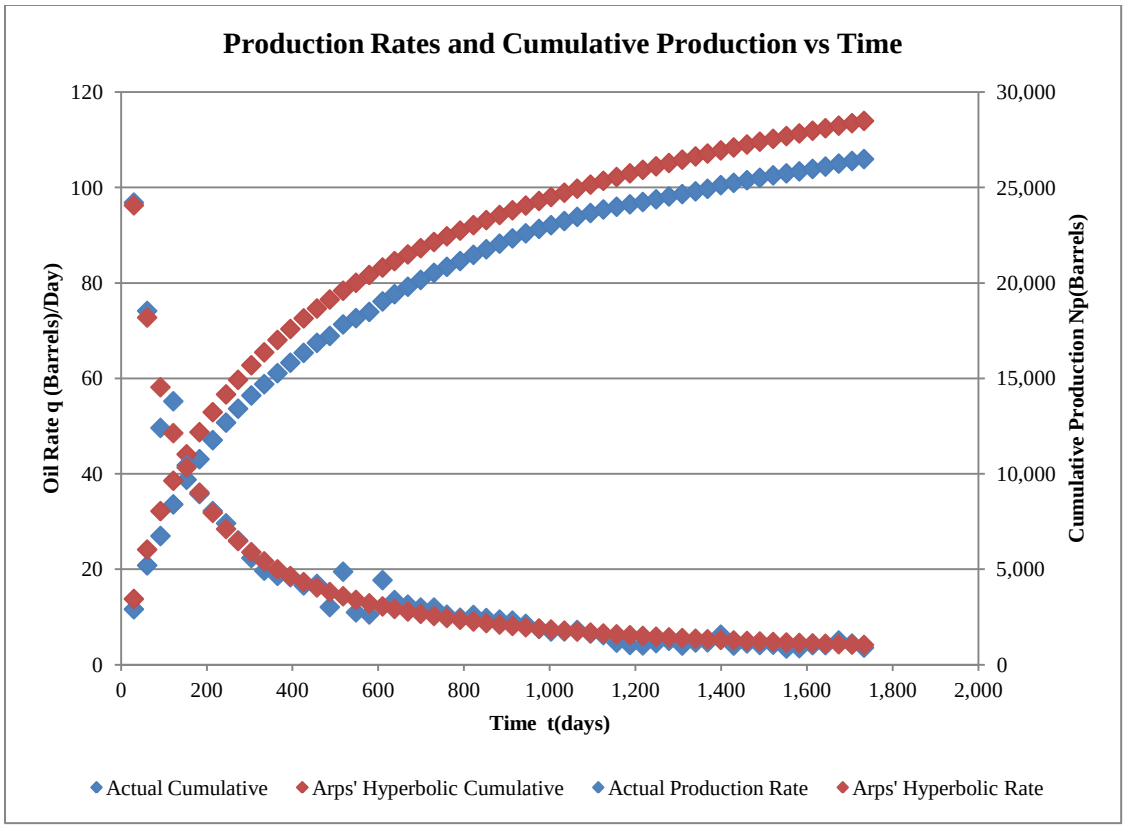

Figure 3.5: Arps' hyperbolic analysis showing cumulative production and rate match between the actual and the modeled data.

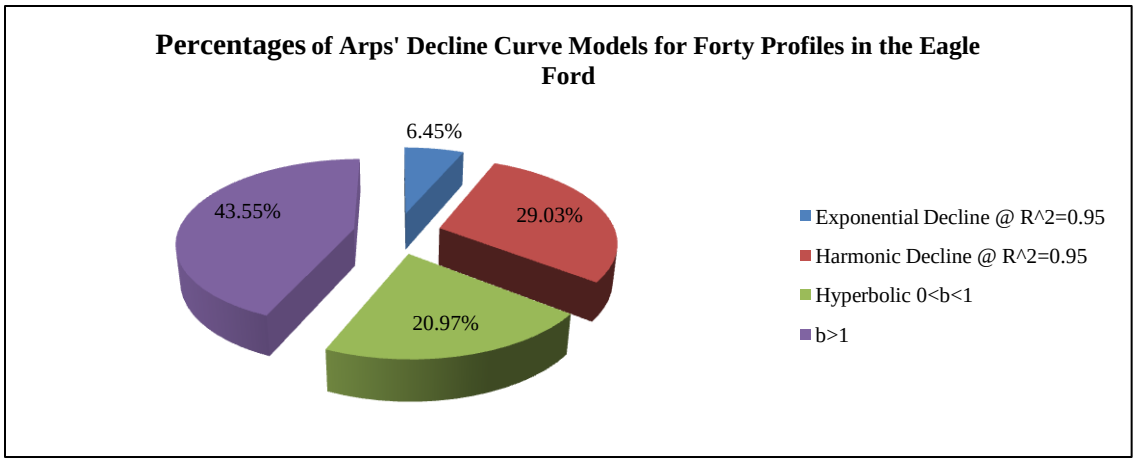

Figure 3.6: Percentage application of Arps' decline curve analyses for Forty Profiles in the Eagle Ford.

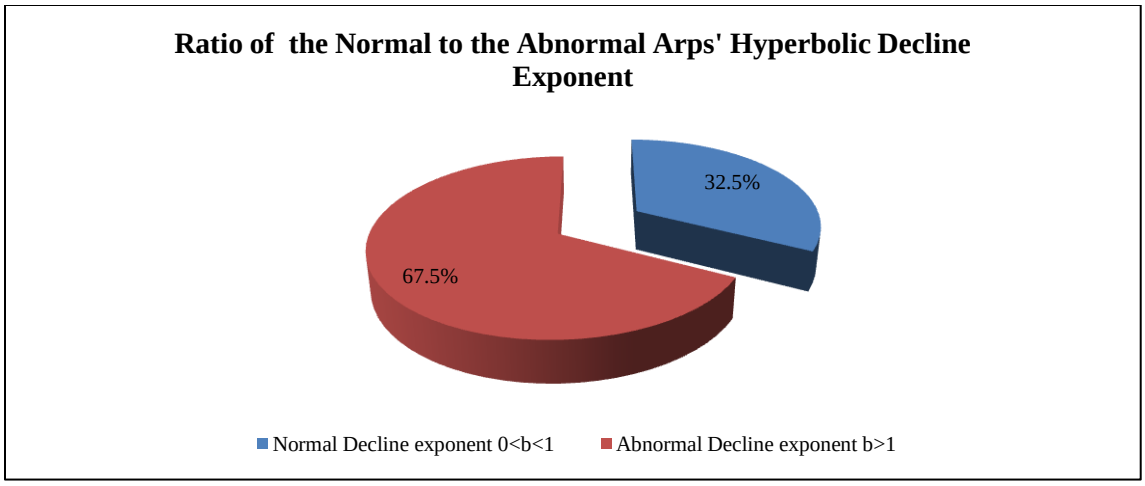

Figure 3.7: The percentage of abnormal decline exponents is more than twice that of the normal decline exponents obtained from Arps' hyperbolic model.

The fittingness of all the forty production profiles by Arps' hyperbolic model resulted specifically in 67.5% abnormal decline exponents (b>1) and 32.5% normal decline exponents 0<b<1) (**Figure 3.7**). Thus, regardless of the values of b, an excellent fit was observed for the forty production profiles. The problem associated with b>1 becomes significant when future performance and reserves are estimated. When b>1, the cumulative production becomes erroneously bigger than expected for some of the wells depending on how much the b value deviates from normal (b=1).

3.2.3 Power Law Exponential Analysis (PLE)

Figure 3.8 and **Figure 3.9** show PLE diagnostic plots for two wells in Leon County where I eliminated data necessary to achieve $R^2 \geq 0.97$. **Figure 3.10** illustrates the outcome of modeling one of the forty production profiles using the PLE. The PLE, however, did not fit all the production profiles of the forty wells in this fashion as one can see in **Figure 3.11**.

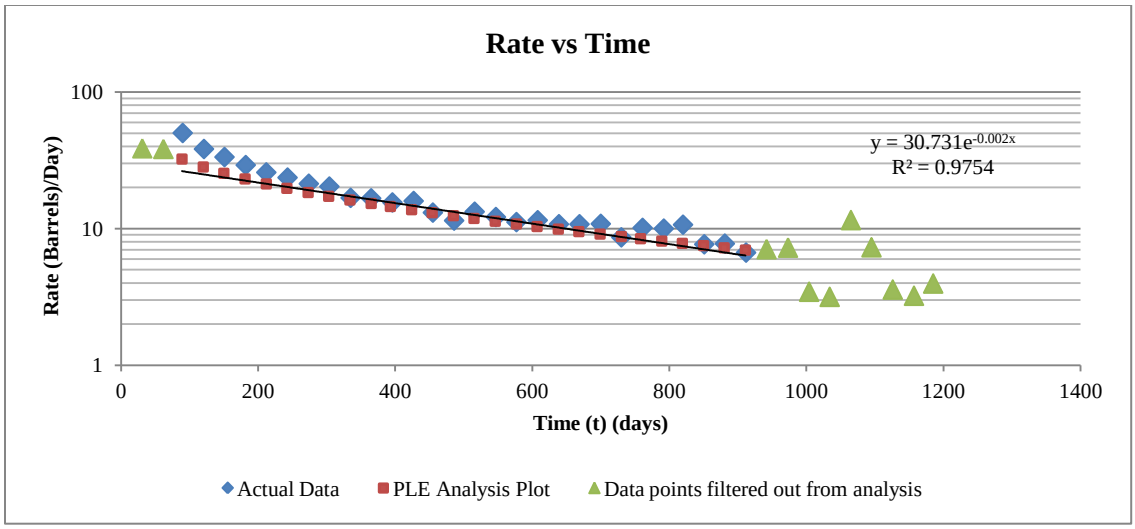

Figure 3.8: PLE diagnostic plot for the Simms lease achieved $R^2 \geq 0.97$ only when initial and erratic data sets were filtered out.

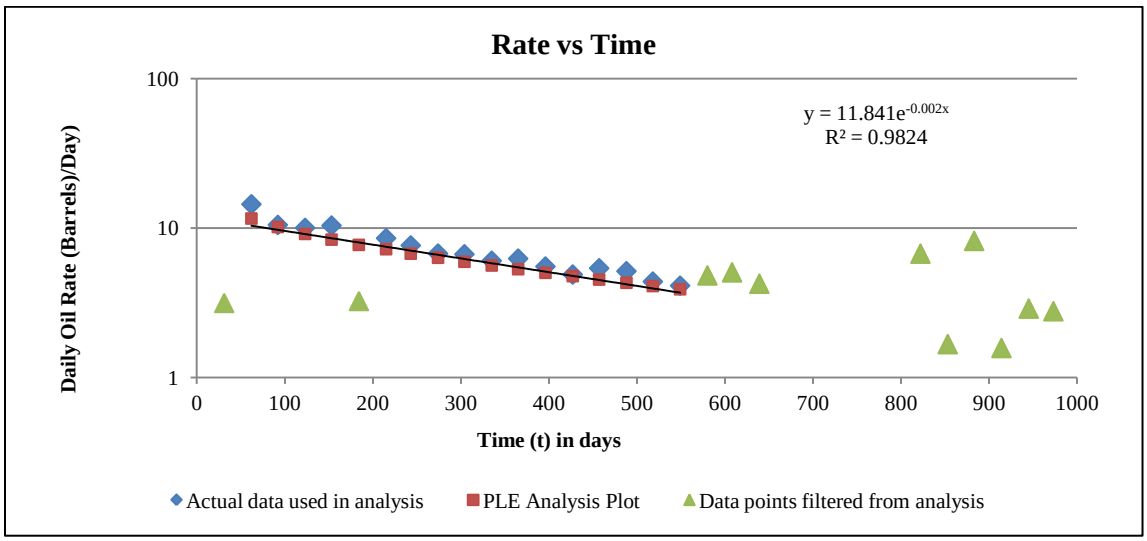

Figure 3.9: PLE diagnostic plot for the Easterling well achieved R2≥0.97 only when erratic data sets and no production sections were filtered out.

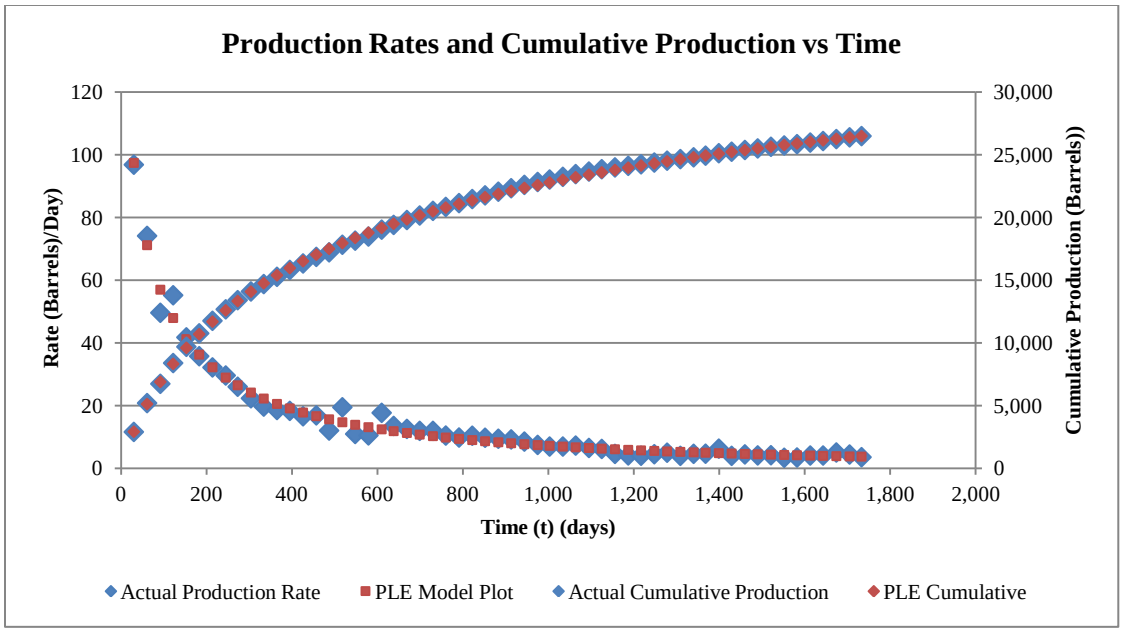

Figure 3.10: Power law exponential analysis showing cumulative production and rate match between the actual and the modeled data for Giesenschlag W.H. well in Burleson County.

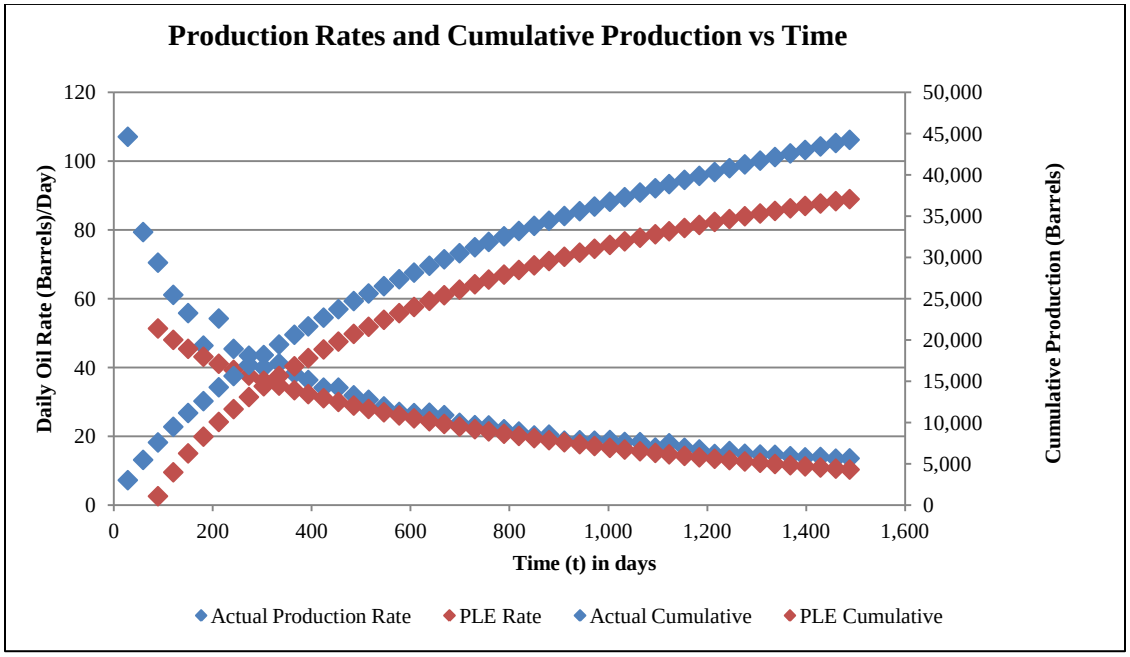

Figure 3.11: Power law exponential analysis showing not very good cumulative production and rate match between the actual and the modeled data for Hullabaloo well in Brazos County.

3.2.4 Logistic Growth Analysis (LGA)

The results of the logistic growth analyses (LGA) for forty oil cumulative productions have closely fitted the past production profiles. **Figure 3.12** is one example of the outcome of a good fitting of the cumulative productions, as well as the corresponding production rates, generated from the logistic growth analysis, to the actual production profile.

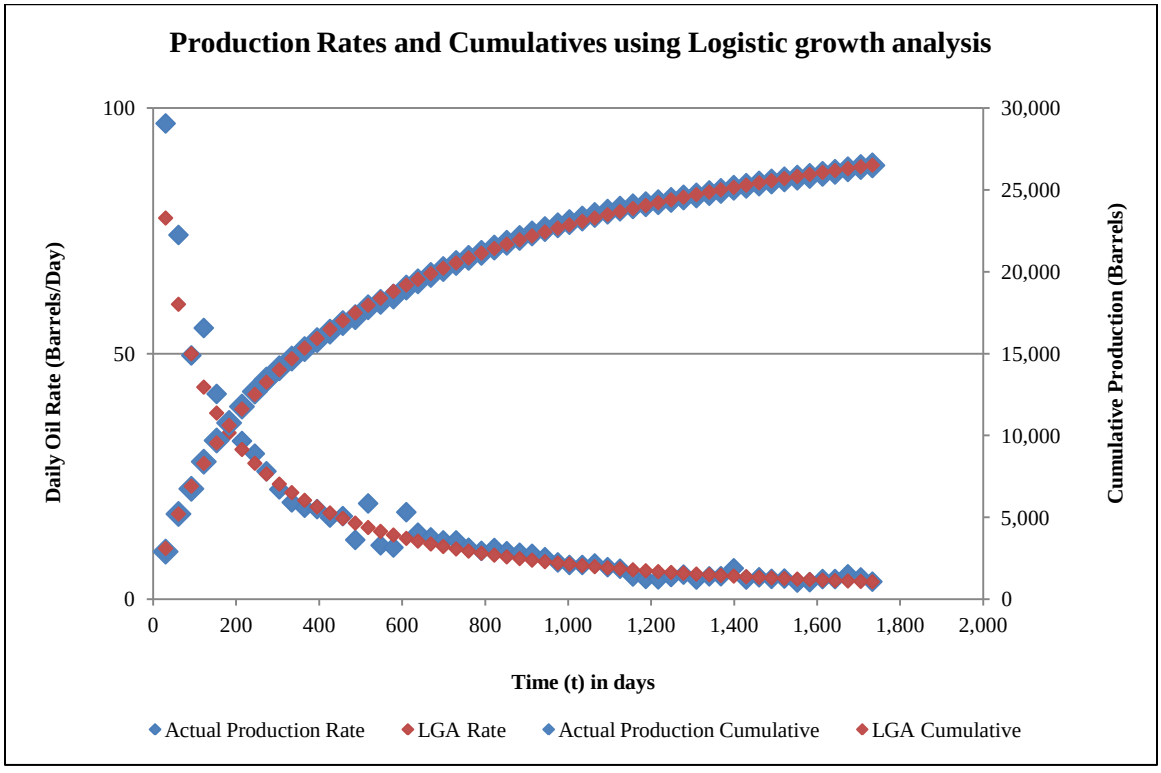

Figure 3.12: Logistic growth analysis showing cumulative production and rate match between the actual and the modeled data for Giesenschlag W.H. well in Burleson County.

3.2.5 Duong's Decline Curve Analysis Method

The Duong's method diagnostic plots determined the required parameters such as a (the intercept constant, day^{-1}), m (the slope), q_i (Oil rate on day 1, stb) and q_∞ (Oil rate at infinite time, stb) for all forty wells investigated. In the diagnostic plot presented in **Figure 3.13**, the values of a=13.533, m= 1.67, q_1=0.0032 and q_∞=11.432 have been defined by the equation of the line of least square regression. Note that in this example, the value for q_∞ will be zero if the line passes through the origin, but this is not the case for all forty production profiles, unless it is made to do so by Excel tools.

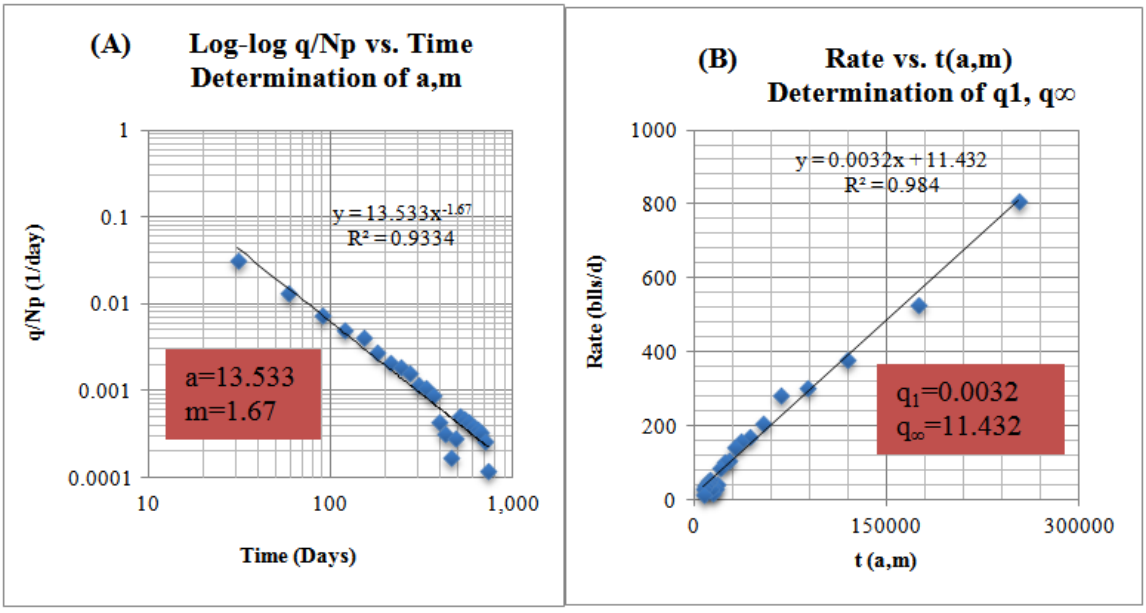

Figure 3.13 (A, B): Duong's method diagnostic plots for a production profile to determine a, m, q_1 and q_∞. (q_i= Oil rate at Day 1, q_∞= Oil rate at infinite time, t= Production time, days, t ($_{a, m}$) = Time function based on **Equation 2.17**)

The outcomes of Duong's method fitting the past production history are consistently better when the value of q_∞ is zero compared to when it is nonzero. In **Figure 3.14 (A, B)**, the cumulative production corresponding to q_∞ = -1.3 does not fit the actual production history as much as it does for **Figure 3.14 (A, B),** corresponding to q_∞ = 0. Another example of a similar result is presented in **Figure 3.15 (A, B)**. There are other cases where no significant difference in the cumulative trends between history and the Duong's method profiles exist. The rates at infinite time are -0.1 and 0.0 (zero) for **Figure 3.16 (A, B)** respectively; i.e., both rates are approximately zero; hence their cumulative production profiles are similar.

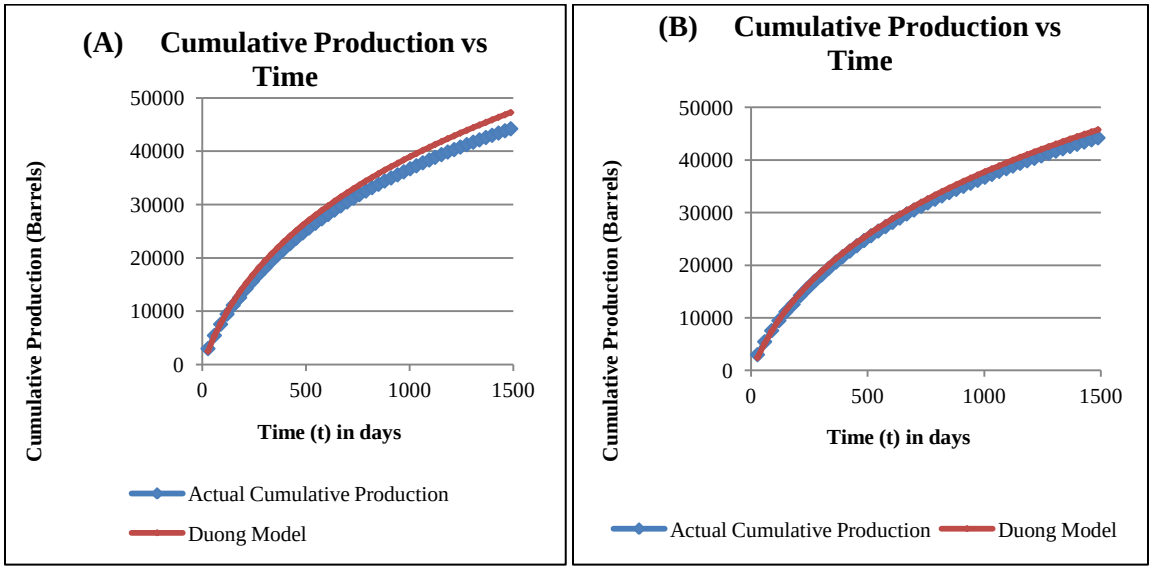

Figure 3.14 (A, B): Different results are obtained in fitting past cumulative production profile of a well (Hullabaloo) with Duong's method when the rate versus time function does or does not pass through the origin.

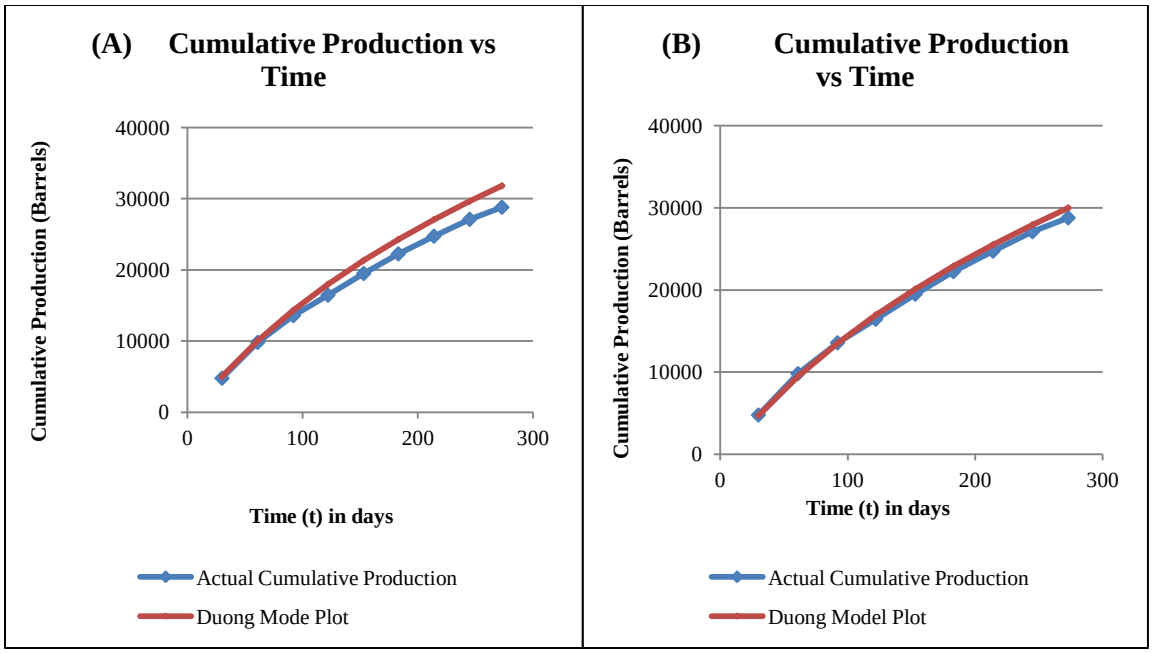

Figure 3.15 (A, B): Different results are obtained in fitting past cumulative production profile of a well (Donaho Unit) with Duong's method when rate versus the time function does or does not go through the origin.

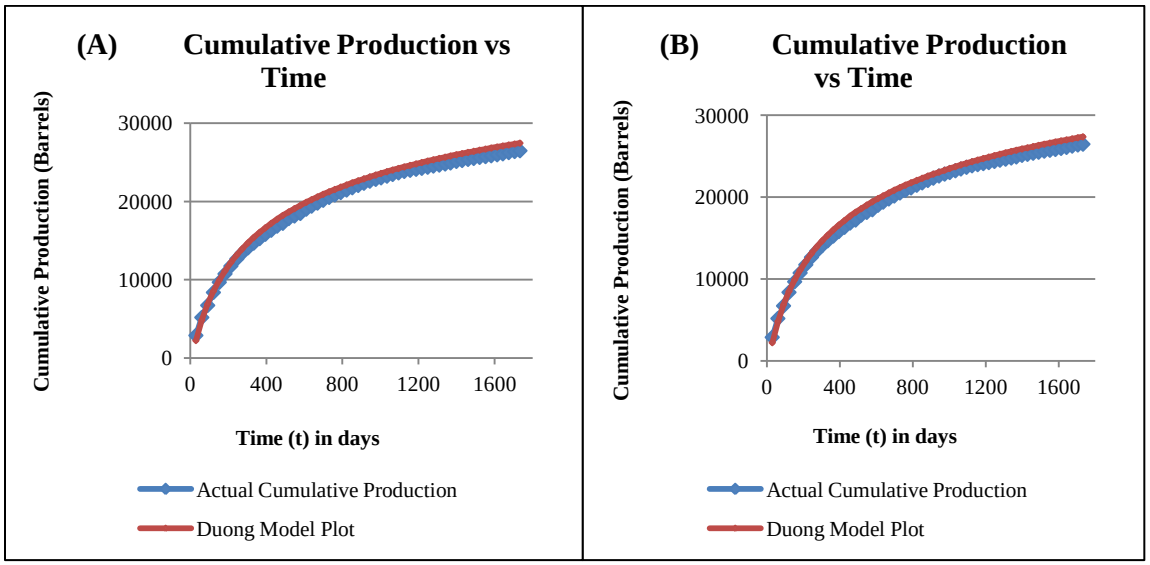

Figure 3.16 (A, B): No significant differences are obtained in fitting past cumulative production profile of a well (Giesenchlag W.H.C) with Duong's method when rate versus the time function does or does not pass through the origin.

The results for an entire process of evaluating one of the wells (Cannon Unit) in the Karnes County using Duong's method are presented in **Figure 3.17 (A, C)**. The model's rate versus time plot is seen overlying the actual data, but does not fit it very well (**Figure 3.17 (A, C)**. In **Figure 3.17 (B)**, the rate at infinity (q_∞) is a nonzero digit of -27.663 stb/d. In the end, there is not a good overlap between the actual cumulative production data and that of Duong's method (**Figure 3.17 (C)**). **Figure 3.18** is one example of the outcome of a fitting of the cumulative productions, as well as the corresponding production rates, generated from the Duong's method, to the actual production profile.

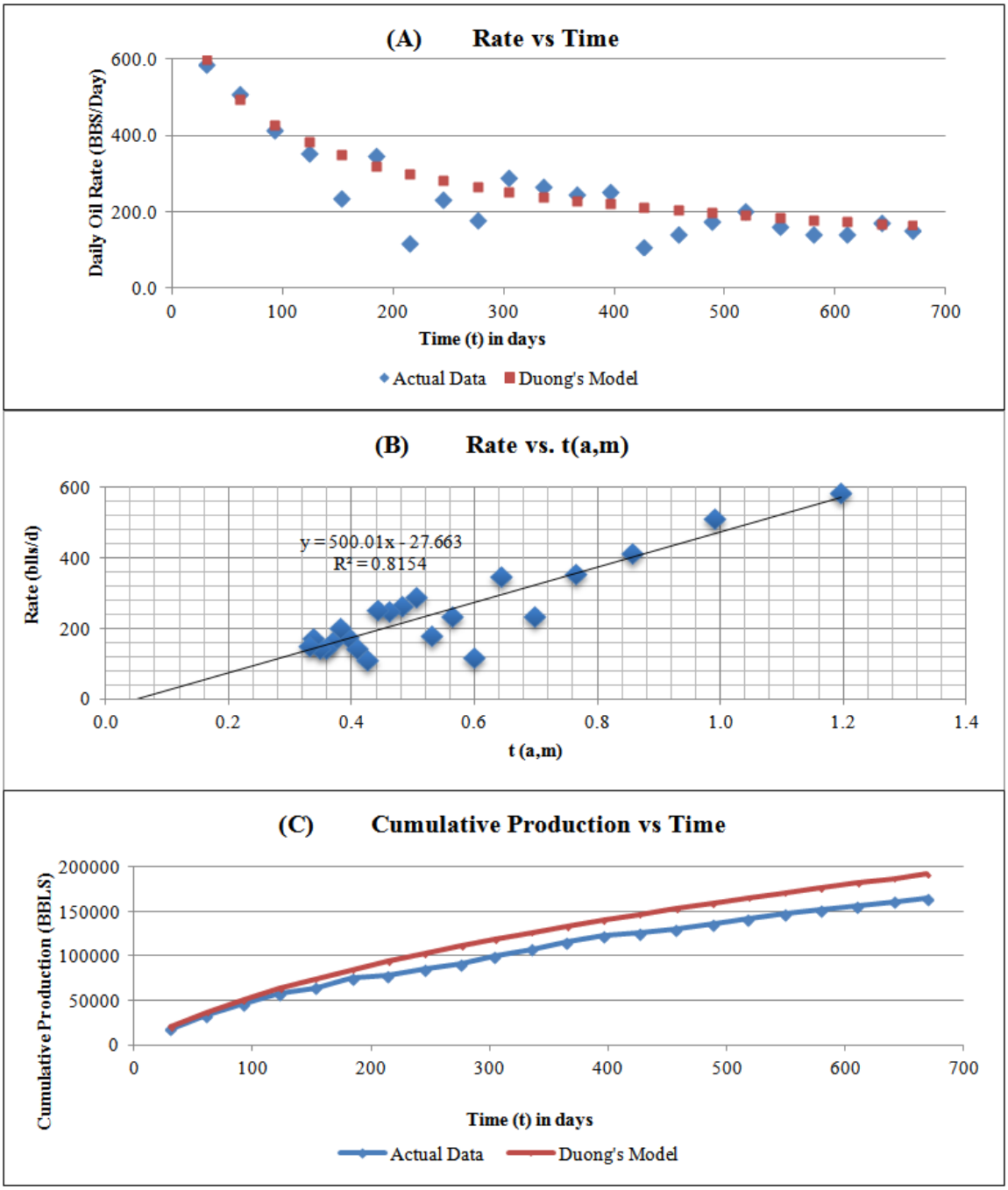

Figure 3.17 (A-C): Duong's method failed to match the production history for unfiltered Cannon # 09607 lease.

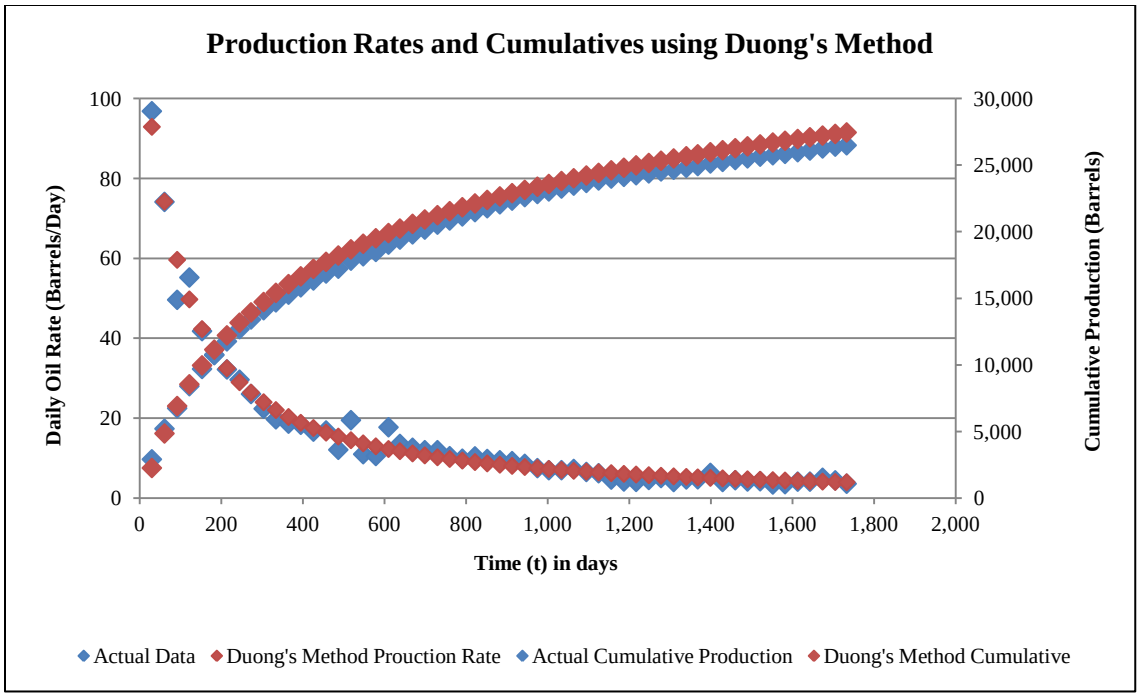

Figure 3.18: Duong's method showing cumulative production and rate match between the actual and the modeled data for Giesenschlag W.H. well in Burleson County.

3.2.6 Logistic Arps Hyperbolic Approach (LAHA)

When the combined real and extended LGA cumulative production data was fed into Arps' hyperbolic, it improved the normal hyperbolic decline (0<b<1) from 32.5% to 80%, and thereby reduced the number of b>1 from 67.5% to 20% (**Figure 3.19 (A, B)**. Recall, Arps' hyperbolic relation achieves reasonable reserve estimate and future production forecast when the decline exponent is within the range 0<b<1. Otherwise when b>1, reserve estimates and future production forecasts become unrealistically optimistic.

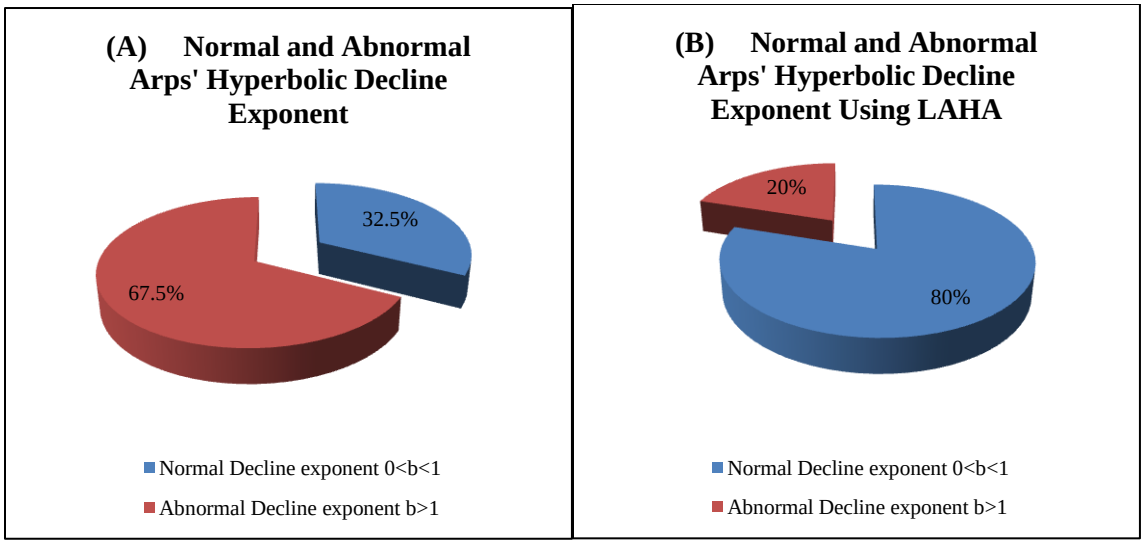

Figure 3.19 (A, B): Percentage of normal decline exponent (0<b<1) improves with the use of the new approach (LAHA).

Figure 3.20 illustrates the effects of the proposed LAHA approach. The number of production profiles with decline exponent 0<b<1 increased from 13 to 32, as presented in **Figure 3.20** and **Appendix Table A.1**. The blue and the red bars on **Figure 3.20** correspond to the normal and abnormal decline exponent values for all forty production profiles. The green bars represent the normal decline exponents of previously abnormal decline exponents (i.e. red bars). They show that LAHA has been successful in eliminating high decline exponents within a certain range of b>1, such as b<1.5.

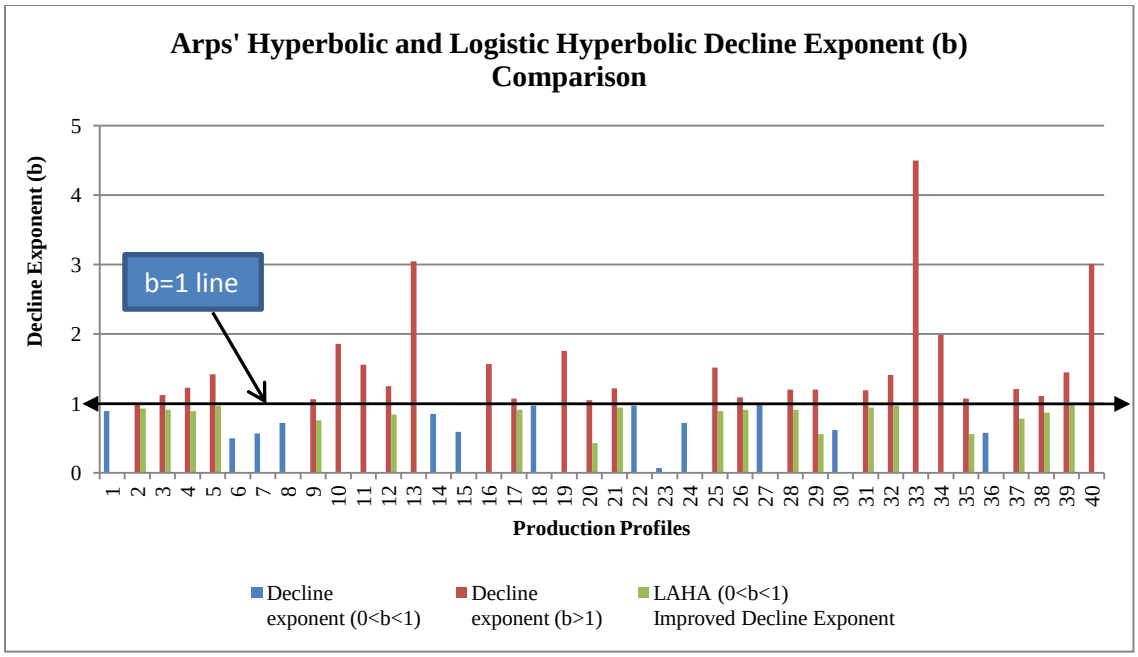

Figure 3.20: Comparison of decline exponents (b) using Arps' hyperbolic and LAHA.

In addition, LAHA lowered the EUR values wherever the decline exponents were shown to improve from abnormal b>1 to normal 0<b<1. EUR results for Arps' hyperbolic decline exponents b>1 and LAHA decline exponents (0<b<1) are presented side by side in **Figure 3.21** and **Appendix Table A.2**.

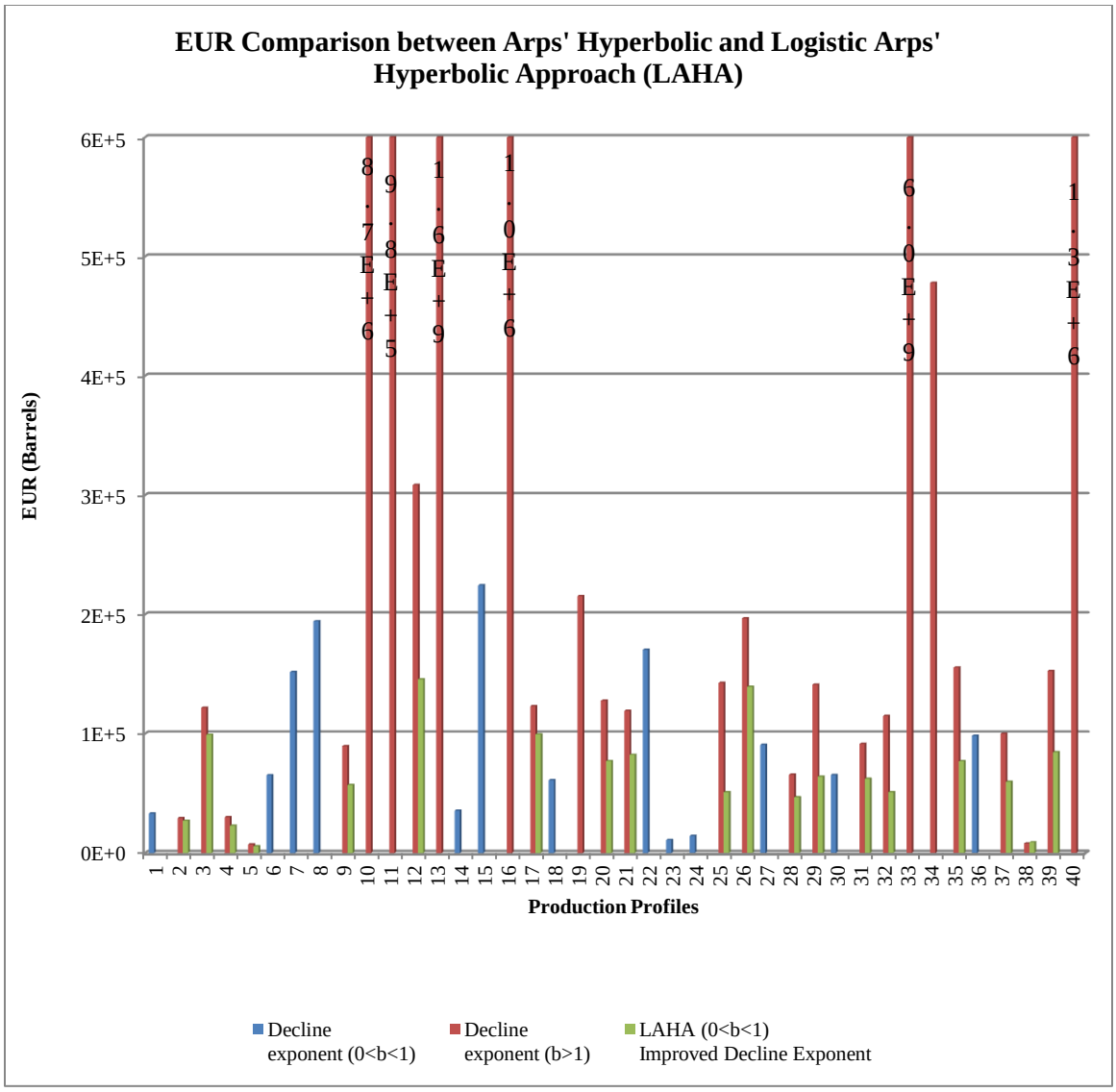

Figure 3.21: Expected ultimate recoveries (EUR) generated by LAHA are expectedly lower than that of Arps' hyperbolic decline for cases where b>1 under Arps' hyperbolic method became 0<b<1 under LAHA.

3.3 Discussion of General Results

The consequences of not filtering the data include unexpected results such as:

1. Duong's method diagnostic plot for q_1 and q_∞ determination may fail to pass through the origin, resulting in unmatched cumulative production
2. Arps' hyperbolic decline may cause high incidence of decline exponent b>1 resulting in wrong reserves future production forecasts or
3. The PLE may fail to achieve the best least square regression fit (R^2>0.97) resulting in abnormal rate as production time approaches infinity.

Arps' hyperbolic decline model fits reasonably well for all forty past production rate profiles regardless of the values of the decline exponent (b). The problem of abnormal decline exponent (i.e., b>1) becomes significant when estimating future performance and reserves. Thus, the consequences of an abnormal decline exponent are unrealistic overestimation of cumulative production and infinite recoverable reserves. Mathematically, when b>1 is used for cumulative production calculations, the result is infinite over times when the production rate approaches zero.

PLE estimated the least EUR and remaining reserves to abandonment for all forty profiles analyzed. Compared to the other models, the general observation is that PLE is an augmented Arps' exponential model and provided pessimistic forecasts. A better fit is observed when a trendline of R^2>0.97 is passed through the late-time profile (after ignoring the early months' production) of the new production data points.

The strength of LGA against the other models is the determination of the maximum possible recoverable oil (K), which ensures that EUR does not grow infinitely with time. It is consistently more conservative than the optimistic models such as Arps' hyperbolic (includes harmonic) and Duong's method.

Duong's method is particularly sensitive to the level of noise in the production trend data. Even with filtered profiles, Duong's model history-matched the cumulative shale oil production trends the least, compared to the other decline models, for most of the forty production profiles. As a consequence, the forecasted EUR, the remaining reserves, and time to abandonment are sometimes extremely high or low compared to the values of other models. When Excel is used to force the trendline to go through the origin, a slightly closer match is obtained. However, it gives a lower least square regression, changes the curvature of the cumulative production trend, and provides questionably high forecasts. The closer the rate at infinity (q_∞) is to zero, the better the match between past and modeled cumulative production data.

Despite the problems associated with EUR when decline exponent b>1, Arps' model is still applied frequently in the industry. To maintain the useful tradition and conserve the original parameters of decline analysis, I proposed and tested a new technique: Logistic Arps hyperbolic approach (LAHA). In this approach, closely matched production profiles obtained from LGA with reasonable EUR have been used to investigate Arps' hyperbolic decline. The expectation is to find a solution to the occurrence of erroneous b>1 and to eliminate the unrealistically high EUR. The method has been successful in tackling both the abnormal decline exponent (b) and the high EUR when b is greater than unity by up to 0.5. Decline exponents b>1.5 also show significant improvement, but not enough to bring the decline exponent to normal (0<b<1).

Chapter 4 Eagle Ford Shale Oil Production Decline Analysis Specific Results

4.0 Introduction

This chapter discusses the performance history and the results of the decline curve analyses for forty production profiles from the eight counties evaluated in **Chapter 3**. The completion details of these wells are not publicly available from Texas Railroad Commission online data resource. The historical performance and detailed results of the individual production profiles are discussed county by county and, to some extent, well by well. The exact methods for application of the different decline analysis techniques have already been discussed in **Chapter 3**. The detailed results for the expected ultimate recoveries (EUR), remaining reserves, and time to abandonment are tabulated and presented in **Appendix Table A.2**. The relative locations of the various counties for the wells investigated are shown in the arrow labels on **Figure 2.1 and 2.2**.

4.1 Burleson County

4.1.1 Introduction

Three wells with long production histories were examined in this county located up-dip in the oil generation window of the Eagle Ford Shale formation (**Figure 2.2**). The wells are identified by their lease names: Giesenschlag-Groce, AB Childers and Giesenschlag W.H. Hydraulic fracture stage and perforation cluster specifications are not available publicly at the Texas Railroad Commission free webpage.

Well #2H in the Giesenschlag-Groce lease had fifty-four months of production data from September 2008 to February 2013 (**Table 4.1**). The wellbore produced initially at a monthly average rate of 216 barrels/day for 27 days in the first month, but declined to an average rate of

108 barrels/day by January 2009. A total of 65,298 barrels of oil was produced over the entire production period between September 2008 and February 2013.

Well #3H from AB Childers well produced 28,000 barrels of oil within fifty-six months (August 2008-February 2013). Initial and latest rates were 66.5 and 8.4 barrels/day, respectively (**Table 4.1**).

The Giesenschlag W.H lease well #3H was completed in May 2008 and its production profile available were fifty-eight months long as of February 2013. The latest production rate reported, as of February 2013, was 3.6 barrels/day, compared to an initial rate of 96.8 barrels/day in May 2008. It had cumulative oil production of 28,134 barrels (**Table 4.1**). The past production rates versus time for the three wells are presented in **Figure 4.1**.

Table 4.1: Burleson County wells' completion and production history

County	Well Name	Completion date & Recompleted date	Depth (ft) MD /TVD	Horizontal length (ft)	Number of fracture stages	Producing life until now (Months)	Initial rate (Barrels/day)	Cumulative production (Barrels)	Current rate (Barrels/day)
Burleson	GIESENSCHLAG W. H.	5/21/2008	10890 / TVD (not available)	998	Not available	58	53.1	26489	3.6
	A B CHILDERS	7/30/2008	9214 /TVD (not available)	635	Not available	56	66.5	28000	8.4
	GIESENSCHLAG-GROCE	8/3/2008	13558 / 9016	3640	Not available	54	216	65298	20.6

4.1.2 Specific Results of Shale Oil Production Decline Analysis in Burleson County

The production rate profiles of all three wells in Burleson County are similar especially the Giesenschlag W.C and AB Childer wells' production declines (**Figure 4.1**).

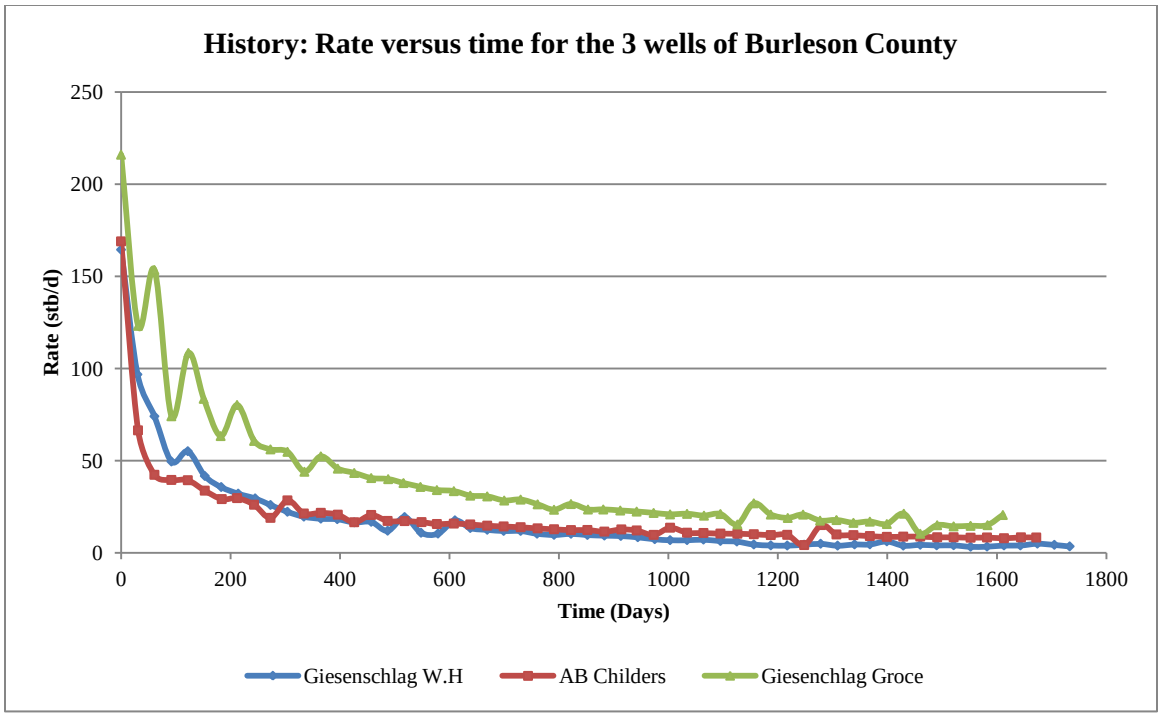

Figure 4.1: Profile of Burleson County wells' production history.

PLE analyses have predicted the least EUR, remaining reserves, and time to reach abandonment for all three wells (**Figures 4.2-4.4** and **Appendix Table A.2**). Of the three wells, Arps' exponential decline curve analysis modeled only the AB Childers successfully, but the other techniques analyzed and generated future production trends for all three wells. LGA production performance predictions are always relatively less compared to Arps' hyperbolic model over predictions. The Duong's method predictions are questionably high in the case of the AB Childers well when compared to the other decline techniques. LAHA has successfully reduced the original predictions of Arps' hyperbolic decline curve analysis, especially for the AB Childers and Giesenschlag Groce wells which had decline exponents greater than unity. LAHA improved the Arps' hyperbolic decline exponent from 1.01 to 0.93 and 1.12 to 0.91 for AB Childers and Giesenschlag-Groce respectively (**Appendix Table A.1**).

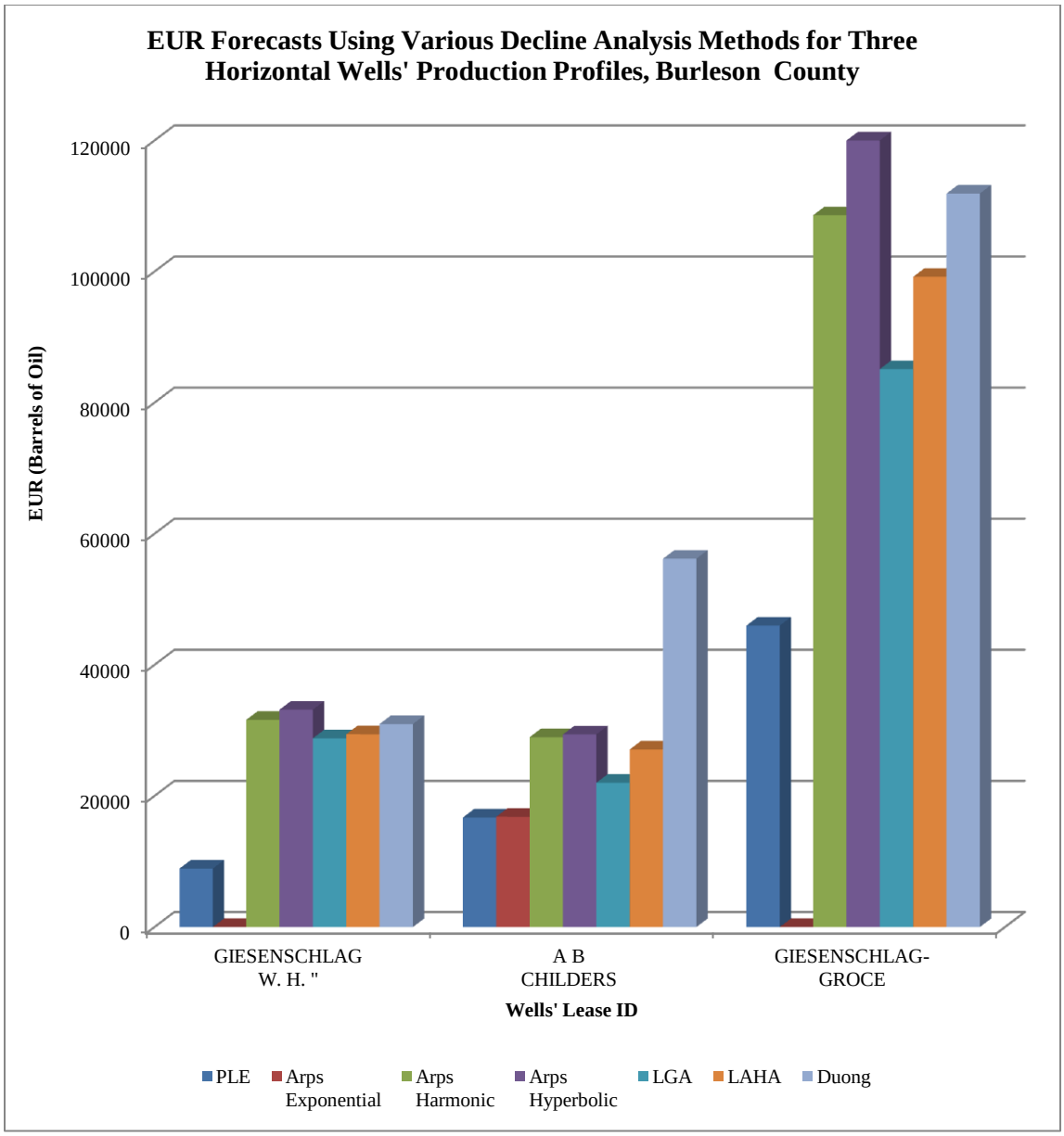

Figure 4.2: EUR generated for three horizontal wells' production profiles Burleson County.

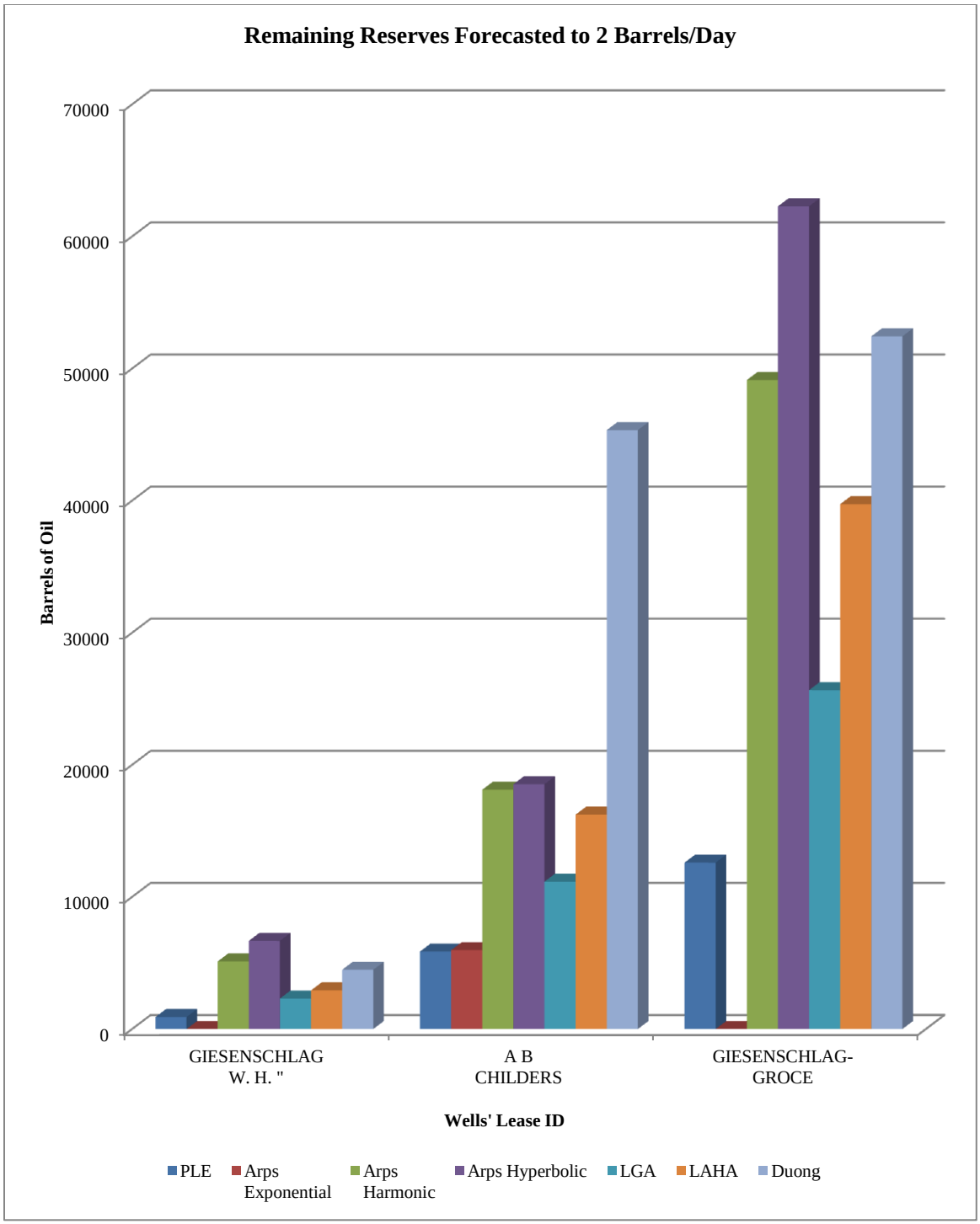

Figure 4.3: Remaining reserves forecasted to 2 barrels/day for three Burleson county horizontal wells' production profiles.

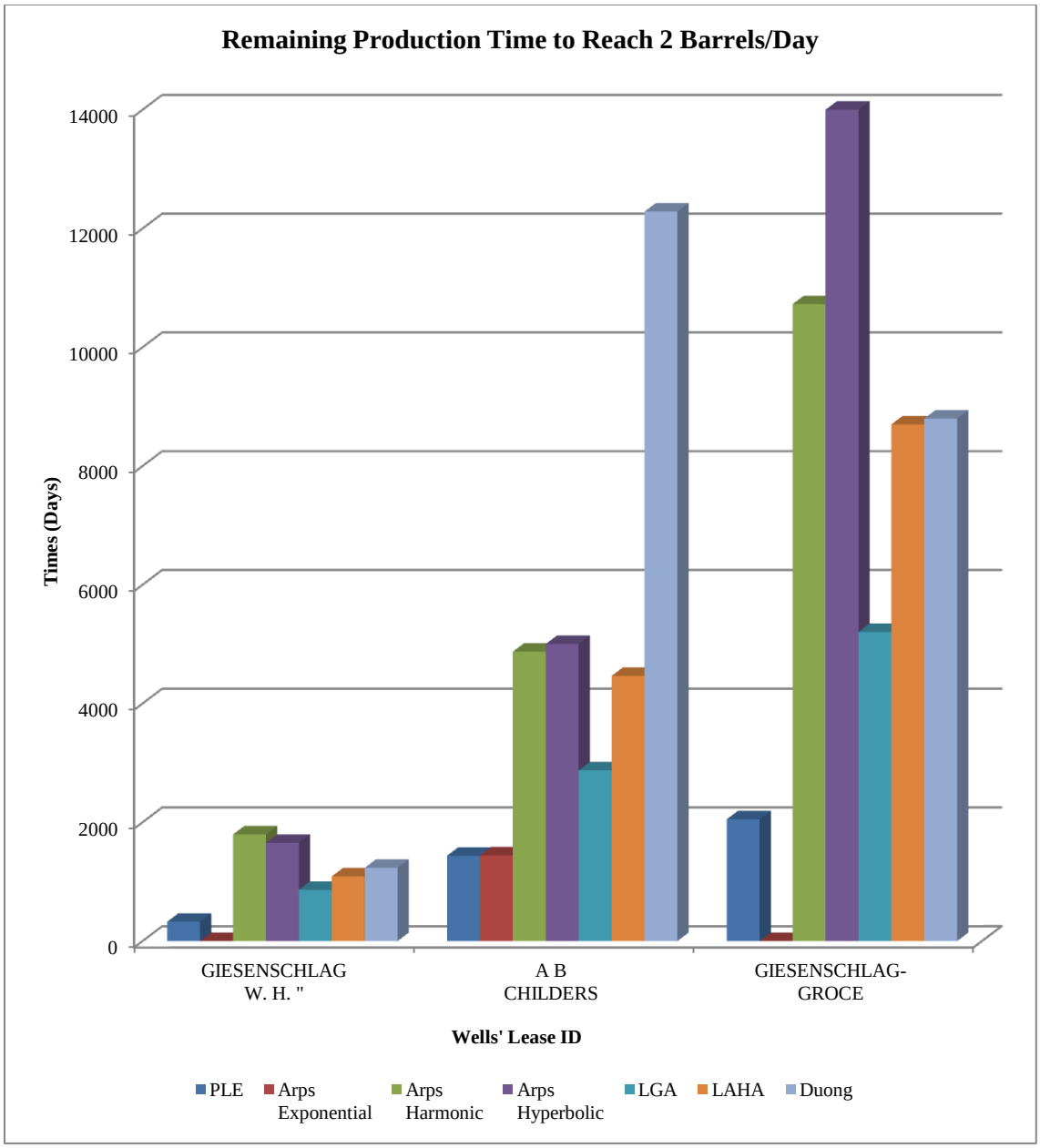

Figure 4.4: Remaining production time to reach 2 barrels/day for three Burleson county horizontal wells' production profiles.

4.2 Leon County

4.2.1 Introduction

Leon County is set in District 05 of the Eagle Ford Shale and encloses the up-dip oil sector of the play (**Figures 2.1 and 2.2**). It is located right above the Brazos County. Three horizontal wells' production profiles were retrieved from the public domain of the TRRC and analyzed (**Table 4.2**).

The horizontal wellbore (#3H) of the Simms lease was completed in December 2009; it comprises thirty-nine months of history as of February 2013. The well's horizontal section is between 7333 ft and 9141 ft measured depth (MD), and its production interval is between 7260 ft and 8885 ft MD. It had an initial production rate of approximately 120 barrels/day for 10 days in December 2009, which declined sharply to approximately 38 barrels/day in January 2010. The rate as of February 2013 was roughly 4.0 barrels/day, and the cumulative oil produced was 18,244 barrels (**Table 4.2**).

The Easterling lease well #2H was completed and brought online in July 2010. It produced at the rate of 14.5 barrels/day in August 2010, but as of February 2013, the rate had declined to 2.8 barrels/day (**Table 4.2**). Thirty-two months' cumulative production as of February 2013 is only 4,929 barrels of oil. The records also indicate no production for the months of May-August 2012 and have late-time erratic production rate profiles indicating tempered operating conditions that can introduce errors into the decline curve analysis.

The Donaho Unit wellbore was completed in May 2012 and had only 10 months of history data at the time of this analysis. This well had an initial flowing rate of 188 barrels/day but has since declined to 60.5 barrels/day, with a cumulative production of 34622 barrels (**Table 4.2**).

Table 4.2: Leon County wells' completion and production history

County	Well Name	Completion date & Recompleted date	Depth (ft) MD /TVD	Horizontal length (ft)	Number of fracture stages	Producing life until now (Months)	Initial rate (Barrels/day)	Cumulative production (Barrels)	Current rate (Barrels/day)
Leon	SIMMS	12/21/2009	9141 / 6989	1881	2	39	120	18244	4.0
	EASTERLING	7/7/2010	9200 / 7300	1875	Not available	32	14.5	4929	2.8
	DONAHO UNIT	5/17/2012	13632 / 7746	4231	Not available	10	188	34622	60.5

4.2.2 Specific Results of Shale Oil Production Decline Analysis in Leon County

The comparison between the past productions profiles of all three wells from Leon County is illustrated in **Figure 4.5**. A continuous early-time section of the Simms well's production profile (29 of the 39 months' data) was analyzed successfully with all the decline analysis techniques, with the exception of Arps' exponential model. The first two data points and later section

comprising seven months are very erratic and questionable to include in the analysis. Arps' hyperbolic model calculated b=1.23 for the Simms well, which became b=0.89 with LAHA (**Appendix Table A.1**). Forecasts of expected ultimate recoveries are very close, but Arps' hyperbolic model predicts 3648 barrels more than Duong's Method does (**Figures 4.6-4.8** and **Appendix Table A.2**). The overestimation by Arps' hyperbolic approach may be due in part to having a decline exponent greater than one.

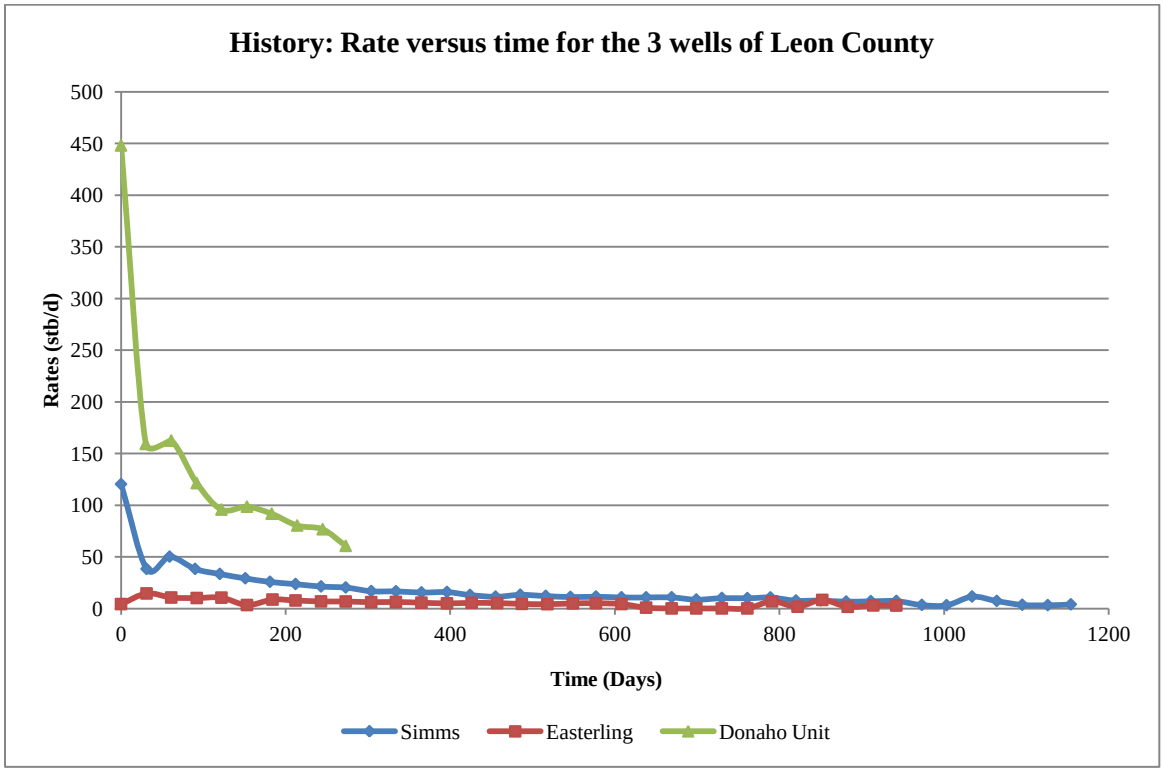

Figure 4.5: Profile of Leon County wells' production history.

A section of the Easterling well's production profile also analyses quite well with all of the techniques except Arps' exponential (**Figures 4.6-4.8** and **Appendix Table A.2**). PLE gives the

lowest, hyperbolic the highest values of EUR and remaining reserves. The differences in the forecasted expected ultimate recoveries are minimal, but Arps' hyperbolic and Duong's method predictions are the most optimistic. The Arps' hyperbolic decline exponent of the actual data was b=1.42, resulting again in the highest future performance predictions. With LAHA it became b=0.97 and the expected ultimate recovery became very close to that of LGA and Arps' harmonic models.

The Donaho Unit well's profile analyzed very well with all the techniques except Arps' exponential and the harmonic. The original decline exponent for Arps' hyperbolic is normal (b=0.5), but LAHA was still used (results shown in **Figures 4.6-4.8** and **Appendix Table A.1** and **A.2**). The PLE also matched the cumulative production, but the Duong's method diagnostic plot deviated slightly from the real data, resulting in high EUR compared to the rest of the models (**Figure 4.6**). Arps' exponential and the harmonic fell short of criteria ($R^2 \geq 0.95$) and so did not apply.

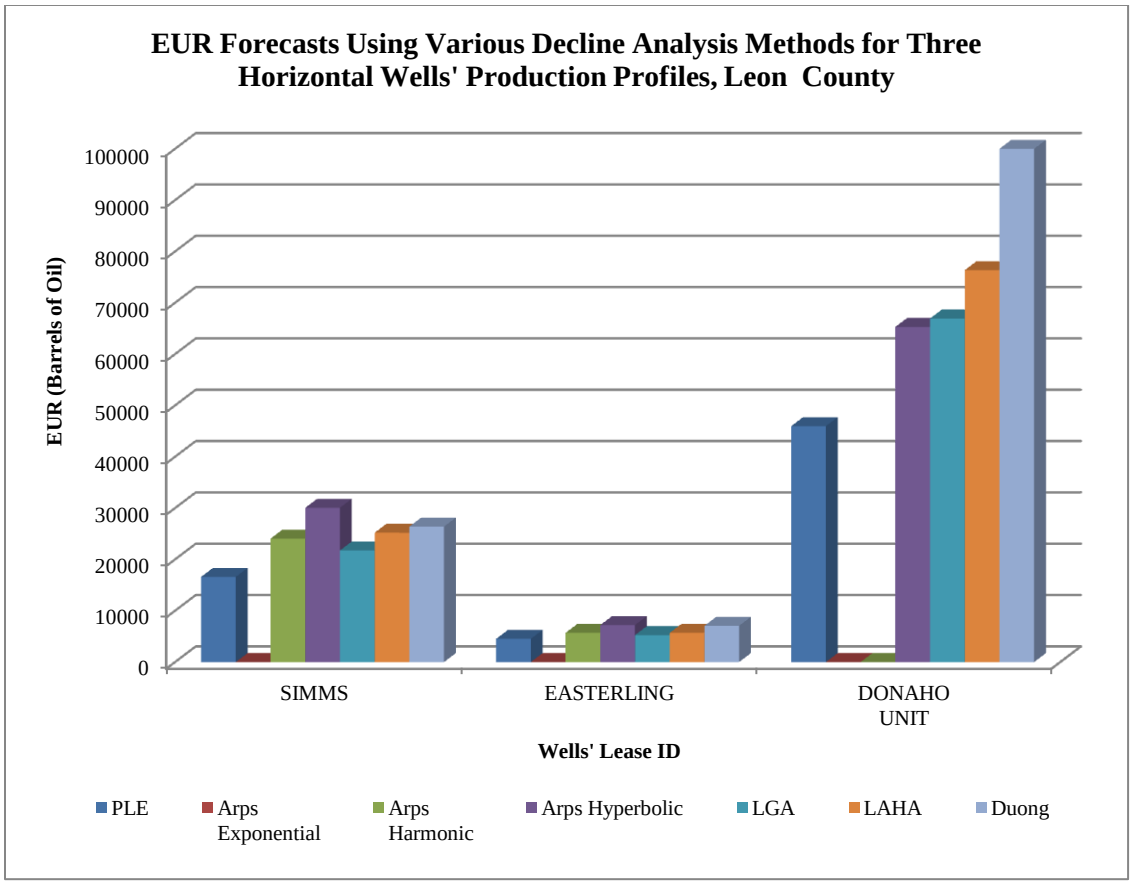

Figure 4.6: EUR generated for three horizontal wells' production profiles in Leon County.

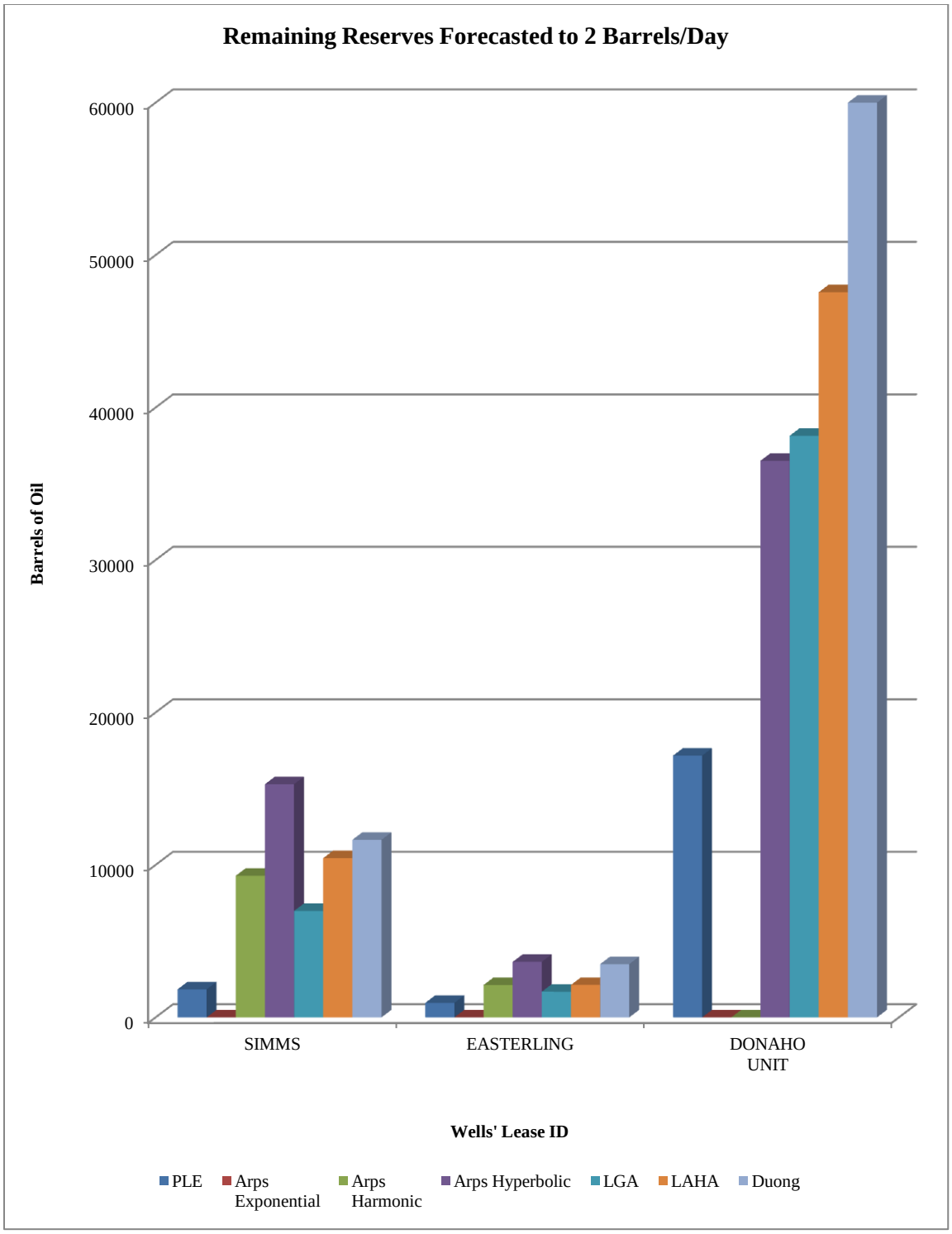

Figure 4.7: Remaining reserve forecasts for three production profiles in Leon County.

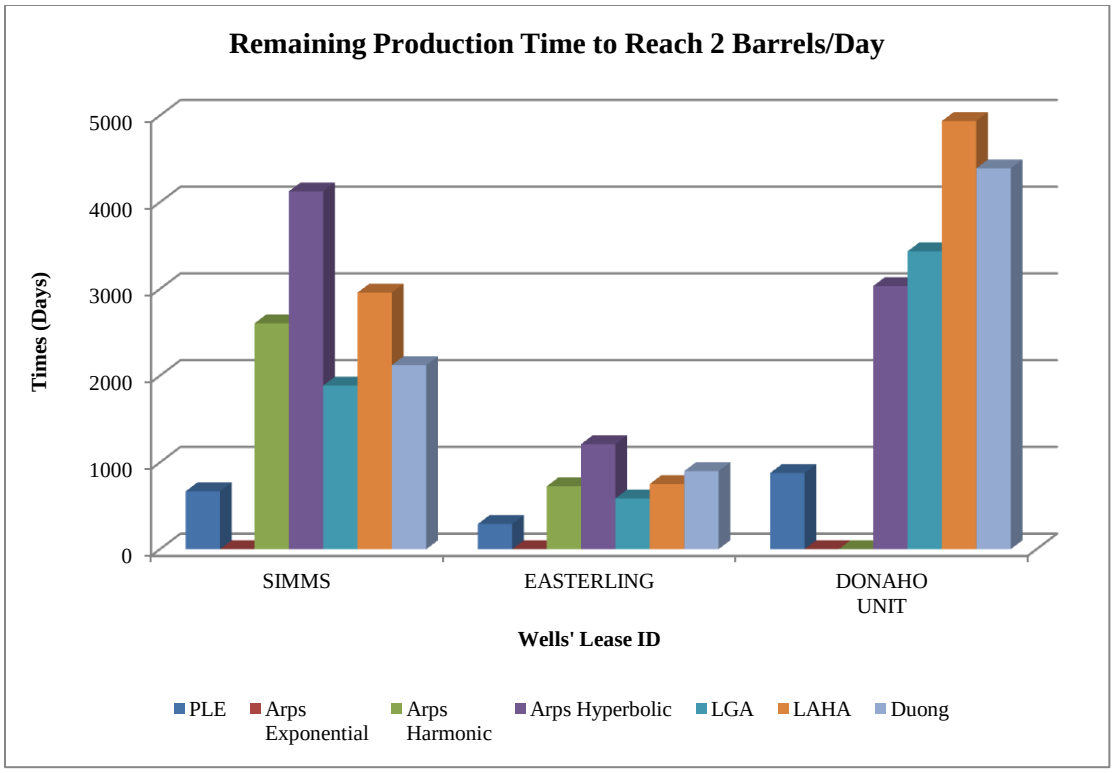

Figure 4.8: Remaining production life to reach 2 barrels/day for 3 wells' in Leon County.

4.3 Brazos County

4.3.1 Introduction

Brazos County is located approximately 90 miles northwest of Houston and shares boundaries with Leon and Burleson Counties on the up–dip segment of the Eagle Ford Shale oil zone. Two production profiles corresponding to oil wells from the Reser-Sanders Unit and Hullabaloo leases are posted online at the TRRC website. The Hullabaloo well has a historic cumulative production of 54,481 barrels of oil for 52 months; it started production at the rate of 193.8 barrels/day, and as of February 2013 it had declined to 13.5 barrels/day (**Table 4.3** and **Figure 4.9**). The Reser-Sanders Unit well started producing at a rate of about 23 barrels/day, which declined to 2.3

barrels/day in February 2013 (**Table 4.3** and **Figure 4.9**). Cumulative oil production for 49 months is only 7,907 barrels.

Table 4.3: Brazos County wells' completion and production history

County	Well Name	Completion date & Recompleted date	Depth (ft) MD /TVD	Horizontal length (ft)	Number of fracture stages	Producing life until now (Months)	Initial rate (Barrels/day)	Cumulative production (Barrels)	Current rate (Barrels/day)
Brazos	RESER-SANDERS UNIT	2/6/2009	15452 / 11763	3520	Not availa-ble	49	22.9	7907	2.3
	HULLABALOO	11/4/2008	12200 / 9518	2255	Not availa-ble	52	193.8	54481	13.5

4.3.2 Specific Results of Shale Oil Production Decline Analysis in Brazos County

The production rate profiles of these wells are dissimilar, as presented in **Figure 4.9.** Examination of the two profiles suggested that the Hullabaloo well is located in a richer oil zone than the Reser-Sanders Unit well (**Table 4.3** and **Figure 4.9**). This observation is also supported by the forecasts in **Appendix Tables 2** and **Figures 4.10-4.12**.

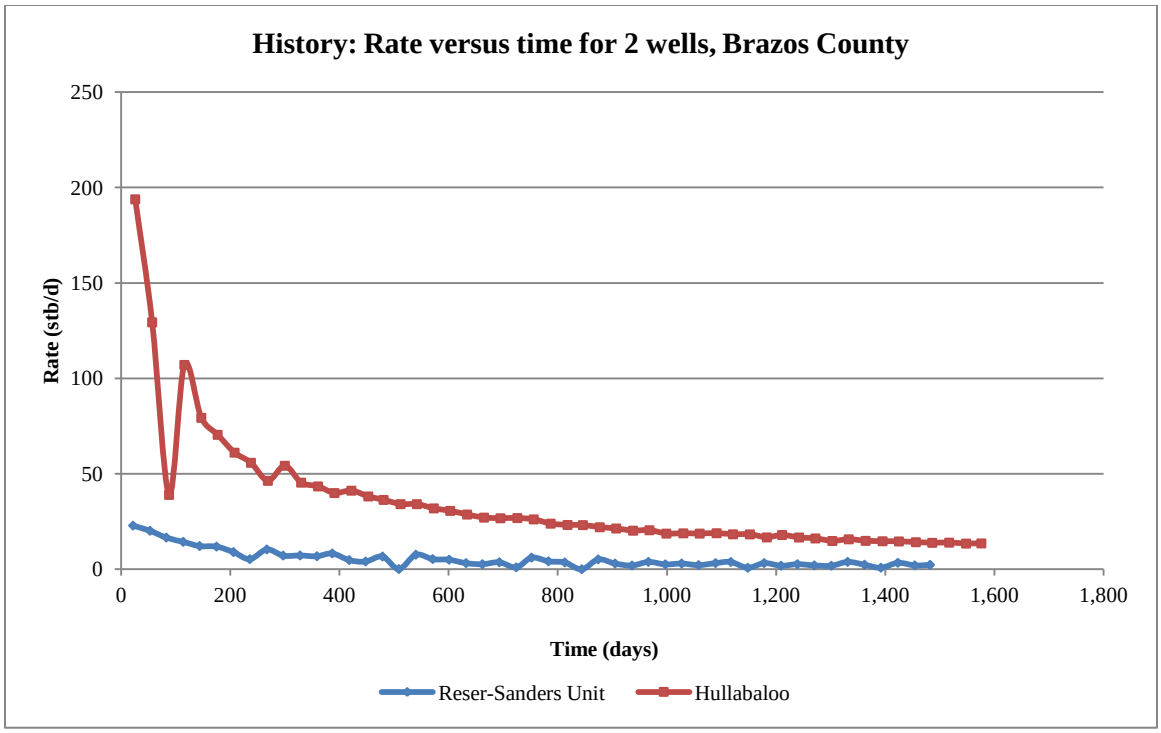

Figure 4.9: Profile of Brazos County wells' production history.

The Reser-Sanders Unit well's production profile cannot be modeled with Arps' exponential or harmonic analyses. The smooth and seemingly undisturbed rate profile of the Hullabaloo well was analyzed by all the decline curve analysis methods. Arps' hyperbolic decline exponents are b=1.45 for Hullabaloo and b=1.11 for Reser-Sanders. These decline exponents did not conform to standards (0<b<1). Consequently, the EUR for Hullabaloo is overestimated above all the other models' predictions; specifically, it is 57,794 barrels more than the Duong's Method prediction, which is the second highest (**Appendix Tables 2** and **Figure 4.10)**. The effect of b=1.11 for Reser-Sander is not obvious, especially with respect to the EUR (**Figure 4.10**). However, with the application of LAHA, the decline exponent became normalized to b=0.99 and b=0.87 for the Hullabaloo and Reser-Sanders wells, respectively. As a result, the predictions for both wells

improved greatly. The Hullabaloo well's profiles indicated possible Arps' exponential and harmonic declines, but neither could be applied to the Reser-Sander Unit well. Arps' exponential and the PLE forecasted very close to each other. Duong's method compares fairly well for estimating the EUR for the Reser-Sanders Unit well; it is in its own class and not particularly similar to any other model results for the Hullabaloo well. LAHA reduced the optimistic EUR of 152627 barrels of oil forecasted by Arps' hyperbolic decline analysis to a more realistic 86418 barrels of oil.

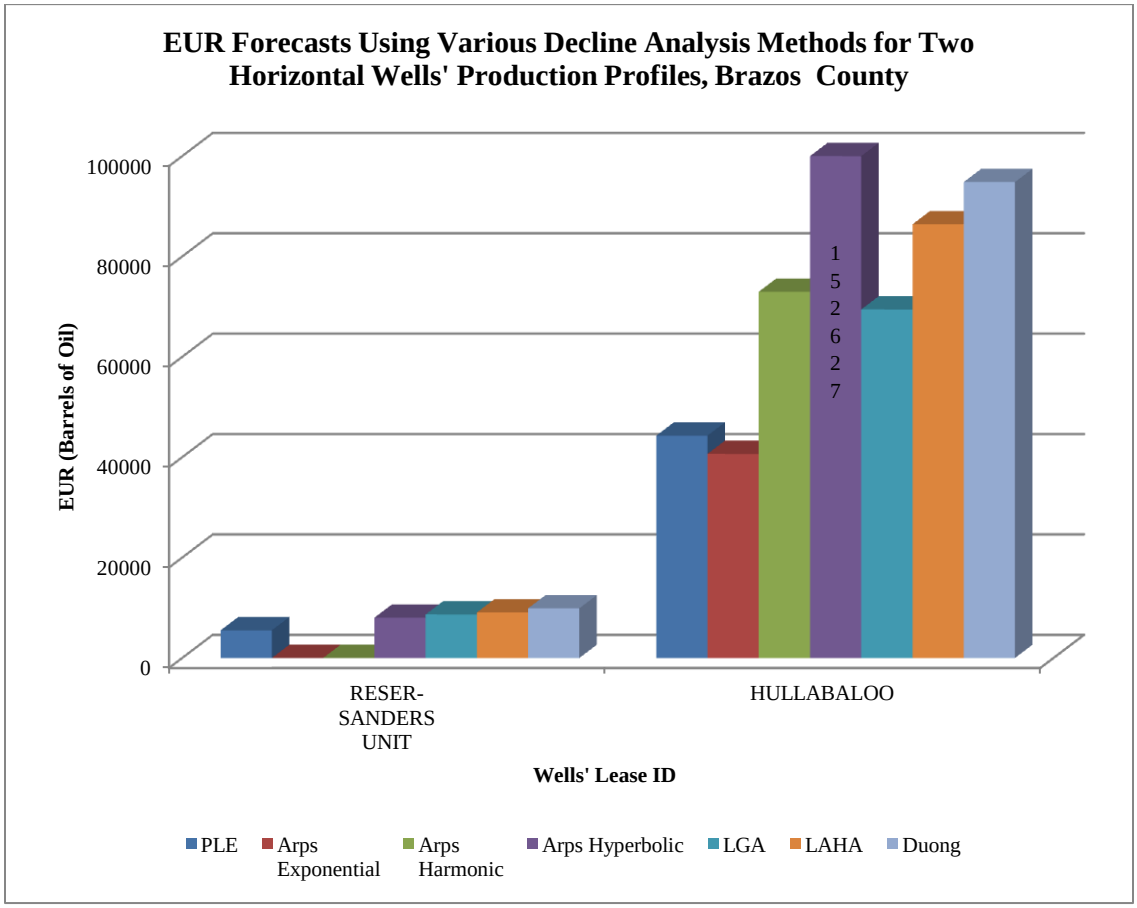

Figure 4.10: EUR generated for two horizontal wells' production profiles in Brazos County.

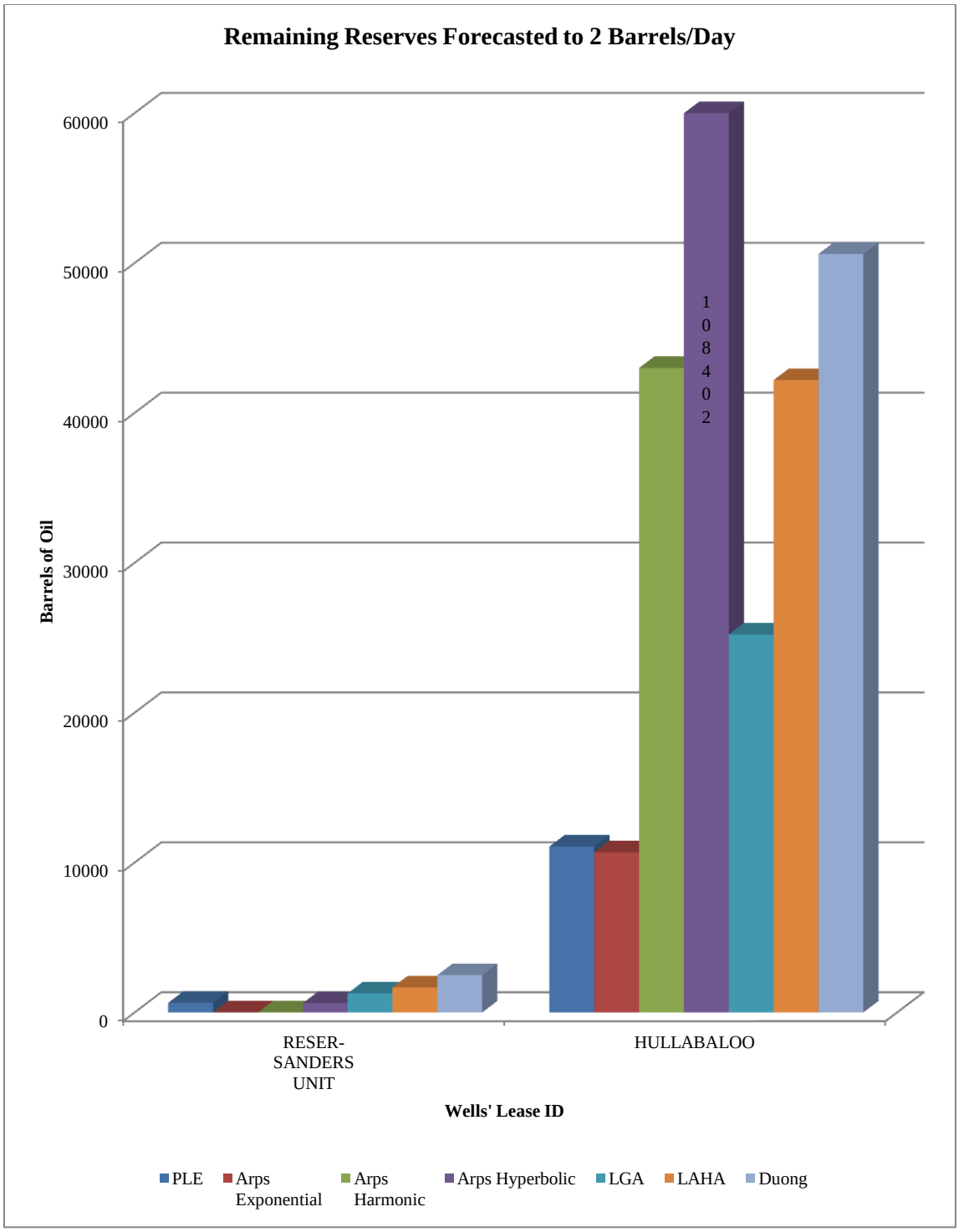

Figure 4.11: Remaining reserve forecasts for two production profiles in Brazos County.

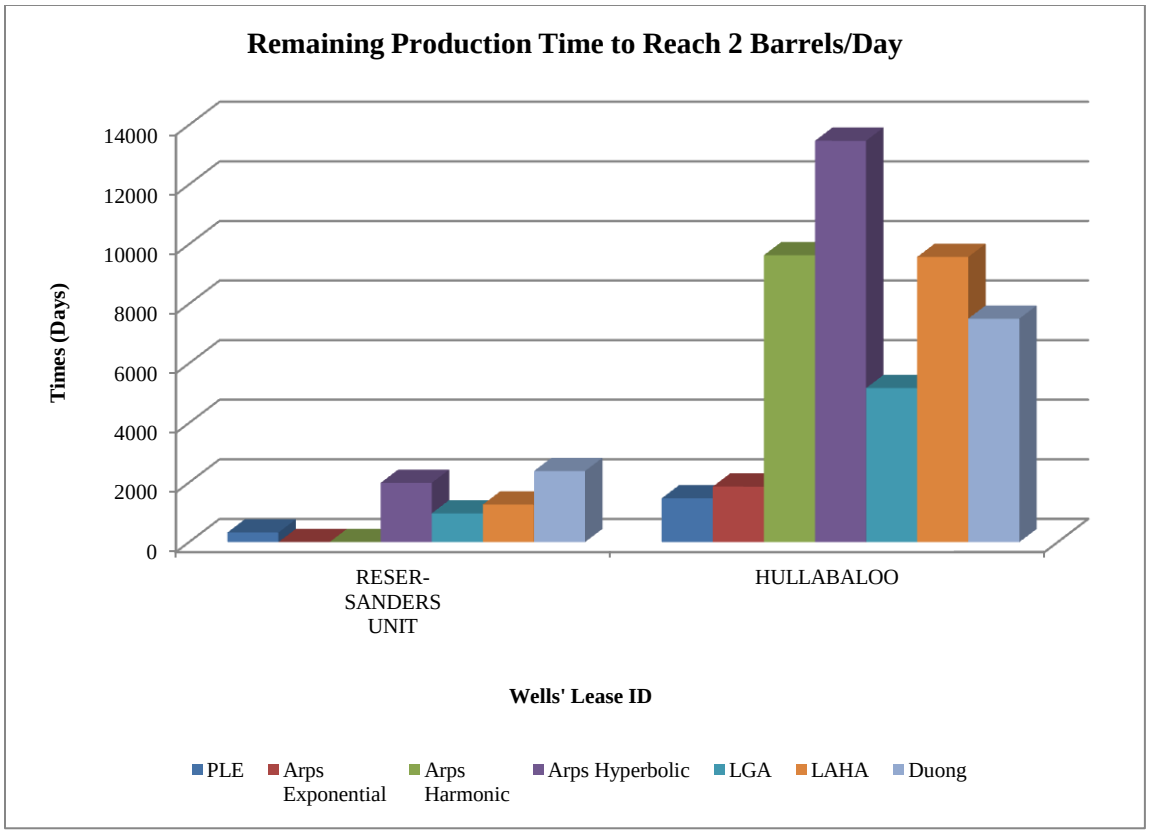

Figure 4.12: Remaining production life to reach 2 barrels/day for 2 wells in Brazos County.

4.4 Lee County

4.4.1 Introduction

Lee County is located adjacent to Burleson County. A horizontal well (E1H) from the Fenn Ranch unit lease was completed in December 2008 and produced at initial rates of 82.8 barrels/day, which declined to approximately 16.1 barrels/day in February 2013. Cumulative oil recovery was 46,957 barrels over the fifty-one month period. The horizontal production interval is approximately 1331ft long and has nine hydraulic fracture stages (**Table 4.4**).

Table 4.4: Lee County wells' completion and production history

County	Well Name	Completion date & Recompleted date	Depth (ft) MD /TVD	Horizontal length (ft)	Number of fracture stages	Producing life until now (Months)	Initial rate (Barrels/day)	Cumulative production (Barrels)	Current rate (Barrels/day)
Lee	FENN RANCH UNIT	12/20/2008	10325 / 8101	1331	9	51	82.8	46957	16.1

4.4.2 Specific Results of Shale Oil Production Decline Analysis in Lee County

In terms of the EUR predictions, the PLE again forecasted the least volume of recoverable reserves; LGA falls behind Duong's method by 10,497 barrels, while Arps' hyperbolic and subsequent LAHA have extremely high predictions (**Figures 4.13-4.15, Appendix Tables 2)**. The Arps' hyperbolic decline exponent b=3.01 resulted in one of the highest volumetric cumulative predictions for all forty production profiles (**Figures 4.13-4.15, Appendix Tables 2)**. LAHA significantly lowered the EUR from the original forecast by Arps' hyperbolic, but could not normalize the high decline exponent of b=3.01.

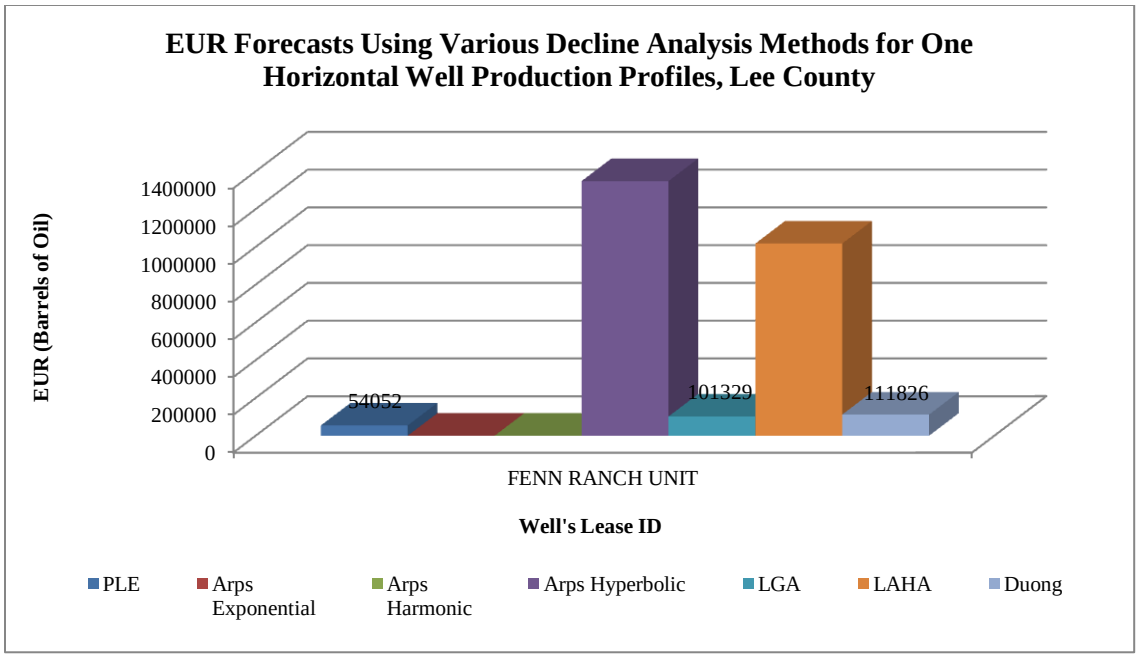

Figure 4.13: EUR generated for one horizontal well's production profile in Lee County.

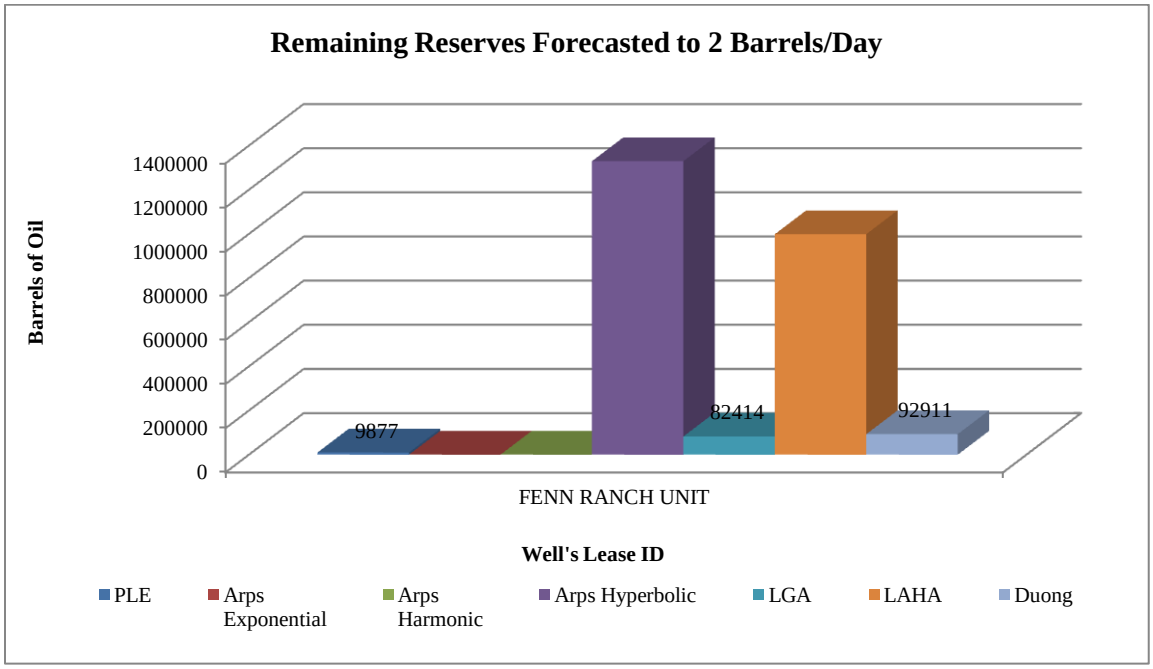

Figure 4.14: Remaining reserve forecasts for one production profile in Lee County.

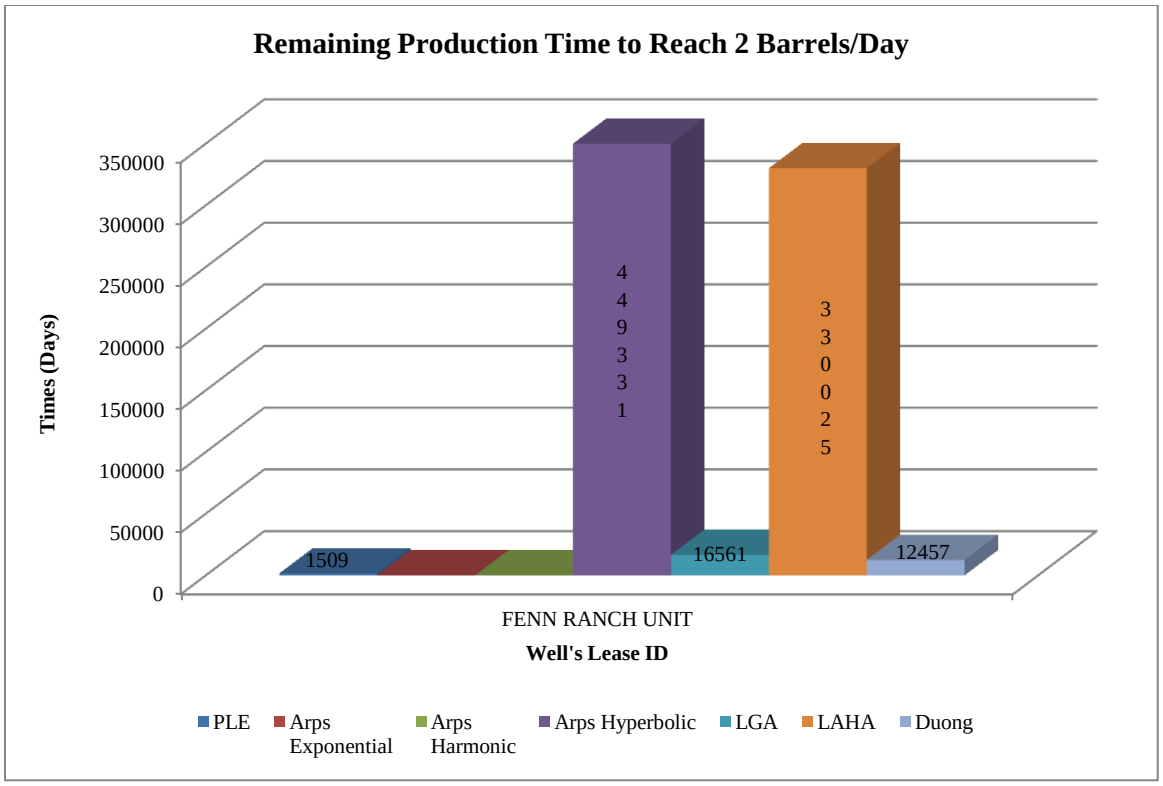

Figure 4.15: Remaining production life to reach 2 barrels/day for one well in Lee County.

4.5 Gonzales County

4.5.1 Introduction

Gonzales County is located south of the up-dip northern section of the Eagle Ford Shale. Eleven oil producing horizontal wells' production profiles were retrieved for decline analysis. The wells' lease names of the respective production profiles are Mostyn, Holmes, Georg, Parr, Bozka, S Duderstadt, Cinco Ranch, Koenning Unit, Gonzo Hunter, Perkins, and Otto. **Table 4.5** is a summary of some of the vital statistics of these wells' completion and production histories.

Table 4.5: Gonzales County wells' completion and production history

County	Well Name	Completion date & Recompleted date	Depth (ft) MD /TVD	Horizontal length (ft)	Number of fracture stages	Producing life until now (Months)	Initial rate (Barrels/day)	Cumulative production (Barrels)	Current rate (Barrels/day)
Gonzales	MOSTYN	Not available	Not availa-ble	Not availa-ble	Not avai-lable	Not availa-ble	Not availa-ble	Not available	Not availa-ble
	HOLMES	6/15/2011	14155 / 7217	7013	23	20	443.3	116014	61.8
	GEORG	5/27/2011	10555 / 6724	3383	12	22	350	16194	1.4
	PARR	5/27/2011	13055 / 7441	4975	17	22	490.2	19448	14.6
	BOZKA	4/1/2011	14240 / 10533	3146	11	23	351.3	41824	25.8
	S. DUDERSTADT	3/8/2011	15890 / 11693	4240	Not avai-lable	22	203.9	85671	44.8
	CINCO RANCH	3/23/2011	15084 / 10029	5066	15	24	359.3	48756	32.6
	KOENNING UNIT	6/16/2010	Not availa-ble	Not availa-ble	Not avai-lable	Not availa-ble	Not availa-ble	Not available	Not availa-ble
	GONZO HUNTER	8/3/2010	13750 / 9537	3290	Not avai-lable	27	323.2	68385	28.3
	PERKINS	Not available	Not availa-ble	Not availa-ble	Not avai-lable	Not availa-ble	Not availa-ble	Not available	Not availa-ble
	OTTO	Not available	Not availa-ble	Not availa-ble	Not avail-able	Not availa-ble	Not availa-ble	Not available	Not availa-ble

4.5.2 Specific Results of Shale Oil Production Decline Analysis in Gonzales County

Figure 4.16 shows the variation in rate profiles of the various horizontal wells in this one county. The various initial production rates, in particular, may be due to local differences in natural fracture density and probable existence of sweet spots. Differences in shale petrophysical properties (mineralogy, organic content and geomechanics) within the same formation may also produce such variations. Koenning Unit and Mostyn wells' production profiles started at the lowest rates, while Parr, Perkins and Holmes had the highest initial rates. The rest of the wells (Georg, Bozka, S Duderstadt, Cinco Ranch, Koenning Unit, Gonzo Hunter, Perkins, and Otto) have initial production rates ranging between 320 and 360 barrels/day. The Gonzo Hunter and Holmes production profiles are also very erratic.

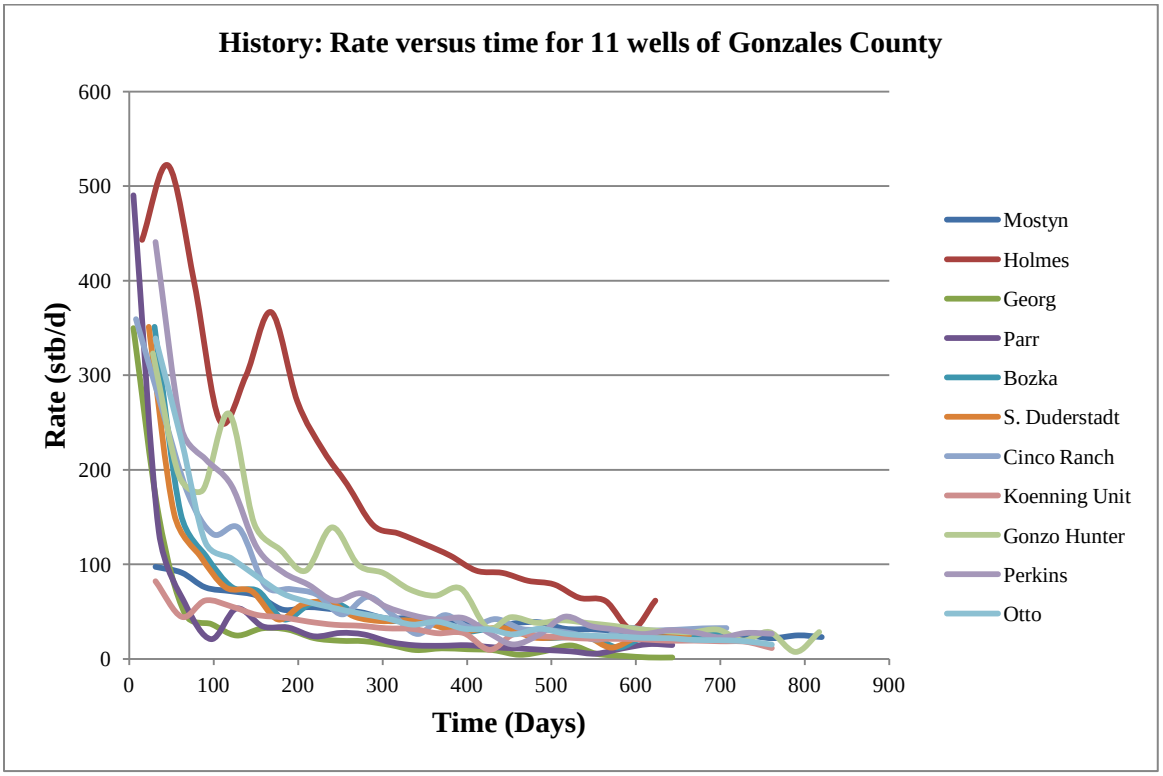

Figure 4.16: Profile of Gonzales County wells' production history.

Figures 4.17-4.19 and **Appendix Table A.2** show the results of assessing the eleven production profiles with the decline models. Analysis of these eleven wells provided the following comments:

1. PLE forecasted in all cases the lowest EUR, remaining reserves, and time to reach abandonment.
2. Arps' exponential decline modeled Koenning Unit only, and it forecasted similarly to PLE. Both Arps' exponential and PLE calculations may underestimate the volumetric oil in place.
3. The forecasts by Arps' harmonic for five of the wells, where diagnostic plots have $R^2 \geq 0.95$, are comparable to the other predictions except in the case of the Perkins lease well, where the model predicts an unrealistically long time to reach 2 barrels/day (**Figure 4.19)**. The cause of having such a high prediction of abandonment time is not clear from the original data. The diagnostic verification for Arps' harmonic decline analysis was obtained for 21 out of 25 months of the production profile for Perkins.
4. The Arps' hyperbolic decline exponents for the various production profiles are shown in **Appendix Table A.1**. The cases where b>1 were the Mostyn, Bozka, S. Duderstadt, Koenning Unit, Hunter Gonzo and Otto production profiles, and the EUR forecasted for these cases soared above the other predictions.
5. The LGA model had decent history matches in all cases, therefore producing reasonable and comparable predictions of EUR, remaining reserves, and time to reach 2 barrels/day.
6. Duong's method did not have good history matches, but its forecasts were comparable to the other models in most cases.
7. LAHA reduced the high values of the Arps' hyperbolic when b>1. The corresponding b values with LAHA are shown in **Appendix Table A.1.**

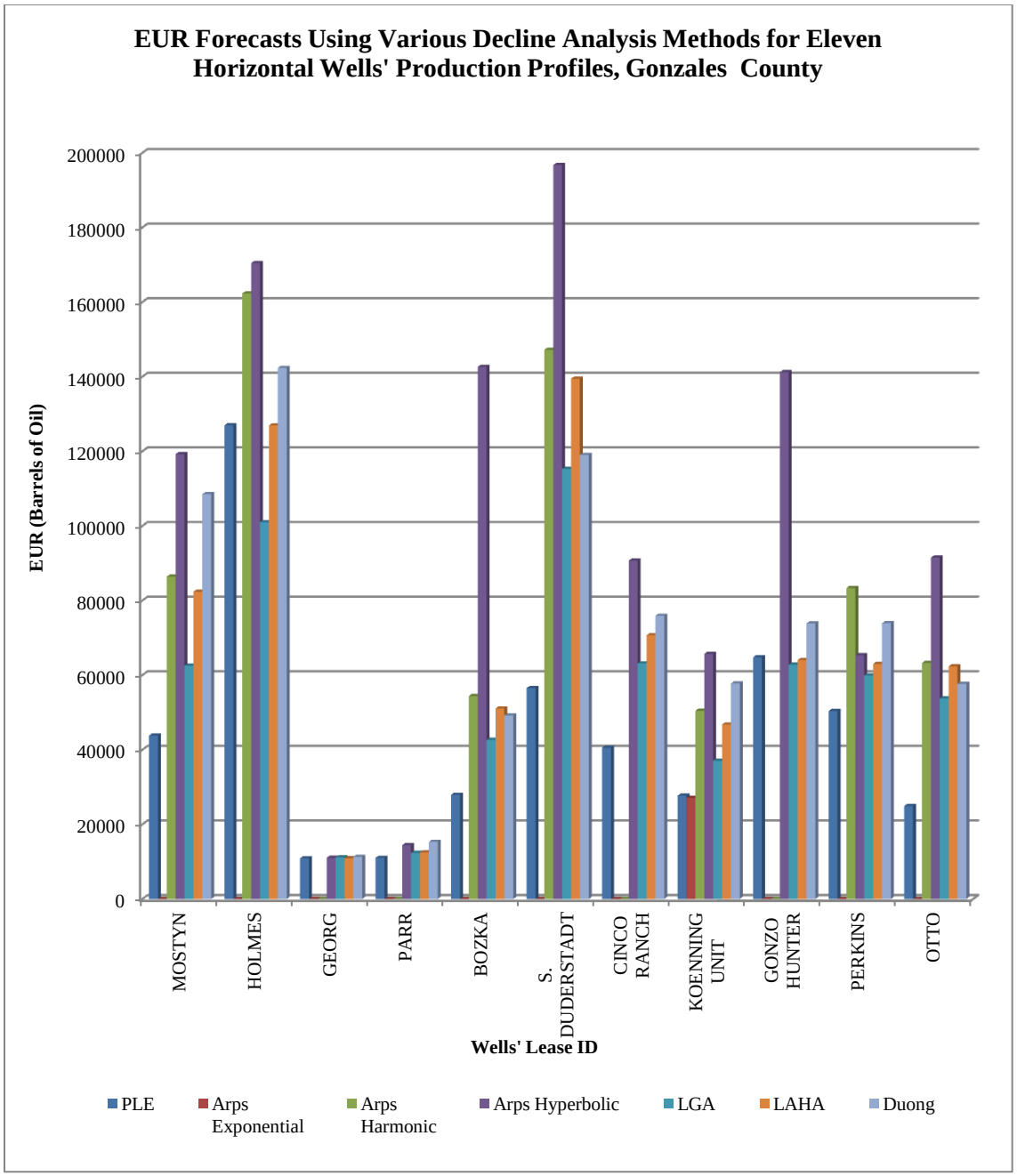

Figure 4.17: EUR generated for eleven horizontal wells' production profiles in Gonzales County.

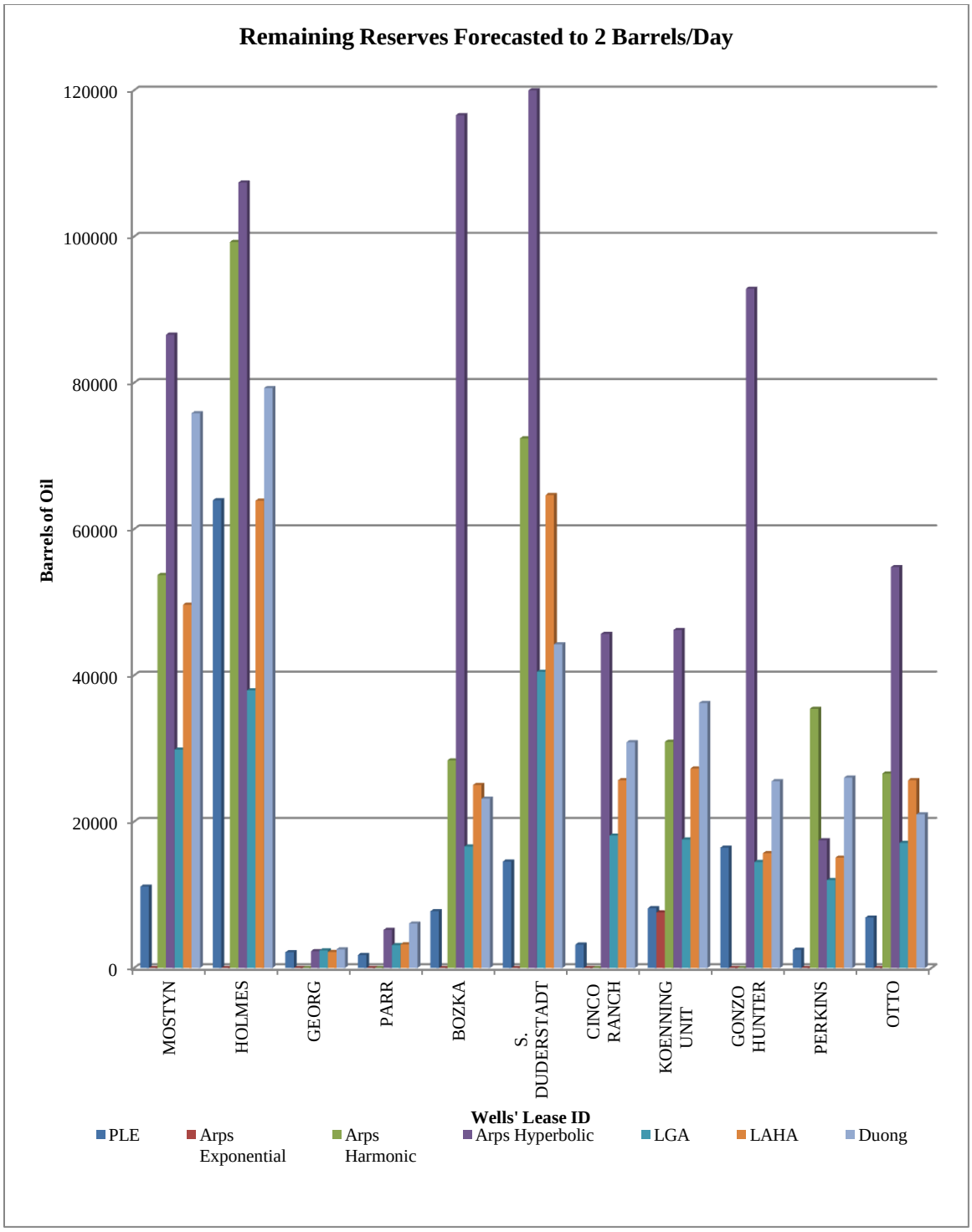

Figure 4.18: Remaining reserve forecasts for eleven production profiles in Gonzales County.

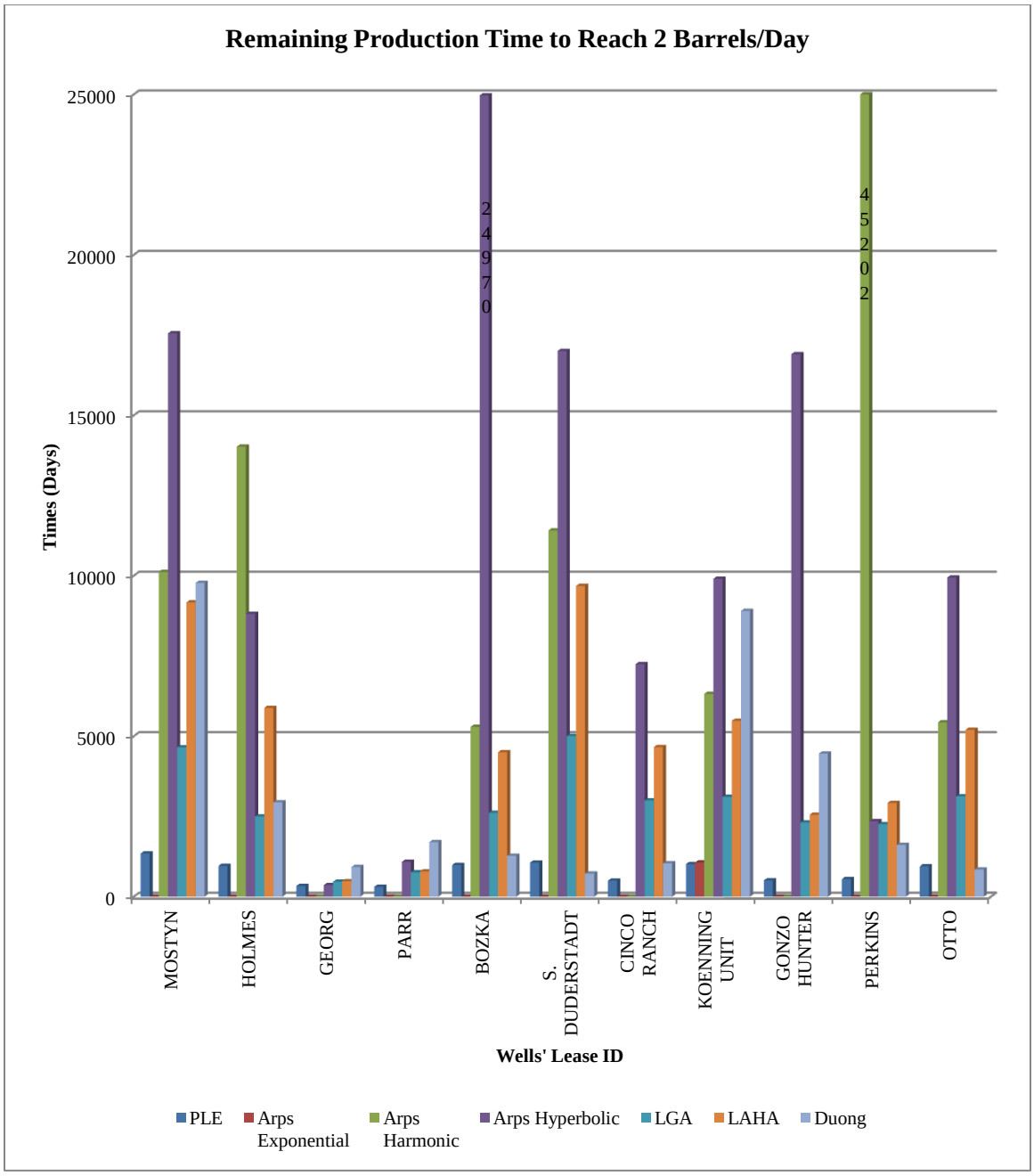

Figure 4.19: Remaining production life to reach 2 barrels/day for 11 wells in Gonzales County.

4.6 Karnes County

4.6.1 Introduction

Karnes County is approximately 50 miles southeast of San Antonio in one of the prolific hydrocarbon zones of the Eagle Ford Shale play. It has all three thermal maturity windows: liquid, condensate and dry gas. Supposedly, wells producing more than 1000 barrels/day are located here, but such information cannot be confirmed through the publicly available database on the TRRC website.

Ten oil production profiles were retrieved from the TRRC website. The wells' lease names are Berry, Coates "A", Muenchow Unit, Cannon, Brysch Jonas, Kathryn Kealey, CEF, Gilley Unit, Yosko Unit, and Carter Unit. Available wells' completion and production data are summarized in **Table 4.6**.

Table 4.6: Karnes County wells' completion and production history

County	Well Name	Completion date & Recompleted date	Depth (ft) MD /TVD	Horizontal length (ft)	Number of fracture stages	Producing life until now (Months)	Initial rate (Barrels/day)	Cumulative production (Barrels)	Current rate (Barrels/day)
Karnes	BERRY	12/5/2010	16752 / 12078	4166	10	26	515.4	128040	13.1
	COATES	1/28/2011	15610 / 9707	5550	20	26	317	110478	59.3
	MUENCHOW UNIT	6/20/2011	15767 / 10943	4397	12	20	502	45621	21
	CANNON	4/3/2011	17105 / 11900	5120	n/a	24	507	179226	151
	BRYSCH JONAS UNIT	08/03/2011 & 03/26/2012	18540 / 12158	6141	20	19	567.8	120058	118.3
	KATHRYN KEALEY UNIT	Not Available	Not availa-ble	Not avail a-ble	Not avai-lable	24	324.5	125725	72.9
	CEF	6/28/2011	16652 / 11095	5564	Not avai-lable	20	547.7	150377	248.8
	GILLEY UNIT	5/4/2011	16969 / 12144	919	Not avai-lable	22	56.4	28923	18.4
	YOSKO UNIT	4/8/2011	17335 / 12200	5010	Not avai-lable	22	741.8	166501	94.6
	CARTER UNIT	6/13/2011	16878 / 5864	4343	Not avai-lable	21	666	95695	110.3

4.6.2 Specific Results of Shale Oil Production Decline Analysis in Karnes County

Figure 4.20 shows a great disparity in the initial production rate for the various profiles for the various horizontal wells in this county. With the exception of Yosko, Gilley, and Muenchow Unit wells, the production profiles are very erratic.

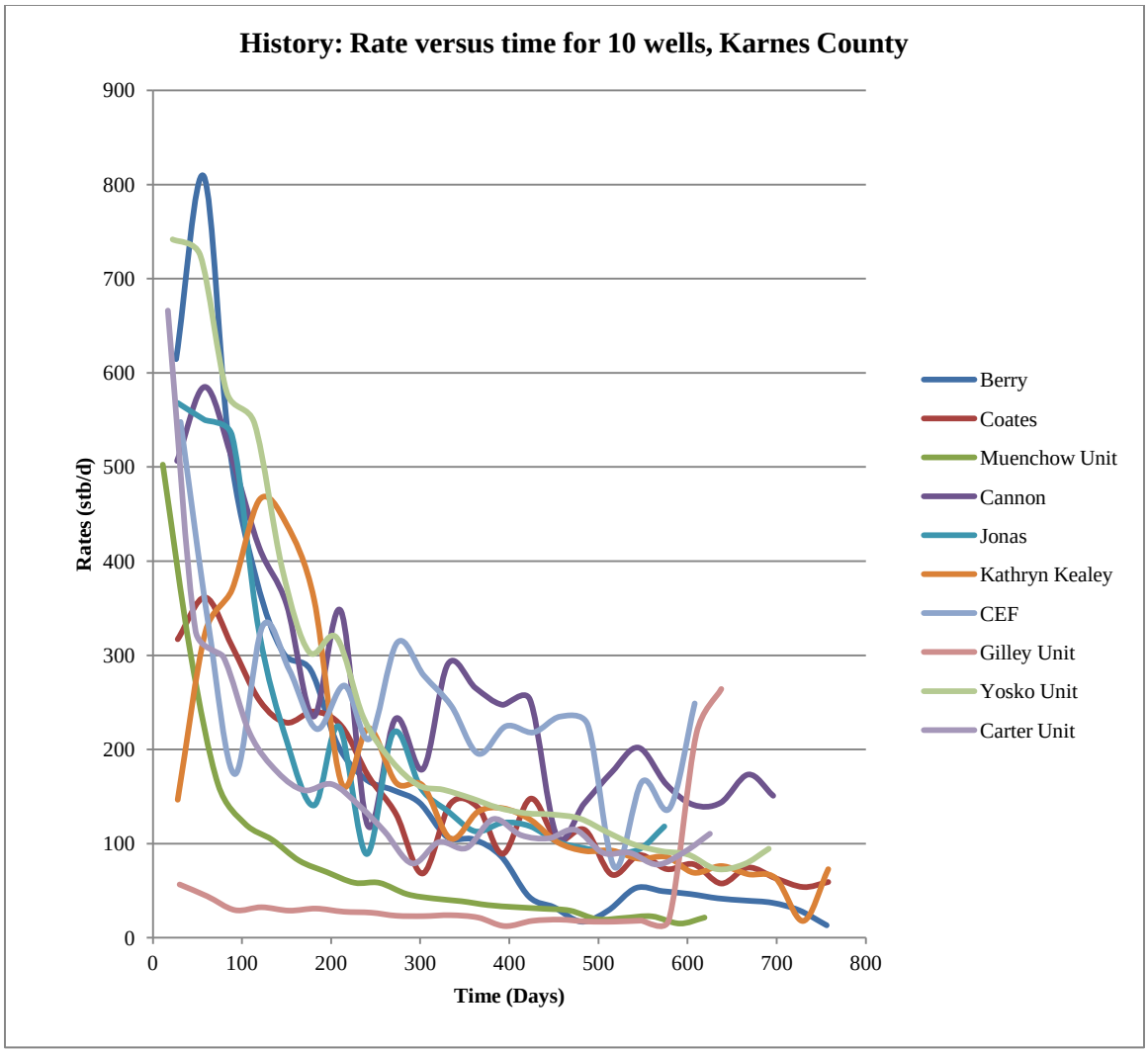

Figure 4.20: Profile of Karnes County wells' production history.

The results of the ten production profiles analyzed by the various decline models are presented in **Figures 4.21-4.23** and **Appendix Table A.2**. From these results the following comments can be made:

1. The PLE did apply to the production profile of all wells' production profiles in this county at the $R^2 \geq 0.97$ acceptance level. The EUR and production forecasts are still low compared to the other models.

2. Arps' exponential decline modeled the Kathryn Kealey well's production profile only. Its forecast was not very different from that of the PLE.
3. Arps' harmonic diagnostic proofs were obtained only for Muenchow, Kathryn Kealey and Yosko Unit wells.
4. CEF well future production performance are extremely high with Arps' hyperbolic techniques because the decline exponent, b=3.05, is greater than unity. In this instance, the PLE and LGA results seem reasonable to use because the EUR and production forecasts generated by the other models are all erroneously high. A close look at the original data suggests that the erratic nature of the production trend, which is difficult to filter, may be the reason for the associated problems analyzing its decline and estimating reserves.
5. The LGA model had very decent history matches in all cases, producing reasonable values of EUR, remaining reserves, and time to reach 2 barrels/day compared to the other models.
6. Duong's method does not have good history matches, but its forecasts are comparable to those of the other models in most cases. In some cases, positive values of q_{∞}, greater than the abandonment rate of 2 barrels/day, predicted excessively long times to reach abandonment.
7. LAHA adjusted the EUR obtained for Arps' hyperbolic with abnormal decline exponents that are by to 0.5 higher than b=1. LAHA could not sufficiently reduce decline exponent values greater than b=1.5. The production trends of most of the wells (Cannon, Brysch Jones, CEF, and Carter Units) do not follow reasonable decline trends; with or without data filtering, neither Arps' hyperbolic nor LAHA predict future performances

accurately. It is my guess that the production profiles reported for these wells individually may instead have multiple producers.

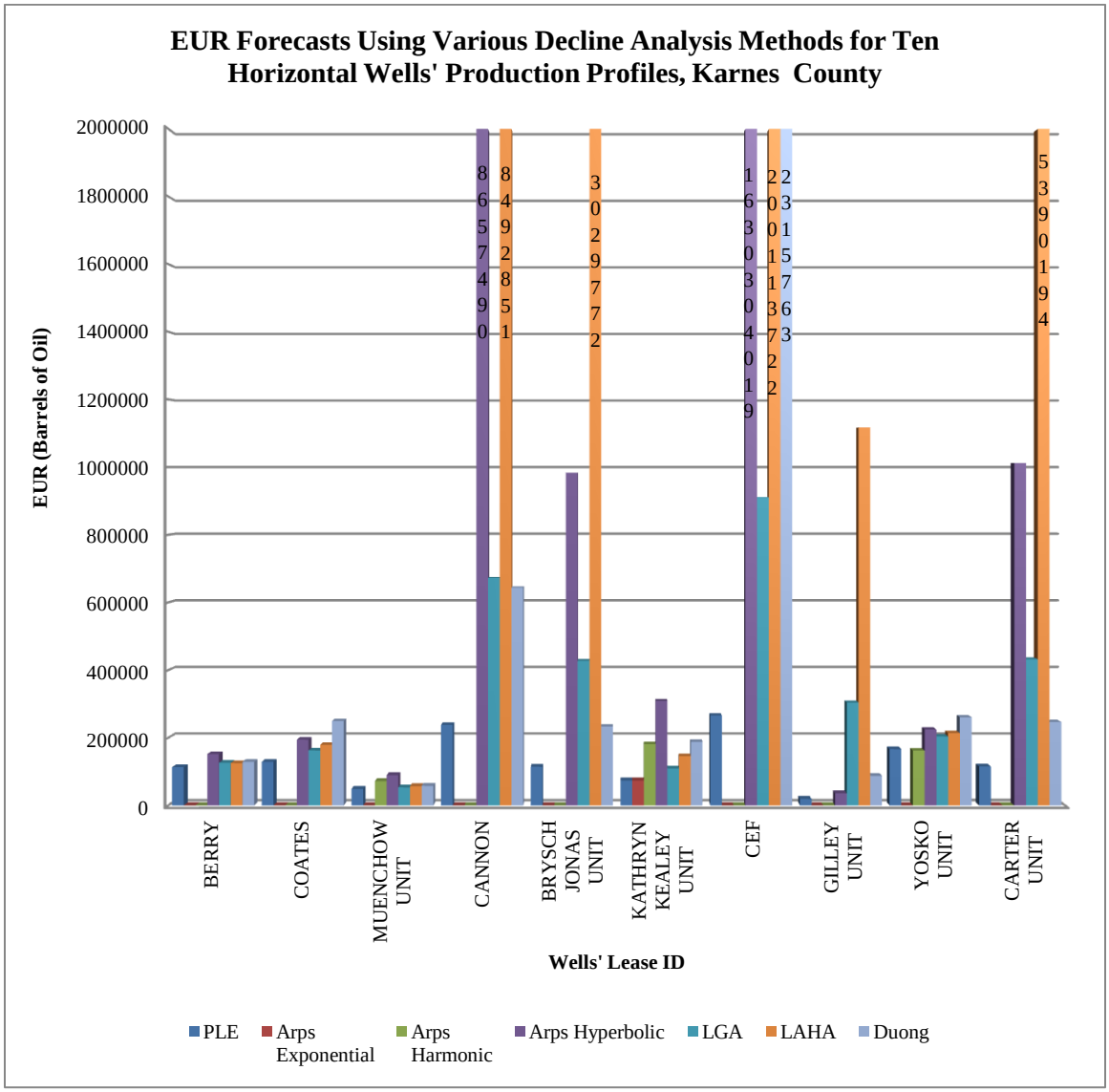

Figure 4.21: EUR generated for ten horizontal wells' production profile in Karnes County.

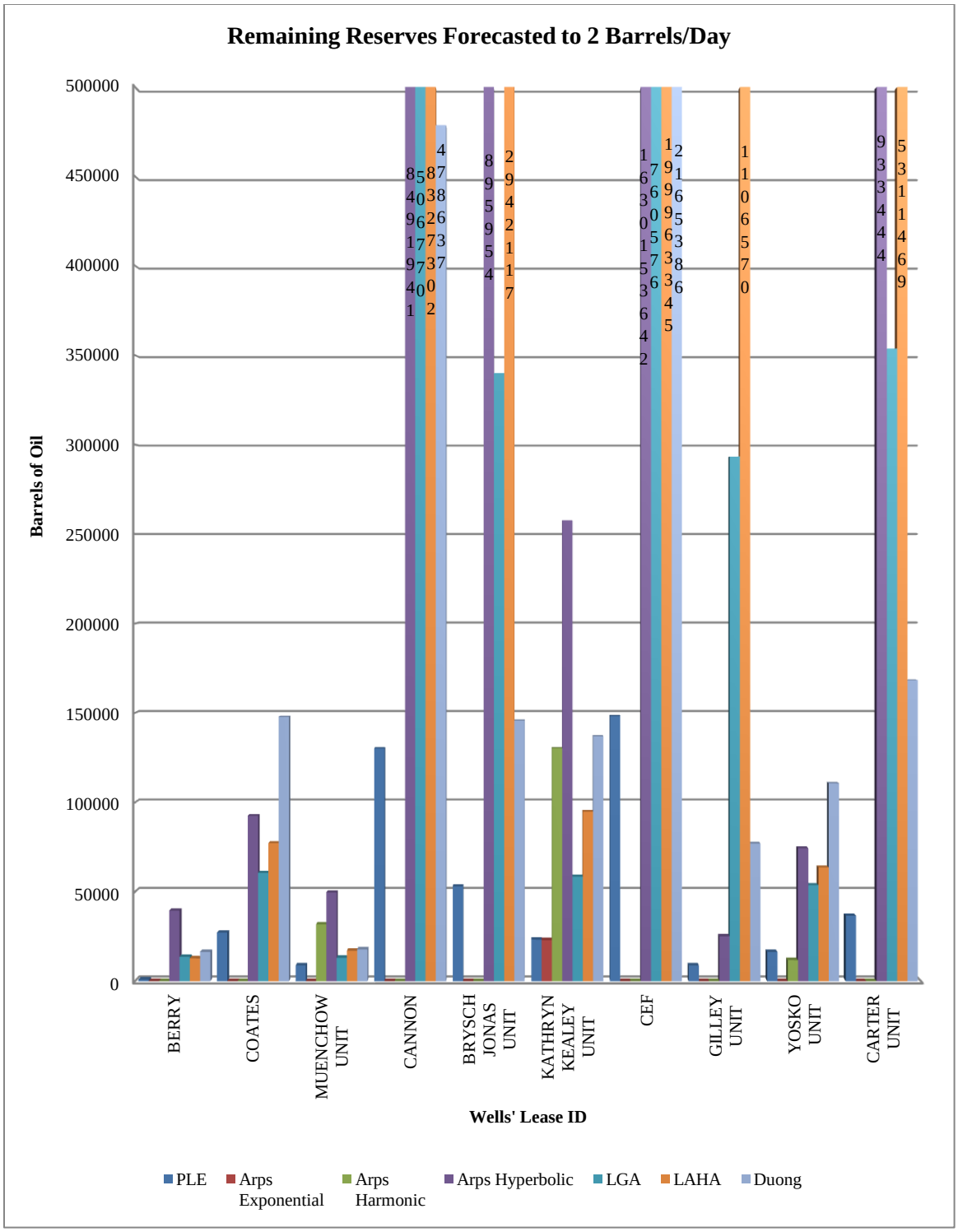

Figure 4.22: Remaining reserve forecasts for ten production profiles in Karnes County.

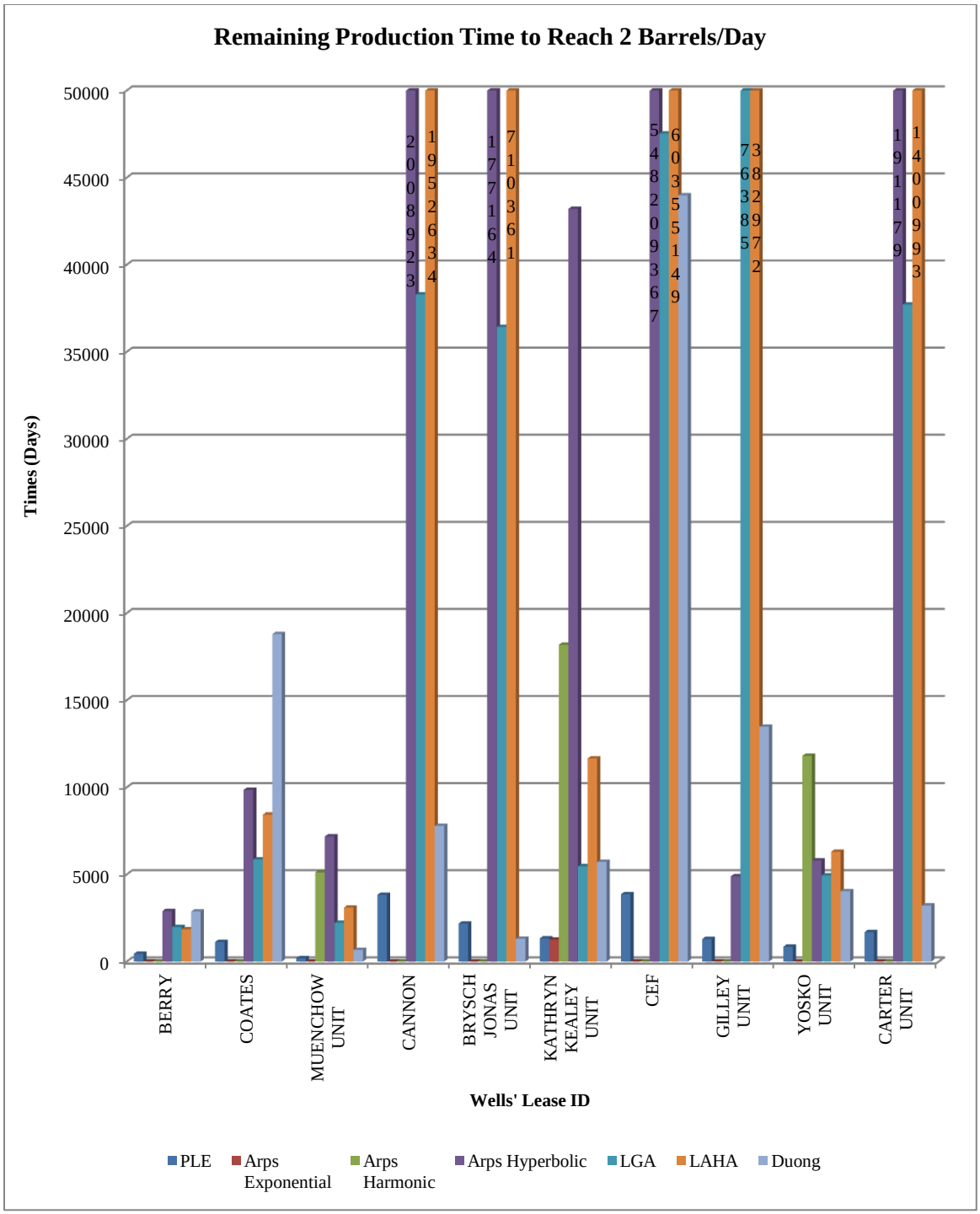

Figure 4.23: Remaining production life to reach 2 barrels/day for ten wells in Karnes County.

4.7 Dimmit County

4.7.1 Introduction

Located in the southern segment of the Eagle Ford Shale formation, Dimmit County is situated in oil-prone and condensate-rich zones of the play. Production profiles of horizontal wells in the Hutch, Voltz Unit, Fog Mount and JBGS leases are available for analysis from the TRRC public webpage. Available statistics of these wells, including completion date, initial and current rates, and cumulative oil production are presented in **Table 4.7**.

Table 4.7: Dimmit County wells' completion and production history

County	Well Name	Completion date & Recompleted date	Depth (ft) MD /TVD	Horizontal length (ft)	Number of fracture stages	Producing life until now (Months)	Initial rate (Barrels/day)	Cumulative production (Barrels)	Current rate (Barrels/day)
Dimmit	HATCH	3/16/2010	11405 / 7292	3789	17	36	217.1	63219	22.4
	VOTLZ UNIT	12/25/2010	13597 / 6948	Not availa-ble	Not availa-ble	24	120	33024	19
	FOG MOUN T	09/06/2010 & 01/15/2011	12275 / 6058	3145	Not availa-ble	26	99.9	35376	22.1
	JBGS	10/13/2010	13820 / 6782	Not availa-ble	Not availa-ble	25	77.1	62743	33.5

4.7.2 Specific Results of Shale Oil Production Decline Analysis in Dimmit County

Figure 4.24 shows the rate profile histories for the four horizontal wells. The similarity of the profiles for the Voltz and Fog Mount wells may be an indication of similar petrophysical

characteristics or completion technique. The JBGS well's production profile is very erratic, especially at early-time performance stages.

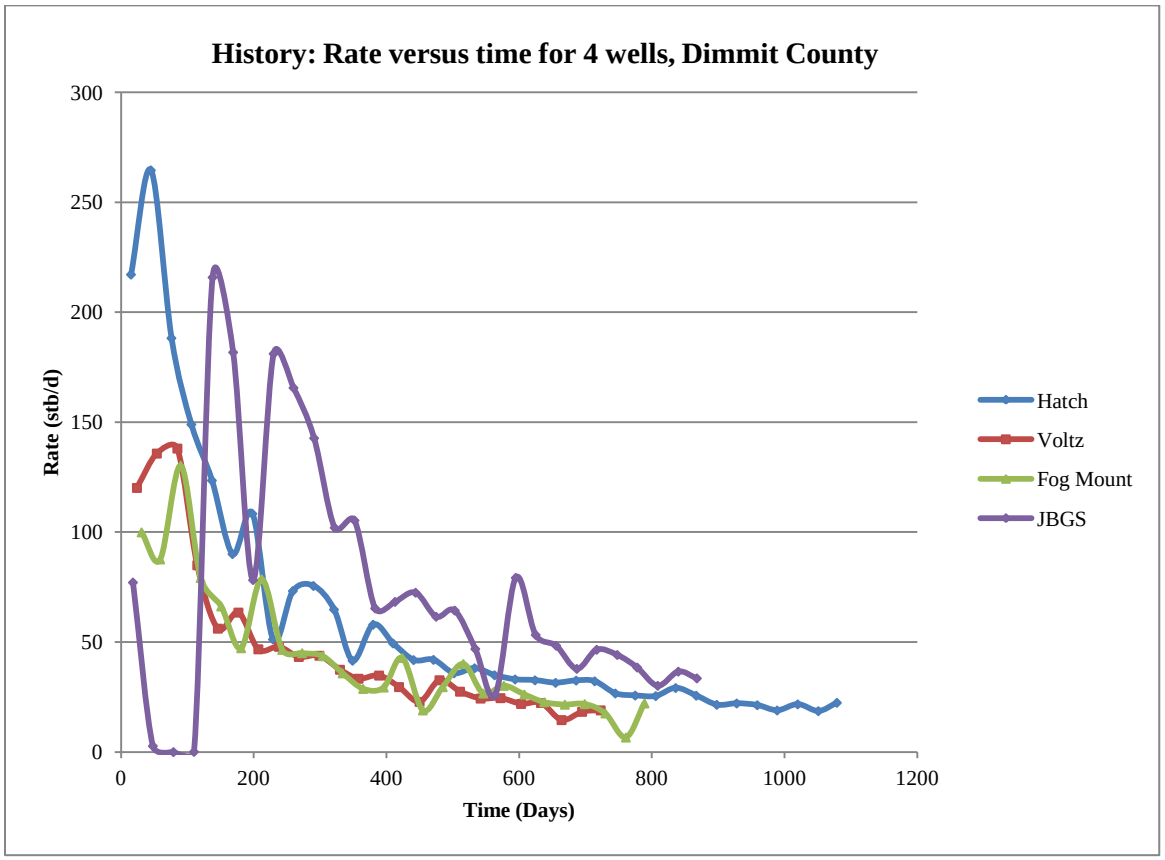

Figure 4.24: Profile of Dimmit County wells' production history.

PLE results are the least for each lease; Arps' hyperbolic and Duong's method share the highest predicted future performance and reserves (**Figures 4.25-4.27, Appendix Tables 2)**. Arps' hyperbolic projected high EUR, remaining reserves and abandonment time for the Fog Mount well, due to excess b=1.76 >1. Arps' exponential cannot model any of the production profiles, and Arps' harmonic was applied to the Hutch lease well only.

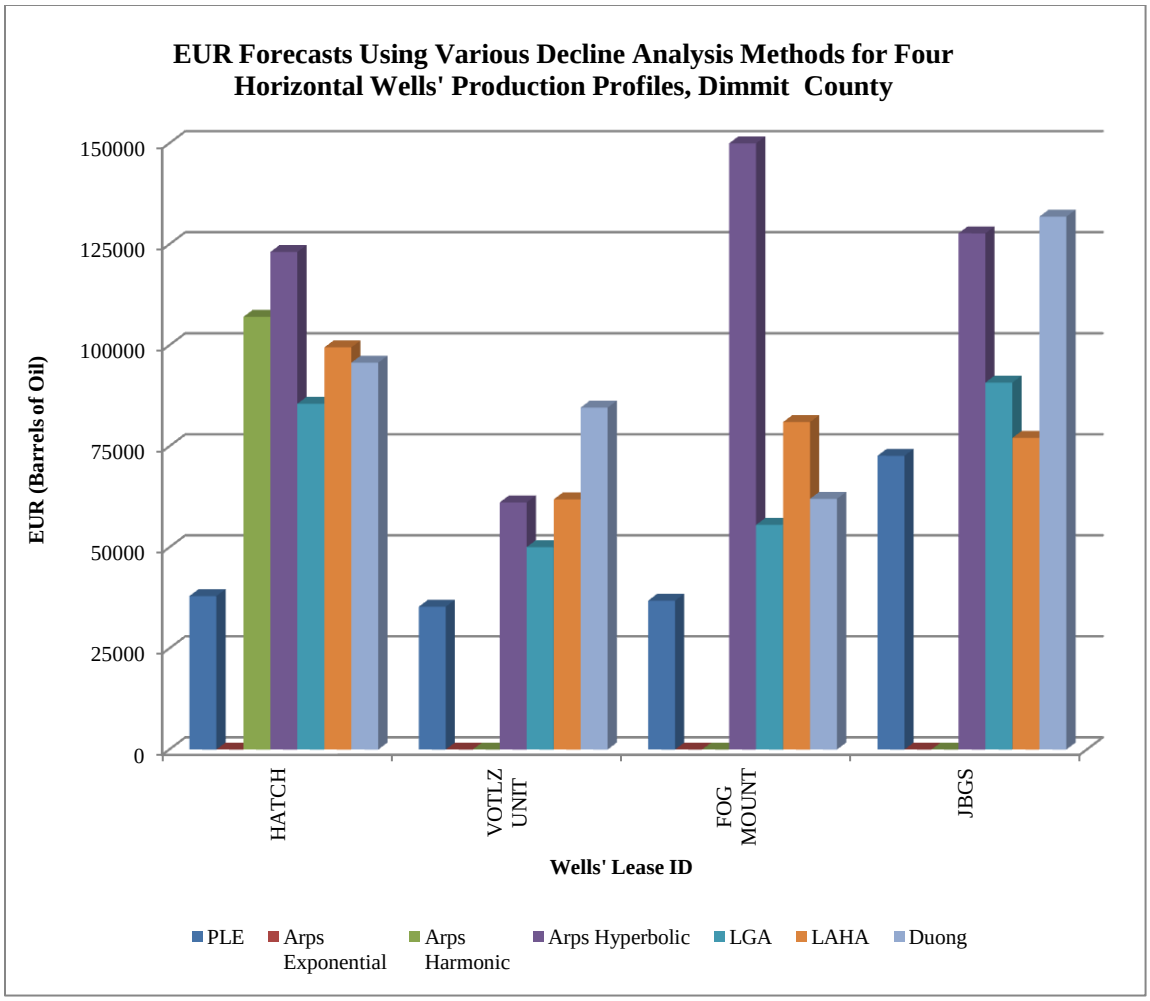

Figure 4.25: EUR generated for four horizontal wells' production profiles in Dimmit County.

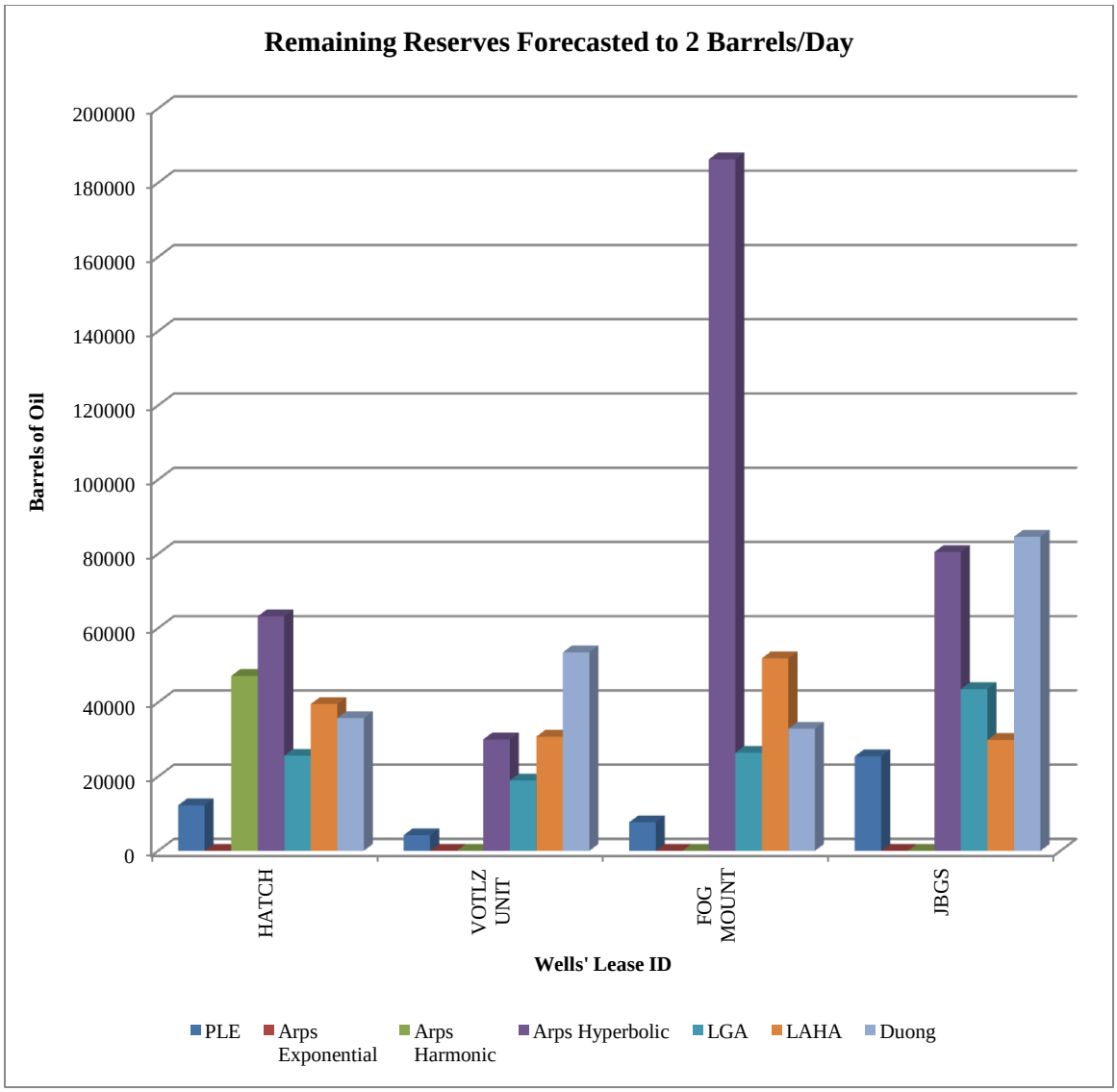

Figure 4.26: Remaining reserve forecasts for four production profiles in Dimmit County.

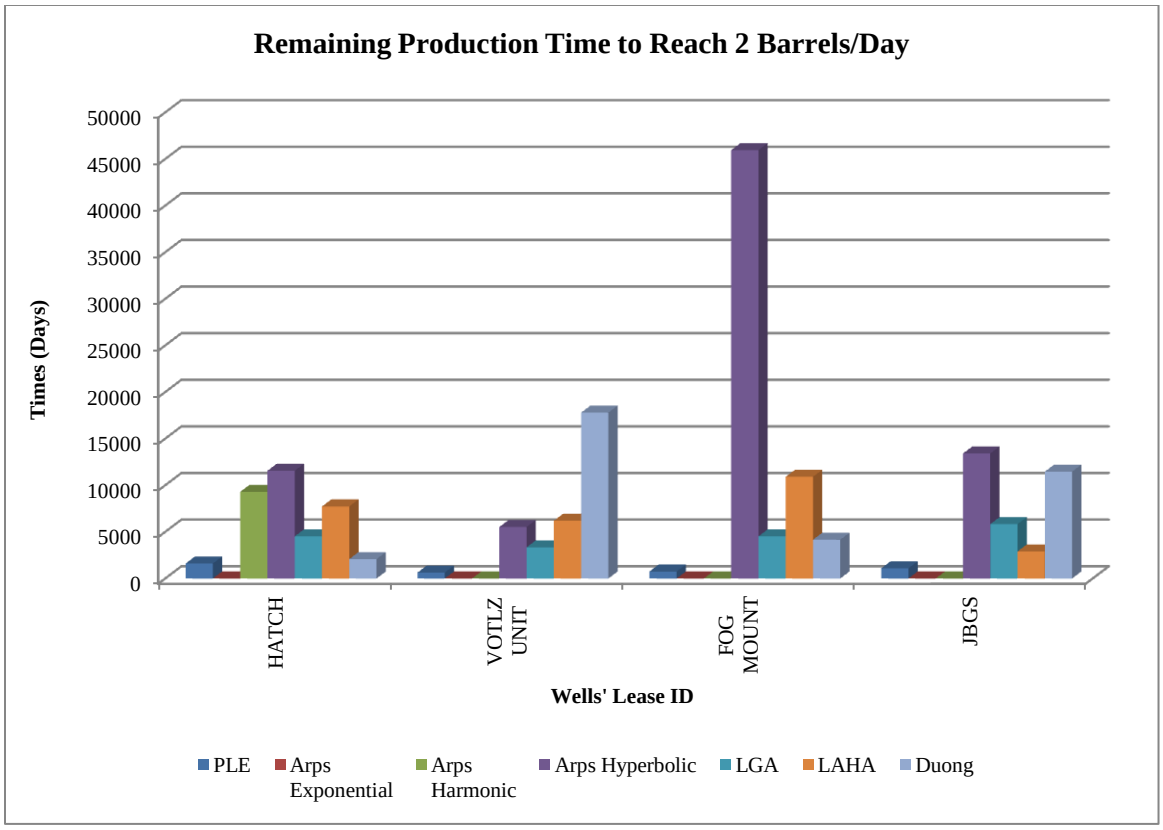

Figure 4.27: Remaining production life to reach 2 barrels/day for four wells in Dimmit County.

4.8 Zavala County

4.8.1 Introduction

Zavala County shares boundaries with Dimmit County. It is situated mainly in the oil generation thermal window of the Eagle Ford play. A total of six wells' production profiles were investigated. The wells' lease names are K.M. Ranch, Mustang Ranch C, Alpha Ware, Felps, Howett and Addison Avery. Available information about these wells is summarized in **Table 4.8** below.

Table 4.8: Zavala County wells' completion and production history

County	Well Name	Completion date & Recompleted date	Depth (ft) MD /TVD	Horizontal length (ft)	Number of fracture stages	Producing life until now (Months)	Initial rate (Barrels/day)	Cumulative production (Barrels)	Current rate (Barrels/day)
Zavala	K.M RANCH	6/27/2011 & 08/08/2012	12627 / 6587	5758	Not avail a-ble	20	577	55503	91.5
	MUSTANG RANCH C	6/30/2010	11684 / 5573	5824	22	29	117.2	57848	55.8
	ALPHA WARE	7/5/2011	11800 / 5693	5458	21	20	247.2	42606	34.2
	FELPS	6/1/2011	9723 / 5616	4717	15	21	111.8	41336	44.8
	HOWETT	10/16/2011	11007 / 6535	3870	Not avail a-ble	17	101.1	52740	51.8
	ADDISON AVERY	4/27/2011	9435 / 5290	4162	12	26	93.5	30768	21.1

4.8.2 Specific Results of Shale Oil Production Decline Analysis in Zavala County

Figure 4.28 shows the rate profiles of all six wells. The K.M Ranch shows two episodes of high initial production, most likely due to recompletion of the well. The Alpha Ware, Mustang Ranch, Felps, and Addison Avery production profiles show established sections of reasonable decline trends.

Six production profiles assessed with the decline models have their results presented in **Figures 4.29-4.31** and **Appendix Table A.2**. From the analyses, the following comments can be made:

1. PLE predictions again forecasted the lowest EUR, remaining reserves, and time to reach 2 barrels/day in all six cases.

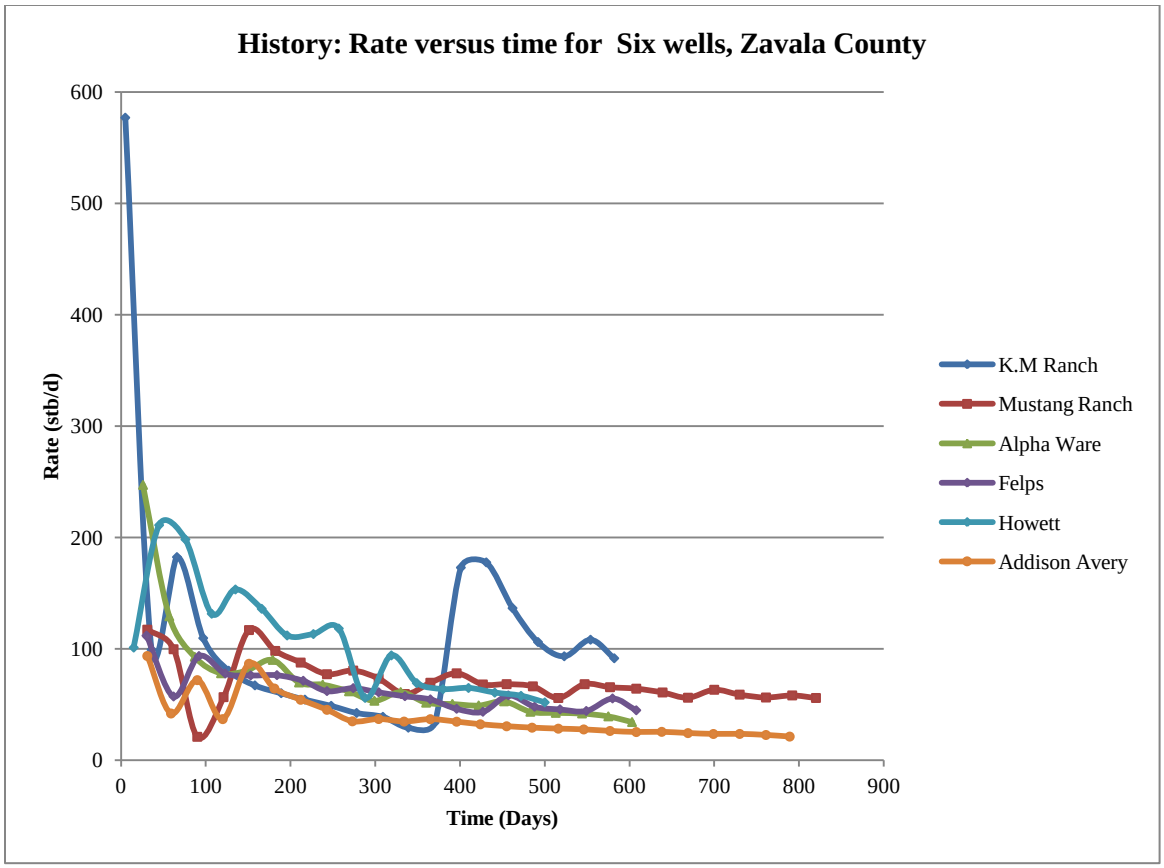

Figure 4.28: Profile of Zavala County wells' production history.

2. Arps' exponential decline modeling of Addison Avery well's production profile calculated a similar EUR value to those calculated by the PLE, hyperbolic, and the LGA models.
3. Arps' harmonic predictions apply to the K.M Ranch and Addison Avery wells only. It estimated results comparable to those of the other models.
4. Two severe cases of high predictions were observed for the Mustang Ranch C and Alpha Ware wells due to high decline exponent values of b=4.50 and b=1.99, respectively. This could come as a result of changing operating conditions. The profiles are difficult to filter without eliminating all data.

5. Duong's method has fairly high production predictions for the Felps, Howett, and Addison Avery wells, because the diagnostic plots of **Equation 3.10** fail to pass through the origins.
6. LAHA reduced the exaggerated values of Arps' hyperbolic decline model when b>1.

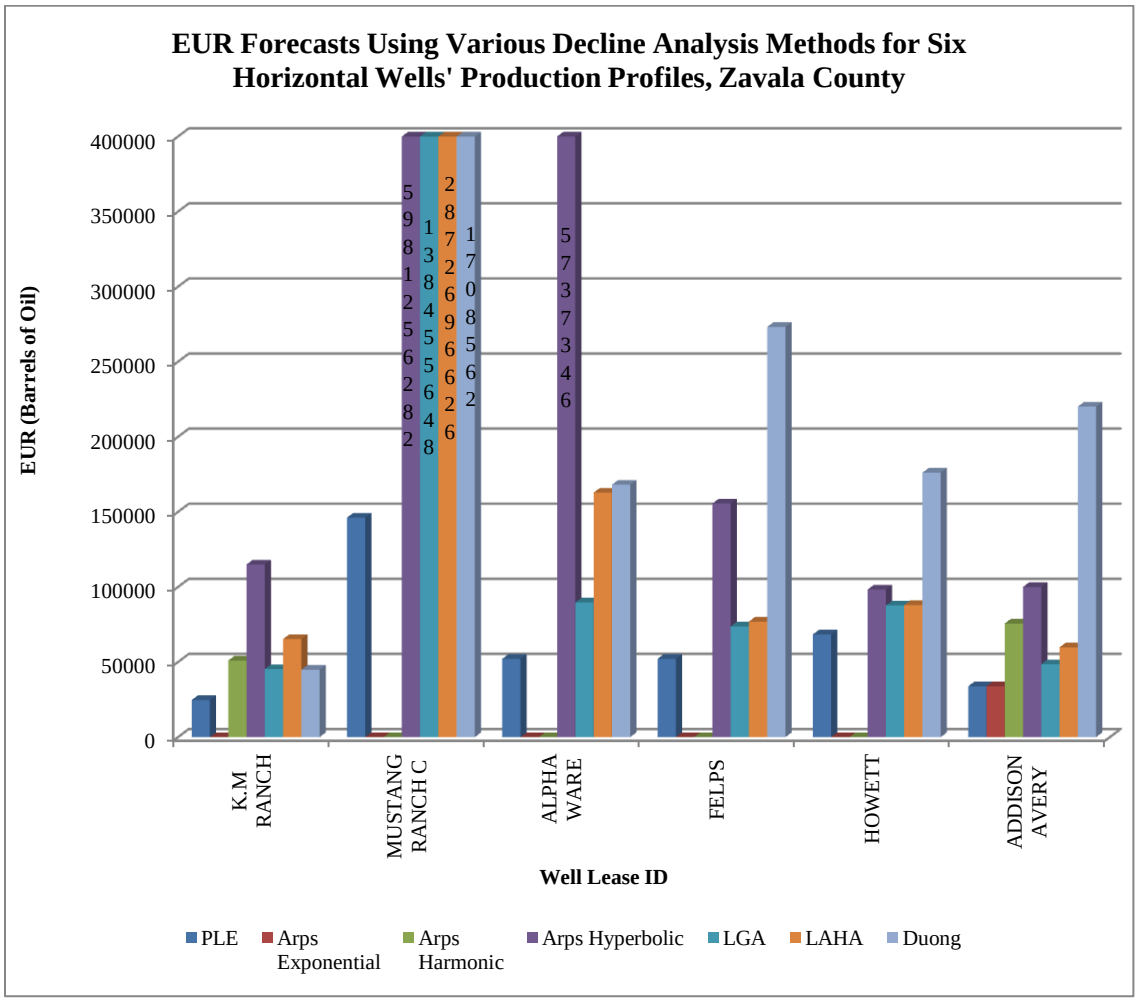

Figure 4.29: EUR generated for six horizontal wells' production profiles in Zavala County.

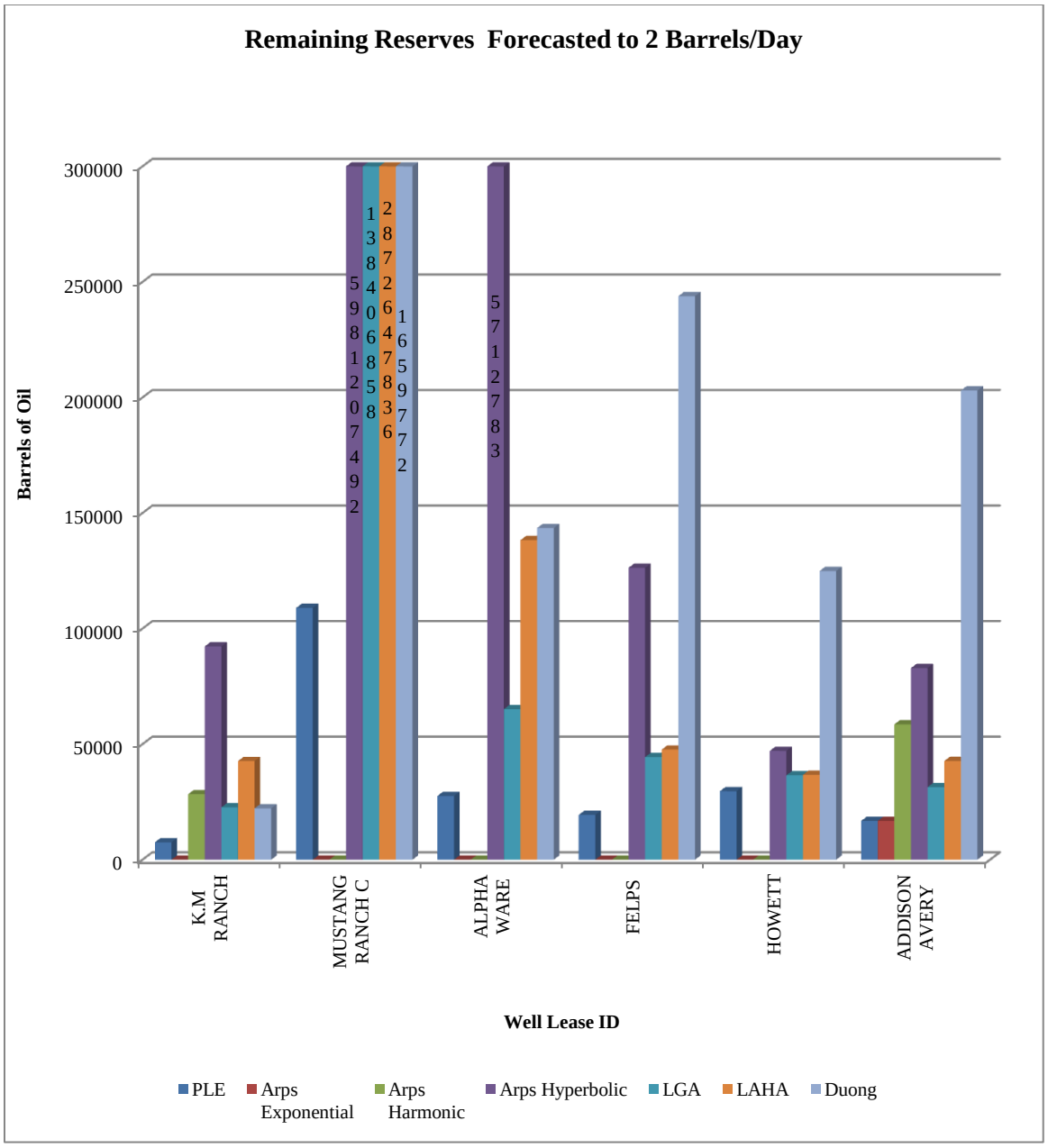

Figure 4.30: Remaining reserve forecasts for six production profiles in Zavala County.

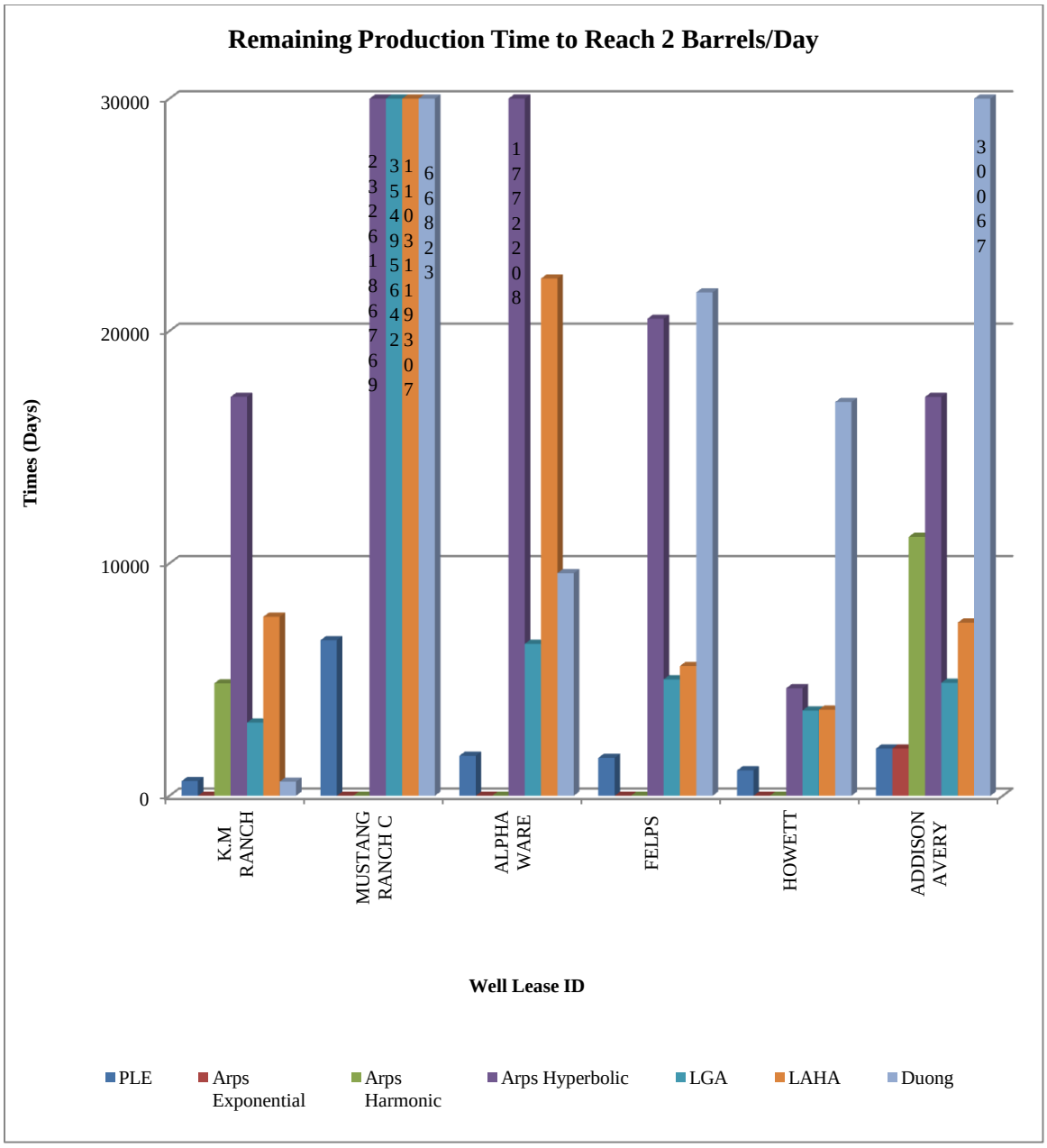

Figure 4.31: Remaining production life to reach 2 barrels/day for six wells in Zavala County.

4.9 Chapter Summary

The observations in this chapter about the individual wells and their respective counties do not suggest any commonality for the production performance of the horizontal wells. The production data analyses results are very unique for each well. A few of the wells in the same county have similar past production trends; this is a good indication for similar shale mineralogy and completion design that can only be confirmed if petrophysical data and completion statistics of the wells are available. The expected ultimate recoveries, remaining reserves and the lifespan of the individual wells indicate wide variability of shale oil distribution within the play. The average initial rates for producing hydraulically fractured horizontal wells show vast disparity from county to county. The Karnes county wells have consistently reported the highest initial production rates for its individual producing wells and may be identified as the most liquid prolific county. For the other counties, the average initial rates are relatively low due to huge rate gaps between the individual wells. These same trends are noticeable in the overall estimates for total recoverable reserves, which indicate the relative liquid hydrocarbon richness among the counties.

Chapter 5 Shale Oil Reservoir Simulations

5.0 Introduction

Numerical Simulation Model (NSM) analysis of all forty horizontal wells could not be done due to insufficient data available, since the reliability of simulation output depends on quality and quantity of wells' and reservoirs' input data. As a consequence, only two Eagle Ford Shale (EFS) wells were simulated for production performance history matching and cumulative production forecast. Future productions forecasted by NSM were compared with the analytical results for these two wells. The chapter also included enhanced shale oil recovery (ESOR) using different configurations of producers and injectors with the reservoir model and parameters of one of the wells that was history matched. The ESOR covers the miscible gas injection displacement processes by CO_2, 1:1 mixture of CO_2-CH_4, and an enriched gas mixture. The injectant methane (CH_4) was also initially considered, but due to low reservoir pressure, it turned out rather as an immiscible gas displacement process.

History matching the production data for each well began with reservoir parameters modification within an acceptable range of values reported in the literature (Chaudhary, 2011 and Orangi et al., 2011). The properties modified include fracture density, porosity, and permeability, matrix porosity and permeability, relative permeability curve end points and Corey exponents, critical and residual saturations, and initial liquid saturations and pressures. The early part of each well's performance was dominated by fracture fluid loading and linear flow regimes, so the remarkably sensitive parameters of primary fracture geometry, porosity, and permeability were modified in order to model and history-match the initial high oil rate. On the other hand, the matrix parameters were adjusted until a match was obtained for the later low rates. It should be noted

that the use of generalized reservoir parameters from the literature and their further adjustment, during the history matching for the very short production periods of the EFS, subject the outcomes to high degrees of uncertainty.

The simulation also covers assessment of pressure waves and hydrocarbon fluids withdrawal from non-stimulated reservoir lease zones adjacent to stimulated reservoir areas. Assuming any shale oil reservoir, pressure depletion was simulated to investigate the extent hydrocarbon fluids withdrawal goes beyond the geometric confines of the simulated reservoir volume.

5.1 Methods: Production Decline and Future Performance Simulations

5.1.1 Building the Reservoir Simulation Models

Two single-well simulation models were built using the data provided earlier **(Table 2.4)** using the Gilman and Kazemi dual permeability option in CMG (GEM) software. Initial reservoir model parameters were based on the knowledge of 3-10% range and an average of 6% porosity, matrix permeability, water saturation, compressibility, reservoir temperature and pressure values quoted in **Tables 2.1** through **2.3**. Eagle Ford Shale synthetic crude compositional model, developed based on the Peng-Robinson equation of state (EOS) by Orangi et al. (2011), was incorporated into CMG Winprop. The gas-oil ratio (GOR) is 500 scf/stb and API gravity of 41^{o} for the compositional model. Subsequently, Two-phase P-T diagram and pressure-dependent phase properties were generated.

Formation volume factor (FVF) of the Eagle Ford Shale, as in **Figure 2.5,** provided by Orangi et al., (2011) was also used to perform reservoir fluid analysis using Winprop. Corresponding pressure-volume-temperature (PVT) values and diagrams at initial composition were generated

by CMG software. A compositional model was used, meaning that the simulator calculated all phase properties at any pressure for any cell using the given initial oil/gas phase composition.

Using Winprop, the minimum miscibility pressure (MMP) for multiple contacts miscibility (MCM) for CO_2 gas, methane, CO_2-CH_4 gas mixtures, and enriched gas mixtures that would be injected for miscible displacement of EFS oil were analyzed.

The tuned-up EOS model of the EFS crude was incorporated into the Builder-GEM, CMG Compositional Software, to build the individual single-well, dual-permeability models needed to simulate horizontal wells of the Giesenschlag-Groce and Hutch leases.

Stimulated reservoirs of two horizontal wells were modeled using researched data summarized below in **Tables 5.1** and **5.2**. **Table 5.2** includes the initial and final reservoir model parameters, literature reviewed and history matched respectively. These two wells, Giesenschlag-Groce and Hutch, have been previously analyzed with empirical decline models in **Chapter 4.** They have been stimulated with 18 and 17 perforations respectively. The models have initial water saturation of 30%. The relative permeability parameters used were provided by Chaudhary (2011) and Orangi et al. (2011) presented in **Chapter 2** (**Tables 2.4** and **2.5**). By sensitivity analysis, the reservoir model parameters were modified until the wells' production histories were matched.
History matching, future production trends, and potential miscible gas injection displacement for enhanced shale oil recovery (ESOR) were modeled and simulated using the Hutch well past performance data. The Giesenschlag-Groce well was only simulated for history matching and generating future production curves. The wells' numerical simulation models estimated future

production to abandonment at 2 stb/d and these were compared with the analytical decline models results in **Chapter 4.**

Table 5.1: Reservoir fluids, depths, lateral lengths and stimulation data (from www.rrc.state.tx.us June 10, 2012)

County/ Well	**Top (TVD) (ft)**	**Depth (TVD) (ft)**	**Height (ft)**	**Lateral Length (ft)**	**Fracture Interval (MD)**	**Thickness Interval (ft)**	**Fracture Stages**	**GOR (scf/stb)**	**API**	**Acres**
Burleson Giesenschlag-Groce	8877	9016	139	3640	9780-13420	8877-9016	Not available	510	42.1	459
Dimmit Hatch	7145	7292	147	3694	7616-11310	Not available	17	506	36	3489

Table 5.2: Initial and final reservoir model parameters of the Eagle Ford Shale (EFS)

Reservoir and Hydraulic Fracture Parameters	Burleson County Well		Dimmit County Well	
	Initial	Final	Initial	Final
Matrix porosity (fraction)- Variable	0.1	0.04	0.1	0.05
Natural fracture porosity (fraction)- Variable	0.001	0.001	0.001	0.001
Shale Matrix Absolute Permeability (md) by History Matching- Variable	0.0001	0.00009	0.0001	0.0001
Natural Fracture Permeability (md) by History Matching- Variable	0.001	0.0004	0.001	0.0007
Hydraulic Fracture Permeability (md) calculated from given conductivity	83300		83300	
Hydraulic Fracture Spacing (ft)	200		220	
Hydraulic Fracture Half Length (ft) by	500		500	
Hydraulic Fracture Width (ft)	0.001		0.001	
Hydraulic Fracture Conductivity (md-ft)	83.3		83.3	
Hydraulic Fracture Stages	18		17	
Reservoir Thickness (ft) from TRRC website	139		147	
Shale Compressibility (1/psi)	5.00E-06		5.00E-06	
Initial Water Saturation	0.3		0.3	
Initial Reservoir Pressure (psi)	3800		3200	
Reservoir Temperature (deg. F)	241		212	

5.1.2 The Reservoir Simulation Initialization Outputs

A two-phase P-T (pressure-temperature) diagram was obtained for the compositional model of the Eagle Ford synthetic crude oil and presented in **Figure 5.1**. It shows the critical point where oil and gas phases coexist in equilibrium, and the enclosure of the 2-phase boundary is the phase envelope, where proportionate amounts of oil and gas mixtures exist. The critical pressure and temperature are 1500 psia and 800 ^{o}F respectively. The cricondentherm and the cricondenbar are 895^{o}F and 2280 psia, respectively.

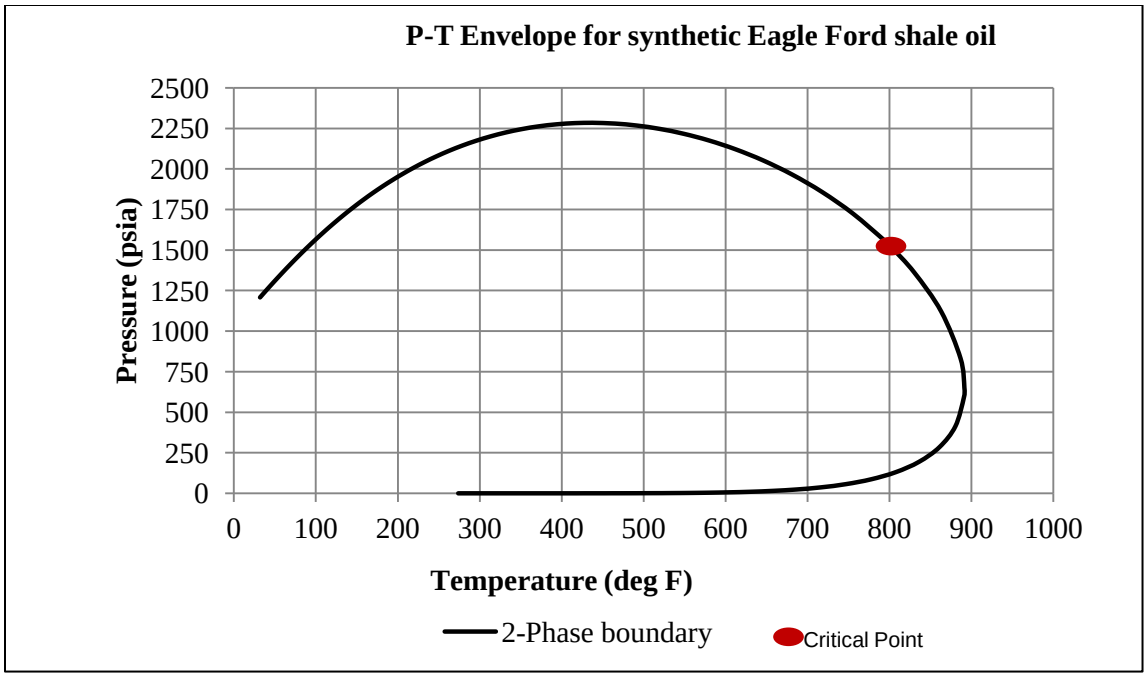

Figure 5.1: Two-Phase P-T envelope of the synthetic Eagle Ford Shale oil.

Winprop also analyzed and generated other pressure-temperature dependent phase properties associated with the analysis of the synthetic Eagle Ford Shale (EFS) crude include liquid and vapor (gas) phase and are presented in **Figures 5.2- 5.5**. These include liquid and vapor volumes versus pressure curves **Figures 5.2** and **5.3**, illustrating liquid and vapor saturations before and after the bubble point pressure of 2054.85 psia. Also, **Figure 5.4** is the plot of gas compressibility with pressure showing increasing gas compressibility at reduced pressures below the saturation pressure of 2054.85 psia. Finally, **Figure 5.5** is the vapor liquid equilibrium (VLE) ratio alterations with pressure for the different components of the EFS synthetic crude. The compositions shown in the legend are those of the EFS synthetic crude (**Table 2.4)**. Equilibrium ratios are very important in compositional model reservoir simulations for the calculation of the vapor and liquid equilibrium composition at various reservoir pressure-temperature (PT) flash

conditions. **Figure 5.5** separates the highly volatile and the non-volatile components of the EFS synthetic crude. It also helps to explain the preference of CO_2, CH_4 and the enriched gas mixtures as the best miscible displacement injectant in enhanced shale oil recovery.

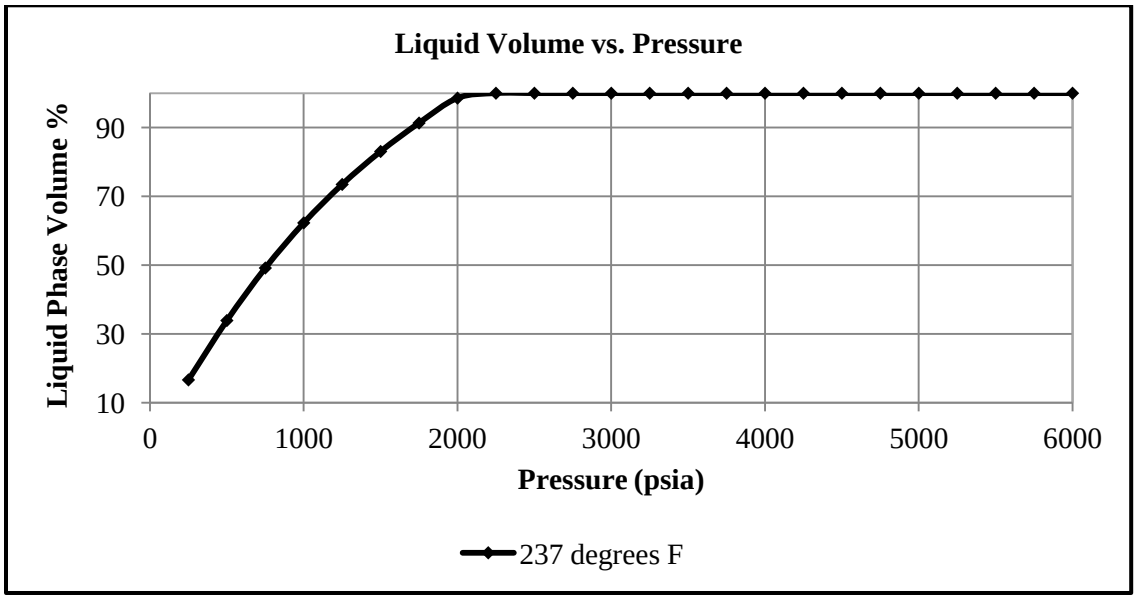

Figure 5.2: Liquid phase volume fraction versus pressure.

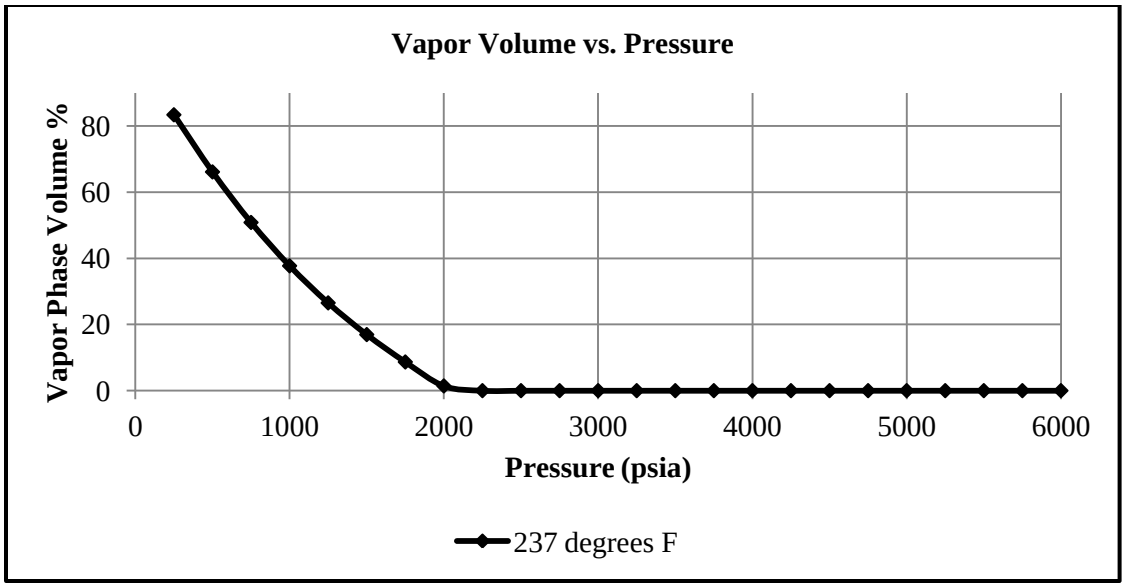

Figure 5.3: Vapor phase volume fraction versus pressure.

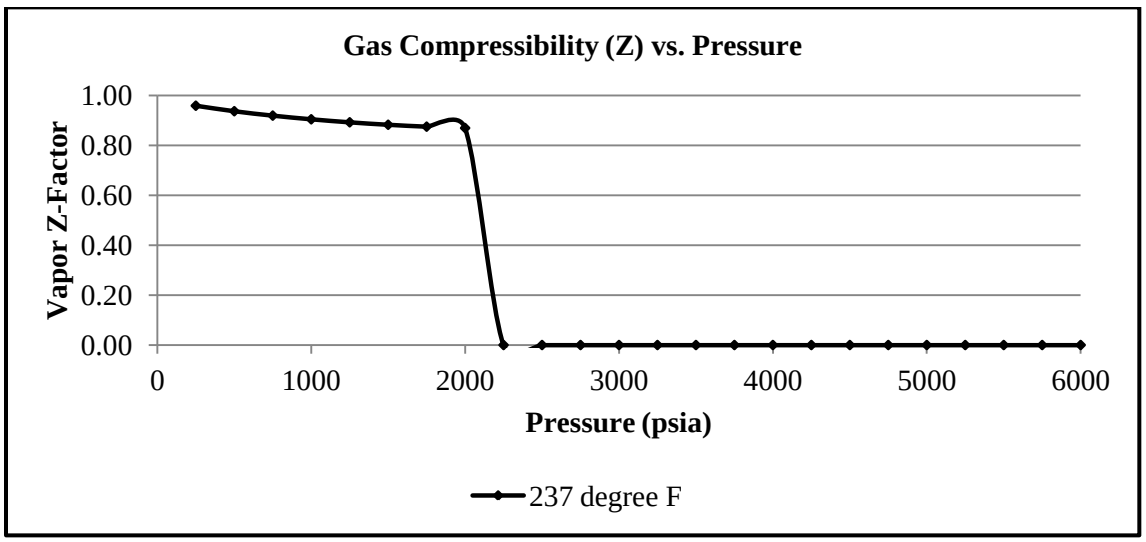

Figure 5.4:Vapor Z-Factor versus pressure.

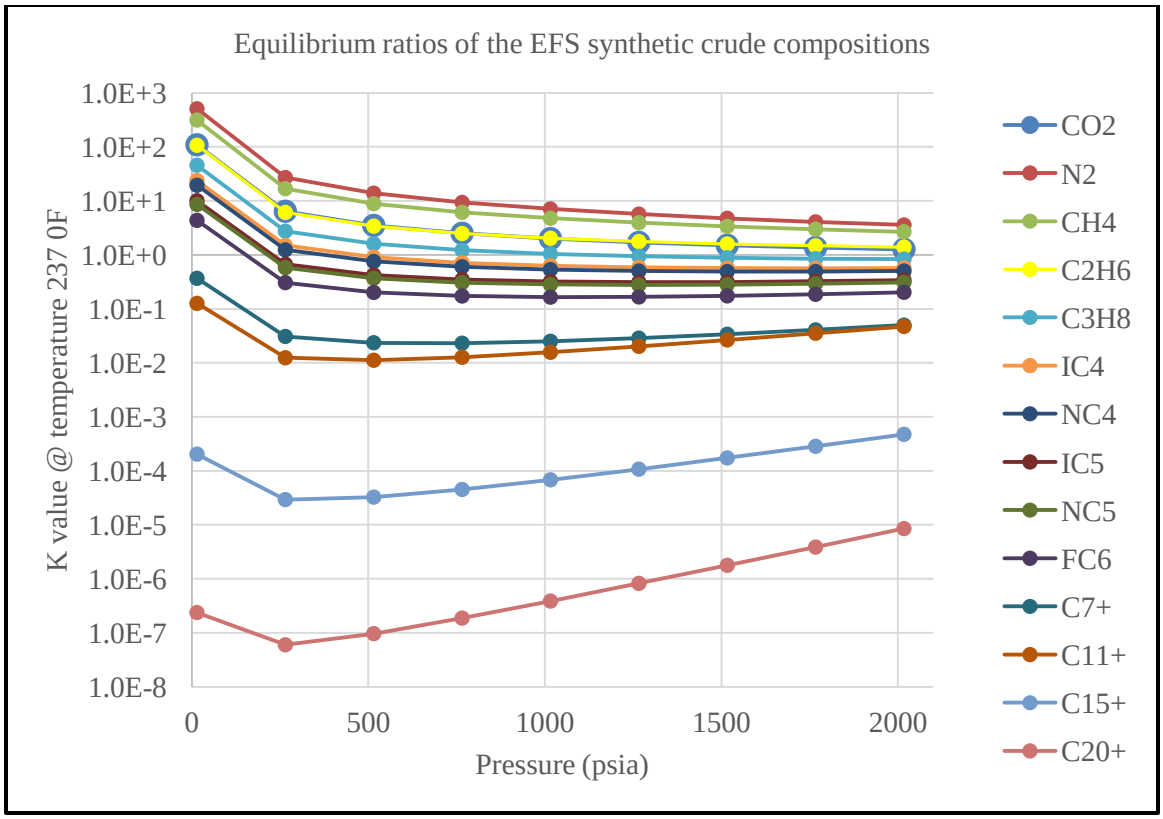

Figure 5.5: Equilibrium ratio (K Value=vapor/liquid) versus pressure.

Further outputs of the Eagle Ford Shale (EFS) synthetic crude fluid analysis using Winprop include PVT tables and figures presented in **Figures 5.6** through **5.9**. The highlighted values are the bubble point parameters of the EFS synthetic crude compositions. These PVT data analysis results illustrate the regression between data provided by Orangi et al., (2011) and Winprop simulation.

Pressure (psia)	Final GOR scf/stb	Pressure (psia)	Exp. GOR scf/stb
6000	504.637	6000	500
3500	504.637		
3000	504.637		
2500	504.637		
2054.85	**504.637**		
2000	492.671		
1800	449.983		
1600	408.64		
1400	368.538		
1200	329.553		
1000	291.52		
750	244.761		
500	197.916		
250	146.704		
14.7	0		

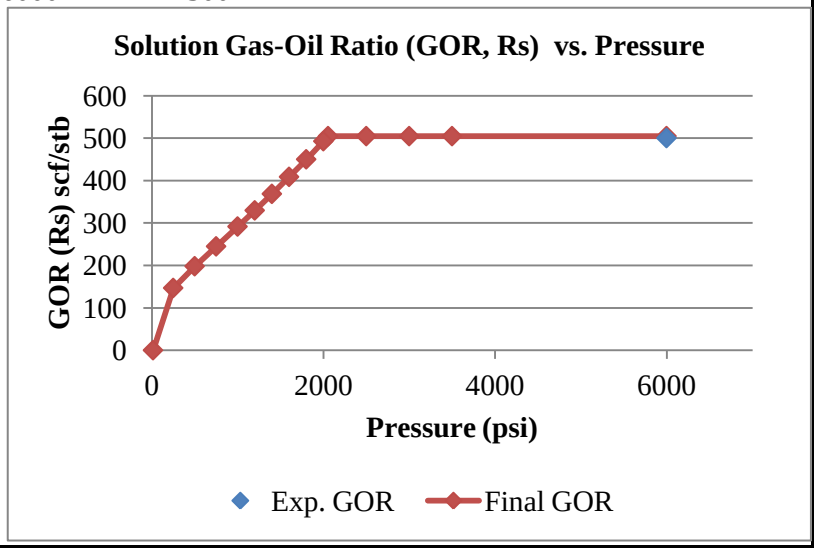

Figure 5.6: Eagle Ford Shale synthetic crude solution gas-oil ratio with pressure.

Pressure (psia)	Final FVF rb/stb (Bo)	Pressure (psia)	Experimental FVF rb/stb (Bo)
6000	1.30	6000	1.3534
3500	1.34	3500	1.366
3000	1.35	3000	1.37
2500	1.37	2500	1.374
2054.85	**1.377**	2000	1.38
2000	1.37	1800	1.355
1800	1.35	1600	1.335
1600	1.33	1400	1.31
1400	1.31	1200	1.29
1200	1.29	1000	1.265
1000	1.27	750	1.23
750	1.25	500	1.2
500	1.22	250	1.16
250	1.19	14.7	1.05
14.7	1.05		

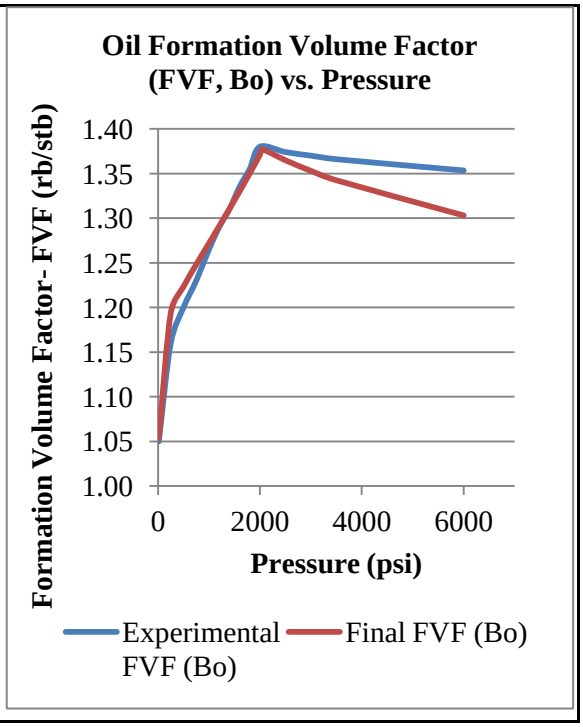

Figure 5.7: Eagle Ford synthetic crude oil formation volume factor with pressure.

Pressure (psia)	Oil Viscosity (cp)
6000	0.132544
3500	0.116668
3000	0.11307
2500	0.109293
2054.85	**0.105758**
2000	0.106071
1800	0.107182
1600	0.108247
1400	0.109246
1200	0.110155
1000	0.110942
750	0.111692
500	0.112059
250	0.111756
14.7	0.108883

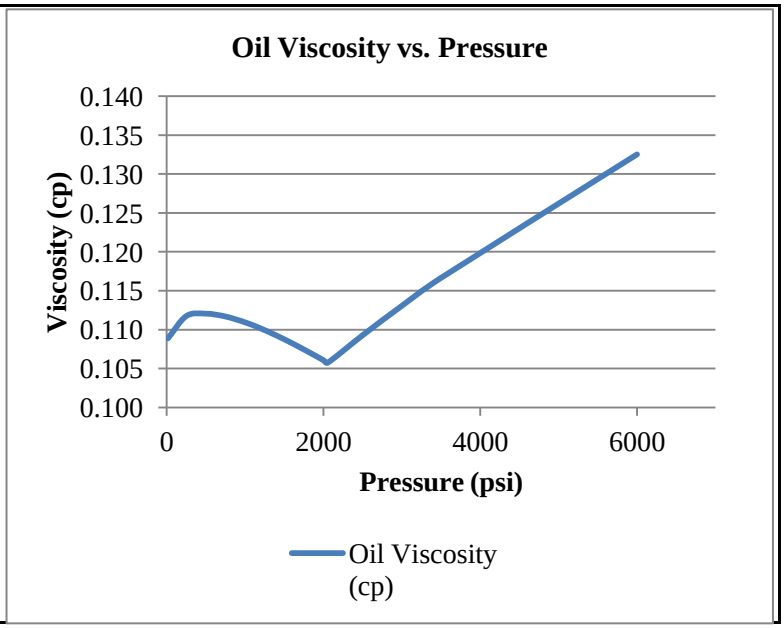

Figure 5.8: Eagle Ford synthetic crude oil viscosity versus pressure at reservoir temperature.

Pressure (psia)	Oil FVF (Bo) rb/stb	GOR (Rs) scf/stb	Z-Factor	Gas FVF Bg (rb/scf)	Bt (rb/stb)
6000	1.30	504.64	1.055	0.00020	1.30
3500	1.34	504.64	0.891	0.00030	1.34
3000	1.35	504.64	0.875	0.00034	1.35
2500	1.37	504.64	0.867	0.00041	1.37
2054.85	1.38	504.64	0.868	0.00050	1.38
2000	1.37	492.67	0.868	0.00051	1.38
1800	1.35	449.98	0.873	0.00057	1.38
1600	1.33	408.64	0.878	0.00065	1.39
1400	1.31	368.54	0.885	0.00075	1.41
1200	1.29	329.55	0.893	0.00088	1.45
1000	1.27	291.52	0.902	0.00107	1.50
750	1.25	244.76	0.915	0.00145	1.63
500	1.22	197.92	0.930	0.00222	1.90
250	1.19	146.70	0.948	0.00452	2.81
14.7	1.05	0	0.983	0.07984	41.34

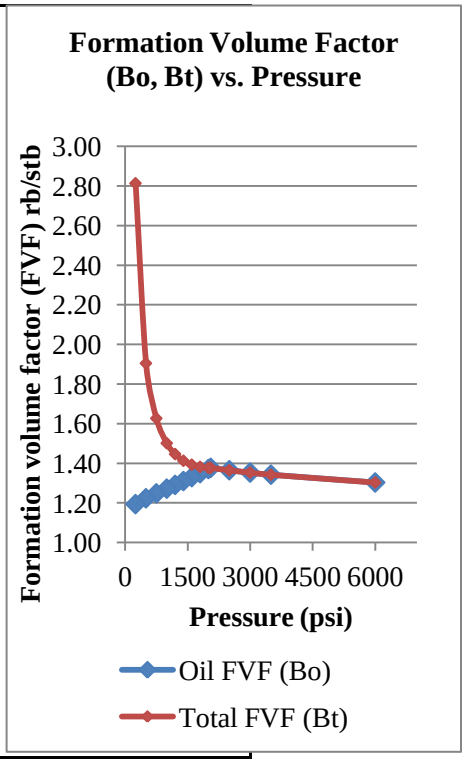

Figure 5.9: Eagle Ford synthetic crude oil two-phase formation volume factor with pressure.

After regression using Winprop, the calculated saturation pressure for the oil of GOR 500 scf/stb is 2054.85 psia at 237^{o}F; it is comparable to Orangi et al.'s (2011) experimental value of 2053 psia (**Table 2.5)**. Also in this simulation, Winprop analyzed minimum miscibility pressure (MMP) for CO_2 gas and reservoir fluids, which was achieved at 3111 psia by the vaporizing gas drive phenomenon explained earlier in the literature review (Holm, 1986 and Rahmatabadi, 2011). Similarly, miscibility for 100% CH_4 was achieved at 6234 psia, which is higher than the reservoir pressure of 3200 psia and, therefore, excludes its consideration from the miscible gas displacement process in this reservoir. Two miscibility pressures, multiple-contact-miscibility (MCM) and first-contact-miscibility (FCM) pressures for a 1:1 CO_2-CH_4 gas mixture were achieved at 3111 psia and 3210 psia, respectively, by vaporizing gas drive. Finally, an enriched gas mixture (arbitrarily composed using one of the CMG user manual's illustrations), comprising 0.1% CO_2, 2.1% N_2, 86.12% CH_4, 5.9% C_2H_6, 3.6% C_3H_8, 1.7% i-C_4, and 0.5% i-C_5, attained MCM at 2964 psia. Thus, a summary of the minimum miscibility pressures obtained from Winprop analysis is provided in **Table 5.3**:

Table 5.3: Miscible gas injectants and multiple contact miscibility pressures

Gas Injected	**Multiple Contact Minimum miscibility pressure (psia)**
CO_2	3111
CH_4	6246
CO_2-CH_4	3111
Enriched Gas	2964

The final oil-water and oil-gas relative permeability data and curves generated by Builder-CMG reservoir simulation software-are provided in **Tables 5.4(a-b**) and **Figures 5.10 – 5.12**.

Note: S_w, S_g, S_l, K_{rw}, K_{row}, K_{rg} and K_{rog} are petroleum engineering standard abbreviations associated with reservoir fluids saturations and relative permeability, which are defined in the nomenclature.

Table 5.4 (a-b): Relative permeability tables generated using CMG Builder.

S_w	K_{rw}	K_{row}
0.30	0.00	0.35
0.33	0.00	0.27
0.35	0.00	0.21
0.38	0.00	0.15
0.41	0.00	0.11
0.43	0.00	0.07
0.46	0.01	0.05
0.49	0.02	0.03
0.52	0.03	0.02
0.55	0.05	0.01
0.58	0.08	0.01
0.60	0.11	0.00
0.63	0.15	0.00
0.66	0.19	0.00
0.69	0.25	0.00
0.72	0.32	0.00
0.74	0.40	0.00
0.77	0.49	0.00
0.80	0.60	0.00

(a)

S_g	K_{rg}	K_{rog}
0.05	0.00	0.35
0.07	0.00	0.27
0.09	0.01	0.21
0.12	0.01	0.15
0.14	0.03	0.11
0.16	0.04	0.08
0.18	0.06	0.05
0.20	0.08	0.04
0.23	0.10	0.02
0.25	0.13	0.01
0.27	0.16	0.01
0.29	0.19	0.00
0.31	0.23	0.00
0.33	0.26	0.00
0.36	0.31	0.00
0.38	0.35	0.00
0.40	0.40	0.00

(b)

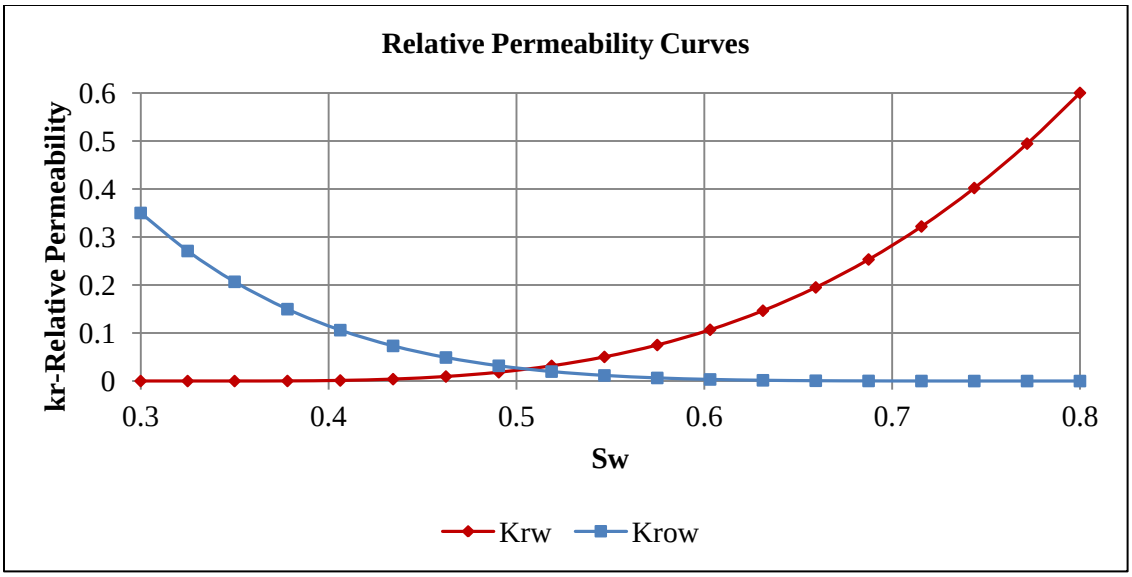

Figure 5.10: Relative permeability curves k_{rw} & k_{row} vs S_w plotted by using Table 5.4.

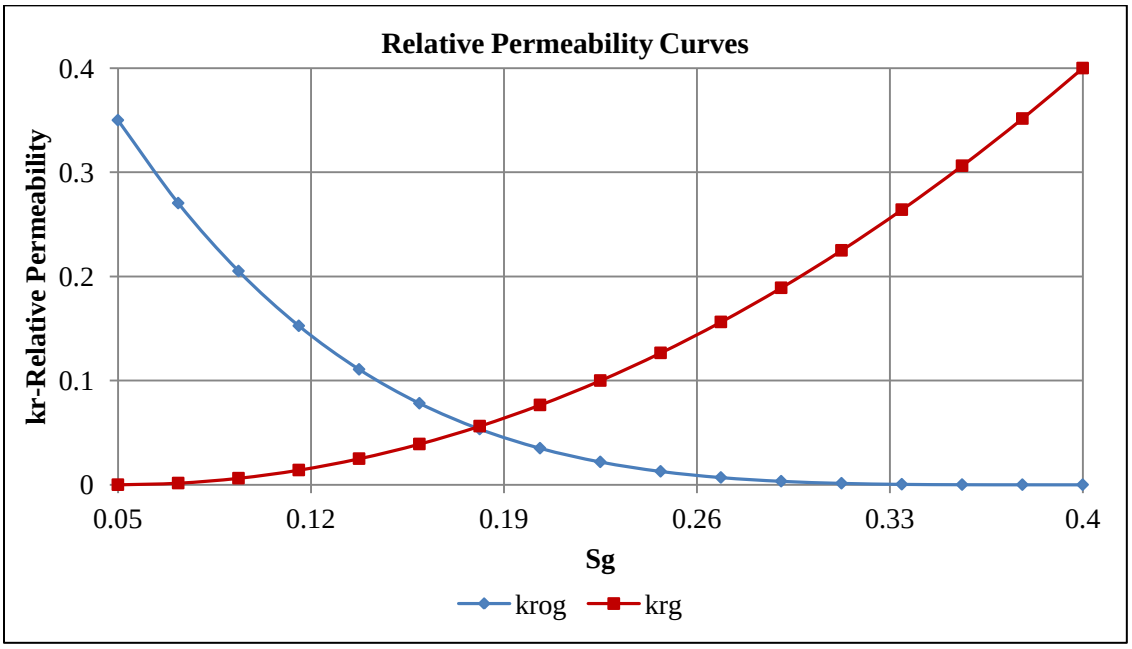

Figure 5.11: Relative permeability curves- k_{rg} & k_{rog} vs. S_g plotted by using Table 5.4.

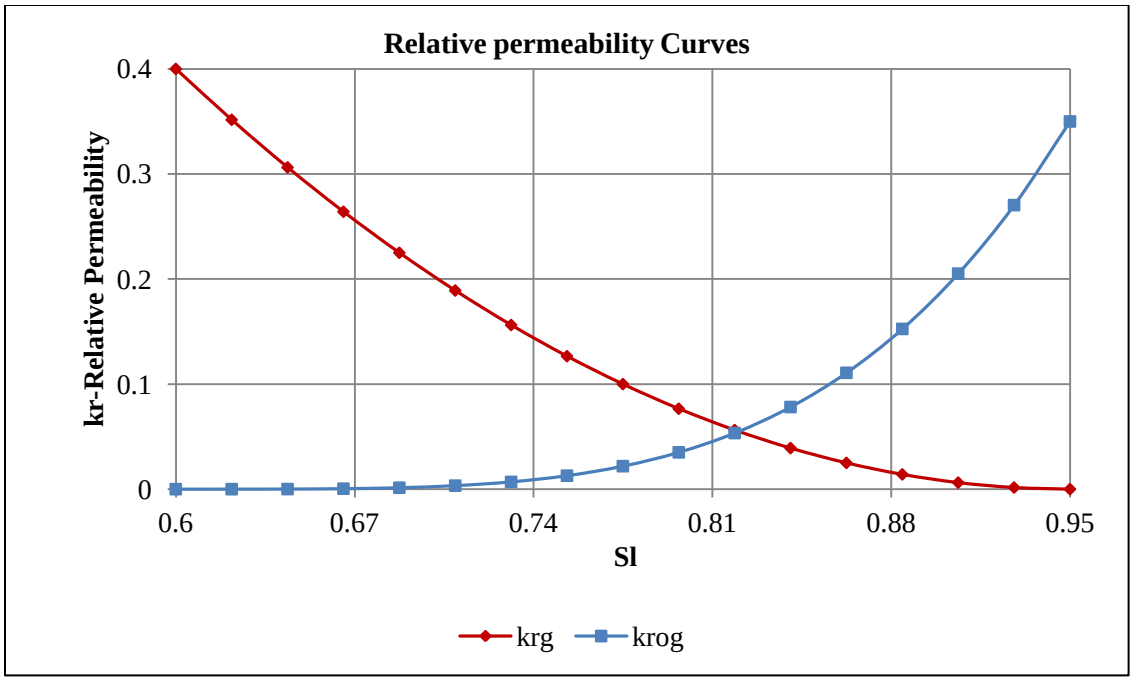

Figure 5.12: Relative permeability curves k_{rg} & k_{rog} vs. S_l plotted by using Table 5.4.

The base model of the Giesenchlag-Groce single horizontal well has Cartesian grid dimensions of 18x5x1 for a total of 90 grid block cells (**Figure 5.13**). Grid block thicknesses of 200 ft x 200 ft x 139 ft result in a modeled volume of 5.0×10^8 ft^3. It includes eighteen hydraulic fracture stages of 200 ft equidistant spacing. The base grid only captures the hydraulic fracture stages without taking into consideration shale petrophysical variations and permeability anisotropy. However, in order to capture the effects of near wellbore and fracture large pressure depletion and saturation changes, smaller size grid blocks were introduced near the wellbore using CMG Builder local grid refinement tool (Chaudhary, 2011). As a result, the total grid presented in **Figure 5.13** is 2484 cells. The calculated original oil in place (OOIP) is 3.11×10^6 STB.

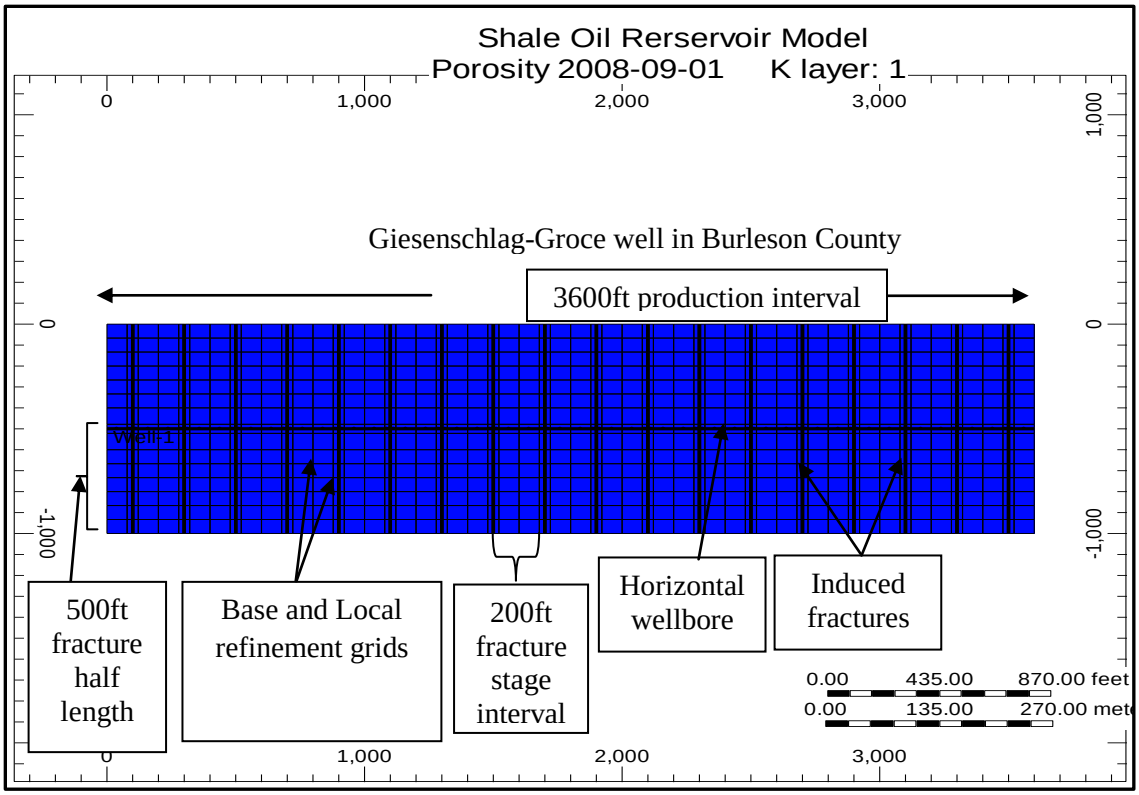

Figure 5.13: Base reservoir model of the Burleson County lease well.

The Dimmit County well (Hutch) was modeled with Cartesian grid dimensions of 221x5x1 for a total of 1105 grid block cells **Figures 5.14** and **5.15**. Grid block thicknesses of 17 ft x 200 ft x 147 ft resulted in a modeled volume of $2.3x10^8$ ft^3. It has 17 hydraulic fracture stages and a total of 3366 grid cells including the effects of local grid refinement capture the effects of near wellbore and fracture large pressure depletion and saturation changes. The calculated OOIP is 2.75x106 STB.

The homogenous reservoir model with abrupt top and bottom is not representative of the EFS. To accurately represent the EFS will require importing geologic tops and bottoms (the horizons) into

the model which are not available at the time of research. Previous EFS models used a similar homogenous system to investigate fracture conductivity; unlike in this case that it was used to history match very short past production performance. The results of the reservoir modeling and simulation investigate the technical feasibility of the concept and may be subject to reservations.

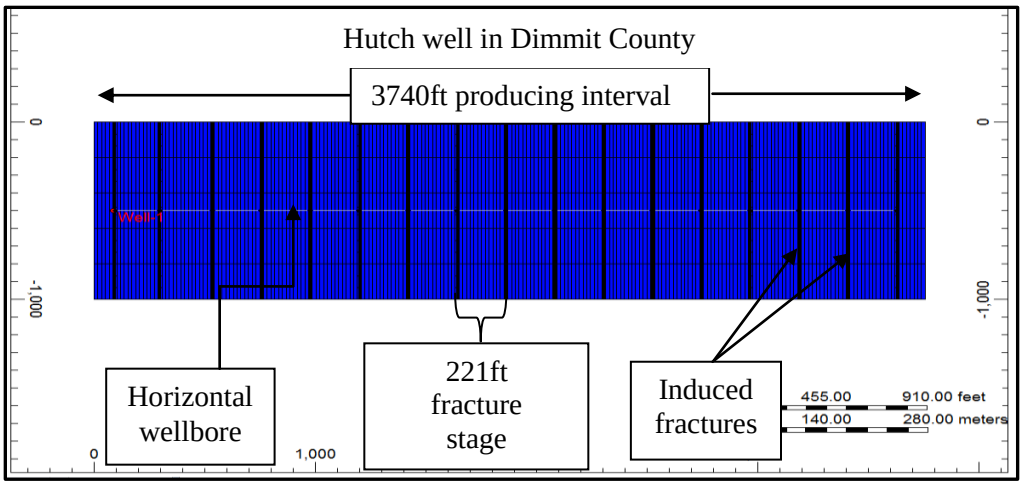

Figure 5.14: Base reservoir model of the Dimmit County well-Hutch.

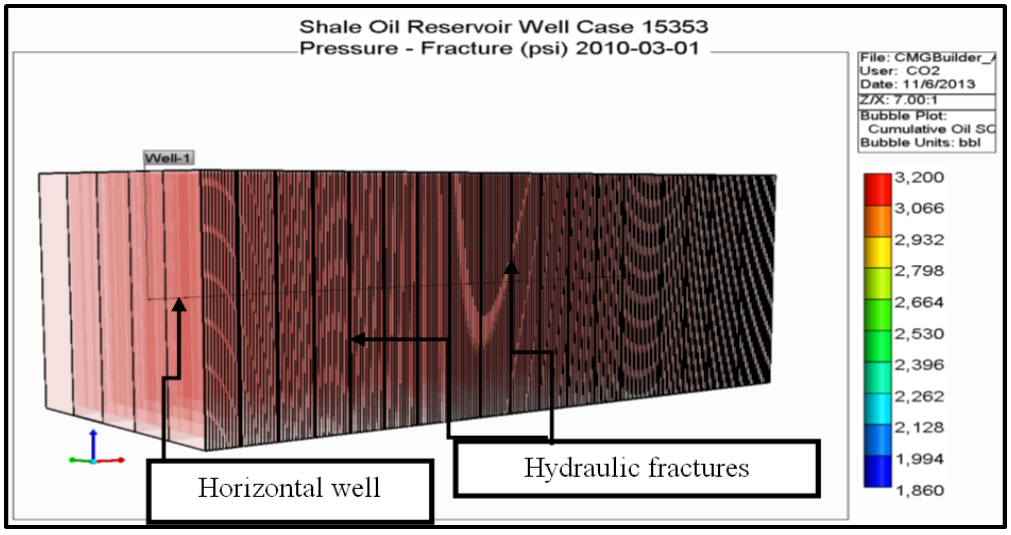

Figure 5.15: 3D view of the Hutch well showing the horizontal well and the hydraulic fractures.

5.2 Results: Production Decline and Future Performance Simulation

Figure 5.16 illustrates the suitable history match between simulation output and the historical oil production rates and cumulative oil production profiles for the Giesenchlag-Groce horizontal well of Burleson County **Figure 5.13**. The numerical simulation model (NSM) forecasted the cumulative productions to abandonment at 2stb/d using the same production history matched model (**Figure 5.17**). In this figure, the expected ultimate recovery (EUR) forecasted by the numerical simulation model (NSM) is not particularly close to any of the decline curve analysis techniques' results for the Giesenschlag-Groce well in the Burleson County.

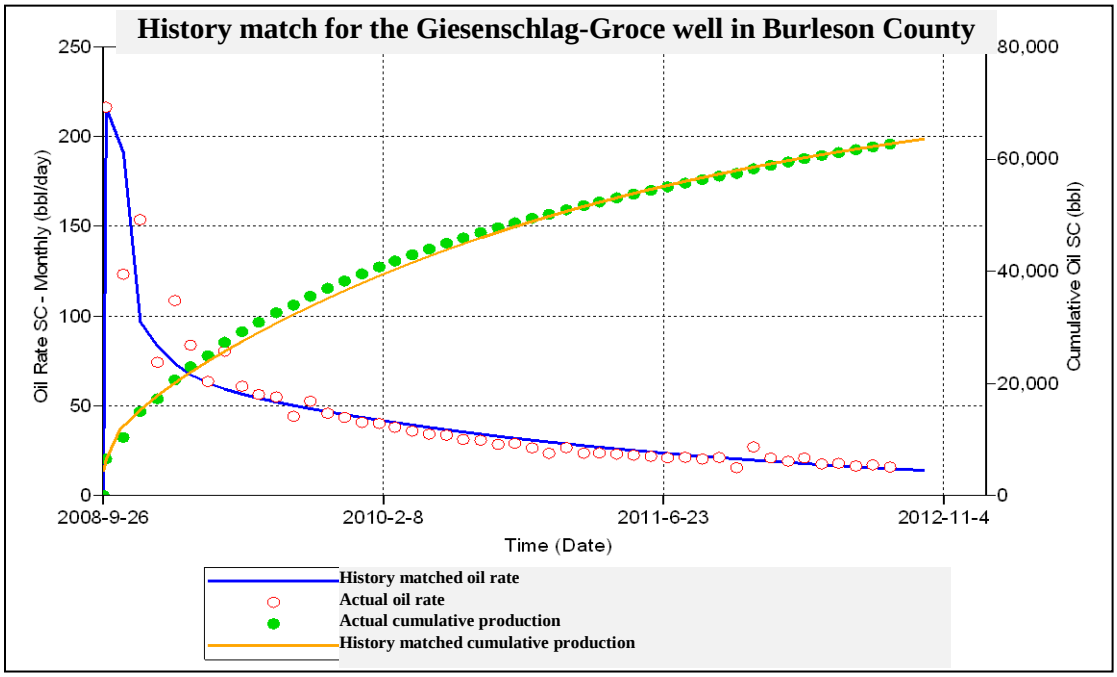

Figure 5.16: History match between simulation output (blue and gold lines) and the past production data (red and green circles) for Giesenschlag-Groce well in the Burleson County.

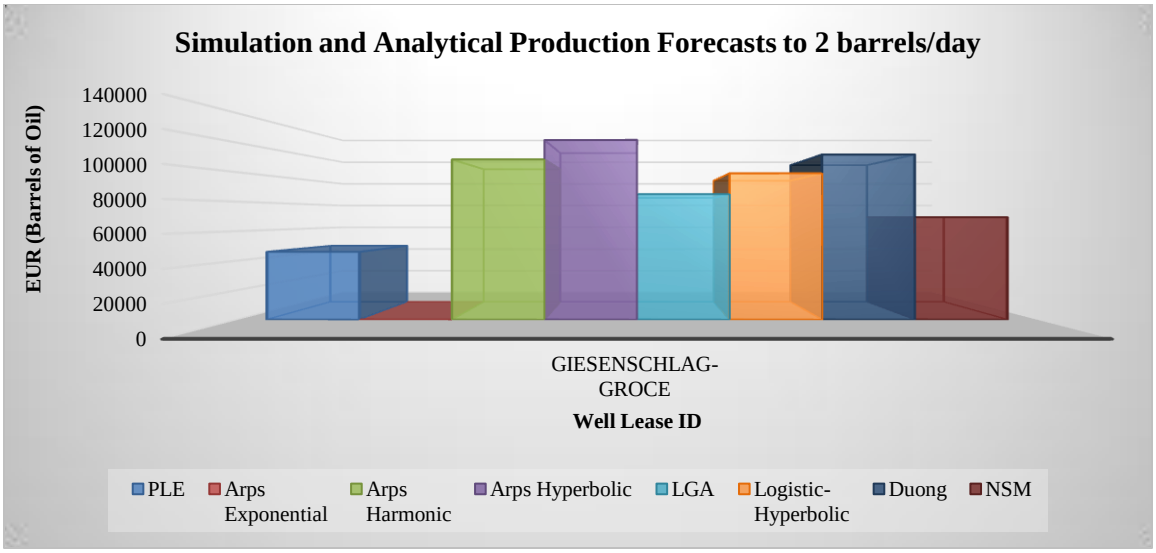

Figure 5.17: Comparison of EUR forecasted to 2 barrels/day, between numerical simulation model (NSM) and various analytical decline curve analysis techniques for Giesenschlag-Groce well.

Figure 5.18 shows the decent history match between simulation outputs and the historical oil production rates and cumulative oil production profiles for the Hutch horizontal well of Dimmit County **Figure 5.14**. The numerical simulation model (NSM) forecasts of cumulative productions associated with the closely matched production history are presented for abandonment at 2stb/d and 5stb/d respectively in **Figure 5.19**. In this figure, the expected ultimate recovery (EUR) forecasted by the numerical simulation model (NSM) is close to the analytical forecasts from Arps' harmonic, Duong's method, and LAHA decline curve analysis.

Pressure variations over the period of history matching the Hutch well reservoir are illustrated in **Figures 5.20 through 5.26**. The pressure drawdown, from the observations at six months intervals in these figures, is highest close to the horizontal wellbore and hydraulic fractures

compared to the rest of the reservoir leading to possible phase saturation and multiphase flow near the wellbore and the hydraulic fractures.

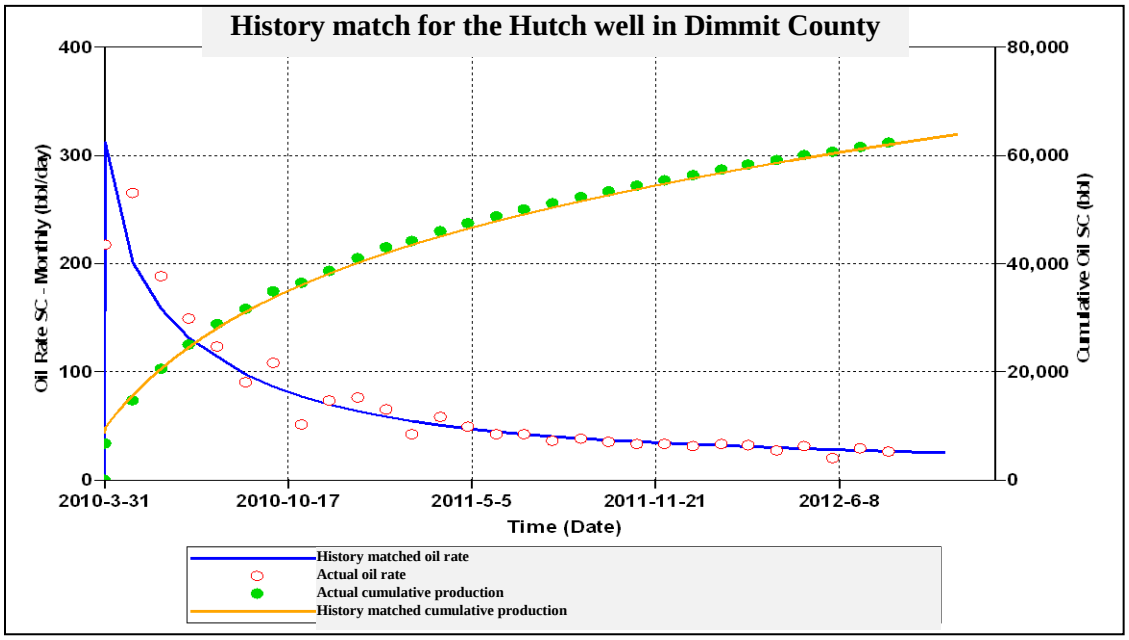

Figure 5.18: History match between simulation output (blue and gold lines) and the past production data (red and green circles) for Hutch well in the Dimmit County.

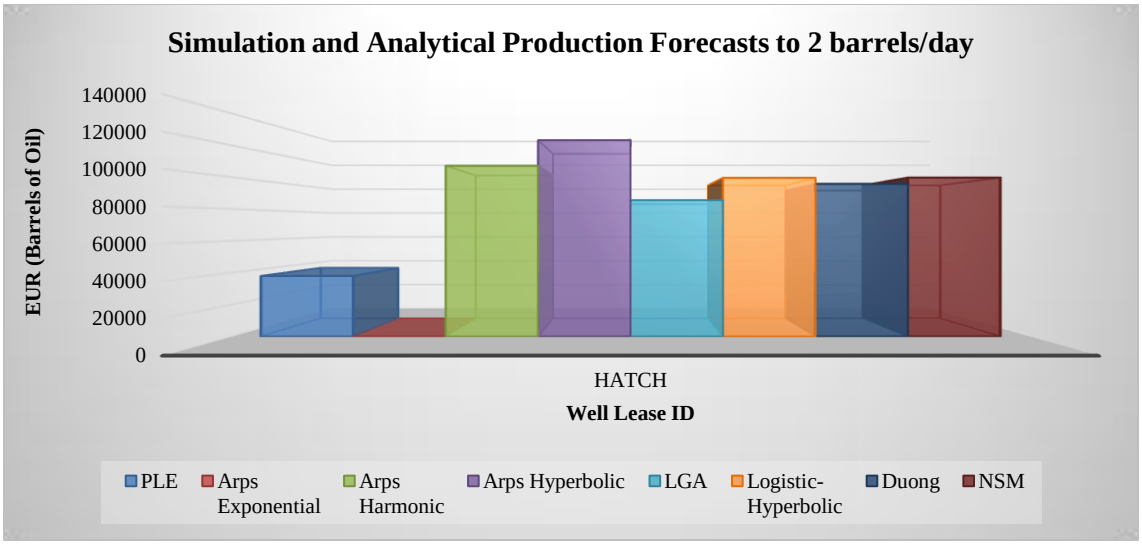

Figure 5.19: Comparison of EUR forecasted to 2 barrels/day, between numerical simulation model (NSM) and various analytical decline curve analysis techniques for Hutch well.

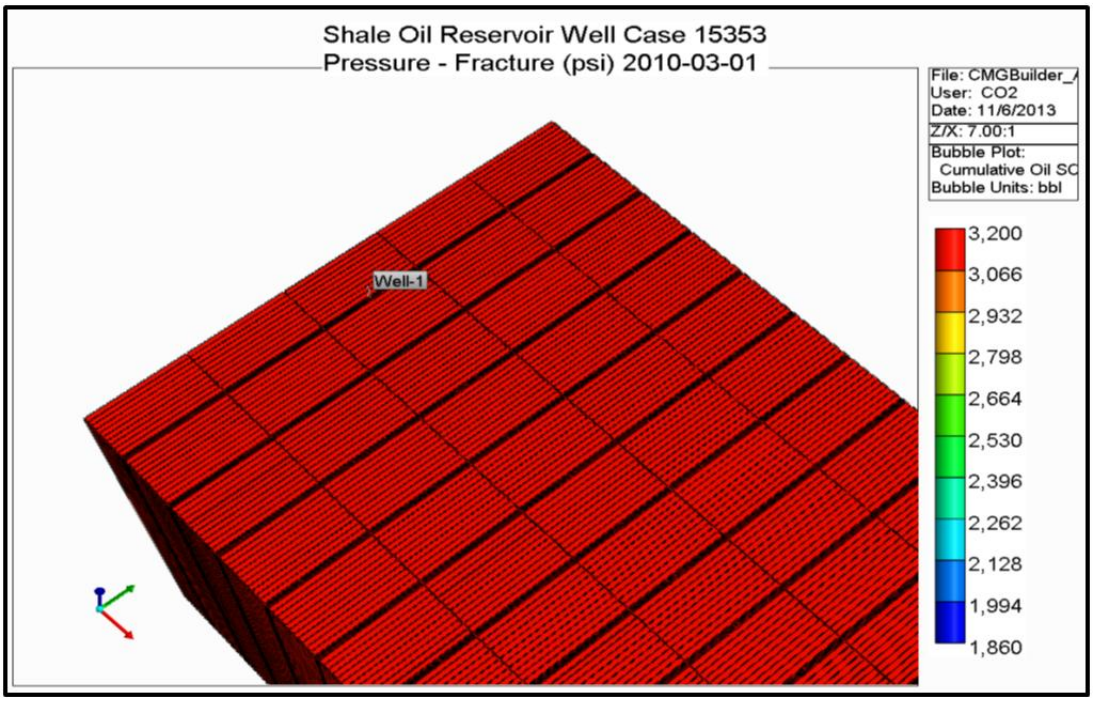

Figure 5.20: Initial pressure of the reservoir for the Hutch well model in Dimmit County.

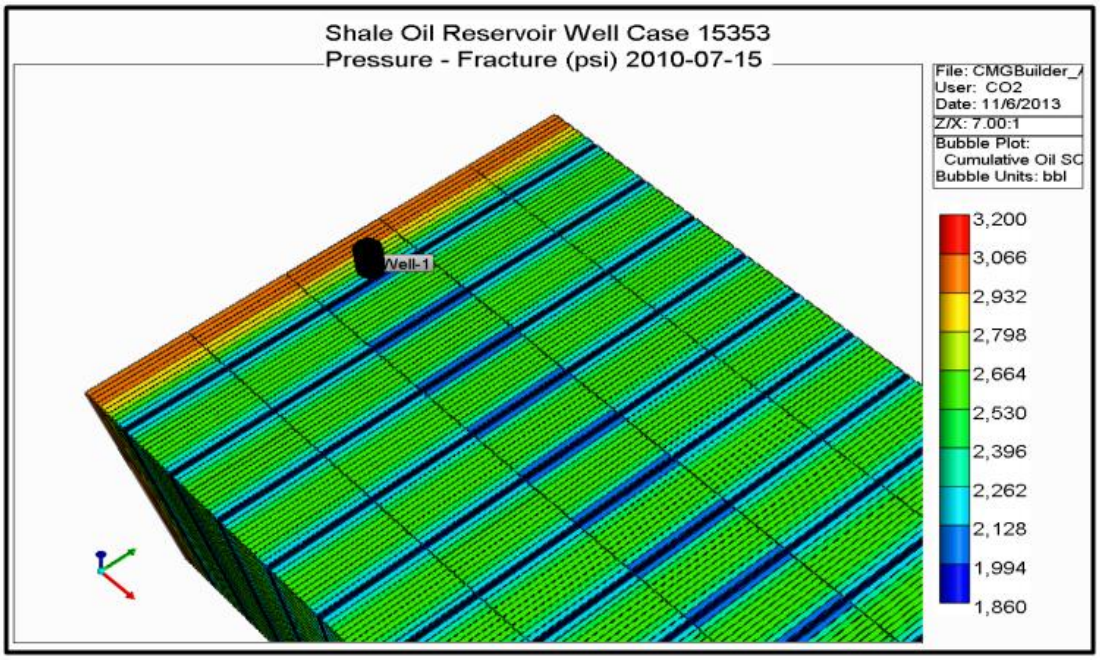

Figure 5.21: Pressure drawdown close to the wellbore, hydraulic fractures and within reservoir after 6 months of production of the Hutch well.

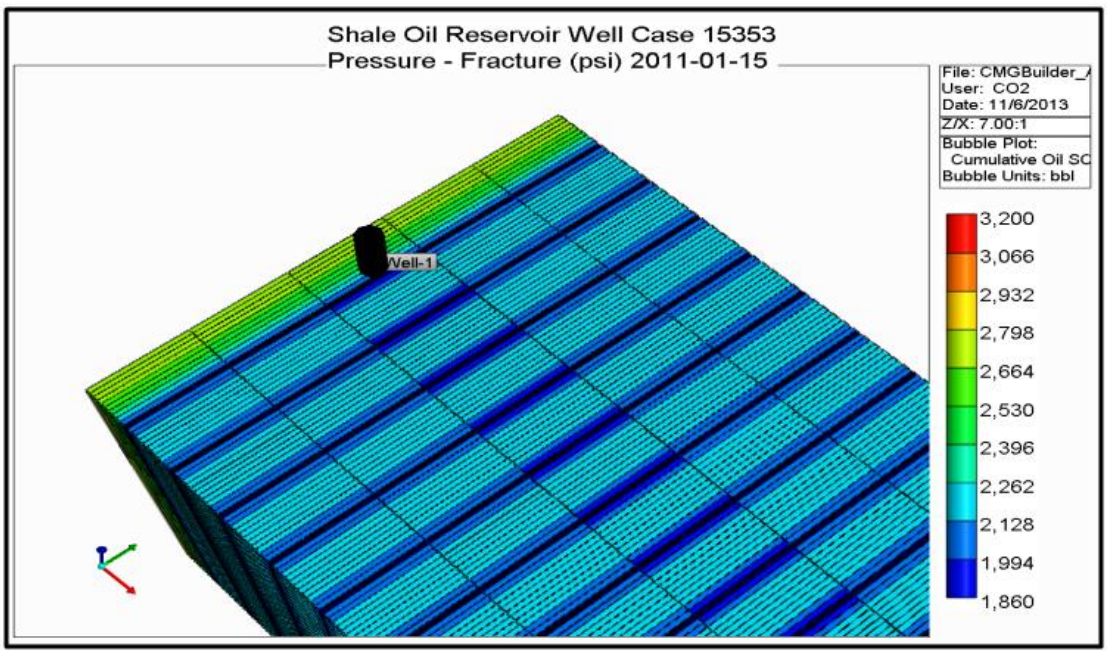

Figure 5.22: Pressure drawdown close to the wellbore, hydraulic fractures and within reservoir after 12 months of production of the Hutch well.

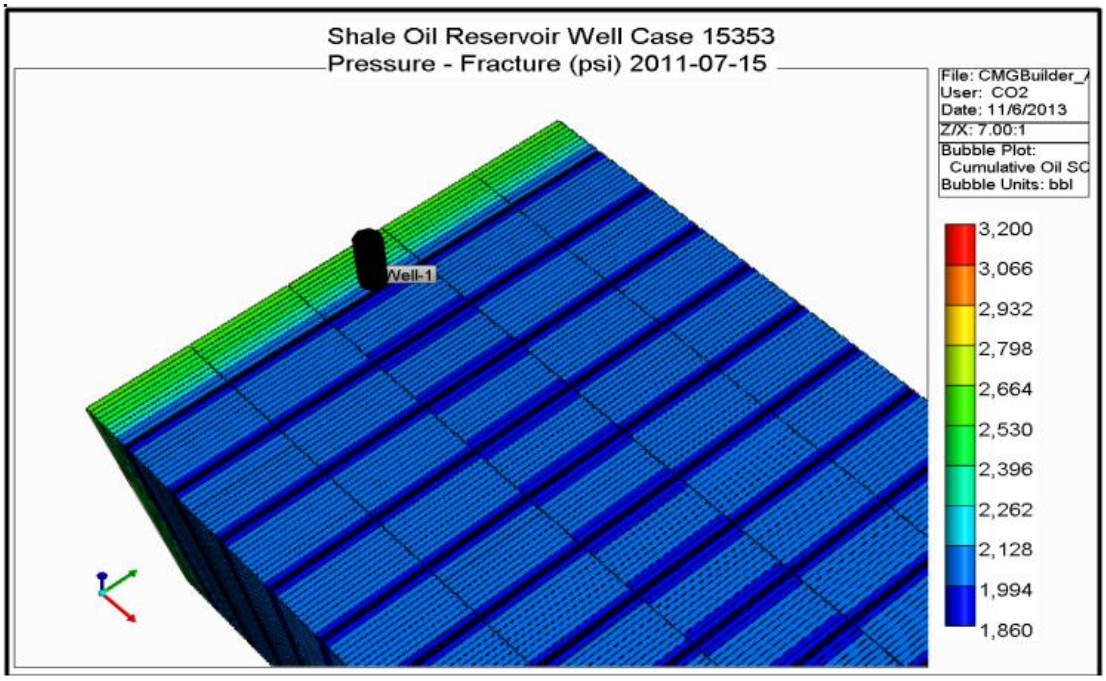

Figure 5.23: Pressure drawdown close to the wellbore, hydraulic fractures and within reservoir after 18 months of production of the Hutch well.

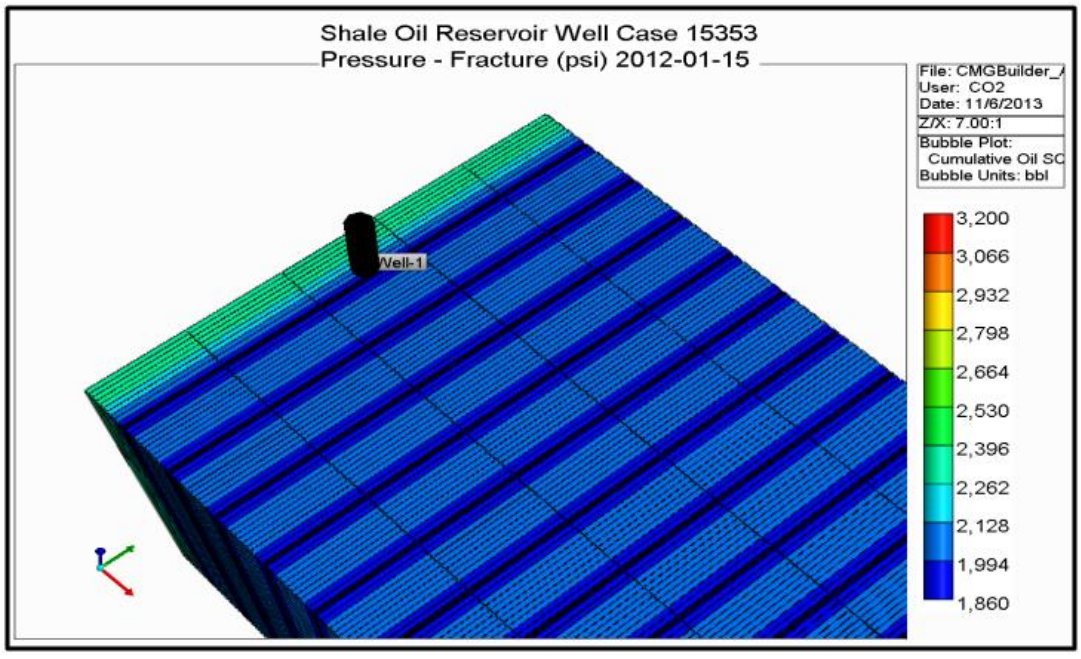

Figure 5.24: Pressure drawdown close to the wellbore, hydraulic fractures and within reservoir after 24 months of production of the Hutch well.

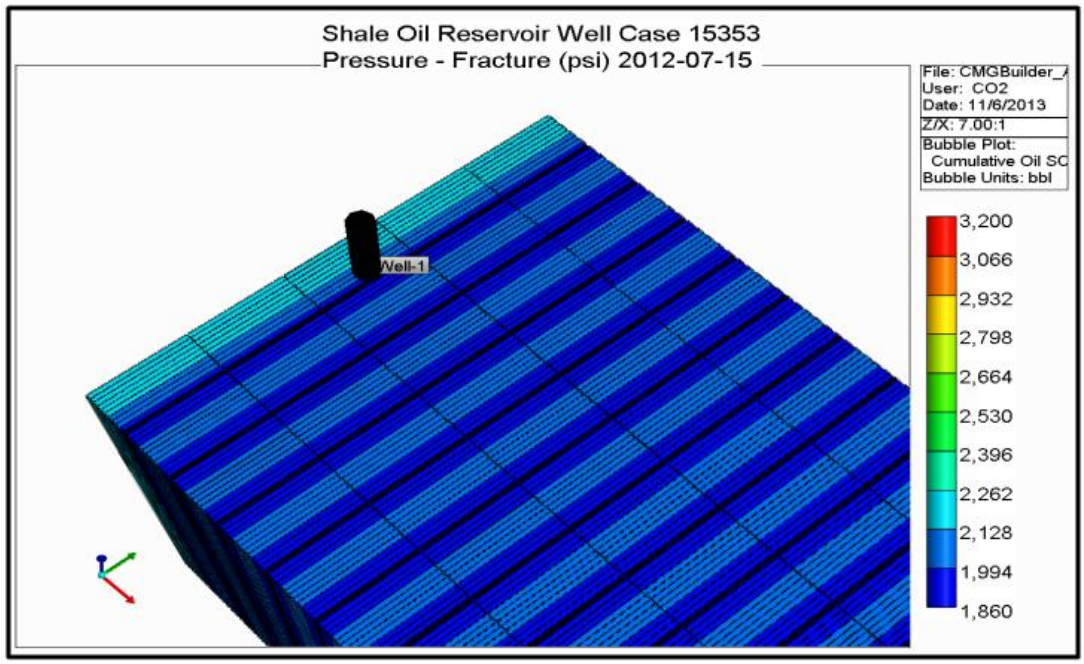

Figure 5.25: Pressure drawdown close to the wellbore, hydraulic fractures and within reservoir after 30 months of production of the Hutch well.

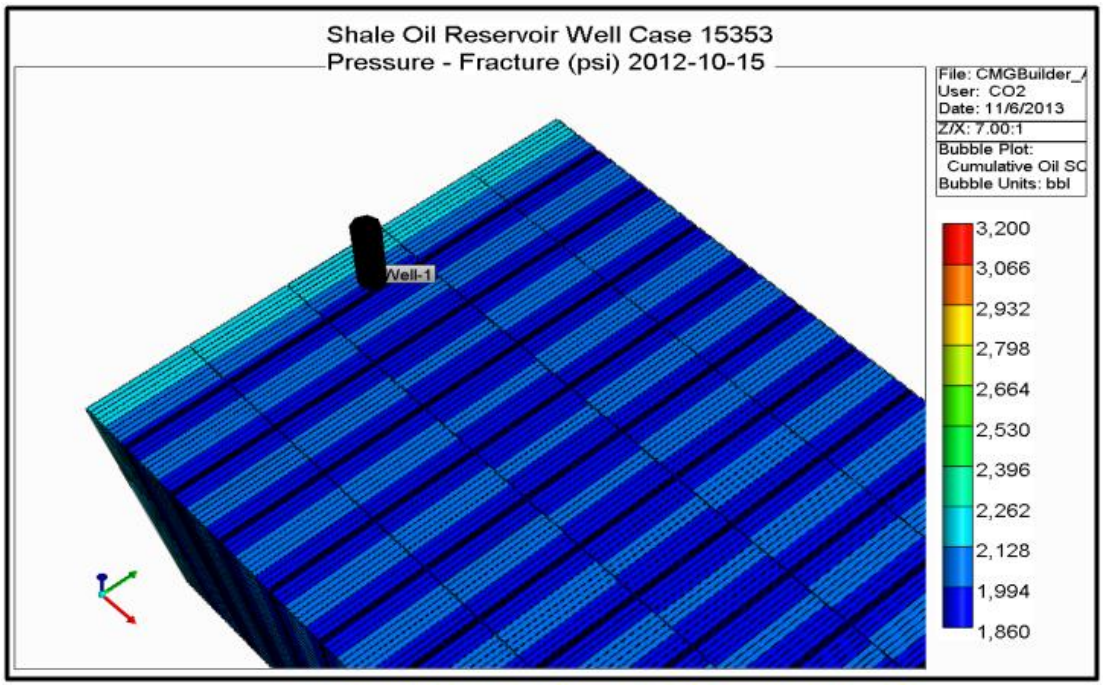

Figure 5.26: Pressure drawdown close to the wellbore, hydraulic fractures and within reservoir after 36 months of production of the Hutch well.

5.3 Methods: Enhanced Shale Oil Recovery Simulation

Oil recovery from shale oil reservoirs by primary depletion is very low. As discussed in the literature review (**Chapter 2)**, it is possible to enhance shale oil recovery by miscible gas injection displacement process. This section investigates the following depletion scenarios:

1. Five and seven horizontal wells, in patterns 5/P and 7/P, with different hydraulic fracture half-lengths but equivalent stimulated reservoir volume (SRV) scenarios were modeled to investigate the effects of the number of horizontal wells and hydraulic fracture half-lengths on oil recovery by primary energy depletion. Both patterns have the same size, shape, and total fracture half-length, while the difference is the number of wells and individual fracture half-length.
2. Three horizontal wells (producers) interspaced with two horizontal wells (injectors) (3-2/P-I), and four horizontal wells (producers) interspaced with three horizontal wells (injectors) (4-3/P-I) were modeled by converting two producers of 5/P and three producers of 7/P, respectively. 3-2/P-I and 4-3/P-I scenarios investigated the effects of the number of producers and injectors and hydraulic fracture half-length on enhanced shale oil recovery.
3. Injection of different gas (es) to investigate their respective effectiveness for enhanced shale oil recovery.

A reservoir of 450 acres was used to simulate the three scenarios. The logic was to test well geometries and spacing versus production volumes with and without enhanced shale oil recovery (ESOR) mechanisms. 5/P and 7/P horizontal wells, hydraulically fractured with approximate half-lengths of 375 ft and 525 ft, respectively, fitted well into the 450-acre reservoir (**Figures 5.27** and

5.28). Reservoir rock and fluid properties were kept the same as that of the previous history match in the Dimmit County (**Table 5.2** and **Figure 5.14**).

Figure 5.27 modeled reservoir as 5/P and 3-2/P-I with two viewpoints; to simulate oil recovery (a) without and (b) with gas injection (primary drive depletion and ESOR scenarios). The primary drive depletion model (5/P) and the ESOR model (3-2/P-I) have hydraulic fractures with approximate half-lengths of 525 ft.

Similarly, 7P and 4-3/P-I well patterns were modeled, with hydraulic fractures with approximate half-lengths of 375 ft for the primary drive depletion model and ESOR. Adjacent wells' stimulated reservoir volumes (SRV) were modeled 50 ft apart (**Figure 5.28**). **Figure 5.29** illustrates the initial pressure condition of the simulated reservoir model.

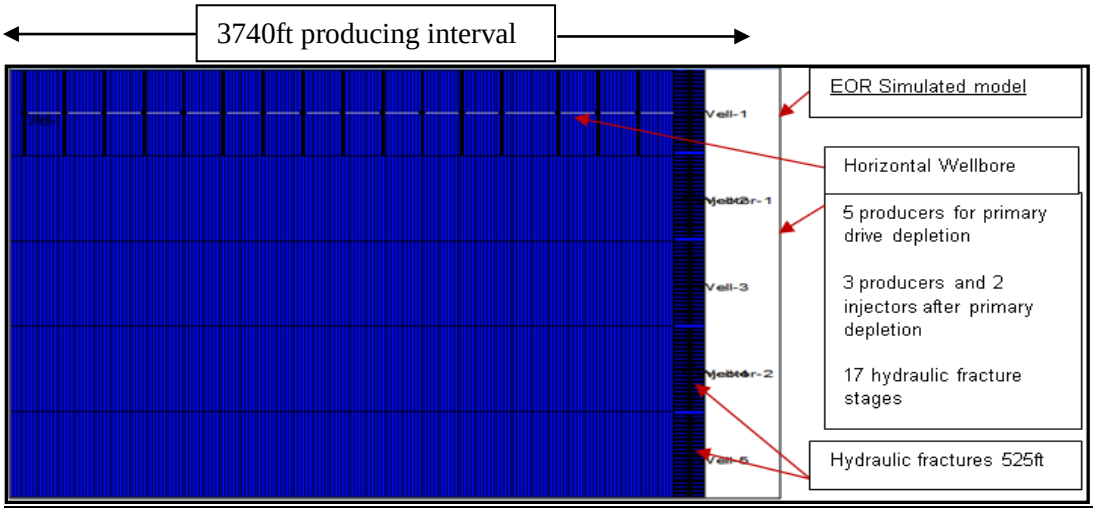

Figure 5.27: Reservoir model (5P) consisting of 5 hydraulically fractured horizontal producers for primary shale oil depletion. This model is later converted to 3-2/P-I with 3 producer and 2 injectors for ESOR

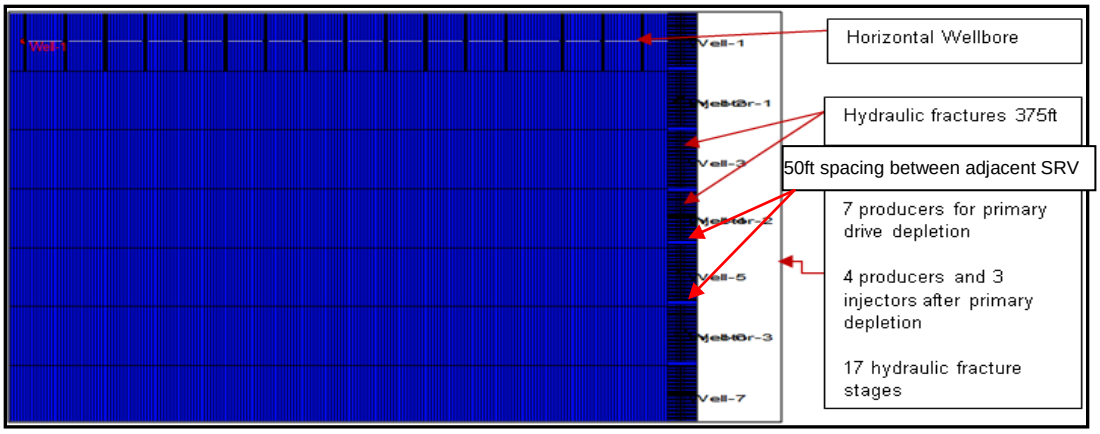

Figure 5.28: Reservoir model (7P) consisting of 7 hydraulically fractured horizontal producers for primary shale oil depletion. This model is later converted to 4-3/P-I with 4 producer and 3 injectors for ESOR.

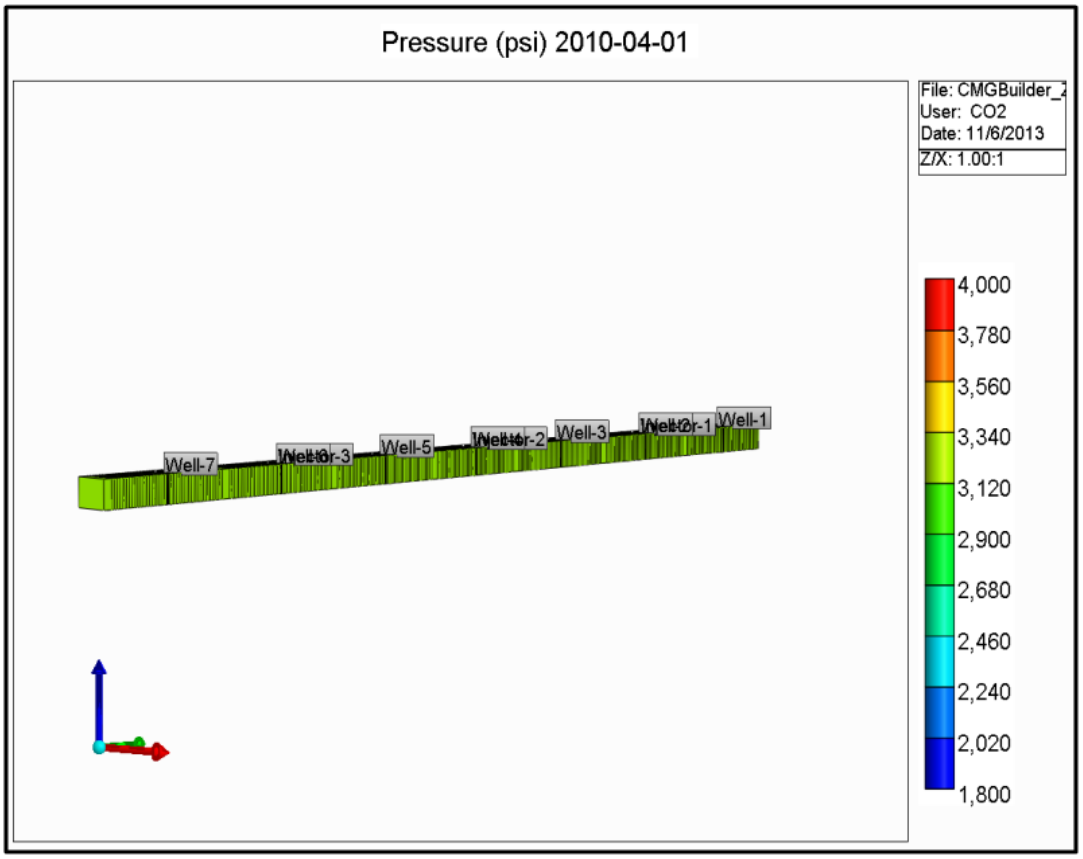

Figure 5.29: Initial pressure condition for the reservoir model (7P) consisting of 7 hydraulically fractured horizontal producers for primary shale oil depletion. This model is later converted to 4-3/P-I with 4 producer and 3 injectors for ESOR.

Seventeen hydraulic fracture clusters were integrated into the model based on completion information available for this the Hutch lease well on the TRRC webpage. However, to lessen the computation time required to simulate the entire reservoir with seventeen clusters, only one hydraulic fracture per well was simulated, and the results multiplied by seventeen.

The compositional model was built with the same reservoir parameters as the Hutch lease wellbore in the Dimmit County (**Table 5.2**). Each of the given patterns was simulated in turn; first, with primary drive mechanism, and second, with gas injection. Primary depletion was simulated to 2 barrels/day/producer with both 5/P and 7/P configurations before the commencement of gas injection. Thus, 5/P and 7/P depleted the field to 10 barrels/day and 14 barrels/day, respectively, before the start of gas injection.

The reservoir was depleted under a minimum bottom hole pressure of 1850 psia. When the primary depletion reached the production limits of 2 barrels/day/producer, then two wells of the 5/P pattern and three wells of the 7/P pattern operated as injectors as described for **Figures 5.27** and **5.28**. The gas injection continued until the production limit of 2 barrels/day/producer was reached, again under enhanced shale oil recovery. The production constraint of 2 barrels/day/producer, in a field-wide sense, implies 10 barrels/day for a 5/P well arrangement. Similarly, the field-wide rate constraints for the 7/P well pattern are 14 barrels/day. Subsequently, final rate limit for ESOR is 6 barrels/day for 3-2/P-I, when the reservoir depletes to 2 barrels/day/producer. For the 4-3/P-I well pattern, the rate is 8 barrels/day for the limit of 2 barrels/day/producer.

Operational conditions were arbitrarily chosen for ESOR, including 1000 rcf/day of gas injected continuously at a bottom-hole pressure of 4000 psia. These conditions did not have the goal of recovery factor optimization or any economic significance, but were used to investigate the technical viability of the miscible gas injection to enhance shale oil recovery.

5.3.1 Results: Enhanced Shale Oil Recovery Simulation

The production rate profiles for both types of reservoir and wells' configurations using the different gas injectants simulated under primary depletion drive and miscible gas displacement process are presented in **Figures 5.30** and **5.31**. These plots show different recovery patterns for the different miscible gas injectants due to differences in respective gas injection properties at the reservoir conditions of temperature and pressure. The miscible gas injectants displacement process occurred at slightly higher rates for the 7 wells' pattern compared to the 5 wells' configuration (**Figure 5.30** and **5.31**).

The peaks are highest for miscible CO2 injectant (**Figure 5.30** and **5.31**). The reason is that supercritical CO2 has a comparable density as the in-situ hydrocarbon fluids, and therefore, it is able to interact and displace more residual oil due to a more efficient mass transfer activity. This argument is justifiable by the discussion of the contents of **Table 5.6.**

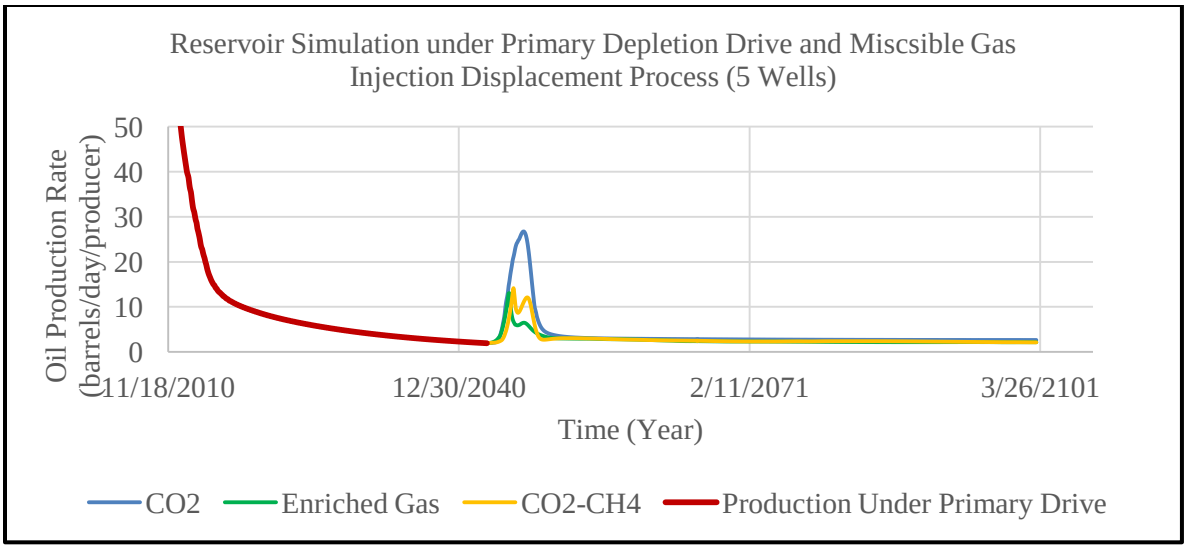

Figure 5.30: Production rates profile of reservoir simulation under primary depletion drive and miscible gas injection displacement process (5P and 3-2/P-I well patterns)

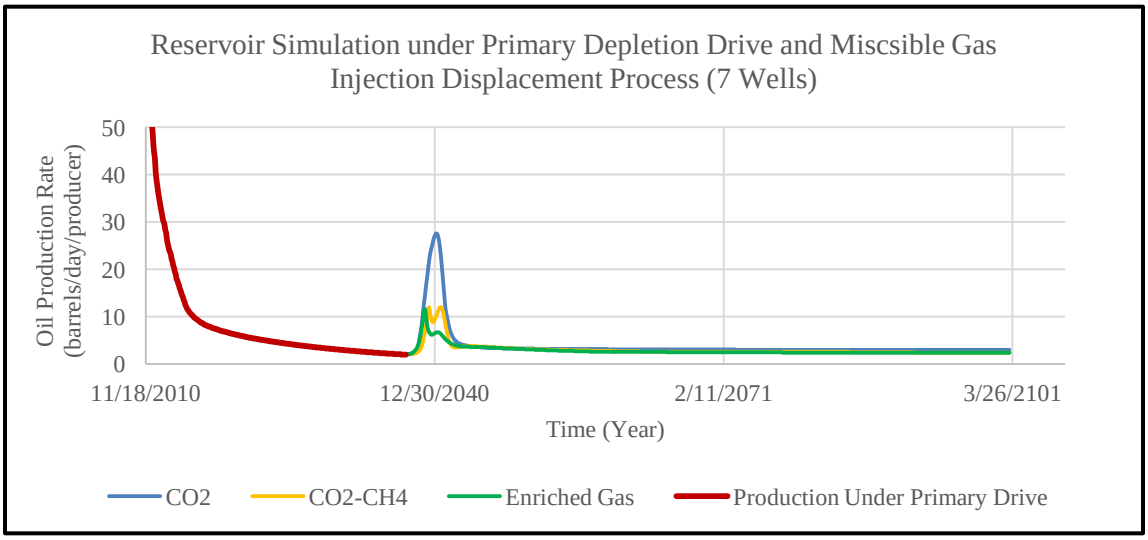

Figure 5.31: Production rates profile of reservoir simulation under primary depletion drive and miscible gas injection displacement process (7P and 4-3/P-I well patterns).

The simulation results of primary depletion and miscible gas injection displacement process in terms of cumulative oil production and recovery factors are summarized in **Table 5.5**. CO2

injection has slightly more enhanced shale oil recovery than the other gas injectants depending on the wells' pattern, production limit rate, and simulation period. For the 7 wells (4-3/P/I) reservoir depletion to 2 barrels/day/producer, the individual gases injected have the recovery factors of CO2 =5.8%, CO2-CH4=5.44 and enriched gas=5.37% (**Table 5.5**). The corresponding observations for the 5 wells (3-2/P-I) are CO2 =5.4%, CO2-CH4=5.1 and enriched gas=5.0% (**Table 5.5**).

In terms of total recovery factors and depletion to 2 barrels/day/producer, the 7 well patterns (4-3/P-I) performs slightly better than the 5 well pattern (3-2/P-I) (**Table 5.5**). The ultimate justification of these slight advantages depends on economic evaluation for the different scenarios.

Table 5.5: Primary depletion, ESOR cumulative oil produced, and recovery factors

Configuration	Production Limit	Years of Primary Depletion	Primary Depletion Cumulative Oil Produced (STB)	Primary Depletion Recovery Factor	Gas Injected	Years of ESOR Depletion	ESOR Cumulative Oil Produced (STB)	ESOR Recovery Factor
5 Wells Pattern	2 Barrels per day per producer	04/30/2010 - 11/30/2043	827200.3	4.2	CO2	11/30/2043 - 12/1/2100	1069648.5	5.4
					Enriched Gas		997942.5	5.0
					CO2-CH4		1008066.0	5.1
7 Wells Pattern	2 Barrels per day per producer	04/30/2010 - 1/31/2038	804701.1	4.0	CO2	1/31/2038 - 12/1/2100	1162522.2	5.8
					Enriched Gas		1068135.8	5.4
					CO2-CH4		1082924.3	5.4

Presence of natural fractures would reduce the volumetric sweep efficiency during EOR. The interesting features about the enhanced recovery process are the differences in the recovery patterns considering the different peaks/humps of each injectant's (**Figures 5.30 through 5.31**). These differences can be explained by considering the operating conditions of injection wells, the producing GOR (**Figure 5.32**), the Z-factors (measure of the gas compressibility), density, viscosity of the injectants, and subsequently, the ratios of bottom hole injection rates presented in **Table 5.6**. With the operating conditions of 4000 psia bottom hole injection pressure (BHIP) and gas injection rate of 1000 rcf/day, **Table 5.6** pointed to the significant differences between CO_2 and the other miscible gas injectants. These differences include low compressibility of CO_2 compared to the compressibility of the other injectants, and higher density and viscosity of CO_2 in comparison to the others. The effects of these significant differences include high volumetric injection of the CO_2 at relatively high injection rates compared to the volumes and rates of injection of miscible CO_2-CH_4 and enriched gas. Despite injecting much more CO_2 both at the microscopic and macroscopic scale, the GOR plot in **Figure 5.32** indicates only a slight difference between the production of CO_2 and the other injectants of less volumetric injection. This means that a lot of miscible CO_2 tends to remain in the reservoir due to its solubility in oil compared to the others. This favorable behavior of CO_2, results in its low viscosity, later breakthrough, oil swelling and reduction in oil viscosity all of which in favor of higher oil recovery.

Table 5.6: Miscible gas injectants properties at reservoir operating condition during ESOR. (Note: Viscosity ratio (μ) and fraction of rates (q) are relative to the highest property values of CO_2)

Gas	Z-Factor	Density gm/cc	Viscosity cp	Bg (rcf/scf)	1/Bg (scf/rcf)	μ-gas/μ-CO_2 (Ratio)	q-gas/q-CO_2 (Fraction)
CO_2	0.5950	0.6572	0.2488	0.0028243	354.1	100.0	1.00
CH_4	0.9740	0.1464	0.0166	0.0046236	216.3	6.7	0.61
CO_2-CH_4	1.0459	0.1178	0.0148	0.0049648	201.4	5.9	0.57
Enriched Gas	0.9416	0.1808	0.0193	0.0044699	223.7	7.7	0.63

Producing Gas-Oil-Ratios for the miscible gas injectants under primary depletion drive and miscible displacement process is illustrated in **Figure 5.32** indicating a slight difference between the volumes of injectants per barrels of oil produced. This again confirms that at any given time CO_2 is more in the reservoir resulting in higher volumetric efficiency than its counterparts.

The breakthrough time for CO2 injection was 5 years; it was 2.5-3 years for the other miscible gas injectants. These variations in breakthrough time are due to the favorable high viscosity and density as well as high solubility in oil. Thus, less viscous and less dense gases have high mobility and can therefore easily bypass the oil in the reservoir and are easily producible through the fractures.

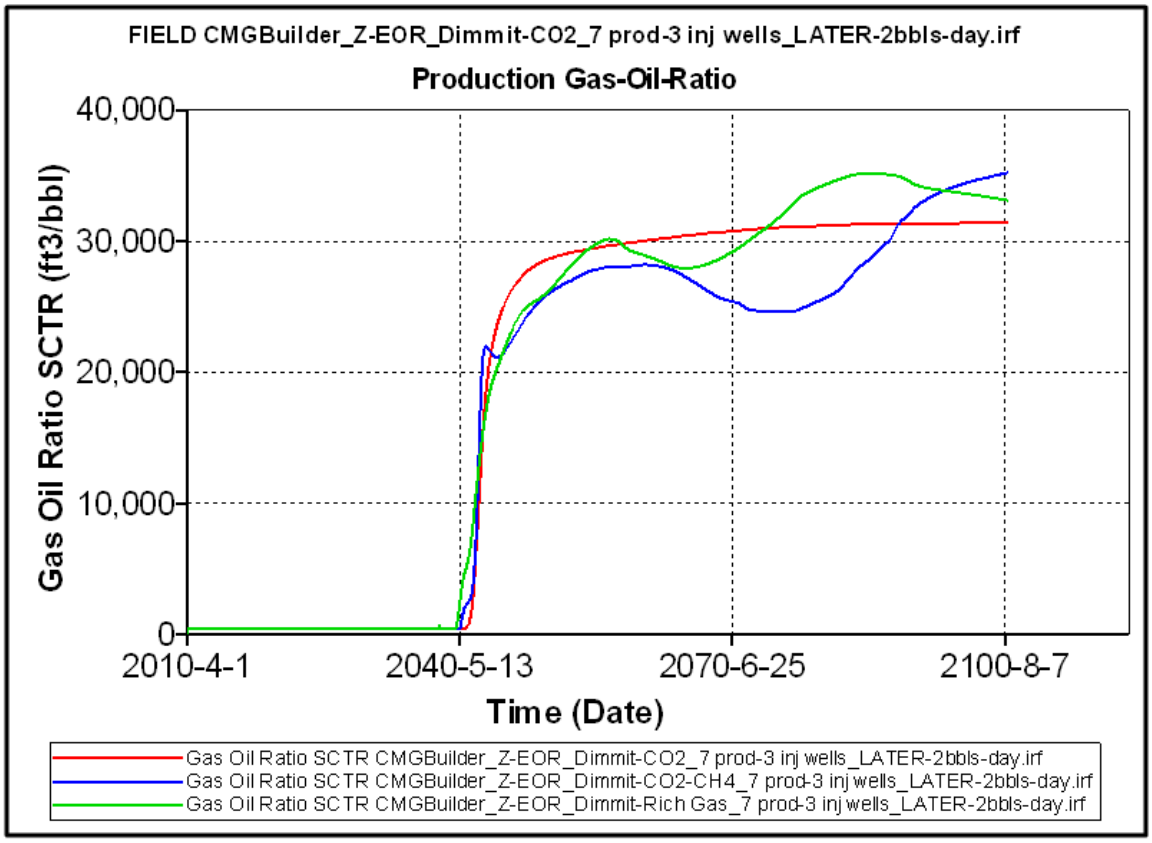

Figure 5.32: Production Gas-Oil-Ratios of the miscible gas injectants under primary depletion drive and miscible displacement process.

The minimum miscibility pressures (MMP) of CO2 and CO2¬-CH4 are the same (**Table 5.3**), but methane is mostly immiscible and has low density than the hydrocarbon fluids. As a result, it segregates and overrides the oil instead of mixing to reduce viscosity and increase swelling factor of the oil.

The enriched gas had the lowest minimum miscibility pressure, but its oil recovery behavior was the poorest. Also, considering (**Table 5.6**), enhanced shale oil recovery by the enriched gas should not have been the lowest since it has a slightly favorable compressibility, density,

viscosity than CO_2-CH_4 and CH_4. This behavior can be attributed to injecting less volume of enriched gas which is only 63% of volume of pure injected CO2.

The pressure profiles (**Figure 5.33** through **5.37**) observed in the reservoirs from start to end of simulation can explain the general low recovery factors. The average reservoir pressure depleted very fast from 3200 psi to 1850 psi (BHP) within 5 years (**Figures 5.33** and **5.34**). Reading from **Figures 5.30** and **5.31**, this period marked the end of the early years of fast production rate decline and the beginning of the very low production rates, which lasted the long transient flow periods till abandonment.

At the onset of miscible gas injection (**Figure 5.35**), pressure gradient returned to the reservoir leading to the peaks observed in **Figures 5.30** and **5.31** associated with increased production of mobilized oil. By 2040, the peak is fully reached (**Figure 5.31**), and since the pressure wave could not penetrate the 50 ft interval between the stimulated zones surrounding producers and injectors, there was a sharp decline in the production rate again. It is observed that the pressure regimes in the reservoir in 2040 and 2100 are similar (**Figures 5.36** and **5.37**); hence pressure depletion rate declined leading to long production plateau for most part of the enhanced shale oil recovery (ESOR).

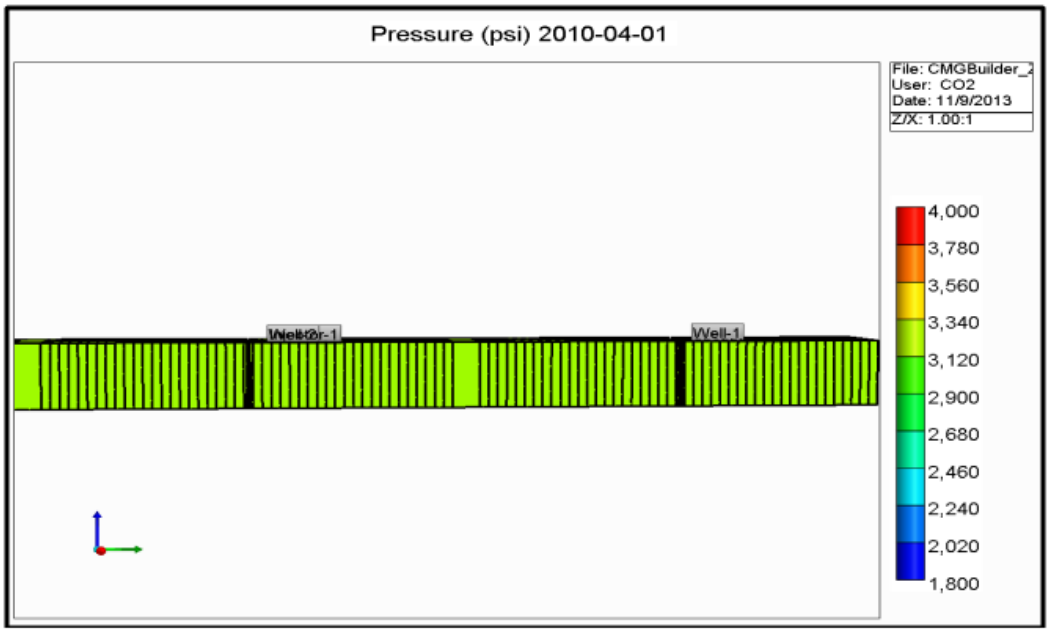

Figure 5.33: Uniform reservoir pressure of 3200 psi at the onset of primary oil recovery

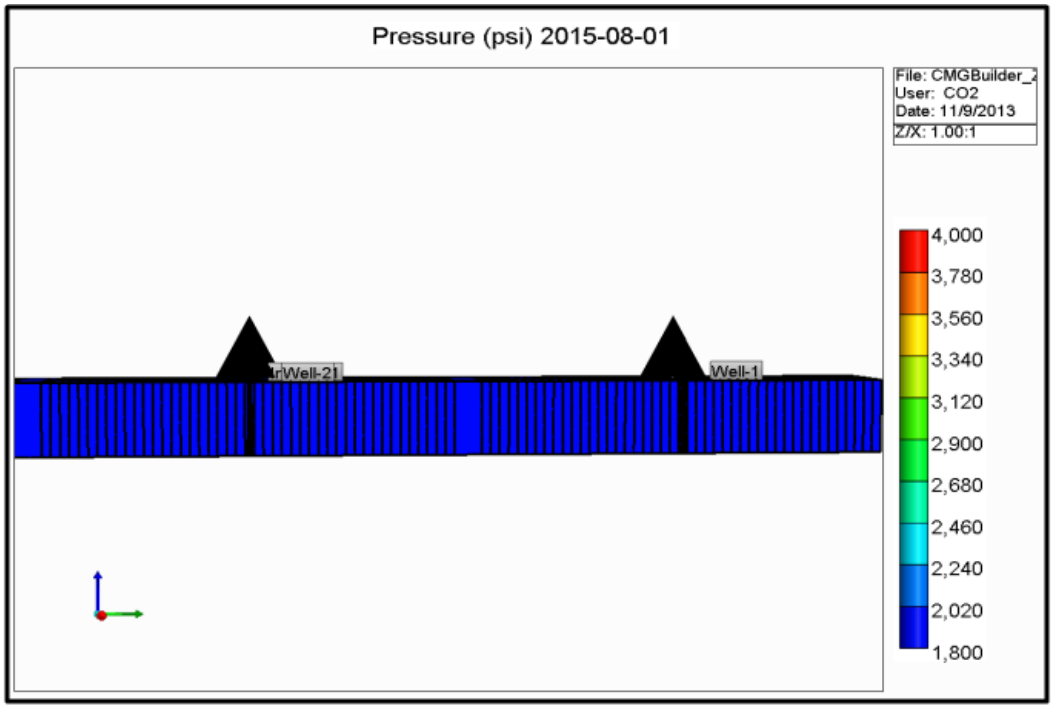

Figure 5.34: The reservoir pressure depleted from 3200 to 1850 psi uniformly by 2015 during the primary depletion drive. Note the wells are all producers, well cone pointing up.

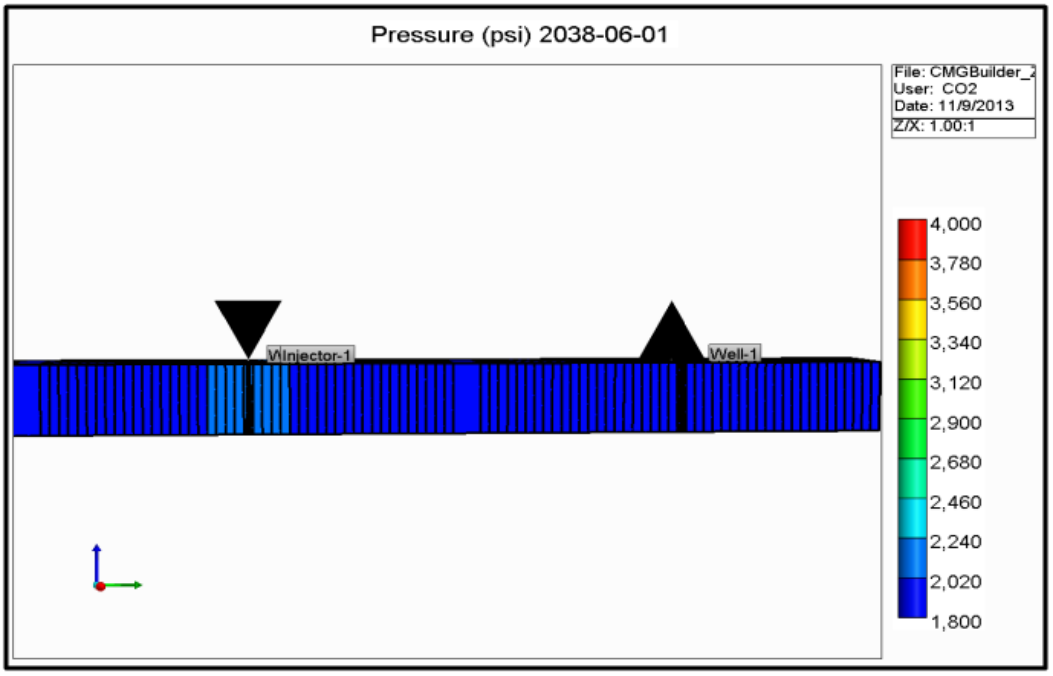

Figure 5.35: Next pressure change in the reservoir was not until 2038 at the onset of miscible gas injection due to injector bottom hole pressure of 4000 psi. Note: cones pointing down are the injectors.

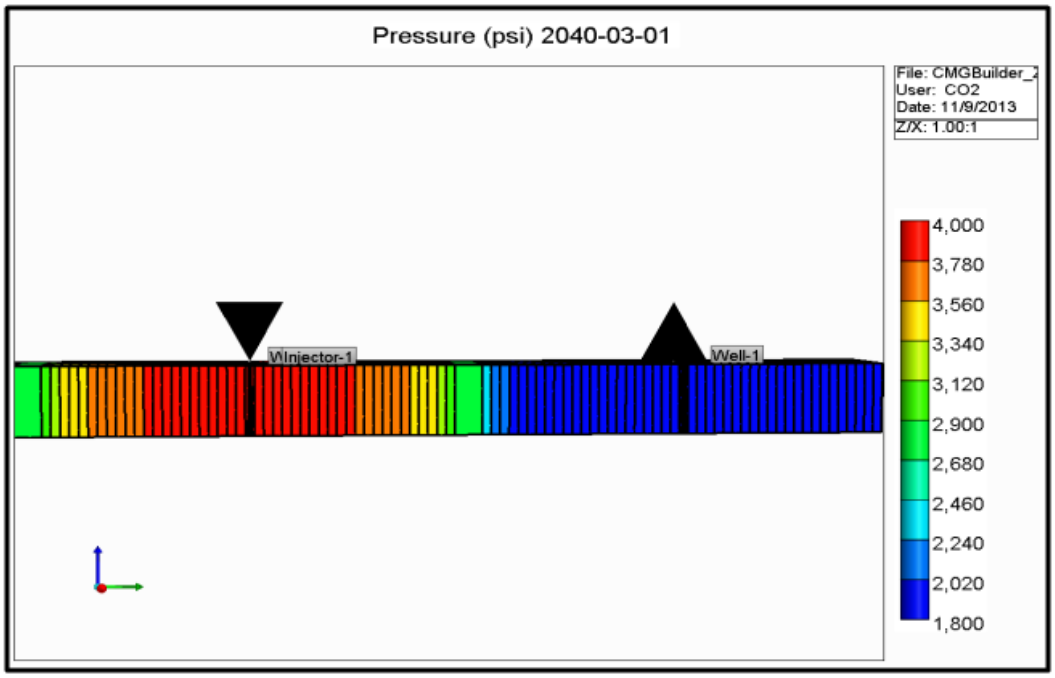

Figure 5.36: Pressure wave is highest at the injectors and least at the producers creating a pressure gradient. This pressure waves moves the oil towards the producers.

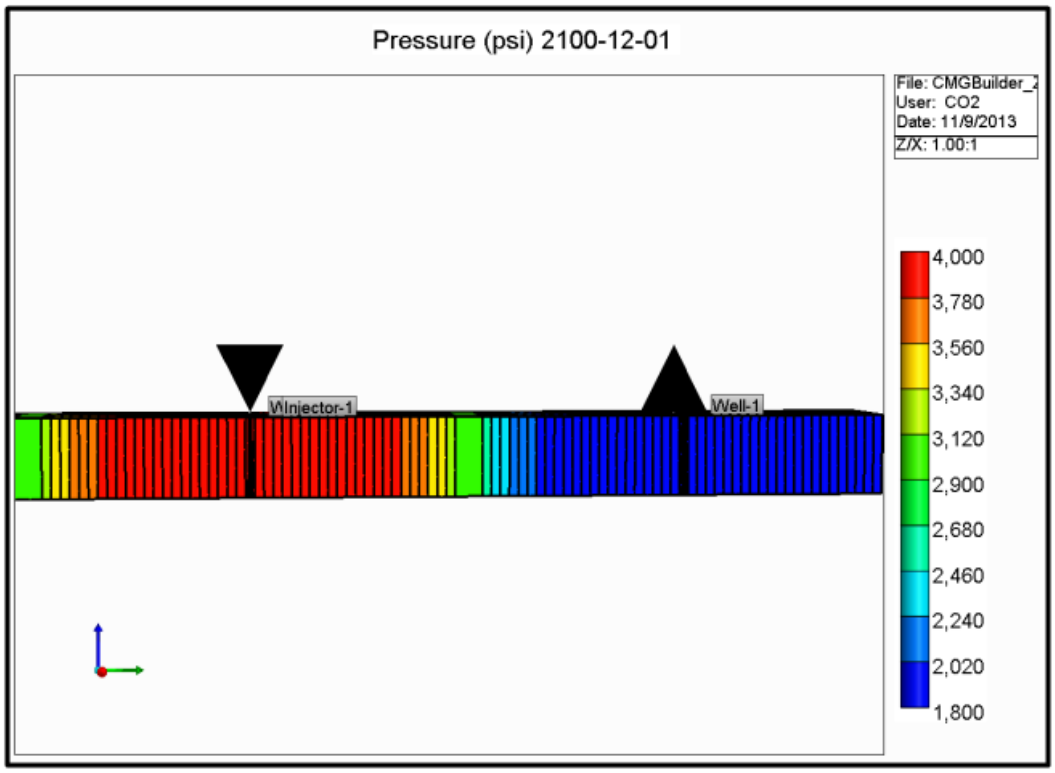

Figure 5.37: Pressure profile did not change much between 2040 and 2100. Almost an abrupt sharp pressure drop can be observed in the spaced zone between producers and injectors.

5.4 Pressure Profiles across Lease Boundaries

Oilfield demarcation into leases limits an owner's acreage in terms of practical development, but subsurface fluid flow behavior cannot obey legal and physical boundaries unless shale reservoirs are completely impermeable. As a result, lease boundaries' integrity with respect to pressure depletion in the subsurface need to be examined. To address this issue, the drainage area was investigated by measurements of pressure profiles across the boundary of the stimulated reservoir volume (SRV) and into adjacent leases using a simulation model.

5.4.1 Methods

I modeled a hypothetical field development scenario with the reservoir parameters as those previously used in the ESOR. It comprised as many as seven producing horizontal wells to create a substantial stimulated reservoir volume and six lateral observation wells in contiguous non-stimulated shales (**Figure 5.38)**. Thus, wells 1-7 are perforated and hydraulically fractured producers; wells 8-10 are observation wells oriented parallel to the large stimulated reservoir zone, at 150 ft, 450 ft and 750 ft away from the lease boundary. Wells 11-13 are observation wells oriented perpendicular to the producing wells at distances 150 ft 450 ft and 750 ft respectively to the right of the large stimulated reservoir zone. The observation wells monitor bottom hole pressure responses across adjoining stimulated reservoir regions. The Cartesian grid dimensions of the reservoir is 60x75x1 for a total of 24611 grid block cells with local grid refinement near wellbores and hydraulic fractures. **Figure 5.37**. Grid block thicknesses of 100 ft x 100 ft x 147 ft resulted in a modeled volume of $6.62x10^9$ ft^3. No assumptions with regards to geological complexities were incorporated in the reservoir model. This model was simulated for 60 years and the wells' pressure profiles were plotted as wells' bottom-hole pressures (BHP) versus time.

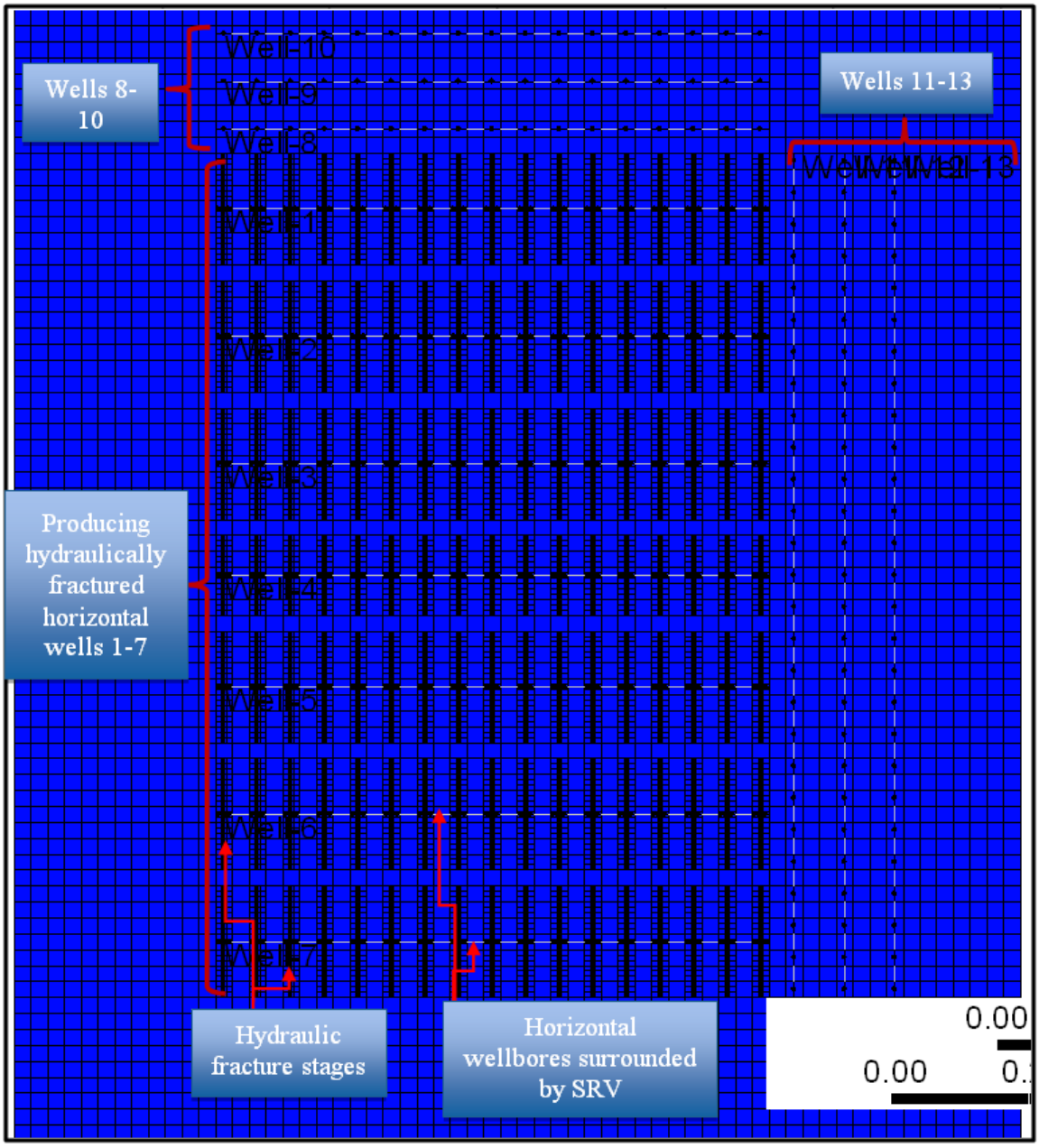

Figure 5.38: Simulation model to investigate bottom hole pressure in adjoining leases during depletion.

5.4.2 Results: Pressure Profiles across Lease Boundaries

The pressure drops vary based the distances of the observation wells away from the tip of the SRV (**Figure 5.38**). The closest to the SRV boundaries are observation wells 8 and 11 at 150 ft away and there is negligible difference in their measured BHP (**Figure 5.39**). Similar insignificant differences are observed at equal distances for the parallel and perpendicular observation wells 9, 12 and 10, 13. However, the most important observation is that the pressure drawdowns in the non-stimulated zone never attain the saturation pressure of 2054 psia of the reservoir. It remained under saturated, and it should be noted that volumetric oil withdrawal associated with large pressure depletion will be insignificant in this circumstance. **Table 5.7** shows the ranges of pressure depletion occurring successively over the entire simulation period of 60 years. Considering the low compressibility of oil, the drainage of fluid away from hydraulic fracture tips is not significant.

Table 5.7: Pressure responses across stimulated reservoir volume into non-stimulated reservoirs

Observation Wells' ID#	Wells' distance from limit of SRV (ft)	Days before first pressure communication	Successive Pressure drawdown (psi)					
			1st January 2015	1st January 2020	1st January 2030	1st January 2040	1st January 2050	1st January 2060
8	150	0.08	225.7	402.8	580.2	672.4	732.8	777.0
9	450	92	6.5	41.4	142.8	231.8	302.9	361.1
10	750	745	0.1	2.1	22.8	60.8	104.9	150.2
11	150	0.74	246.6	421.8	592.8	682.7	740.5	782.8
12	450	122	7.8	46.7	151.1	240.1	310.4	366.8
13	750	716	0.1	2.4	24.9	63.5	106.0	147.1

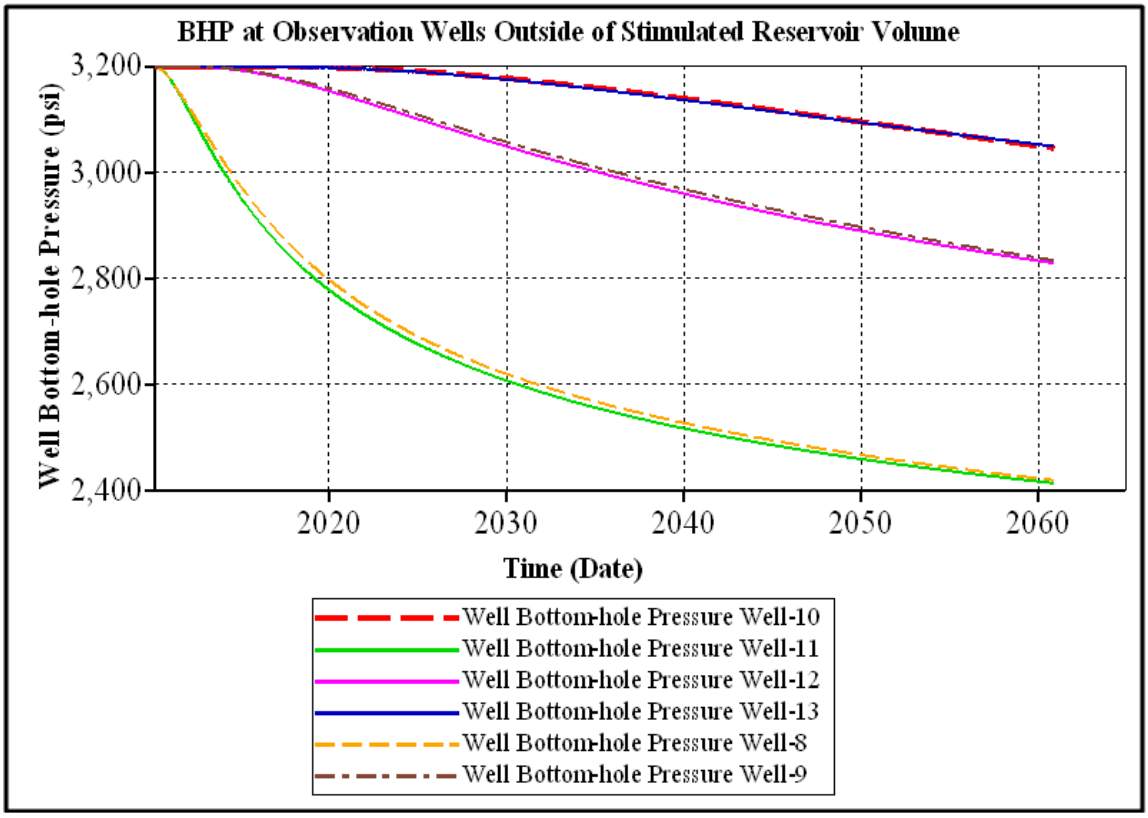

Figure 5.39: Pressure profiles of all observation wells at distances away from the ends of stimulated reservoir volume (SRV).

Chapter 6 Discussion

6.1 Decline Curve Analysis of the Eagle Ford Shale Oil Production

Production profile analyses by the traditional Arps' DCA and various new models have one unique purpose: to evaluate and address the past production performance and future prediction challenges associated with low permeability and transient flow regimes in shale and other tight formations. The outcome of the application of each analytical model to the forty production profiles from wells in the Eagle Ford Shale oil trend varies according to the individual models' fundamental concepts and empirical equations. This section discusses the strengths and weaknesses identified in the use of each decline curve analysis technique.

Traditional methods of Arps' decline curve relations assessed the production profiles to varying degrees based on the decline type (exponential, hyperbolic, or harmonic). Based on $R^2 \geq 0.95$, 6.45% and 29.03% of the wells follow exponential and harmonic decline, respectively.

The Arps' hyperbolic decline model, regardless of the values of the decline exponent (b), closely fitted the past production rate profiles for all forty wells. However, the success of the hyperbolic technique depends on accurate reserves estimation and future production predictions; this accuracy is better when the decline exponent (b) is $0<b<1$ than when $b>1$. The percentage success of the hyperbolic decline model ($0<b<1$) to accurately match the observed decline history is 32.5% for the forty wells investigated. The percentage majority (67.5%) of the forty wells production decline assessment using the Arps' hyperbolic relation resulted in $b>1$. This result may be due to inconsistencies in the actual production trend due to possible changing operating conditions. The unusually high percentage of $b>1$ compromises the reliability of most of the

reserves and future production calculations regarding the use of the Arps empirical decline curve analysis equations.

When Arps' hyperbolic decline model is used in combination with other decline models, such as the logistic growth analysis, Duong's method, and the power law relation techniques, more realistic values of b and subsequent cumulative forecasts may be obtainable. I verified this assertion. The results obtained from the combination of the PLE model data and Arps' hyperbolic relations are slightly less accurate to the logistic Arps' hyperbolic approach (LAHA). When Duong's method is combined with Arps' hyperbolic decline concept, similar percentage improvement of normal decline exponent is observed as in the case of LGA, but the Duong's method still matches the cumulative production less fittingly than the other techniques.

The logistic growth analysis (LGA) technique, one of the established alternatives to the traditional Arps' methods, seems to match cumulative production profiles regardless of operating conditions. However, a suitable cumulative production match does not necessarily translate into an acceptable production rate match. Consequently, the erratic production profiles may affect the outcomes of LGA; hence, data filtering is necessary to accurately estimate reserves and generate future performance curves. The LGA decline exponents (n), equivalent to Arps' hyperbolic decline exponents (b), persistently have values $0 \leq n \leq 1$ (i.e., 95%), except for two: Karnes County well #09667 of the Berry lease and Gonzales County well #15526 of the Georg lease. LGA gives more conservative estimates than do the optimistic decline model types (Arps' hyperbolic, harmonic, and Duong's method).

The PLE predictions are similar to Arps' exponential decline whenever both apply. PLE consistently estimated the lowest values of EUR, future production, and lifetime remaining. It is, therefore, the most conservative approach to generating production forecasts and calculating shale oil reserves.

Duong's method did not match the majority of the wells' past cumulative production because of its high sensitivity to inconsistent decline trends. Nevertheless, Duong's decline analysis method generated volumes comparable to that of other models, especially when the random data points are accurately identified and filtered out.

Finally, the Logistic-Arps' Hyperbolic Approach (LAHA), is the author's proposal to combine two established techniques, the new logistic growth analysis (LGA) model and the traditional Arps' hyperbolic decline relation, to improve the percentage success of the Arps' method. The expectation of LAHA is to translate the advantages of the LGA method by increasing the percentage of $0<b<1$ for the Arps' hyperbolic decline curve analysis, thus improving future production prediction and EUR.

The selection of one technique over the other must be based on longer production data and the feedback from continuous applications of the available techniques. There is not yet a perfect decline model for the Eagle Ford Shale oil, but all of them can be used if their individual limitations are recognized and managed properly until longer production histories become available.

6.2 Production Decline and Forecast, ESOR and Pressure Profiles Simulation

6.2.1 Production Decline and Forecast Simulation

In this section, I discussed the simulation results of the two wells compositional models in the Burleson and Dimmit Counties in comparison to the results obtained from decline curve analysis methods.

Production decline simulation using the two horizontal wells' production profiles resulted in satisfactory history matches. Comparison of expected ultimate recovery (EUR) between the two wells' simulation results and the corresponding analytical methods do not show similar trends. Thus, the EUR for the Burleson County well's production profile is not particularly close to any of the decline models' results. On the other hand, prediction based on simulations of the well in Dimmit County are similar to the forecasts obtained using the Arps' harmonic, Duong's method, and LAHA decline techniques.

However, conducting simulations of only two of the 40 horizontal wells production profiles evaluated analytically was insufficient for a fair performance comparison between the various decline curve analyses techniques. It should also be noted that history matching, especially for a short production history and a small model, is not unique. This suggests that comparisons of the simulation and analytical results be done with caution.

6.2.2 Enhanced Shale Oil Recovery (ESOR) Simulation

This section discusses the results of using different wells' configuration and gas injections to enhance shale oil recovery. As noted earlier in the literature review, the oil recovery factor for the

Eagle Ford Shale play during primary energy reservoir depletion is roughly 5% (Hart 2011). In this research, simulation results showed recovery factors improved from 4.0% under primary depletion drive to as much as 5.8% for ESOR using CO_2 injectant and the seven wells pattern (4-3/P-I). The recovery factor is very low compared to significant recovery factor improvements by miscible gas injection displacement processes associated with conventional reservoirs. The difference is due to broad range of mobility of hydrocarbon phases in conventional reservoir; whereas in shale reservoirs, the mobility is restricted to a much narrower saturation range because of the nano- Darcy permeability of the matrix. Most of the gas injectants for the miscible displacement take the path of hydraulic fracture conduits instead of infiltrating the micro pores to mobilize the residual oil of the shale reservoirs. This leads to poor volumetric sweep efficiency.

The results of the miscible gas injection displacement process vary for the different gas injectants, but the best scenario is for well pattern (4-3/P-I), CO_2 gas injection and depletion to 2 barrels/day/producer. The likelihood for this to occur is CO_2 relative high ability to attain solubility and multiple contact miscibility with reservoir oil compared to other gases. Different interactions between the in-situ crude and the different gas compositions resulted in different rate-time profiles and breakthrough time. CO_2 took the most time to breakthrough compared to the other gases injected. These differences are the result of differences in phase behavior-solubility and first or multiple contact miscibility with the in-situ crude-of the various gas compositions.

Depending on well configuration and rate constraints, depletion under primary drive took different time periods. Enhanced shale oil recovery (ESOR) simulation could not deplete the reservoir to the production limit of 2 barrels/day/producer 60 years after primary drive depletion. Since shale reservoirs are expected to advance to stripper status and could last 100 or more years,

ESOR to lower production limits could be worthwhile, depending on its economic viability. After more than 60 years of ESOR, 3-2/P-I and 4-3/P-I well configurations flow at 2.4 and 3.0 barrels/day/producer respectively. Thus, with ESOR by gas injection, the Eagle Ford Shale oil reservoir may produce above 2 barrels/day/producer. However, whether ESOR is economically realistic will be determined by crude oil prices, plus maintenance and operating costs.

The 4-3/P-I well pattern generally recovers more oil than the 3-2/P-I well arrangement under ESOR to 2 barrels/day/producer (**Table 5.5**). This may be as a result of increased displacement or sweep efficiency by the gases in the 4-3/P-I arrangement. This could be due to better volumetric sweep and higher pressure gradient between producer/injector pairs.

6.2.3 Pressure Profile Simulation

Pressure profiles across the extent of the stimulated reservoir volume (SRV) and adjacent leases were modeled and simulated in order to investigate the drainage zone. The simulation result could apply to any tight nano-Darcy permeability reservoir such as the shale reservoirs. Shale reservoir leases are like sharing a piece of a globe (pie), and it is important to investigate the level of encroachment going on in the subsurface, with regards to hydrocarbon fluid depletion, from one piece to the other. The pressure profile simulation results show that the total pressure depletion outside of the SRV over a long period of 60 years is about 780 psi. This drop in pressure is insignificant considering the fact that oil compressibility is very low and, in unsaturated oil reservoir, a little fluid withdrawal can lead to high pressure drops. Hence, it can be concluded that the volumetric oil flow from outer leases adjacent to the SRV is not significant.

Chapter 7 Conclusions and Recommendations

7.1 Conclusions

The purpose of this research was to evaluate the effectiveness of various established decline curve analysis methods of evaluating past production performance and predicting future performance of the Eagle Ford Shale oil reservoirs. Both analytical and simulation techniques modeled production profiles and were compared.

Furthermore, since the Eagle Ford Shale oil recovery factor is low, this research explored the technical feasibility of enhanced shale oil recovery (ESOR) by miscible gas injection displacement process.

In addition to the above two objectives, this thesis investigates pressure profiles across lease boundaries and analyzes possible drainage area outside of the stimulated reservoir volume (SRV).

Based on the above objectives, the following conclusions were deduced from this study. These conclusions are limited to the data and the results from this study.

1. The actual production profiles from production wells of the Eagle Ford Shale are often erratic; it is difficult to discern a reasonable decline trend without filtering out off-trend data. This may affect the results of the decline curve analyses; filtering may be biased and introduce errors in future estimates.

2. Arps' exponential and PLE analysis are conservative approaches for estimating reserves and forecasting future performance. Arps' exponential decline relation rarely applies at $R^2 \geq 0.95$. Arps' hyperbolic, Logistic growth analysis, Duong's method and Logistic

Arps hyperbolic approach consistently provided high estimates, and these methods may be said to be the optimistic approach to generating future productions. The Power law exponential technique, on the other hand, consistently provided the least EUR estimates, and the method may be said to be the pessimistic approach to generating future productions

3. Arps' hyperbolic DCA method proves unsuccessful to estimate reserves and generate future production trends correctly as a consequence of unusual high Arps' decline exponent (b). Forecasting transient production with Arps' hyperbolic equations led to a severe overestimation of EUR, and for that matter, remaining reserves.

4. Duong model did not always fit the cumulative production despite closely fitting most of the production rates. The EUR mostly converges to finite/reasonably recoverable reserves. There were 5 cases where it forecasted the highest.

5. Logistic growth analysis maintained the greatest success in modeling the past production performance, both production rates and the cumulative fitted closely. It also consistently generated the conservative EUR of all the optimistic DCA techniques.

6. Logistic Arps Hyperbolic Approach (LAHA) is my innovation. It successfully improved the occurrence of $0<b<1$ associated with Arps' hyperbolic from 32.5% to 80%, thereby reducing $b>1$ from 67.5% to 20%. EUR forecasted by LAHA were relatively realistic predictions compared to the high (unrealistic) value associated with the original Arps'

hyperbolic. It is close to the forecasts of LGA, and it is reported in terms or parameters to which industry, analyst and investors are accustomed.

7. With CO_2 gas injection displacement process, the 4.0% primary recovery factor increased to 5.8%. Favorable performance of the CO_2 compared to the other miscible gas injectants is due to its higher density, viscosity and solubility which reduce the oil viscosity and causes it to swell. More CO_2 remains in the reservoir increasing its volumetric efficiency compared to the other gases. Optimization scenarios and economic analyses were not involved. If proven economically viable, stripping shale oil reservoirs are good candidates for ESOR by CO_2 injection.
8. Finally, based on pressure drop, drainage area of SRV does not significantly extent into the adjacent non-stimulated shale zones of extremely low permeability. Integrity of lease boundaries cannot be said to be compromised unless where the formation is naturally fractured. The volumetric oil withdrawal outside of the SRV is insignificant considering the low mobility of oil. This could be different for gas wells with low viscosity.

7.2 Recommendations

Further work to be done may include the following:

1. Production data publicly available at the time this research was conducted was insufficient for accurate determination of wells' individual performance in terms of decline analysis and production forecast. It is strongly recommended that any future work include more data from a larger number of wells to ensure statistically significant results.
2. Initial rates, decline rates, and EUR should be analyzed together with the wellbore dynamics and geometry, i.e., perforation clusters, hydraulic fracture intervals, fracture

half-lengths, and lateral length of horizontal wells, whenever available, to assess their interdependency.

3. Since reservoir simulation models depend on accurate static and dynamic reservoir and hydraulic fracture data, the study strongly recommends that future simulation input parameters be considerably augmented beyond the very basic ones available at the time of this research.
4. Reservoir simulation of production decline should include a larger number of wells. This creates a broader range of well behavior to assess past and future performance and evaluate the difference between simulation results and other analytical methods.
5. Miscible gas displacement process to enhance shale oil recovery should include optimization scenarios such as gas mobility control measures to avoid early bypass and breakthroughs. These should include sensitivity of the inter-spacing of the ends of the hydraulic fractured zones and polymer augmented miscible gas injection.

REFERENCES

Agboada, D., and Ahmadi, M. (2013). Production Decline and Numerical Simulation Model Analysis of the Eagle Ford Shale Oil Play. SPE 165315-P, 1-30.

Arps, J. J. (1945). Analysis of decline curves. Transactions of the American Institute of Mining, Metallurgical and Petroleum Engineers, 160, 228.

Berg, R. R., and Gangi, A. F. (1999). Primary Migration by Oil-Generation Microfracturing in Low-Permeability Source Rocks: Application to the Austin Chalk, Texas. AAPG Bulletin , 83 (5), 727-756.

Bui, L. H. (2010). Near Miscible Carbon-dioxide Application to Improve Oil Recovery. Kansas City: University of Kansas.

Chaudhary, A. (2011). Shale Oil Production Performance From A Stimulated Reservoir Volume. College Station: Texas AandM University.

Chaudhary, A. S., Ehlig-Economides, C., and Wattenbarger, R. (2011). Shale Oil Production Performance from a Stimulated Reservoir Volume. SPE 147596 , 1-21.

Clark, A. J. (2011). Decline Curve Analysis in Unconventional Resource Play using Logistic Growth Models (2011 ed.). The University Texas at Austin.

Duong, A. (2010). An Unconventional Rate Decline Approach for Tight and Fractured-Dominated Gas Wells. SPE 137748 , 1-15

Duong, A. (2011). Rate-Decline Analysis for Fractured-Dominated Shale Reservoirs. SPE 137748 , 377-387.

Fan, L. et al., 2011. An Integrated Approach for Understanding Oil and Gas Reserves Potential in Eagle Ford Shale Formation. SPE 148751, p. 15.

Fertl, W. H., and Rieke III, H. H. (1980). Gamma Ray Spectral Evaluation Techniques Identify Fractured Shale Reservoirs and Source-Rock Characteristics. SPE 8454 , 1-10.

Ghoodjani, E., and Bolouri, S. (2012). Numerical and Analytical Optimization of Injection Rate During CO2-EOR and Sequestration Processes. Orlando: Carbon Management Technology Conference.

Ghoodjani, E. and Bolouri, S., (2011). Experimental Study of CO2-EOR and N2-EOR with Focus on Relative Permeability Effect. Petroleum and Environmental Biotechnology, pp. 1-5.

Government-Report. (2011, July 12). Government Report Details Vast Shale Wealth. Retrieved July 06, 2013, from http://eaglemap.com/news/bid/61474/Government-Report-Details-Vast-Shale-Wealth

Gui, P., Jia, X., Cunha, J., and Cunha, L. (2008). Economic Analysis for Enhanced CO2 Injection and Sequestration Using Horizontal Wells. JCPT, 47 (11), 34-37.

Gupta, D., and Bobier, D. (1998). The History and Success of Liquid CO2 and CO2/N2 Fracturing System. SPE 40016, 1-8.

Hart, N. (2011, September 30). How Long Will Eagle Ford Shale Wells Produce? Retrieved from Eagle Ford Shale Blog Web site: http://eaglefordshaleblog.com/2011/09/30/how-long-will-eagle-ford-shale-wells-produce

Holditch, A. S. (2003). The Increasing Role of Unconventional Reservoirs in the Future of the Oil and Gas Business. JPT Archives, 55 (11), 34-37.

Holm, L. (1986). Miscibility and Miscible Displacement. SPE 15794, 1-2.

Hsu, S.C., and Nelson, P. P. (2002). Characterization of Eagle Ford Shale. In Engineering Geology (pp. 169-183). Elsevier Science B.V.

Ilk, D., Rushing, J., Perego, A. & Blasingame, T., 2008. Exponential vs. Hyperbolic Decline in Tight Gas Sands: Understanding the Origin and Implications for Reserve Estimates Using Arps' Decline Curves. SPE 116731, 1- 23.

Lillies, A. T., and King, S. R. (1982). Sand Fracturing With Liquid Carbon Dioxide. SPE 11341, 1-8.

Malik, Q. M., and Islam, M. (2000). CO2 Injection in the Weyburn Field of Canada: Optimization of Enhanced Oil Recovery and Greenhouse Gas Storage with Horizontal Wells. SPE 59327, 1-16.

Martin, R., Baihly, J., Malpani, R., Lindsay, G., Atwood, K. W., and Schlumberger. (2011). Understanding Production from Eagle Ford-Austin Chalk System. SPE 145117, 1-28.

McFarland, G. (2010). Petroleum Geochemistry and Shale Plays. Richardson: Obsidian Energy Company, LLC.

McNeil, R., Jeje, O. and Renaud, A., 2009. Application of the Power Law Loss-Ratio Method of Decline Analysis. Canadian International Petroleum Conference (CIPC) 2009-159, pp. 1-7.

Medeiros, F., Kurtoglu, B., Ozkan, E., and Kazemi, H. (2007). Analysis of Production Data from Hydraulically Fractured Horizontal Wells in Tight, Heterogeneous Formations. SPE 110848, 1-11.

Medeiros, F., Ozkan, E., and Kazemi, H. (2008). Productivity and Drainage Area of Fractured Horizontal Wells in Tight Gas Reservoirs. SPE 108110, 1-10.

Mendoza, E., Aular, J., and Sousa, L. (2011). Optimizing Horizontal-Well Hydraulic-Fracture Spacing in the Eagle Ford Formation, Texas. SPE 143681, 1-16.

Miskimins, J.L. (2008). Design and Life Cycle Considerations for Unconventional Reservoir Wells. Paper SPE 114170 presented at the SPE Unconventional Reservoirs Conference, Keystone, Colorado, USA, 10-12 February.

Mullen, J. (2010). Petrophysical Characterization of the Eagle Ford Shale in South Texas. SPE 138145, 1-19.

Nielson, J. (1989). Recovery of oil from oil-bearing formation by continually flowing pressurized heated gas through channel alongside matrix. US Patent 4856587, 1-4.

Nwabuoku, K. C. (2011). Increasing Lateral Coverage in Eagle Ford Horizontal Shale Completion. SPE 147549, 1-12.

Odusina, E., Dr. Sondergeld, C., and Dr. Raj, C. (2011). NMR Study of Shale Wettability. SPE147371, 1-15.

Orangi, A., Nagarajan, N., Honarpour, M., and Rosenzweig, J. (2011). Unconventional Shale Oil and Gas-Condensate Reservoir Production, Impact of Rock, Fluid, and Hydraulic Fractures. SPE 140536, 1-15.

Passey, Q., Bohacs, K., Esch, W., Klimentidi, R., and Sinha, s. (2010). From Oil-Prone Source Rock to Gas-Producing Shale Reservoir - Geologic and Petrophysical Characterization of Unconventional Shale Gas Reservoirs. SPE 131350, 1-29.

Perkins, T., and Kern, L. (1961). Widths of Hydraulic Fractures. Journal of Petroleum Technology-SPE 89, 13 (9), 1-13.

Rahmatabadi, K. A. (2011). Advances in Calculation of Minimum Miscibility Pressure. Austin: University of Texas Austin (http://www.pge.utexas.edu/theses11/ahmadi.pdf).

Rickman, R. et al., 2008. A Practical Use of Shale Petrophysics for Stimulation Design Optimization: All Shale Plays Are Not Clones of the Barnett Shale. SPE 115258-MS, 1-11.

Roussel, N. P., Manchanda, R., and Sharma, M. M. (2012). Implications of Fracturing Pressure Data Recorded during a Horizontal Completion on Stage Spacing Design. SPE 152631, 1-14.
Rubin, B. (2010). Accurate Simulation of Non Darcy Flow in Stimulated Fractured Shale Reservoirs. SPE 132093-MS, 1-16.

Settari, A., Bachman, R., and Morrison, D. (1986). Numerical Simulation of Liquid CO2 Hydraulic Fracturing. Petroleum Society of CIM (Paper No: 86-37-67), 399-418.

Shelley, R., Saugier, L., Al-Tailji, W., Guliyev, N., Shah, K., and Godwin, J. (2012). Data-Driven Modeling Improves the Understanding of Hydraulic Fracture Stimulated Horizontal Eagle Ford Completions. SPE 152121, 1-11.

Shoaib, S., and Hoffman, T. B. (2009). CO2 Flooding the Elm Coulee Field. SPE 123176, 1-11.

Sinal, M. L., and Lancaster, G. (1987, Sept.-Oct.). Liquid CO2 Fracturing: Advantages and Limitations. JCPT-87-05-01, pp. 26-30.

Sondhi, N., 2011. Petrophysical Characterization of the Eagle Ford Shale, Norman, Oklahoma: Mewbourne School Of Petroleum And Geological Engineering.

Stegent, N., and Ingram, S. (2011). Hydraulic Fracture Stimulation Design Considerations and Production Analysis. SPE 139981, 1-10.

Stegent, N., Wagner, A., Mullen, J., and Borstmayer, R. (2010). Engineering a Successful Fracture-Stimulation Treatment in the Eagle Ford Shale. SPE 136183.

TRRC-Website. (2012, May 22). Railroad Commission of Texas. Retrieved June 10, 2012, from http://www.rrc.state.tx.us/eagleford/index.php

Tuttle, S. (2010, September 24). Oil Resource Plays-Examples and Technology. Society of Independent Professional Earth Scientists (SIPES): Houston Chapter, pp. 1-37.

Vassilellis, G., Li, C., Seager, R., and Moos, D. (2010). Investigating the Expected Long-Term Production Performance of Shale Reservoirs. SPE 138134, 1-12.

Vincent, M. C. (2011). Optimizing Transverse Fractures in Liquid-Rich Formations. SPE 146376, 1-16.

Wang, J., and Liu, Y. (2011). Well Performance Modeling in Eagle Ford Shale Oil Reservoir. SPE 144427, 1-9 (1).

Wang, X., Luo, P., Er, V., and Huang, S. (2010). Assessment of CO2 Flooding Potential for Bakken Formation, Saskatchewan. CSUG/SPE 137728, 1-14.

Waters, G., Dean, B., Downie, R., Kerrihard, K., Austbo, L., and McPherson, B. (2009). Simultaneous Hydraulic Fracturing of Adjacent Horizontal Wells in the Woodford Shale. SPE 119635, 1-22.

Wei, Y., and Economides, M. (2005). Transverse Hydraulic Fractures from a Horizontal Well. SPE 94671, 1-12.

NOMENCLATURE

a = Constant of t^n when half the oil has been recovered, (variable used in LGA)

a = Intercept constant, day-1 (variable used in Duong method)

b = Arps' decline exponent

B_o = Oil formation volume factor

BHP = Bottom hole pressure

CH_4 = Methane

CO_2 = Carbon dioxide

d = Day

DCA = Decline curve analysis

D_1 = Decline constant "intercept" at 1 time unit, (t=1,time^{-1}) (variable used in PLE)

D_∞ = Decline constant at "infinite time"($t = \infty, \mathrm{time}^{-1}$) (variable used in PLE)

$\widehat{D}_i$ = Decline constant ($\widehat{D}_i = D_1/n$), time^{-1}(variable used in PLE)

D = Arps' decline constant, 1/day or 1/time

EOS = Equation of state

EOR = Enhanced oil recovery

ESOR =Enhanced shale oil recovery

EUR = Expected ultimate recovery

FCM = First contact miscibility

FVF = Formation volume factor

GOR = Gas oil ratio

K = Carrying capacity (maximum physically recoverable oil), (variable used in LGA)

K_{rg} = Relative permeability to gas

K_{rog} = Relative permeability to oil in a gas-oil system

K_{row} = Relative permeability to oil in a oil-water system

K_{rw} = Relative permeability to water

LAHA = Logistic Arps' hyperbolic approach

LGA = Logistic growth analysis

MCM = Multiple contact miscibility

MMP = Minimum miscibility pressure

m = Slope (variable used in Duong method)

NSM = Numerical simulation model

N_2 = Nitrogen

n = Time exponent, dimensionless (variable used in PLE)

n = LGA hyperbolic exponent (variable used in LGA)

N_g =Corey gas exponent

N_o = Corey oil exponent

N_p = Cumulative oil production, STB

OOIP = Original oil in place

PLE = Power law exponential

P-T = Pressure-temperature

PVT = Pressure-volume-temperature

q = Production oil rate at time t, stb/day or stb/time

q_i = Initial rate, stb/day or stb/time, and

$\hat{q}_i$ = Rate "intercept" t=0, stb/d (variable used in PLE)

q_i = Oil rate at Day 1(variable used in Duong method)

q_∞ = Oil rate at infinite time (variable used in Duong method

S_l = Total liquid saturation

S_g = Gas saturation

S_w = Water saturation

STB = Stock tank barrel (same as stb)

stb/d = Stock tank barrel/day

SRV = Stimulated reservoir volume

TOC = Total organic content

TRRC = Texas railroad commission

t = Production time, days

$t_{(a, m)}$ = Time function based on **Equation 3.11** (variable used in Duong method)

Z-factor = Gas compressibility

Appendix

Table A.1: Table of decline exponents (b) when Arps' hyperbolic and LAHA models are applied

Production Profile Counts	Well's County	Well Lease Names	Decline Exponent (0<b<1)	Decline Exponent (b>1)	LAHA (0<b<1) Improved Decline Exponent
1	BURLESON	Giesenschlag W. H. "	0.89		
2		A B Childers		1.01	0.93
3		Giesenschlag-Groce		1.12	0.91
4	LEON	Simms		1.23	0.89
5		Easterling		1.42	0.97
6		Donaho Unit	0.50		
7	KARNES	Berry	0.57		
8		Coates	0.72		
9		Muenchow Unit		1.06	0.76
10		Cannon		1.86	
11		Brysch Jonas Unit		1.56	
12		Kathryn Kealey Unit		1.25	0.84
13		CEF		3.05	
14		Gilley Unit	0.85		
15		Yosko Unit	0.59		
16		Carter Unit		1.57	
17	DIMMIT	Hatch		1.07	0.91
18		Votlz Unit	0.97		
19		Fog Mount		1.76	
20		JBGS		1.05	0.43

Table A.1: Continued:

Production Profile Counts	Well's County	Well Lease Names	Decline Exponent (0<b<1)	Decline Exponent (b>1)	LAHA (0<b<1) Improved Decline Exponent
21	GONZALES	Mostyn		1.22	0.94
22		Holmes	0.97		
23		Georg	0.07		
24		Parr	0.72		
25		Bozka		1.52	0.89
26		S. Duderstadt		1.09	0.91
27		Cinco Ranch	0.98		
28		Koenning Unit		1.20	0.91
29		Gonzo Hunter		1.20	0.56
30		Perkins	0.62		
31		Otto		1.19	0.94
32	ZAVALA	K.M Ranch		1.41	0.97
33		Mustang Ranch C		4.50	
34		Alpha Ware		1.99	
35		Felps		1.07	0.56
36		Howett	0.58		
37		Addison Avery		1.21	0.78
38	BRAZOS	Reser-Sanders Unit		1.11	0.87
39		Hullabaloo		1.45	0.99
40	LEE	Fenn Ranch Unit		3.01	

Table A.2: EUR, remaining reserves and well's life to 2stb/day for Eagle Ford horizontal wells

Well's County	Well's Lease Names	Reserves in Barrels & Time to Reach 2 Barrels/day	PLE	Arps' Exponential	Arps' Harmonic	Arps' Hyperbolic	LGA	LAHA	Duong
BURLESON	GIESENSCHLAG W. H. "	EUR	8915	-	31606	33162	28795	29416	30976
		Remaining Reserves	907	-	5117	6673	2306	2927	4487
		Remaining Life	326	-	1796	1654	863	1090	1234
	A B CHILDERS	EUR	16722	16828	28971	29391	22014	27091	56199
		Remaining Reserves	5864	5970	18113	18533	11156	16233	45341
		Remaining Life	1437	1443	4874	5003	2876	4466	12285
	GIESENSCHLAG-GROCE	EUR	45996	-	108595	121748	85119	99202	111905
		Remaining Reserves	12598	-	49131	62284	25655	39738	52441
		Remaining Life	2052	-	10727	14026	5205	8701	8800
LEON	SIMMS	EUR	16590	-	24044	30047	21734	22906	26399
		Remaining Reserves	1836	-	9290	15293	6980	8152	11645
		Remaining Life	668	-	2603	4125	1887	2291	2123
	EASTERLING	EUR	4513	-	5686	7204	5248	5692	7057
		Remaining Reserves	949	-	2122	3640	1684	2128	3493
		Remaining Life	291	-	725	1212	586	752	900
	DONAHO UNIT	EUR	45959	-	-	65300	66938	76359	122874
		Remaining Reserves	17165	-	-	36506	38144	47565	94080
		Remaining Life	878	-	-	3035	3435	4937	4391
DIMMIT	HATCH	EUR	37971	-	107057	123119	85566	99506	95714
		Remaining Reserves	12247	-	47095	63157	25604	39544	35752
		Remaining Life	1606	-	9293	11557	4521	7729	2080
	VOTLZ UNIT	EUR	35333	-	-	61152	50099	61893	84619
		Remaining Reserves	4192	-	-	30011	18958	30752	53478
		Remaining Life	632	-	-	5523	3342	6194	17794
	FOG MOUNT	EUR	36842	-	59641	215465	55588	54195	62045
		Remaining Reserves	7681	-	30480	186304	26427	25034	32884
		Remaining Life	742	-	6257	45950	4516	10909	4153
	JBGS	EUR	72692	-	-	127734	90817	77105	131864
		Remaining Reserves	25448	-	-	80490	43573	29861	84620
		Remaining Life	1086	-	-	13410	5832	2903	11463
LEE	FENN RANCH UNIT	EUR	54052	-	60422	1348154	101329	1017639	111826
		Remaining Reserves	9877	-	41507	1329239	82414	998724	92911
		Remaining Life	1509	-	8959	449331	16561	330025	12457

Table A.2: Continued

Well's County	Well's Lease Names	Reserves in Barrels & Time to Reach 2 Barrels/day	PLE	Arps' Exponential	Arps' Harmonic	Arps' Hyperbolic	LGA	LAHA	Duong
KARNES	BERRY	EUR	113208	-	-	151792	125904	125086	128690
		Remaining Reserves	858	-	-	39442	13554	12736	16340
		Remaining Life	444	-	-	2900	1982	1850	2874
	COATES	EUR	129078	-	-	194380	162457	179139	249748
		Remaining Reserves	27148	-	-	92450	60527	77209	147818
		Remaining Life	1117	-	-	9860	5861	8433	18797
	MUENCHOW UNIT	EUR	48885	-	71910	89673	53138	57098	57860
		Remaining Reserves	8791	-	31816	49579	13044	17004	17766
		Remaining Life	195	-	5122	7185	2228	3100	672
	CANNON	EUR	238393	-	671093	8657490	672319	349323	644186
		Remaining Reserves	130145	-	505544	8491941	506770	183774	478637
		Remaining Life	3830	-	59201	2008923	38291	12350	7787
	BRYSCH JONAS UNIT	EUR	114286	-	264765	983609	427641	144368	233354
		Remaining Reserves	56269	-	180422	899266	343298	60025	149011
		Remaining Life	2210	-	23566	177192	36450	4522	1338
	KATHRYN KEALEY UNIT	EUR	74118	73881	181062	308584	109331	145672	187824
		Remaining Reserves	23226	22989	130170	257692	58439	94780	136932
		Remaining Life	1332	1262	18189	43213	5471	11653	5719
	CEF	EUR	266087	-	802971	1630304019	910953	479021	2315763
		Remaining Reserves	155230	-	659561	1630160609	767543	335611	2172353
		Remaining Life	3892	-	74578	548209395	74199	24844	44016
	GILLEY UNIT	EUR	19250	-	-	35558	303815	1117057	87412
		Remaining Reserves	8763	-	-	25071	293328	1106570	76925
		Remaining Life	1291	-	-	4896	76385	382972	13478
	YOSKO UNIT	EUR	166491	-	161924	224487	203877	213767	260796
		Remaining Reserves	16309	-	11742	74305	53695	63585	110614
		Remaining Life	850	-	11812	5801	4947	6302	4041
	CARTER UNIT	EUR	115278	-	272867	1012169	432453	158008	247024
		Remaining Reserves	36553	-	194142	933444	353728	79283	168299
		Remaining Life	1688	-	25889	191179	37713	6448	3217

Table A.2: Continued

Well's County	Well's Lease Names	Reserves in Barrels & Time to Reach 2 Barrels/day	PLE	Arps' Exponential	Arps' Harmonic	Arps' Hyperbolic	LGA	LAHA	Duong
GONZALES	MOSTYN	EUR	43801	-	86403	119258	62536	82340	108520
		Remaining Reserves	11130	-	53732	86587	29865	49669	75849
		Remaining Life	1346	-	10118	17558	4655	9171	9778
	HOLMES	EUR	126992	-	162311	170451	100998	126946	142343
		Remaining Reserves	63944	-	99263	107403	37950	63898	79295
		Remaining Life	960	-	14023	8813	2500	5883	2944
	GEORG	EUR	10890	-	-	11033	11140	10926	11295
		Remaining Reserves	2145	-	-	2288	2395	2181	2550
		Remaining Life	338	-	-	365	466	484	926
	PARR	EUR	11017	-	-	14437	12352	12466	15313
		Remaining Reserves	1778	-	-	5198	3113	3227	6074
		Remaining Life	311	-	-	1086	759	791	1702
	BOZKA	EUR	27919	-	54416	142638	42643	51054	49172
		Remaining Reserves	7755	-	28386	116608	16613	25024	23142
		Remaining Life	988	-	5291	24970	2613	4503	1275
	S. DUDERSTADT	EUR	56522	-	147211	196735	115295	139452	119047
		Remaining Reserves	14559	-	72417	121941	40501	64658	44253
		Remaining Life	1065	-	11412	17007	5008	9683	721
	CINCO RANCH	EUR	40546	-	-	90723	63144	70705	75906
		Remaining Reserves	3197	-	-	45687	18108	25669	30871
		Remaining Life	503	-	-	7246	2999	4663	1042
	KOENNING UNIT	EUR	27696	27113	50445	65699	37065	46753	57770
		Remaining Reserves	8171	7588	30920	46213	17579	27266	36225
		Remaining Life	1017	1067	6322	9909	3112	5481	8907
	GONZO HUNTER	EUR	64796	-	-	141216	62834	64044	73870
		Remaining Reserves	16455	-	-	92875	14493	15703	25529
		Remaining Life	508	-	-	16906	2314	2554	4459
	PERKINS	EUR	50388	-	83345	65357	59918	62989	73930
		Remaining Reserves	2485	-	35442	17454	12015	15086	26027
		Remaining Life	546	-	45202	2353	2265	2924	1617
	OTTO	EUR	24932	-	63274	91498	53775	62347	57675
		Remaining Reserves	6897	-	26594	54818	17095	25667	20995
		Remaining Life	947	-	5436	9945	3131	5201	850

Table A.2: Continued

Well's County	Well's Lease Names	Reserves in Barrels & Time to Reach 2 Barrels/day	PLE	Arps' Exponential	Arps' Harmonic	Arps' Hyperbolic	LGA	LAHA	Duong
ZAVALA	K.M RANCH	EUR	24706	-	50994	114960	45298	51049	44888
		Remaining Reserves	7534	-	28352	92318	22656	28407	22246
		Remaining Life	632	-	4841	17169	3150	4870	606
	MUSTANG RANCH C	EUR	146185	-	376235	5981256282	138455648	2872696626	1708562
		Remaining Reserves	108957	-	327445	5981207492	138406858	2872647836	1659772
		Remaining Life	6695	-	47698	2326186769	35495642	1103119307	66823
	ALPHA WARE	EUR	52147	-	108824	478005	89691	77868	168091
		Remaining Reserves	27584	-	84261	453442	65128	53305	143528
		Remaining Life	1722	-	13624	1772208	6539	6959	9579
	FELPS	EUR	52147	-	-	155600	73713	76968	273177
		Remaining Reserves	19374	-	-	126288	44401	47656	243865
		Remaining Life	1631	-	-	20525	5009	5585	21664
	HOWETT	EUR	68404	-	-	98311	87739	87975	176165
		Remaining Reserves	29655	-	-	47087	36515	36751	124941
		Remaining Life	1095	-	-	4627	3669	3706	16945
	ADDISON AVERY	EUR	33879	33879	75666	100021	48495	59793	220122
		Remaining Reserves	16800	16800	58587	82942	31416	42714	203043
		Remaining Life	2033	2033	11143	17164	4862	7451	30067
BRAZOS	RESER-SANDERS UNIT	EUR	5511	-	-	8022	8673	9073	9891
		Remaining Reserves	644	-	-	621	1272	1672	2490
		Remaining Life	320	-	-	1988	965	1260	2384
	HULLABALOO	EUR	44298	40664	72974	152627	69446	84623	94833
		Remaining Reserves	11076	10690	43000	108402	25221	40398	50608
		Remaining Life	1467	1862	9629	13469	5166	9223	7499